Alma Mater Studiorum – Università di Bologna

DOTTORATO DI RICERCA IN
INGEGNERIA CIVILE, CHIMICA,
AMBIENTALE E DEI MATERIALI

Ciclo 30°

Settore Concorsuale: 04/A3

Settore Scientifico Disciplinare: GEO/05

Impacts of climate change on groundwater: numerical modelling of a northern Apennines catchment

Presentata da: Francesca Petronici

Coordinatore Dottorato	**Supervisore**
Prof. Luca Vittuari	**Prof. Lisa Borgatti**

Esame finale anno 2018

ABSTRACT

Estimating the impacts of climate change on groundwater, and the numerical modelling of fractured aquifers, represent two of the most difficult tasks faced by water resources specialists and hydrogeologists. Some difficulties have to be faced in the representation of the hydrological system and in accounting for the uncertainties of climate change scenarios. In this context, the objective of this study is to provide a methodology for the estimation of climate change impacts on groundwater resources. This methodology has been applied to the Tresinaro stream catchment (147 km^2) in the northern Apennines (Italy), and to the main water source of the stream, the Mulino delle Vene springs (420 m a.s.l., Carpineti, Reggio Emilia province). In particular, the springs outflow is very sensitive to a shortage in water recharge, as it was the case in 2003 and 2017, when prolonged periods of drought caused severe water management issues. Only few studies about the impacts of climate change on groundwater have been carried out in the last years in Italy, and no one in the northern Apennines area. This is of concern because mountainous water resources are fundamental to the civil water supply and to sustain the ecosystem, especially during dry periods. Moreover, it has to be pointed out that this study represents the first effort to model the Tresinaro stream catchment and it has allowed an in depth analysis of the correlated hydrological system.

Firstly, some finite elements models of the fractured aquifer feeding the Mulino delle Vene springs have been developed, with the codes FEFLOW and TRANSIN, in order to investigate the groundwater flow system. An Equivalent Porous Medium (EPM) approach has been adopted, simplifying the whole system with a porous medium. The models have been calibrated on the data observed in the area (monitored piezometric levels in three observation points and daily springs discharge). Results show the complexity of the heterogeneous system and suggest some adjustments of the conceptual model to be carried out in further studies. In particular, some sensitivity analyses and transient state simulations have been carried out, and a range of calibrated conductivity values for the fractured rock masses (between 1.16 x 10^{-4} m/s and 1.16 x 10^{-7} m/s) has been identified.

In the second place, an innovative methodology for the assessment of the impacts of climate change on groundwater has been developed, with the objective of analyse more in detail the low flow period. In particular, some rainfall-runoff models of the Mulino delle Vene springs have been built and calibrated on the daily springs discharge observed data. To the knowledge of the Author, the present work represents one of the first attempt to apply a rainfall-runoff model to groundwater studies. More in detail, two rainfall-runoff model structures have been developed. The first model is inspired to the Hymod model structure (modified Hymod model) and the calibration performance is very good (Erel equal to 0.83 in the calibration period and to 0.73 in the validation period). The second model belongs to the multiple reservoir models group and the calibration is satisfactory (Erel equal to 0.89 and to 0.72 for the calibration and validation period respectively), as well.

Then, the calibrated and validated models have been combined with climate change scenarios for the study area. Climate change data have been obtained from five Regional Climate Models (RCMs) of the European Union Sixth Framework Programme project ENSEMBLES from the A1B family. These RCM scenarios have been statistically downscaled using two different statistical methods: the delta change and the Cumulative Distribution Function transform method (CDF-t). The first method is able to apply corrections only to the mean values of the climatic variables, whereas the second method considers the statistical distributions of these variables as well. In fact, the statistical distributions of the climatic variables are expected to change in the future, with more intense rainfall events, separated by longer dry periods. The downscaling techniques have been used to generate the weather variables for the future 30-years period between the 2021 and the 2050, on the basis of the observed 30-years period between the 1984 and the 2013. More in detail, the climate change scenarios of the Mulino delle Vene area predict warmer years with drier summers and wetter winters. In fact, comparing future downscaled data with baseline data, an increase of temperature in the future is forecasted during each month (average increase of about +1.3 °C) with both the downscaling techniques. Instead, the average annual rainfall decreases by the 3% or the 2.3% respectively with the delta change or the CDF-t method. Moreover, the CDF-t method forecasts a change in the monthly rainfall distribution. In particular,

rainfall decreases mostly during the summer months (e.g. -30 mm in June) and it increases during the winter months (e.g. +25 mm in February). All these scenarios have been applied as input of the calibrated rainfall-runoff models.

Considering the results of this study, it is very likely that groundwater flow rates of the Mulino delle Vene springs will decrease, especially during the summers, exacerbating the water stress condition in the area. In particular, even if the average annual effective recharge does not significantly change in the future, the springs discharge during low flow period will decrease due to the different rainfall pattern throughout the year (e.g. maximum discharge decrease in September by the 26.3%). Moreover, low flow indexes will be adversely affected (e.g., increase of the duration of the continuous time interval of low flow below the threshold Q(80)). This is of concern because the Mulino delle Vene springs are the main water source of the Tresinaro stream and they sustain the stream discharge especially during the dry period (as highlighted from the low flow assessment performed in this study). Therefore, the estimated intra-annual springs discharge changes for the future period (2021-2050) will slightly modify the river flow downstream from their confluence. Furthermore, it has to be emphasized that rivers flowing from the northern Apennines supply the porous aquifers in the alluvial plain of the river Po. These aquifers are largely exploited for civil and industrial purposes to satisfy the needs of hundreds of thousands of people. Therefore, due to the interdependency between river water level and groundwater, the reduction of groundwater input from mountainous aquifers to the river network will result in a decrease of the plain aquifers recharge. This is of concern because these aquifers are already displaying signs of water shortage, because of severe over-exploitation.

Finally, a physically based surface-subsurface flow model has been developed for the Tresinaro stream catchment with the finite elements code HydroGeoSphere. The model has been built according to the results of the hydrological and hydrogeological investigations of the area. Moreover, some simulations and a sensitivity analysis of the rainfall have been carried out. In particular, the reduction by the 10% of the precipitation affected the Tresinaro discharge with a reduction by the 20% of the average stream discharge. Further studies will consider the calibration of a more in detailed model and the combination with the RCMs data of the area.

In conclusion, this work has allowed a comprehensive hydrogeological investigation to be carried out in a sensitive area of the northern Apennines, which has never been object of previous studies, and several numerical models to be implemented. Moreover, the quantitative vulnerability of groundwater resources to climate change has been assessed in a representative springs of the northern Apennines. Results of this analysis represent the first answer to the lack of researches in the field of climate change and groundwater in Italy. Further studies, and the application of the developed methodology to other case studies, will allow a wider framework to be taken into account. Moreover, results of these analyses could be used by policy makers and water resources managers in the development of the best management practice of the water resource in the area and to prevent, or at least reduce, the damage from water scarcity in the future.

TABLE OF CONTENTS

LIST OF FIGURES

LIST OF TABLES

1. INTRODUCTION

Bates et al. (2008) states that warming of the climate system in recent decades is unequivocal, as it is now evident from observations of increases in global average air and ocean temperatures, widespread melting of snow and ice, and rising global sea level. The last Intergovernmental Panel on Climate Change reports (IPCC, 2007; IPCC, 2014) assert that climate change will affect the quantity and quality of the global hydrological cycle with an increase in the risk of flooding and drought in many regions. In particular, groundwater bodies will be affected, as stated by Taylor et al. (2012), firstly by the decreasing of the water table, then an increment in the irrigation demand will occur contributing to the drying of the aquifers. Moreover, the global water demand has increased 35 fold in the last 330 years and it is continuing to grow (Kundzewicz & Doll, 2009). In detail, communities rely more on groundwater during dry periods and more on surface water during wet periods (Alley, 2001). Therefore, as an exacerbating of the water stress conditions is expected in the future, further studies on the effects of climate change on groundwater bodies are necessary to understand and consciously face the drought issue (Dragoni & Sukhija, 2008; Garnier et al., 2015).

Italian water resources are particularly sensitive to a shortage of the water recharge, as it was the case in 2003 and 2017, when a prolonged drought period caused severe water management issues. In Italy, according to ISTAT (Istituto Nazionale di Statistica, 2012), the 85.6% of drinking water comes from groundwater (35.7% from springs and 49.8% from wells). In fact, thanks to the hydrogeological characteristics of its territory, Italy is rich of groundwater resources of better quality than surface water. Therefore, the best management practices of the Italian water resources start from a comprehensive analysis and a conscious use of groundwater (IAH-Italy, 2017). To develop a good water management approach, an in-depth investigation of the hydrogeological processes is necessary, especially in the mountainous watersheds, which are important sources of water for local and downstream ecosystems and human population. In particular, groundwater is fundamental to mitigate the impacts of dry summers and hot waves and it is essential to manage water resources during dry periods.

Even if the vulnerability of groundwater to climate change is well known, nowadays the projections of the direct impacts of climate change of groundwater systems are highly uncertain. Several studies have analysed the impacts of climate change worldwide, but still few works have been carried out in Italy and especially over the Apennines area.

Considering this general context, the thesis deals with the evaluation of climate change effects on the groundwater resources of a basin in the northern Apennines of Italy (Tresinaro stream catchment, Reggio Emilia Province). The study intends to investigate a frame of different modelling approaches relevant for climate change impacts assessment, and to assess the effects of climate change on a catchment representative of several northern Apennines catchments. In particular, the study has been developed, on a local scale, analysing and modelling the main springs system of the basin (Mulino delle Vene springs). Then, on a large scale, analysing the stream low flow and modelling the hydrological catchment from the mountainous part to the alluvial plain. Several modelling approaches have been applied and compared. During this work, the recommendations of Holman et al. (2012) and the advice of the IPCC have been taken into account to define the main modelling strategies to be considered in the groundwater related climate change studies. For example, Holman et al. (2012) suggests using multiple climate change scenarios and complex downscaling techniques, which allow the statistical distribution of climate variables. Moreover, the use of integrated models is recommended to properly represent all the variables of the hydrological cycle. The work has been feasible thanks to the data and the instruments provided by the regional environmental agency (Agenzia Regionale per la Prevenzione, l'Ambiente e l'Energia dell'Emilia-Romagna, ARPAE E-R).

In section 2 of this thesis, a review of the scientific literatures performed in the field of groundwater, fractured aquifers and climate change is displayed. Section 3 describes the geological and hydrological setting of the Tresinaro stream catchment. Section 4 presents the methodology used in the current research. Section 5 exposes the main outcomes of the research, as obtained following the methodology described in the previous section. Finally, section 6 provides conclusion and research perspectives.

2. SCIENTIFIC REVIEW

2.1 MODELLING CLIMATE CHANGE EFFECTS

In the recent years, literature about the effects of climate change on the hydrological cycle is wide and constantly increasing in number (Green et al., 2011), but most of the papers are site-specific.

To date, most of the works have been directed to forecasting the potential impacts of climate change on surface water hydrology, even if groundwater plays a key-role in meeting the demand for drinking water and to sustain the ecosystem and, in addition, to supply agricultural and industrial activities. In fact, groundwater constitutes the major resource of fresh water (Taylor et al., 2012) and it sustains baseflow in rivers during periods of low flow. Only in the last two decades, the research community interest in the impacts of climate change on subsurface water has started to increase (Green et al., 2011). The classical way to approach the problem is numerical modelling; different code and approaches have been developed throughout the years. In particular, several Authors have evaluated the effects of climate change on groundwater combining different modelling code.

For example, Allen et al. (2004) have modelled the sensitivity of the Grand Forks aquifer (Canada) to changes in recharge or in river flow, using three separate code. In particular, a 3D groundwater flow model has been built with MODFLOW (WHI, 1997), combined with Visual HELP (WHI, 1999) to estimate the recharge and BRANCH (Schaffranek, 1987) to compute the river stage. Results have suggested that variations in the recharge have smaller impacts on the groundwater system compared with the river stage elevations. Later, Scibek & Allen (2006) and Scibek et al. (2007) have confirmed the close relationship between the stream flow and the aquifer water resources modelling the climate change effects in the Grand Forks hydrological catchment. Therefore, where river-aquifer interactions occur, groundwater levels respond significantly and more directly to shifts in the river hydrograph than to recharge changes.

Secondly, Woldeamlak et al. (2007) have evaluated the effects of climate change on the water balance and groundwater system of a sandy aquifer (Grote-Nete, Belgium) under temperate climate conditions, using WetSpass (Batelaan & al., 2001) to assess the annual recharge and MODFLOW to simulate the groundwater levels in steady-state conditions. Modelling results have shown the potential impacts of a recharge change on the hydrogeological system, highlighting the sensitivity of the water cycle to climate change.

In addition, Toews & Allen (2009) have evaluated the sensitivity of recharge to different climate models in an irrigated agricultural region (Okanagan Basin, Canada). All the scenarios used in this work have predicted an increase of temperature together with a potential reduction of precipitation during late summer months. An increase of precipitation has been forecasted during winter. The recharge has been assessed with the HELP model (Berger, 2004) obtaining a modest increase in future time periods.

Furthermore, Pulido-Velazquez et al. (2015) have used the Visual-Balan tool to assess the future recharge in a Spanish basin, starting from a calibrated model and regional climate change projection. Instead, Touhami et al. (2015) have applied the HYDROBAL model in a Spanish basin. For the Spanish regions, a decrease of recharge has been always forecasted even if using different regional climate models.

Moreover, a well-known code used in the hydrological modelling and analysis is the Soil Water Assessment Tool (SWAT). Numerous works have applied the SWAT code to investigate the effects of climate change on water supply availability (Borah & Bera, 2003; Jayakrishnan et al., 2005; Romanowicz et al., 2005; Ficklin et al., 2009; Bekele & Knapp, 2010; Raposo et al.; 2012). In particular, Mango et al (2011) have analysed both climate change and land use change (i.e. deforestation) finding that the conversion of forest to agriculture or grassland in the basin is likely to reduce dry season flows, exacerbating water scarcity problems into the future.

Apart from this, several works have taken into account also the irrigation and the water demand, quantifying the possible future groundwater shortage in basins (Kreins et al., 2015).

Recently, one of the most used software to simulate surface and groundwater flow is MIKE SHE coupled with MIKE11 (DHI, 2007). Several Authors have used this code to simulate stream flow at the catchment outlets

and groundwater levels in the basin (Xevi et al., 1997; Feyen et al., 2000; Liu et al., 2007; van Roosmalen et al., 2009; Sultana & Coulibaly, 2011). For example, Voeckler et al. (2014) have developed a coupled surface water – groundwater model for a small steep mountainous headwater catchment (Upper Penticton Creek watershed, in the Okanagan Alpine zone, Canada) with the aim to explore the role of deep groundwater flow in the catchment dynamics. The aquifer is a fractured one but it has been treated as an equivalent porous medium with uniform conductivity values. Actually, the Upper Penticton Creek watershed is characterised by a network of fractures, which act as preferential pathways for infiltration and groundwater flow. To better represent the fractured medium, a heterogeneous bedrock can be built with the FracMan Reservoir Edition (FRED) software (Golder Associates Ltd., 2006) as in Voeckler & Allen (2012).

Moreover, MIKE SHE has been applied by Foster & Allen (2015) to assess the surface-groundwater interactions in a mountain to coast watershed (Cowichan watershed, British Columbia, Canada) and to assess the climate change effects on the water resources of the catchment. Furthermore, a small and detailed model of a chalk valley riparian wetland (Berkshire, UK) has been developed by House et al. (2016) with the MIKE SHE software in order to assess impacts of climate change to the wetland ecosystem.

All these works represent interesting examples, but the all of them evaluate separately the surface and the subsurface components of the water cycle. Instead, Holman et al. (2012) assert that the simultaneous solution of surface and subsurface flow equations improve the simulation of the hydrogeological processes, like the recharge that is fundamental in the climate change effect assessment. An important condition for estimating the impacts of climate change on the water resources of a catchment is that the hydrogeological model is capable of consistently represent observed phenomena, coupling the hydrological processes. This standard is achieved by integrated code.

Barthel & Banzhaf (2016) pointed out the importance of the use of an integrated code capable of reproducing groundwater-surface water interactions.

Several code and integration techniques have been applied in recent years. For example, Huntington & Niswonger (2012) have highlighted the need for integrated hydrologic models in climate change studies. They have built an integrated surface and groundwater model to simulate climate impacts on surface water/groundwater interactions under several climate change scenarios in the eastern Sierra Nevada (United States). They have used GSFLOW (Markstrom et al., 2008) which is an integration of the Precipitation Runoff Modelling System (PRMS) and of MODFLOW. Due to the interactions between surface water and groundwater, they have found that snow-dominated watersheds may become more arid during the hottest period of the year, and water stress in the low flow period will become more severe even if annual precipitation increases.

Moreover, Sulis et al. (2011) have evaluated the sensitivity to climate change of a small river basin in Canada with the coupled hydrological model CATHY.

Lastly, one of the most effective tool developed for the integrated hydrogeological modelling is HydroGeoSphere (HGS; Aquanty, 2013). This powerful software allows a fully integration of processes capable to reproduce groundwater-surface water exchange in complex systems. Therefore, the number of applications are increasing (Jones et al., 2009; Bolger et al., 2011; Ala-aho et al., 2015). Hereafter some example of HGS applications are reported.

Firstly, Goderniaux et al. (2009) have combined the physically based integrated model of HGS with advanced climate change scenarios, assessing the impacts of climate change on the groundwater resources in the Geer Basin (Belgium). The use of the HGS software has allowed a better simulation of all the hydrological processes in the basin, especially actual evapotranspiration, which has been calculated as a function of the soil moisture. In particular, Goderniaux et al. (2009) have forecasted dryer summer and wetter winter for the Belgian catchment, and modelled outputs have showed a significant decrease of groundwater levels and surface flow rates. The previous model has been improved by Goderniaux et al. (2011) and Goderniaux et al. (2015) estimating the uncertainty around projected impacts and using a sophisticated transient weather generator to

assess impacts in a probabilistic way respectively. At this moment, these methodologies are among the best applied practices to assess the impact of climate change on the water resources. Moreover, the discretization problem has been analysed from Wildemeersch et al. (2014) who have assessed the effects of the discretization on the flow performance of HGS. They have pointed out that a coarse model poorly simulated the runoff and the surface water-groundwater interaction due to a rough representation of the surface.

Moreover, von Gunten et al. (2014) have carried out an interesting work dealing with the problem of calibration and time consumption. Indeed, HGS is very powerful but it requires high computational time. They have proposed to calibrate the model gradually, with progressively increasing mesh resolutions, obtaining a reduction of the calibration time duration. Then, the HGS calibrated model has been used by von Gunten et al. (2015) and von Gunten et al. (2016) to assess climate change effects under various irrigation conditions and to estimate future drought indices of a small catchment in northern Spain. HGS allows irrigation or other man activity on the catchment to be easily taken into account, reaching a better representation of the system also in the future. This allows the evaluation of drought indices in order to predict hydrological impacts of droughts under changing climate conditions.

Even if the literature about the hydrogeological modelling of springs is still poor, an application with the HydroGeoSphere code has been recently carried out. Levison et al. (2014) have developed a groundwater modelling study simulating fractured bedrock springs flow in Covey Hill (Canada). The model has been built with the HydroGeoSphere software simulating springs flow in the actual and future periods from climate change scenarios and investigating the ecological habitats in different flow conditions.

Furthermore, HGS is capable to simulate fractured matrix with a DFN approach as shown in Cey et al. (2006), Gleeson & Manning (2008) and Blessent et al. (2009). An in-depth knowledge of the system is necessary but results are quite interesting.

2.2 MODELLING A FRACTURED AQUIFER

In addition to climate change effects assessment, a second issue taken on in this work is the modelling of fractured aquifers, topic which is frequently coupled with climate change.

A fractured aquifer is a complex hydrogeological system and a lot of structural data and hydrogeological information are necessary to build a representative model. Several Authors have dealt with the heterogeneity of the fractured systems with different modelling solutions. Most of the works have applied an Equivalent Porous Medium approach (Gburek et al., 1999; Rayne et al., 2001; Paradis et al., 2007; Piccinini & Vincenzi, 2010) even if studies about Discrete Fracture Network and Hybrid models are increasing (Long et al., 1982; Shapiro & Andersson, 1983; Wang et al., 2001; Surrette et al, 2008; Renz et al., 2009; Garzonio et al., 2014). For example, Voeckler & Allen (2012) have modelled a regional fractured aquifer (Okanagan Basin, Canada) estimating the bedrock hydraulic conductivity through lineament and outcrop mapping in combination with inverse Discrete Fracture Network modelling.

In this work, the Equivalent Porous Medium approach has been applied and finite elements models have been built. Future studies will apply a Hybrid or a Discrete Fracture Network approach to better represent the domain heterogeneity.

Moreover, a further approach for the groundwater modelling of highly heterogeneous aquifers is the application of rainfall-runoff models. They represent an alternative way to the finite elements / finite differences codes and they demand a lower number of data. Different model structures have been applied in the last years from the simple lumped model to more complex ones (Eisenlohr et al., 1997; Fiorillo, 2011; Fiorillo, 2013; Diodato et al., 2014; Katsanou et al., 2014). In this work, several model structures have been tested.

2.3 MODELLING CLIMATE CHANGE EFFECTS IN ITALY

In Italy, groundwater is a significant economic resource being the 23% of the total water abstracted (Hiscock et al., 2011). Major aquifers are contained in the plain alluvial sediments that are recharged twice each year with snowmelt in the spring and rainfall in the autumn (Morari et al., 2004). Antolini et al. (2016) have analysed changes in temperature and precipitation in the Emilia-Romagna region from the 1961 to the 2010. The data set shows a significant increase in mean annual temperatures all over the region about +0.5 °C/decade. Precipitation shows a less clear behaviour with both local decrease and increase (e.g. -100 mm/decade over the wester mountains; increase in some areas close to the Po River Delta). For the future, Global Circulation Models (GCMs) forecast, by the end of this century, increases in winter recharge for southern Europe, whereas summers will be drier with a longer period of limited or no groundwater recharge (Hiscock et al., 2011). Therefore, Italy is expected to become more water stressed than at the present. Future drinking and irrigation water demand has to be managed sustainably in order to face the water stress conditions. One possibility is the protection of the mountainous water resources, which feed the river and supply the alluvial plain aquifers.

In the past, water resources managers and researchers have not focused their attention on the Apennines water resources due to the small volumes of the mountainous aquifers compared to the regional water resource. Instead, the mountainous aquifers host water of good quality and their supply is essential for the surface water bodies maintenance and for the mountain villages.

To the knowledge of the Author, works about the effects of climate change on the groundwater resources of the northern Apennines are not published on scientific journals. The Italian works published during the last years are list below.

Firstly, Cambi & Dragoni (2000) have carried out one of the first attempt to assess the effects of climate change on groundwater for a central Italian aquifer (the Bagnara spring). They have found a higher decrease in spring discharge than in the recharge decrease highlighting the vulnerability of Italian water sources. Later, this result has been confirmed by Dragoni et al. (2015).

Moreover, Gattinoni & Francani (2010) have published an interesting work about the hydrogeological modelling of an Italian spring in a fractured system. They have modelled the Nossana spring (northern Italy) with the software MODFLOW. In detail, they have assessed the effects of different recharge conditions on the depletion curve of the spring. Similarly, Dragoni et al. (2013) have built a MODFLOW model of a spring in the central Apennines fed by a fractured limestone massif (Scirca spring). The calibrated model has been used to test the efficiency of various management schemes of the water resources.

Other works concerning the south of Italy have been published by D'Agostino et al. (2014) and Liuzzo et al. (2014). The first Author has evaluated impacts of climate change on the water balance and water use in an area of the Puglia region with a coupled hydro-economic model. The second Author has investigated different recharge conditions in the Sicilian region. Results have shown a worsening of water stress due to a negative trend in precipitation and an increase in evapotranspiration. Moreover, Fiorillo et al. (2007) have carried out a statistical analysis of the rainfall-spring discharge correlation in the Terminio massif (Campania region, southern Italy), highlighting the sensitivity of springs to climatic parameters.

Finally, Vezzoli et al. (2015) have analysed the effects of climate change scenarios on the Po river discharge with a hydrological model. During summer, they have forecasted a reduction of precipitation that leads to an increase of low flow duration. Instead, the high flows frequency will increase in autumn and winter when precipitation shows a positive variation.

The present work constitutes the first effort to apply the most used modelling techniques to a northern Apennines catchment. Results will be also useful for future research in the area.

3. STUDY AREA

The object of this study is the Tresinaro stream catchment, located in the SE of the Reggio Emilia Province (Italy), in the northern Apennines. The stream originates in the municipality of Carpineti (562 m a.s.l.) and it flows in the valley for 47 km through the municipalities of Baiso (542 m a.s.l.), Viano (275 m a.s.l.), Scandiano (95 m a.s.l.) and Rubiera (53 m a.s.l.) where it joins the river Secchia (tributary of the Po River). In the last centuries, the natural stream path was modified by human activities, especially in the alluvial plain, in order to reduce the flood risk. In particular, the so-called "Taglio Tresinaro" was built in the XIV century at Fellegara (95 m a.s.l., Scandiano) to divert the stream directly in the Secchia river and to protect from floods the village located downstream. After this event, in the former section of the stream the "Cavo Tresinaro" was cut with the main function to drain water excess.

The mountainous part of the catchment is scarcely urbanised, with a population density of 45.7 people for km^2 at Carpineti, 44.9 people for km^2 at Baiso and 75.7 people for km^2 at Viano. Instead, in the plain, the population density increases at 507.3 people for km^2 at Scandiano and 590 people for km^2 at Rubiera (Istat, 2014). In addition, an important industrial zone is located in the Scandiano and Casalgrande municipalities. For these reasons the mountainous parts of the stream could be considered as only slightly influenced by human activities, whereas the plain part discharge is strongly affected by human sewage, especially during dry period, when the stream discharge is less than 100 l/s.

This study focuses mainly on the mountainous part of the catchment and on the apex of the alluvial fan. In particular, in the hydrological analysis the basin is closed at the 35th km of the stream, where the gauge station of Ca' de Caroli is set to monitor the stream discharge (Fig. 3.1). With this assumption, the Tresinaro stream hydrological catchment covers approximately an area of 147 km^2. Moreover, the main source of the Tresinaro stream, the Mulino delle Vene springs (420 m a.s.l.), are comprehensively analysed.

Figure 3.1 Study area.
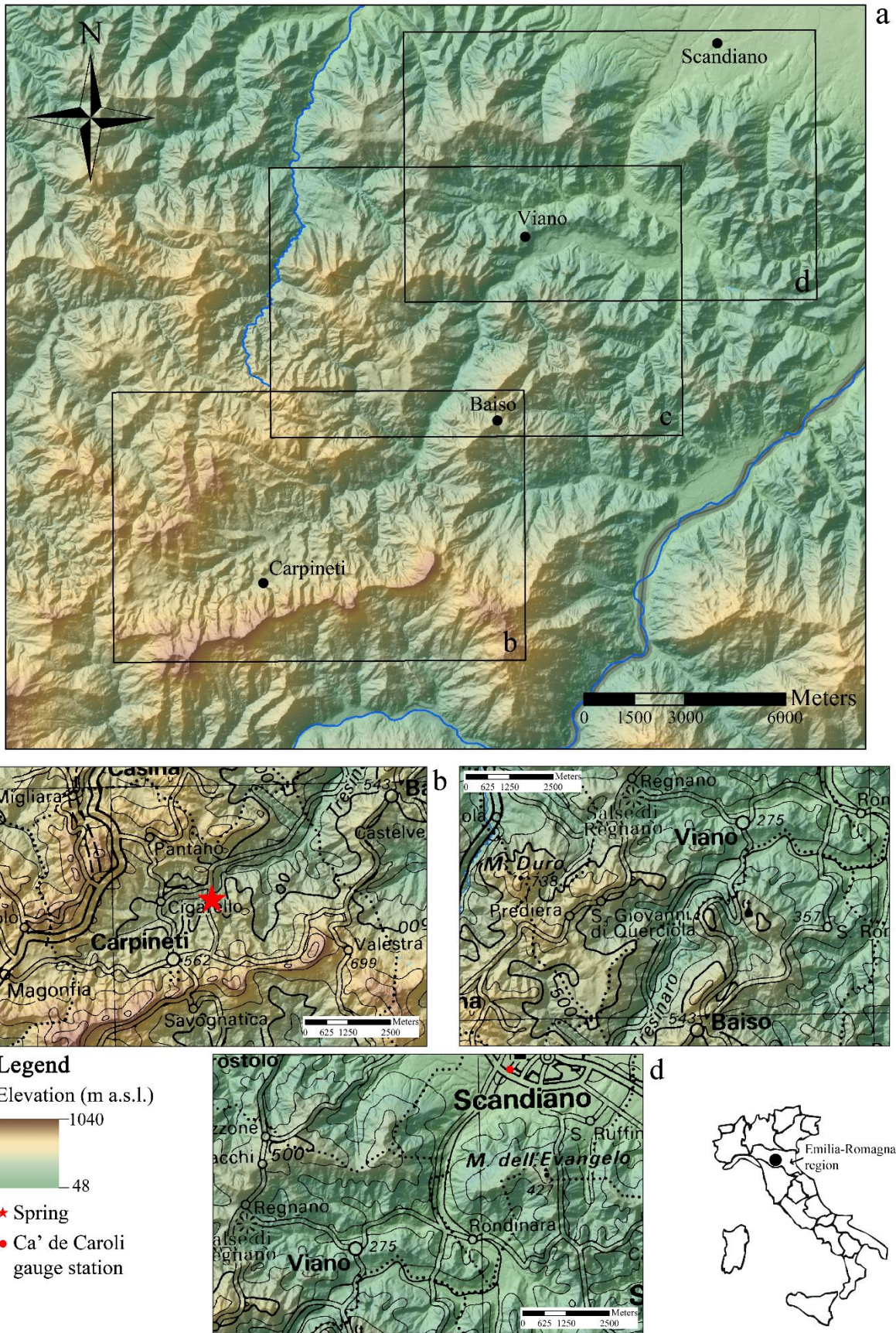
3.1 HYDROLOGICAL FEATURES

A hydrological analysis of the area has been carried out in order to describe the hydrological catchment of the Tresinaro stream. The work starts from a Digital Terrain Model (5x5m) of the Emilia-Romagna region treated with the Hydrology Tools of Arc Map (ESRI). Selecting the point of the Ca' de Caroli gauge station as closing point, the Tresinaro stream catchment (Fig. 3.2) has a total area of 147 km^2 and a stream length of 35 km. Furthermore, the catchment is characterized by a steep topography in the upper sector, whereas it is gentler down valley. Elevation ranges from 972 m a.s.l. to 98 m a.s.l., with a mean value of 322 m a.s.l.. The alluvial fan apex is located about 3 km upstream the Ca'de Caroli stream gauge.

Being a relatively small catchment and still sparsely urbanized, it can be considered as an interesting and representative case study for similar catchment in the Apennines. In the method and the result sections, a detailed description of the hydrological analysis of the climate data is reported (sections 4.1 and 5.1). Results allow a better characterization of the basin to be obtained.
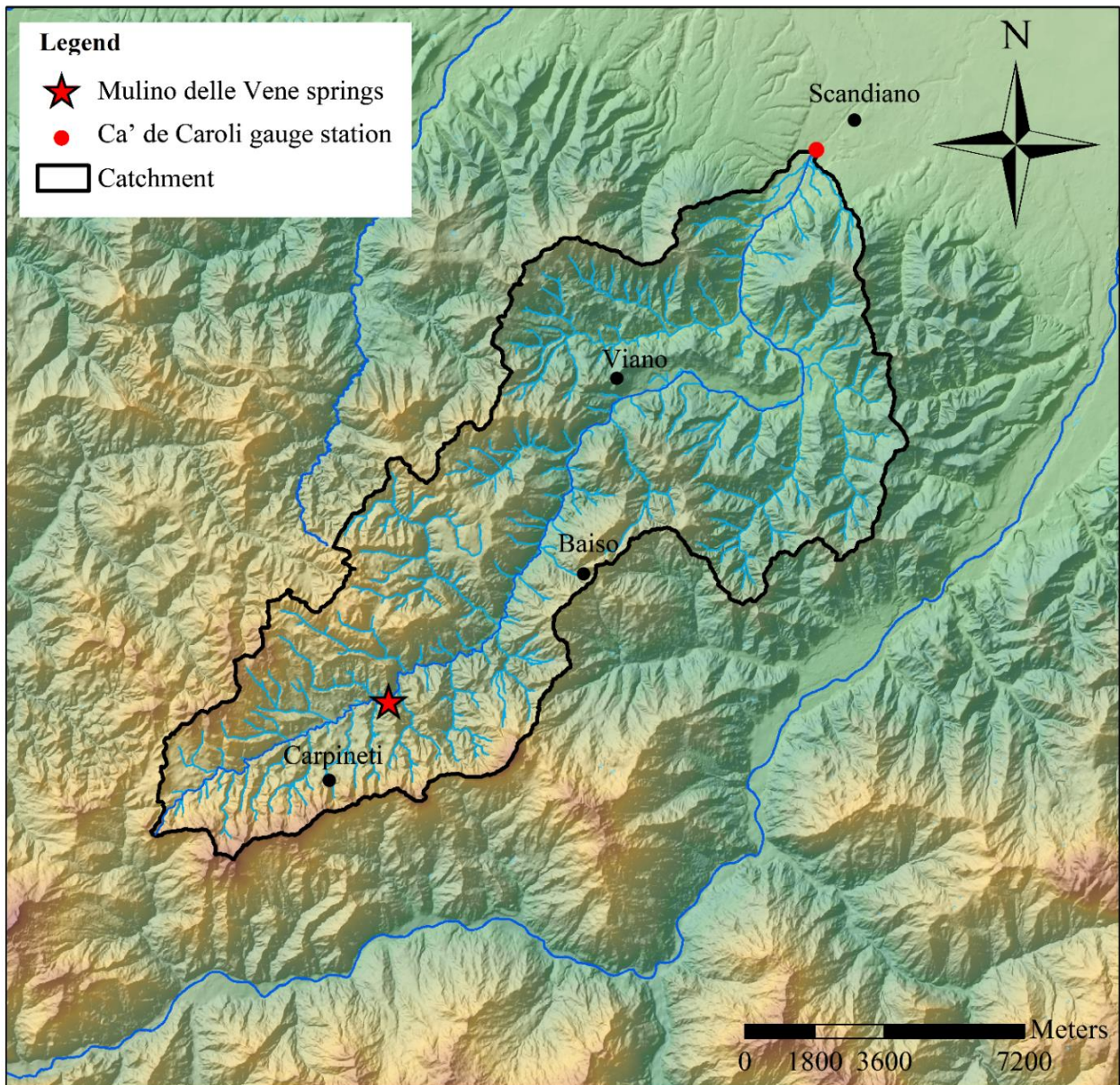
Figure 3.2 Hydrological catchment.

HYDROLOGY OF THE EMILIA-ROMAGNA REGION

The Environmental Protection Agency of Emilia-Romagna, Hydro Meteo Climate Service (ARPA SIMC E-R) performed a comprehensive study of the climate variables (precipitation and temperature) registered in the Emilia-Romagna region covering the period 1961-2010 (Antolini et al., 2016). A significant increase in mean annual temperature was observed all over the region, about 0.5 °C/decade, between the 1961 to the 2010. Moreover, average precipitation was decreasing with a trend of about -155 mm/decade. The mean temperatures, averaged over 1961-2010, range from 5 °C to over 14 °C, estimated at the highest mountain peaks and at the urban areas in the plain, respectively. The cumulated annual precipitations, averaged over 1961-2010, range from 600 mm in the eastern plain areas to over 2300 mm in the mountain areas. To better analyse the climate variables in the study area, a more detailed analysis was carried out, as described in the sections 4.1 and 5.1.

3.2 GEOLOGICAL AND HYDROGEOLOGICAL FEATURES
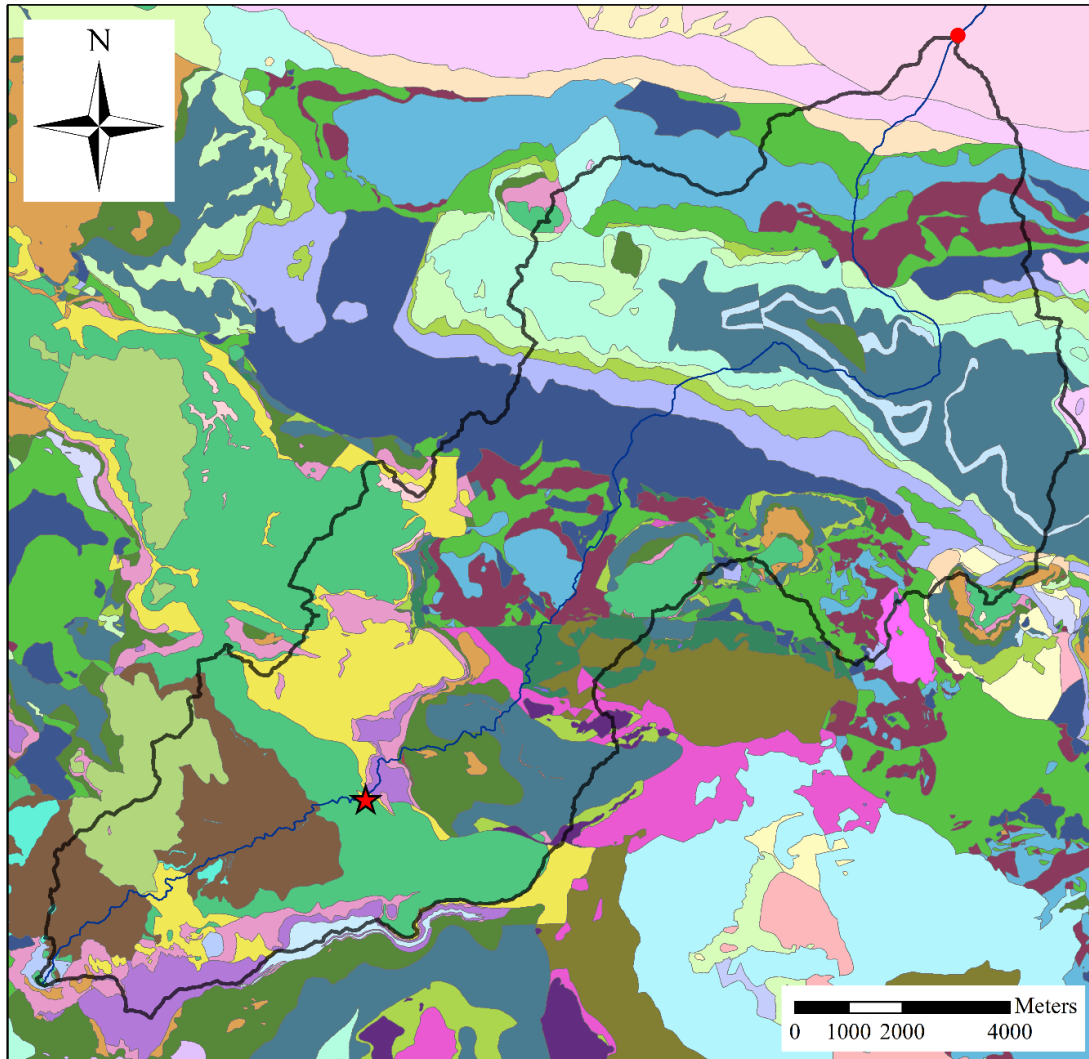
Legend

- ★ Mulino delle Vene springs
- ● Ca' de Caroli gauge station
- — Tresinaro stream
- ▭ Hydrological catchment
- Scabiazza sandstones
- Varicolori clay of Cassio
- Palombini shale
- Brecce Argillose of Baiso - included Flysch elmintoidi
- Brecce Argillose of Val Tiepido - Canossa
- Brecce Argillose of Baiso - unit of Costa dei Buoi
- Brecce Argillose of Baiso
- Monte Cassio Flysch
- Ranzano formation- unit of Varano de' Melegari
- Ranzano formation - litofacies arenaceo-conglomeratica
- Ranzano formation - unit of Val Pessola
- Blue clay
- Blue clay - litofacies pelitico-sabbiosa

- Cigarello formation
- Cigarello formation - unit of Marola sandstones
- Cigarello formation - sandstones litofacies
- Contignaco formation
- Contignaco formation - unit of Villaprara
- Contignaco formation - unit of Carpineti
- Loiano formation
- Monte Venere formation
- Pantano formation
- Pantano formation - unit of Santa Maria
- Pantano formation - unit of Bismantova
- Antognola marls
- Antognola marls - unit of Anconella
- Marls of Monte Piano
- Viano clay
- Chalk formation
- Sintema di Costamezzana

Figure 3.3 Geological map of the study area (from the Geological, Seismic and Soil Survey).

11

The Tresinaro stream crosses Epiligurian and Ligurian geological units (Papani et al., 2002). In particular (Fig. 3.3), the Cigarello formation (CIG), constituted by clay-shales, crops out in the uppermost part of the basin, then the stream crosses some outcrops of the Pantano formation (PAT). The PAT is made up by sandstones and it is subdivided in different sub-units according to the ratio of arenitic to pelitic layers (A/P ratio), for example the unit of Santa Maria (PAT4), that has a high A/P ratio (Papani et al., 2002) and it is the unit hosting the main aquifer of the area for secondary permeability. In the upper part of the stream path, we can find the Contignaco (CTG) and the Antognola (ANT) formations, which are mainly marly rock masses. In the middle part of the basin, clay rich units are outcropping (AVI, Clay of Viano; APA, Palombini shale; AVV, Varicolori clay of Cassio) and flysch deposits (BAI, Brecce Argillose of Baiso; SCB, Scabiazza sandstones). Then we can find the Ranzano formation (RAN) constituted mainly by sandstones and the Monte Cassio Flysch (MCS). In the final part of the hydrological catchment, different types of clay-shale units (APA; AVV; FAA, Blue clay), the chalk formation (GES) and finally the plan deposits constituted by sand and gravel outcrop.

Resuming, the catchment is characterized by the outcropping of clay-rich units with very low hydraulic conductivity (marls or clay-shales: hydraulic conductivity K of about $10^{-10} \div 10^{-13}$ m/s, Freeze & Cherry, 1979), associated with sandstone rock masses (hydraulic conductivity K equal to $10^{-5} \div 10^{-10}$ m/s, Freeze & Cherry, 1979) of which the PAT4 unit represents the main aquifer in the area (Vizzi, 2014). Most of the mountainous part of the hydrological catchment is bounded by clay-rich units (K of about $10^{-10} \div 10^{-13}$ m/s, Freeze & Cherry, 1979) or rock masses with a high A/P ratio, therefore the exchanges of groundwater from the borders could be considered equal to zero.

The Mulino delle Vene springs originate at the bottom of a 50 m long slope (Fig. 3.4). This slope is the southern termination of a continuous and poorly-deformed sandstone plateau (Pantano Sandstones, Santa Maria formation, PAT4) bonded by sub-vertical normal faults overlying almost impermeable marls (Contignaco Marls, CTG). These faults have important effects on the fractures system observed in the PAT4 unit. The most evident discontinuity has generated the Rio Fontanello deep valley (Fig. 3.4).
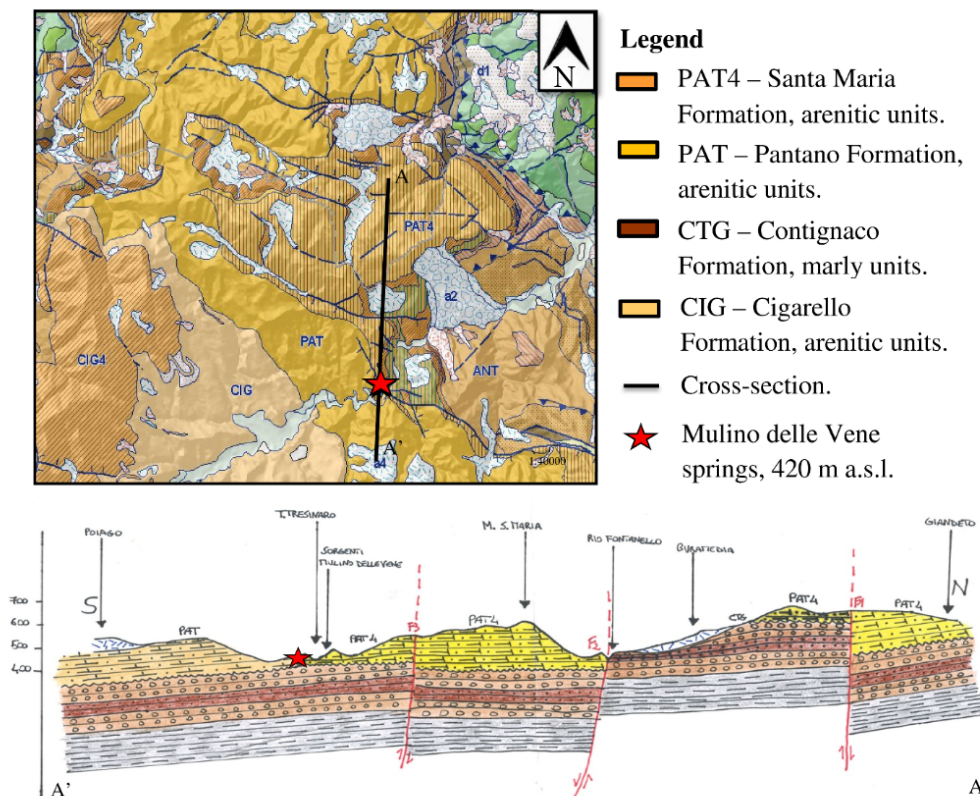
Figure 3.4 Geological map of the Mulino delle Vene springs area and cross-section (Vizzi, 2014).

The Mulino delle Vene springs area has been object of a comprehensive hydrogeological investigation by Vizzi (2014). This Author has gathered the geological units outcropping in the area in hydrogeological structures with a small variation of the hydraulic conductivity, according to Civita (2005). In particular, the following hydrogeological units have been defined:

- MK-HK: Medium conductivity ($10^{-2}<K<10^{-6}$ m/s) - High conductivity ($K>10^{-2}$ m/s) unit constituted by the S. Maria sandstone (PAT4);

- MK: Medium conductivity ($10^{-2}<K<10^{-6}$ m/s) units gathering the Cigarello sandstones (CIG4) and the Contignaco (CTG) formation;

- LK-MK: Low conductivity ($10^{-6}<K<10^{-9}$ m/s) - Medium conductivity ($10^{-2}<K<10^{-6}$ m/s) unit grouping the Pantano unit (PAT), the Scabbiazza sandstones (SCB) and the Ranzano formation (RAN) with a low-medium conductivity;

- LK: Low conductivity ($10^{-6}<K<10^{-9}$ m/s) structure constituted by the pelite of the Cigarello formation (CIG);

- I: Impermeable ($K<10^{-9}$ m/s) structure grouping the Antognola formation (ANT) and the shale units.

The map of the hydrogeological units is reported in Fig. 3.5. This characterization is supported by the geomechanical analysis and the hydraulic conductivity assessment carried out in the study area, in particular in Tab. 3.1 are resumed the results of Vizzi (2014), Terenziani (2014) and Petronici (2014) for the conductivity assessment (as in Snow, 1968; Gattinoni et al, 2005; Scesi & Gattinoni, 2007) of the outcrops in Fig. 3.5. In particular, fracture-network data measurement from outcrops have provided estimates of hydraulic properties such as hydraulic conductivity by using fluid-flow theory (Caine & Tomusiak, 2003). The assessed hydraulic conductivity of the PAT4 outcrop ranges from a minimum of 10^{-4} m/s to a maximum of 2.7×10^{-2} (average value equal to 6.1×10^{-3} m/s), whereas the PAT conductivity ranges between 9.1×10^{-5} and 4.4×10^{-4} (average value equal to 2.1×10^{-4} m/s). Moreover, a well test executed in the study area in the PAT unit (well 4 of Fig. 3.5) allows the assessment of the hydraulic conductivity of the rock mass which is of about 5×10^{-7} m/s (Petronici, 2014). In Fig. 3.5 the location of three investigated wells (points 1, 2 and 4) and of a small lake (point 3) are also displayed. A schematic representation of the structure of well 4 is reported in Appendix A, the well is 71 meters deep and crosses sandstone, marls and clay-shale units. Unfortunately, data about the geometry and the stratigraphy of the other wells are not available.

Table 3.1 Hydraulic conductivity (K) assessment.

Outcrop	Unit	K	Hydrogeological classification
n.		m/s	
1	PAT 4	2.7×10^{-2}	HK
2	PAT 4	1.9×10^{-4}	MK
3	PAT 4	1.1×10^{-3}	MK
4	PAT 4	9.3×10^{-4}	MK
5	PAT 4	1.0×10^{-4}	MK
6	PAT 4	5.5×10^{-3}	MK
7	PAT 4	8.0×10^{-3}	MK
8	PAT 4	1.1×10^{-2}	HK
9	PAT 4	8.2×10^{-3}	MK
10	PAT	closed fractures	I

Outcrop	Unit	K	Hydrogeological classification
n.		m/s	
11	PAT	1.1×10^{-4}	MK
12	PAT	4.4×10^{-4}	MK
13	PAT 4	2.8×10^{-4}	MK
14	PAT	9.1×10^{-5}	MK
15	CTG	7.8×10^{-3}	MK
16	PAT 4	5.8×10^{-3}	MK
17	CTG	6.0×10^{-4}	MK
18	CTG	closed fractures	I
19	CTG	3.7×10^{-3}	MK
Well 4	PAT	5×10^{-7}	LK
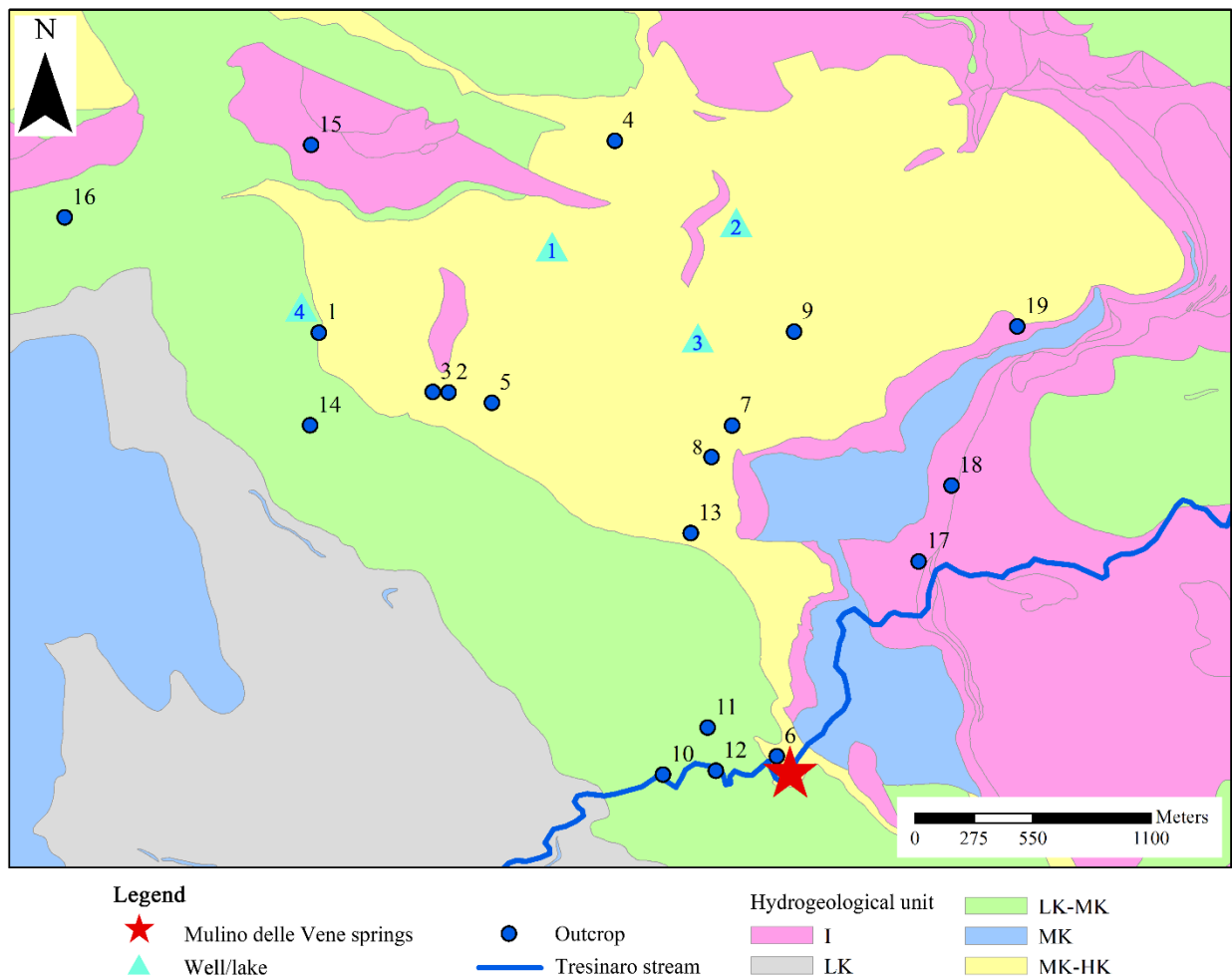
Figure 3.5 Map of the hydrogeological structures in the Mulino delle Vene springs area.

In conclusion, the PAT4 unit displays a higher hydraulic conductivity than the sourrounding units (including the sandstone unit called PAT). Furthermore, the bedding of the PAT4 plateau is gently dipping towards the southeast, where the Mulino delle Vene springs are located (see the geological cross-section, Fig. 3.4), facilitating the groundwater flow towards the Mulino delle Vene springs which thus represent the final and only source point of the analyzed hydrogeological system. Based on this data, Cervi et al (2014) identified the recharge area of the springs as the PAT4 outcrop and they found that the aquifer behaviour is strongly controlled by the network of discontinuities affecting the whole plateau. In this work, groundwater exchanges from the PAT4 outcrop border and especially from the PAT sandstone unit have also been tested in the numerical modelling in order to take into account the variability of the fractured system.

Thereafter, the hydrogeological map of Tresinaro stream catchment (Fig. 3.6) is reported. In the southern-eastern part of the catchment some MK units outcrop on the hydrological catchment border and LK-MK units are spread on the basin, however most of the catchment is impervious (I). Moreover, field surveys executed in the past years (Ghirotti, 2016) have not found sources of water besides the Mulino delle Vene springs. Therefore, in the modelling part, the collected data have supported the choice of considering the catchment and its border as impervious, with the exception of the PAT4 outcrops and of the alluvial fan deposits. In particular, the hydrological catchment has been considered as coinciding with the hydrogeological catchment.
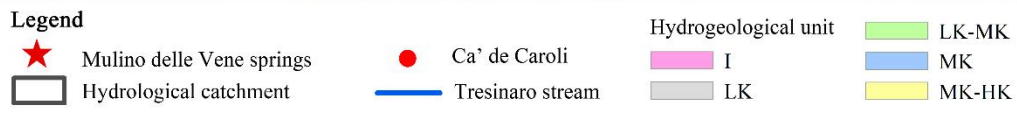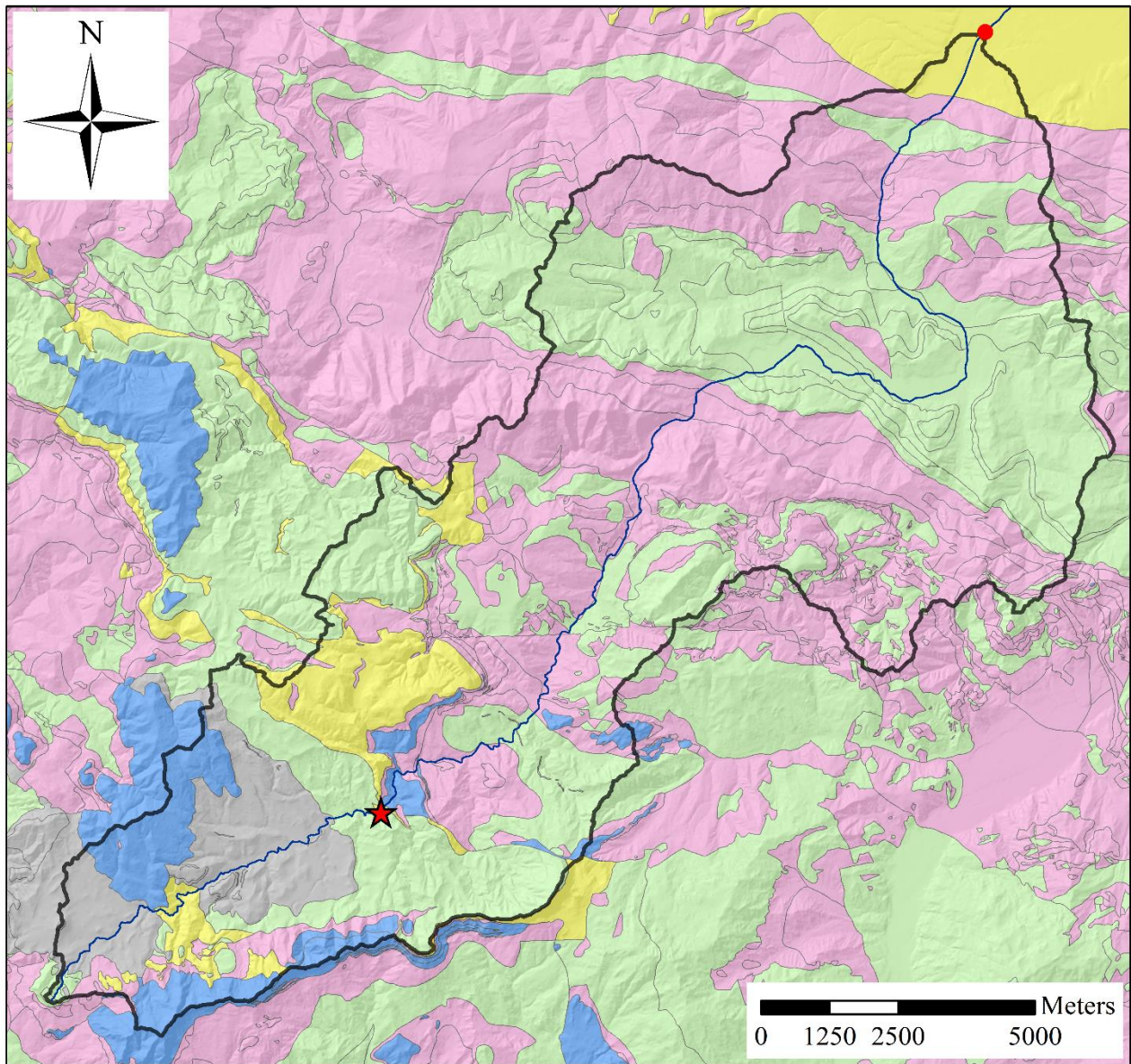
Figure 3.6 Hydrogeological map of the Tresinaro stream catchment.

3.3 MONITORING SYSTEM

The area is the object of a comprehensive study and analysis since 2013. The main water source of the Tresinaro stream are the Mulino delle Vene springs (Carpineti, RE, Fig. 3.2), about 25 km upstream the Ca' de Caroli stream gauge. They are among the largest in the Apennines for mean annual discharge (96.8 l/s) and dynamic storage (1.53 Mm^3) and they are considered as the main water resources in the area (Cervi et al., 2014). ARPAE ER (Agenzia Regionale per la Prevenzione, l'Ambiente e l'Energia dell'Emilia-Romagna) is carrying out continuous monitoring at the Mulino delle Vene springs collecting discharge, electric conductivity and temperature data from March 2013 (section 5.2). Tracer tests carried out during the 2015 low flow period allowed the evaluation of the discharges in several stream sections (section 4.4.3) and highlighted that no other major source of groundwater can be found downstream of the Mulino delle Vene springs. This reveals that a decrease of springs discharge could lead to a decrease of the stream discharge and to an increase of drought events affecting the stream ecosystem and the drinking water supply. Furthermore, it is likely that the impacts could be similar for all the northern Apennines basins. In fact, the northern Apennines are characterized by the presence of hundreds of springs whose discharge is lower than few l/s during the low flow period and renew the groundwater stored within the aquifer almost completely every hydrological year (Cervi et al., 2015). These hydrogeological characteristics make the water resource management in the area quite difficult, especially during the dry season, when an increase of potable water consumption associated to tourism also occurs. Thus, it is important to assess the effects of climatic variability on the springs discharge. In particular, forecast the springs discharge is a pivotal point in the water resources planning and exploitation.

Furthermore, several wells are distributed over the whole catchment but they are all exploited for civil needs and with no significant water extraction. In particular, a well near the Mulino delle Vene springs was continuously monitored during the 2013-2014 winter and three other wells were periodically monitored during the 2013 autumn. These data were used for the calibration of the numerical models of the aquifer feeding the springs (section 4.6) developed in this work.

Downstream, the Tresinaro stream feeds the aquifer in the alluvial plain, infiltrating in the porous sediments of the alluvial fan. Such aquifer is extensively exploited for human and industrial activities by several civil and public wells. In particular, a civil well at the apex of the alluvial fan is equipped with an electric transducer recording the hourly level of the water table and electric conductivity since November 2015 (Fig. 3.7).
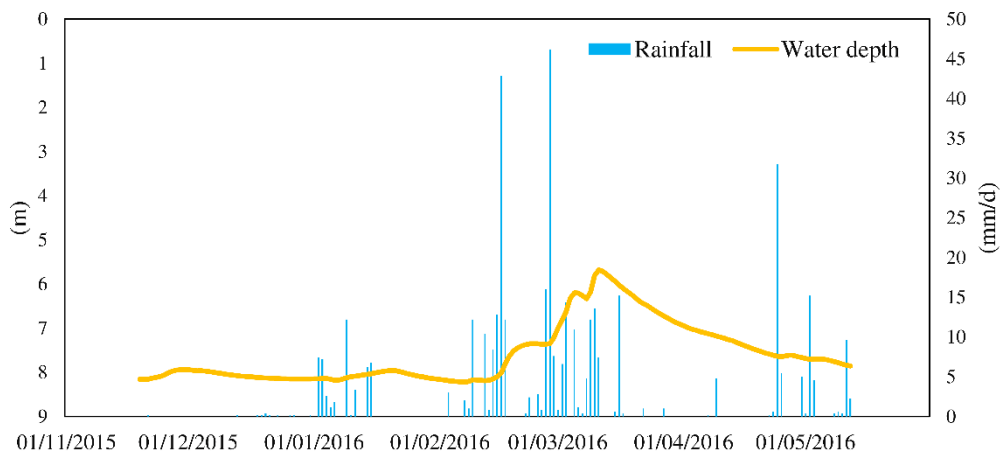
Figure 3.7 Monitored daily water depth in the well of the alluvial fan along with the daily rainfall observed at the Carpineti weather station from November 2015 to June 2016.

The closing point of the catchment is set to the Ca' de Caroli stream gauge (98 m a.s.l.; Scandiano, RE), in the foothills of the northern Apennines chain. The gauge records the daily stream discharge about 3 km downstream the apex of the alluvial fan since 2003, with lack of data in short periods (Fig. 3.8). The average discharge is equal to 1489 l/s. The maximum observed discharge value occurs the 11th of April 2005 and it is equal to 117000 l/s; minimum discharge corresponds to 0 l/s during the 2011 summer period. Unfortunately, no other gauge stations are set along the Tresinaro stream. The only information of discharge distribution along

the stream comes from field surveys and tracer tests executed during the PhD activities.
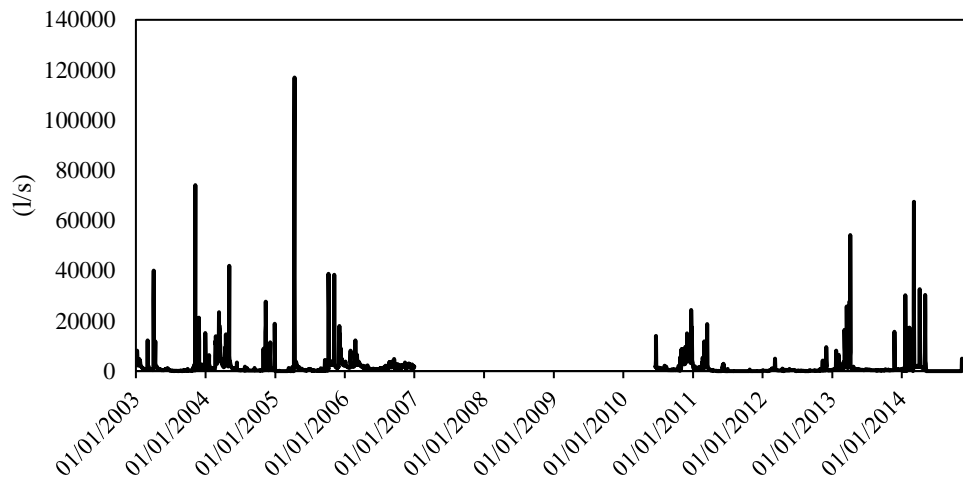
Figure 3.8 Ca' de Caroli monitored discharge in the period 2003-2014.

4. METHODS

4.1 HYDROLOGICAL ANALYSIS

For the hydrological study, precipitation and temperature data from 9 weather stations in the area (Reggio Emilia Province, Fig. 4.1) were used:

- Ca' de Caroli, 98 m a.s.l.

- San Valentino, 302 m a.s.l.

- Baiso, 550 m a.s.l.

- La Stella, 729 m a.s.l.

- Carpineti, 580 m a.s.l.

- Predolo, 751 m a.s.l.

- Ponte Cavola, 367 m a.s.l.

- Castelnovo né Monti, 729 m a.s.l.

- Villa Minozzo, 676 m a.s.l.

Daily data from the 2004 to the 2014 were used to analyse the actual meteorological condition of the catchment. In particular, the rainfall and temperature data were analysed and the potential evapotranspiration was assessed with the equations described hereafter. Some stations register also the daily wind speed and the air humidity necessary to assess the daily evapotranspiration with the Penman-Monteith formula. Finally, data registered at the Carpineti weather station, only two km from the Mulino delle Vene springs location, were used for the modelling.

These data were provided by ARPAE E-R (Agenzia Regionale Prevenzione, Ambiente e Energia dell'Emilia-Romagna) with the online free service Dext3r (http://www.smr.arpa.emr.it/dext3r/) or they were extracted from the yearly regional reports (Annali idrologici).
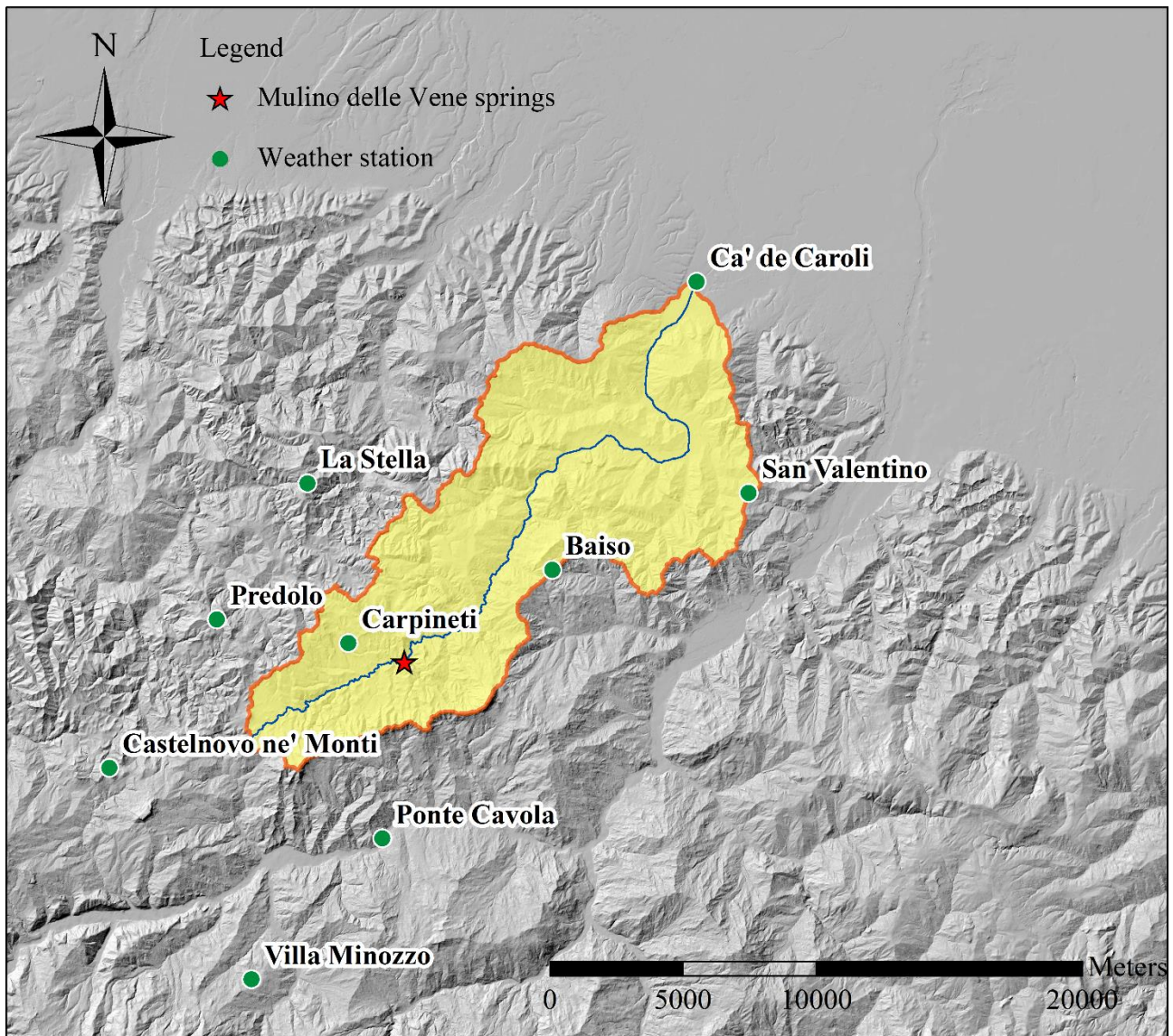
Figure 4.1 Hydrological catchment and weather stations location.

4.1.1 POTENTIAL EVAPOTRANSPIRATION

Evapotranspiration (ET) is the sum of water lost from the soil surface by evaporation and by transpiration from the vegetation cover. Evaporation and transpiration occur simultaneously and there is no easy way of distinguishing between the two processes (Allen et al., 1998). The principal weather parameters affecting evapotranspiration are radiation, air temperature, humidity and wind speed. Several equations have been developed to assess the evapotranspiration from these parameters. Hereafter the more common equations are described.

THORNTHWAITE EQUATION

The potential evapotranspiration from a reference surface can be assessed as (Thornthwaite, 1946):

$$ET_0 = c\,T^a \tag{4.1}$$

Where:

ET_0 is the potential monthly evapotranspiration for a light duration of 12 h, T (°C) is the average temperature of the month, c and a are parameters depending of the weather of the studied area. In particular, they were assessed as follows (Moisello, 2003):

$$a = 0{,}016\,I + 0{,}5 \tag{4.2}$$

$$c = 1{,}6 \left(\frac{10}{I}\right)^a \tag{4.3}$$

Where:

$$I = \sum_{i=1}^{12} \left(\frac{T_i}{5}\right)^{1{,}514} \tag{4.4}$$

and T_i is the average monthly temperature.

PENMAN-MONTEITH EQUATION

The Penman-Monteith method is recommended by the FAO to assess evapotranspiration from the reference surface (ET_0). The reference surface is a hypothetical grass reference crop with an assumed crop height of 0.12 m, a fixed surface resistance of 70 s m^{-1} and an albedo of 0.23. The reference evapotranspiration is the evaporative demand of the atmosphere, independently of crop type, crop development and management practices. Typical values of ET_0 in a temperate region ranges from 2 to 7 mm/d (Allen et al., 1998). All the equations reported below are from Allen et al. (1998).

The Penman-Monteith equation is:

$$\lambda ET = \frac{\Delta(R_n - G) + \rho_a c_p \dfrac{(e_s - e_a)}{r_a}}{\Delta + \gamma(1 + \dfrac{r_s}{r_a})} \tag{4.5}$$

where: Rn is the net radiation; G is the soil heat flux; (e_s - e_a) represents the vapour pressure deficit of the air; ρ_a is the mean air density at constant pressure; c_p is the specific heat of the air; Δ represents the slope of the saturation vapour pressure temperature relationship; γ is the psychometric constant, and r_s and r_a are the (bulk) surface and aerodynamic resistances; λ is the latent heat of vaporization.

In particular, for calculation periods from 1 to 10 days, the soil heat flux G could be ignored.

The vapour pressure could be assessed in function of the air relative humidity (RH) and temperature (T), as the difference between the mean saturation vapour pressure (e_s) and the actual vapour pressure (e_a) with the equations:

$$e_s = 0.611 * \exp\left(\frac{17.27T}{237.3 + T}\right) \quad [kPa] \tag{4.6}$$

$$e_a = \frac{e_s(T_{min})\dfrac{RH_{max}}{100} + e_s(T_{max})\dfrac{RH_{min}}{100}}{2} \quad [kPa] \tag{4.7}$$

The latent heat of vaporization is equal to:

$$\lambda = 4.148 * 10^3 (597.3 - 0.57T) \quad [J/kg] \tag{4.8}$$

The slope of the relationship between saturation vapour pressure and temperature is given by:

$$\Delta = \frac{de_s}{dT} = \frac{4098\left[611\,exp\left(\dfrac{17.27T}{T + 237.3}\right)\right]}{(T + 237.3)^2} \quad [k\,Pa/°C] \tag{4.9}$$

The psychometric constant equation is:

$$\gamma = \frac{c_p P_a}{0.622\lambda} \quad [kPa/°C] \tag{4.10}$$

Where c_p is the specific heat at constant pressure equal to 1.013*10^{-3} [MJ/kg°C]; λ is the latent heat of vaporization; P_a is the atmospheric pressure assessed as function of the topographic height above sea level (z):

$$P_a = 101.3 \left(\frac{293 - 0.0065z}{293}\right)^{5.26} \quad [kPa] \tag{4.11}$$

The Penman-Monteith equation for a daily time step and inserting all the constant values become:

$$ET_o = \frac{0.408\Delta(R_n - G) + \gamma\frac{900}{T + 273}u_2(e_s - e_a)}{\Delta + \gamma(1 + 0.34u_2)} \tag{4.12}$$

R_n = Net radiation [MJ m^{-2} d^{-1}]

G = Soil heat flux [MJ m^{-2} d^{-1}]

T = Average daily air temperature [°C]

u_2 = Wind speed at 2 m above ground surface [m s^{-1}]

e_s-e_a = Vapour pressure deficit of the air [kPa]

Δ = Slope of the relationship between saturation vapour pressure and temperature [kPa °C^{-1}]

γ = psychometric constant [kPa °C^{-1}]

If the net radiation is not measured it could be assessed as the difference between the net shortwave radiation (R_{ns}) and the outgoing net longwave radiation (R_{nl}).

The net shortwave radiation [MJ m^{-2} day^{-1}] resulting from the balance between incoming and reflected solar radiation is given by:

$$R_{ns} = (1 - \alpha)R_s \tag{4.13}$$

Where α is the albedo or canopy reflection coefficient, which is 0.23 for the hypothetical grass reference crop [dimensionless]; Rs is the incoming solar radiation [MJ m^{-2} day^{-1}].

The Solar radiation could be derived from air temperature difference with the equation:

$$R_s = k_{R_s}\sqrt{(T_{max} - T_{min})}R_a \tag{4.14}$$

Where T_{max} and T_{min} are respectinely the maximum and minimum average daily air temperature (°C); k_{R_s} is an adjustment coefficient ($\sqrt{°C}$) and R_a is the extraterrestial radiation [MJ m^{-2} day^{-1}].

The adjustment coefficient k_{Rs} is empirical and differs for 'interior' or 'coastal' regions:
- for 'interior' locations, where land mass dominates and air masses are not strongly influenced by a large water body, $k_{Rs} = 0.16$;
- for 'coastal' locations, situated on or adjacent to the coast of a large land mass and where air masses are influenced by a nearby water body, $k_{Rs} = 0.19$.

The extra-terrestrial radiation (R_a) for each day of the year and for different latitudes can be estimated from the solar constant, the solar declination and the time of the year by:

$$R_a = \frac{24(60)}{\pi}G_{sc}d_r[\omega_s \sin\varphi \sin\delta + \cos\varphi \cos\delta \sin\omega_S] \tag{4.15}$$

Where G_{sc} is the solar constant equal to 0.0820 MJ m^{-2} min^{-1}; d_r is the inverse relative distance Earth-Sun (equation 4.16); ω_s is the sunset hour angle (equation 4.18) [rad]; φ is the latitude [rad] and δ is the solar declination (equation 4.17) [rad].

In particular, the equations are:

$$d_r = 1 + 0.033\cos\left(\frac{2\pi}{365}J\right) \tag{4.16}$$

$$\delta = 0.409\sin\left(\frac{2\pi}{365}J - 1.39\right) \tag{4.17}$$

where J is the number of the day in the year between 1 (1 January) and 365 or 366 (31 December).

$$\omega_s = \arccos(-\tan\varphi \tan\delta) \tag{4.18}$$

The last term necessary to assess the net radiation is the outgoing net longwave radiation (R_{nl}) [MJ m^{-2} day^{-1}],which is equal to:

$$R_{nl} = \sigma \left(\frac{T_{max,K}{}^4 + T_{min,K}{}^4}{2} \right) \left(0.34 - 0.14\sqrt{e_a} \right) \left(1.35 \frac{R_s}{R_{so}} - 0.35 \right) \tag{4.19}$$

where σ is the Stefan-Boltzmann constant [4.903 10-9 MJ K^{-4} m^{-2} day^{-1}], $T_{max,K}$ is the maximum absolute temperature during the 24-hour period [K = °C + 273.16], $T_{min,K}$ is the minimum absolute temperature during the 24-hour period [K = °C + 273.16], e_a is the actual vapour pressure [kPa], Rs is the solar radiation [MJ m^{-2} day^{-1}] and R_{so} is the clear-sky radiation [MJ m^{-2} day^{-1}].

In particular, the clear sky solar radiation is a function of the elevation above sea level (m) and is equal to:

$$R_{so} = (0.75 + 2 * 10^{-5}z)R_a \tag{4.20}$$

In this work, instead of using the reference crop albedo about 0.23 we have assessed the potential evapotranspiration from different types of soil changing the albedo.

The different albedo values are reported in Tab. 4.1.

Table 4.1 Albedo values from different surfaces (Ahrens, 2006).

Surface	Characteristic	Albedo
Soil	Wet-Dry	0.05-0.4
Sand		0.15-0.45
Grass	Long-Short	0.16-0.26
Crop		0.18-0.25
Forest		0.05-0.20
Water		0.03-1
Snow	Old-New	0.40-0.95

In particular, an albedo of 0.12 was used for forested area and a value of 0.2 for crop and grassland.
Finally, the total evapotranspiration is equal to the weighted mean function of the area.

HARGREAVES EQUATION

When weather data as relative humidity and wind speed are missing, evapotranspiration should be estimated using the Hargreaves equation. Allen et al. (1998) suggested the formula:

$$ET_o = 0.0023(T_{mean} + 17.8)(T_{max} - T_{min})^{0.5}R_a \tag{4.21}$$

where all parameters have been previously defined. Units for both ET$_0$ and R$_a$ in equation 4.21 are mm d^{-1}.
The equation can be calibrated in each new region by comparing with estimates on the Penman-Monteith equation at weather stations where all the necessary data are measured. Then the ET$_0$ is equal to a+b ET$_0$ (Hargreaves). The empirical coefficients a and b can be determined by regression analysis of the value assessed with the Penman-Monteith and the Hargreaves equation.

ACTUAL EVAPOTRANSPIRATION

The potential reference evapotranspiration (ET$_0$) represents the evaporation power of the atmosphere and it is the amount of water that would be evaporated and transpired if there were sufficient water available. Instead, the actual evapotranspiration (AET) is the quantity of water that is actually removed from a surface due to the processes of evaporation and transpiration. In this work the rainfall-excess model (section 4.6.2) was used to assess the daily actual evapotranspiration depending on the spatial variability of the soil moisture capacity (Moore & Clarke, 1981; Moore, 2007).

4.2 SPRINGS MONITORING

The Mulino delle Vene springs are perennial springs located on the left side of the Tresinaro stream, on the bottom of a 50 m long slope (Fig. 4.2). They flow out from a fractured aquifer hosted in a sandstone plateau overlying almost impermeable marls (Cervi et al., 2014). The source points appears at the contact between the unit of Contignaco (CTG) and the Pantano of S. Maria (PAT4). Two springs are equipped with weirs while others outflow diffusively along the 50 m slope. Then, all the source water flows in the Tresinaro stream few meters below.
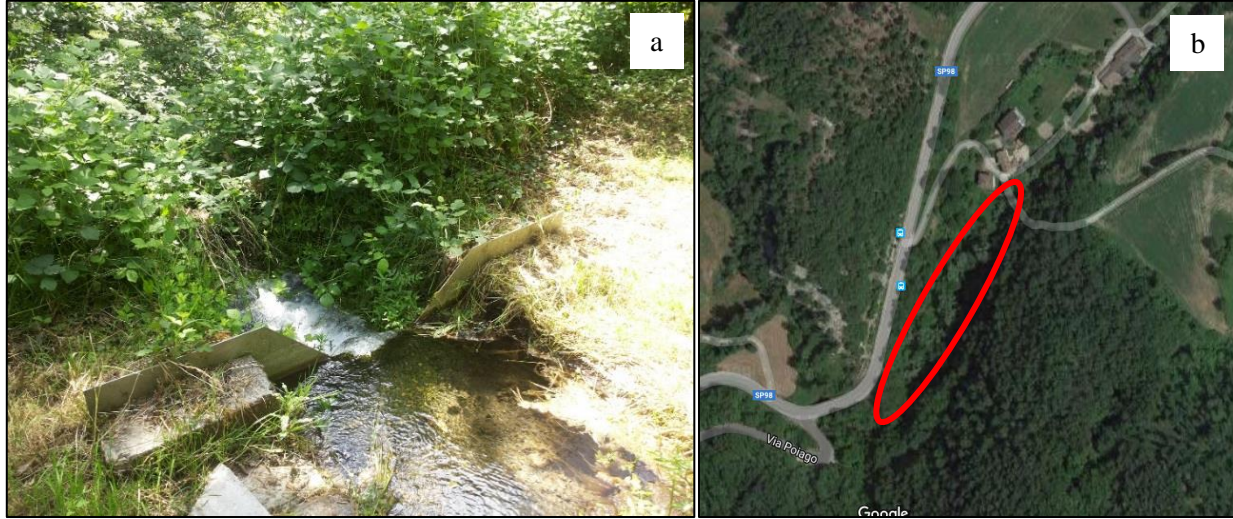
Figure 4.2 Mulino delle Vene springs point (a) and location (b).

Cervi et al. (2014) assessed the total outflow from the springs as a function of the outflow from one weir, which is monitored in continuous. In particular, they carried out an extensive field campaign during the period 2012-2013 repeating the measures of the discharge in the weirs and in the Tresinaro stream, upstream and downstream the springs. Then they processed the discharge data to assess a curvilinear regression (eq. 4.23; Petronici, 2014) between the weir discharge and the total springs discharge.

A triangular weir with angle of 90° is installed at Mulino delle Vene (Fig. 4.3). Applying the mass balance equation to the flow on the weir is possible writing the equation of the flow in function of the height of water on the weir (Citrini & Noseda, 1987):

$$Q_{weir} = 0.0142 \tan\left(\frac{\alpha}{2}\right) h_m^{2.5} \qquad (4.22)$$

Where Q_{weir} is the flow (l/s), α is the angle of the weir outflow, h_m (cm) is the height of water on the weir as in Fig. 4.3.

A STS DL/70/N probe (provided by ARPAE E-R) is installed in the weir that registered every hour the level, the temperature and the conductivity. From the measured levels, the weir discharge is assessed (Q_{weir}).

Thereafter, the eq. 4.23 is used to assess the total discharge from the Mulino delle Vene springs ($Q_{springs}$).

$$Q_{springs} = 24.0530 + 0.8728\, Q_{weir} + 0.1398\, Q_{weir}^2 \qquad (4.23)$$
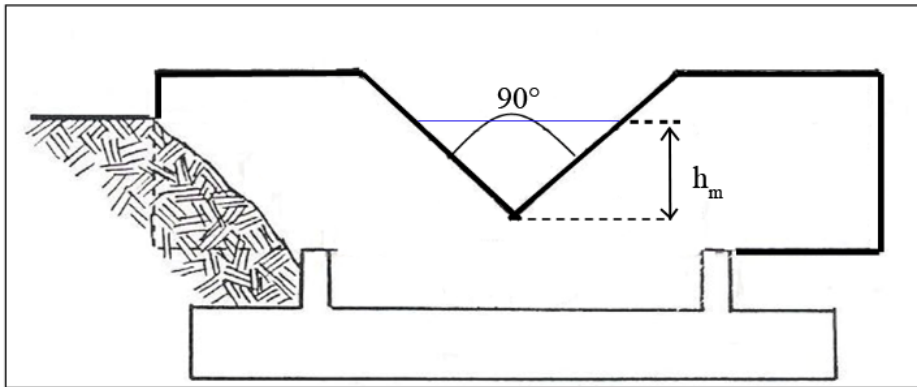
Figure 4.3 Schematic representation of a weir and image of the monitored weir.

4.3 RECESSION CURVE ANALYSIS

The daily Mulino delle Vene springs discharge dataset has been used to apply the hydrograph decomposition in exponential components, as in Kovacs & Perrochet (2008), in order to evaluate some important parameters of the fractured aquifer.

The more common exponential curve is the Maillet equation (1905) which has been used successfully in the hydrograph analysis of water springs (Kovács & Perrochet, 2008; Angelini & Dragoni, 1997):

$$Q_t = Q_0 e^{-\alpha t} \ (m^3/d) \tag{4.24}$$

where t (d) is the time since the beginning of the recession, Q_t and Q_0 are the spring discharges (m^3/d) respectively at time t and at the initial time t=0, α is the depletion coefficient.

The depletion coefficient α is equal to:

$$\alpha = \frac{lnQ_0 - lnQ_t}{t} \ (1/d) \tag{4.25}$$

Integrating between 0 and ∞ the volume (W_0) stored in the system at the beginning of the discharge period (*dynamic yield*) can be calculated:

$$W_0 = \int_0^\infty Q_0 e^{-\alpha t} dt = \frac{Q_0}{\alpha} \ (m^3) \tag{4.26}$$

where Q_{0i} and α_i are the spring discharge (m^3/d) at time t=0 and the depletion coefficient for the specific i-th system.

Being the springs fed by fractured aquifers, the recession curves are composed of an ensemble of parts, which show different slopes. This is due to the presence of different discontinuity sets, with different aperture implying different permeability promoting the development of different yields (Amit et al., 2002). Therefore, each slope represents a sector of the aquifer releasing groundwater with a specific depletion coefficient α and dynamic yields. According to the methods proposed by Forkasiewicz & Paloc (1967), the recession curve can be described by the sum of the several exponential functions characterising the specific reservoir as in the following formula:

$$Q_t = Q_1 e^{-\alpha_1 t} + Q_2 e^{-\alpha_2 t} + \cdots + Q_n e^{-\alpha_n t} \ (m^3/d) \tag{4.27}$$

where n is the number of reservoirs, t is the time, Q_t is the total spring discharge at time t, α and Q are respectively the depletion coefficient and the spring discharge (m^3/d) of the i-th sector at the time t=0.

Consequently, the volume $W_{0,i}$ (m^3/d) stored in each sector at the beginning of the recession can be calculated through the following equation:

$$W_{0,i} = \frac{Q_{0,i}}{\alpha_i} \ (m^3) \tag{4.28}$$

The total volume of water stored in the aquifer can be calculated as the sum of the volumes stored in each sector.

4.4 LOW-FLOW ANALYSIS

4.4.1 DEFINITION - LOW FLOW VS DROUGHT

Low flows are defined as the 'flow of water in a stream during a prolonged dry weather' (WMO, 1974) and, in a catchment without large lakes or wetlands, they are sustained essentially by groundwater.

Droughts are defined as continued and extensive occurrence of below-average water availability (EEA, 2008). Droughts can affect both high and low rainfall areas and they can develop over short or long periods until year or decades. The most common types of droughts are:

- Meteorological drought: lack of precipitation for an extended period of time longer than the average ;

- Hydrological drought: reduction in lake storage, lowering of groundwater levels and decrease of streamflow discharge of magnitude major than the usual one;

- Agricultural drought: deficit of soil moisture affecting a crop at a particular time;

- Socio-economic drought: imbalance between water supply and demand for human activities.

Smakhtin (2001) clarifies the difference between low flows and droughts in the seasonality. In fact, low flows are seasonal phenomena whereas droughts are natural events resulting from lower precipitation for an extended period of time.

4.4.2 LOW FLOW ASSESSMENT

Low flow measurements are important to assess the surface water - groundwater interactions in streams. In this work, low flows have been measured over the 2015 summer period (low flow season) in several sections along the length of the Tresinaro stream (Fig. 4.4). Measurements have been repeated in time to investigate the variation of the low flow during the summer and in space in order to identify the main geological units contributing to the discharge in terms of groundwater flows.

The low flow measurement have been carried out with an artificial tracing method. This method requires the injection of a known tracer concentration in a section of the stream, and the determination of the tracer concentration in a downstream measurement section (Tazioli, 2011). As suggested by Tazioli (2011) in cases of minimum flow with very low height of the water level, an electrolyte tracer (NaCl) has been used. Moreover, the NaCl is very economical, manageable and, if kept within low levels of concentration, it is not pollutant for the ecosystem. The distance between the injection and the measurement section has been chosen in order to have a good mixing length. In particular, the segment has to be regular and without no-flow area, with a length of about 100 m. To investigate the effect of different lengths, in one zone the measurements have been repeated for a distance from the injection point of 60 m, 80 m, 100 m and 120 m. Moreover, to assess the repeatability (significance of measurement error) of the measurements, the measurements have been consecutively repeated in one section as described in Berg & Allen (2007). In particular, the standard deviation of measured values (σ) and the coefficient of variation (ratio between σ and the mean value m in percentage) have been assessed in order to quantify the measurement uncertainty. The total number of the monitored sections is of thirteen along the Tresinaro stream and one section (called 14) along the Rio Dorgola stream, few meters upstream the inflow in the Tresinaro. In section 0 the observed flow during the summer is always almost zero. The measurement have been executed in several days of the 2015 summer (20 June, 2nd July, 23 July, 31 August, 22 September, 29 September and 9 October) but not all the section have been analysed every time.
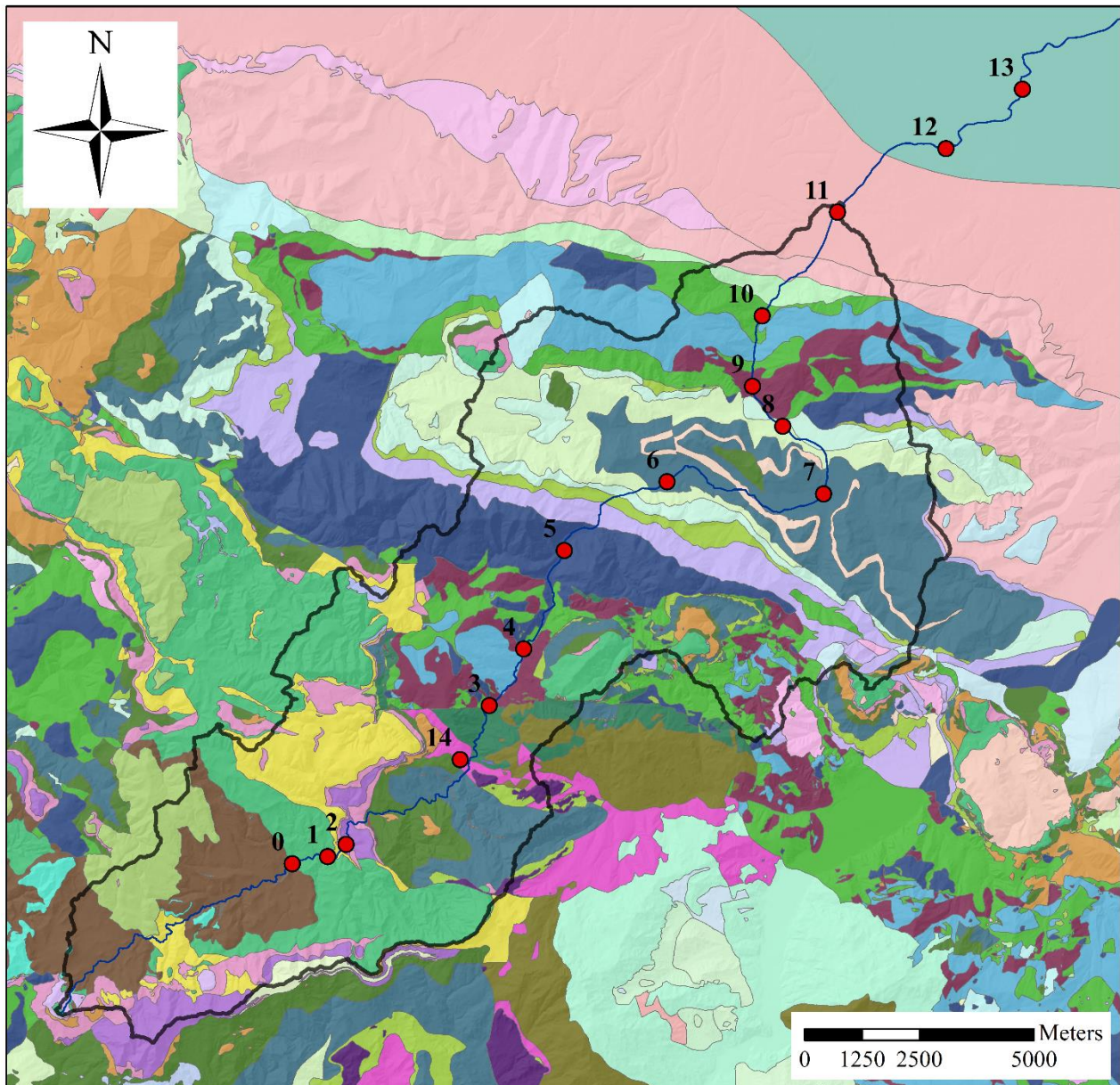
Figure 4.4 Geological map of the Tresinaro stream catchment and tracer test points (geological map legend as in Fig. 3.3).

ARTIFICIAL TRACING METHOD

Firstly, a hyper-concentrated solution has been prepared by diluting 1 kg of NaCl in 10.0 l of water and successively it has been injected instantly (slug-injection) into the river. Conductivity has been measured in-continuous about 100 m downstream the injection-point by using a conductivity-probe DL/N 70 (provided by ARPAE E-R); the acquisition-time has been set at 6 seconds. No pools or back-water areas are present and it is assumed that no subsurface seepage is possible. In Fig. 4.5 the typical curve registered during a measurement is reported. The curve shows the arrival of the tracer with an increase in the conductivity values that ends with the peak, after which starts the gradual disappearance of the tracer and the return of the conductivity to the initial value. Then, the conductivity values measured by the probe are transformed in concentration using a calibration curve verified in the laboratory by Vizzi (2014).
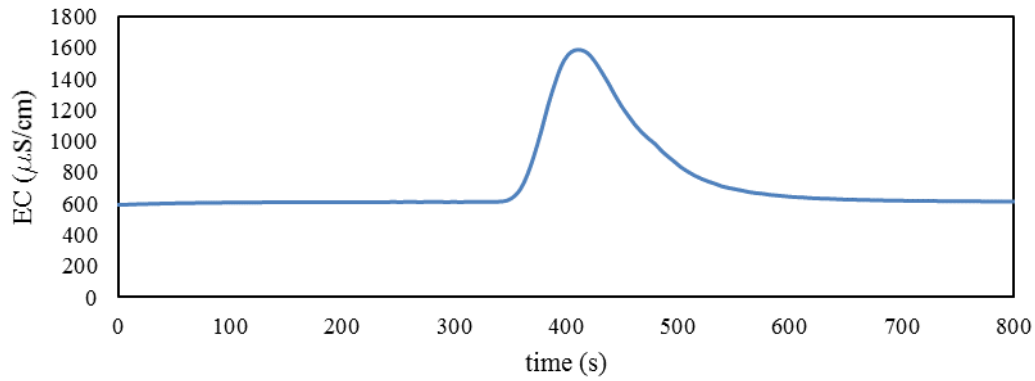
Figure 4.5 EC (Electric Conductivity) curve measured during a tracer test executed with an electrolyte tracer.

The tracer, which has a concentration C_0, is introduced in the water course with discharge Q. The budget is:

$$C_0 = Q \int_0^\infty c\, dt \qquad (4.29)$$

and the stream discharge Q could be assessed as:

$$Q = \frac{c_0}{c} \frac{V}{T} = \frac{C_0}{\int_0^\infty c\, dt} \qquad (4.30)$$

Where c_0 is the concentration of the tracer in the volume V where it is diluted, $c_0 V$ is equal to the tracer injected C_0; c is the concentration measured at the time t; T is equal to the time needed for the tracer to be transported downstream.

Finally, the concentration values are used to assess the term in the denominator of the equation numerically solving the integral term and assessing the total discharge.

4.4.3 MONITORED SECTIONS

In this part, a brief description of all the monitored stream sections is reported as in Ghirotti (2016).

Stream section n. 0

Section upstream of the Mulino delle Vene springs, in the Carpineti area. This section has been almost dry during all the field surveys (Fig. 4.6) and no discharge assessment has been possible.

Figure 4.6 Stream section n. 0.

Stream section n. 1

Section located 50 m upstream of the Mulino delle Vene springs. In this point (Fig. 4.7) the low flow discharge is small and it is largely composed by drains from the Carpineti sewage treatment plant. The section is about 1 km downstream of section n. 0.
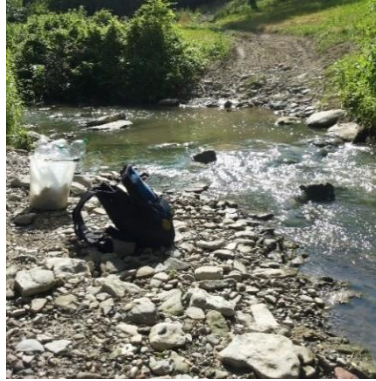
Figure 4.7 Stream section n. 1.

Stream section n. 2

This section is located downstream the Mulino delle Vene springs (420 m a.s.l.). Comparing Fig. 4.7 to Fig. 4.8 the increment of the stream discharge after the springs is evident. In this section, repeated measures to assess the estimating error of tracer test have been executed. The section is about 1.5 km downstream of section n. 0, located in the Contignaco formation.

Figure 4.8 Stream section n. 2.

Stream section n. 3

Section located near the village of Pizzarotto (Carpineti), at 6 km from section n.0 (Fig. 4.9). In the area clay rich units are outcropping. The tracer test has been performed twice.
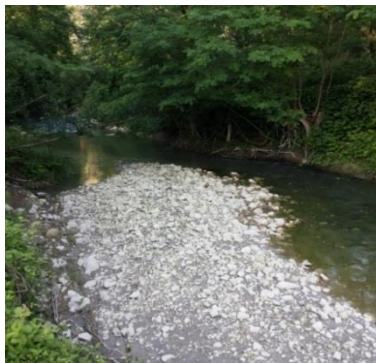
Figure 4.9 Stream section n. 3.

Stream section n. 4

Section located near the village of Baiso, at 7.7 km from section n. 0. In this part of the stream the ideal conditions for a good measurement is not respected at all so only one assessment was done (Fig. 4.10).

Figure 4.10 Stream section n. 4.

Stream section n. 5

Section near the village of Benale (Viano) at 10.4 km from the section n. 0. The point is located in the Flysch of Monte Cassio (Fig. 4.11).

Figure 4.11 Stream section n. 5.

Stream section n. 6

Section in the Viano area, at 13.5 km from the section n. 0 (Fig. 4.12). The straight segment allows a good measurement and the repeated measures at different distances between the injection and the measurement section have been carried on.
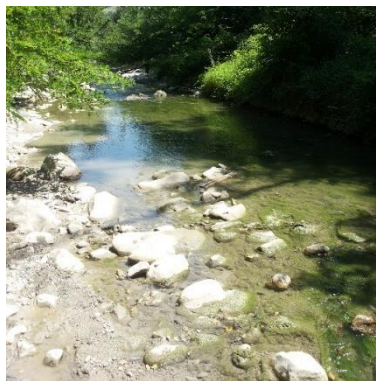
Figure 4.12 Stream section n. 6.

Stream section n. 7

Section in the village of Rondinara (Scandiano) at 18.1 km from section n. 0 (Fig. 4.13).

Figure 4.13 Stream section n. 7.

Stream section n. 8

Section in the Rondinara village (Scandiano), at 20 km from section n. 0 (Fig. 4.14). This section has been added to the monitored ones only the last day of the field campaign in order to have a better assessment of the stream discharge in the area immediately upstream of the alluvial fan.

Figure 4.14 Stream section n. 8.

Stream section n. 9

Section between the village of Rondinara and Iano (Scandiano) at 21 km from section n. 0 (Fig. 4.15). As for section 8, the measure has been carried out only the last day of the field campaign in order to have a better assessment of the stream discharge in the area immediately upstream of the alluvial fan.

Figure 4.15 Stream section n. 9.

Stream section n. 10

Section in the apex of the alluvial fan, in the village of Gessi-Mazzalasino, at 22.5 km from section n. 0 (Fig. 4.16). In this point, the clay units outcropping along the river start to be covered by the deposits of the alluvial fan.
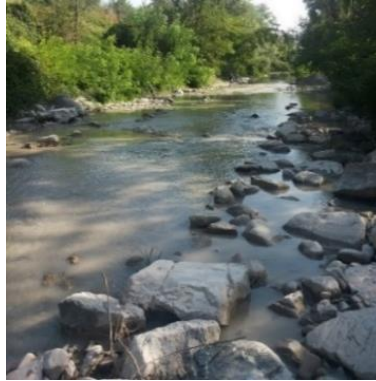
Figure 4.16 Stream section n. 10.

Stream section n. 11

Section in the Scandiano village, near the bridge of the SP37 (Pedemontana street) where the in-continuous gauge station of Ca' de Caroli set by ARPAE E-R is located (Fig. 4.17). This section is 25.6 km downstream of the Section n.0 and represent the closing point of the catchment used in the hydrogeological simulations. Moreover, the section is located on the alluvial deposits.

Figure 4.17 Stream section n. 11.

Stream section n. 12

Section located between the villages of Scandiano and Arceto, at 28.6 km from the section n. 0 (Fig. 4.18). This section is downstream of the Ca' de Caroli gauge station, which has been selected as closing point of the catchment.

Figure 4.18 Stream section n. 12.

Stream section n. 13

Section located in the area of Arceto at 31 km from the section n. 0, downstream of a channel connected to the Secchia river (Fig. 4.19).

Figure 4.19 Stream section n. 13.

Stream section n. 14

Section in the Rio Dorgola stream (Fig. 4.20), upstream of the confluence into the Tresinaro stream (Pizzarotto, Carpineti). This is the only monitored section that is not along the Tresinaro stream but on a small tributary.

Figure 4.20 Stream section n. 14.

4.5 CLIMATE CHANGE SCENARIOS

4.5.1 SCENARIOS

The Special Report on Emissions Scenarios (SRES) have developed four scenario families describing different ways in which the world may develop. Each family represents different demographic, social, economic, technological and environmental developments. Nakićenović (2000) gives the definition of these families as above:

- A1: the A1 family describes a future world of very rapid economic growth, global population that peaks in mid-century and declines thereafter, and the rapid introduction of new and more efficient technologies. The A1 scenario family develops into three groups that describe alternative directions of technological change in the energy system. The three A1 groups are distinguished by their technological emphasis: fossil intensive (A1FI), non-fossil energy sources (A1T), or a balance across all sources (A1B).

- A2: the A2 family describes a very heterogeneous world. The underlying theme is self-reliance and preservation of local identities. Fertility patterns across regions converge very slowly, which results in continuously increasing global population. Economic development is primarily regionally oriented and per capita economic growth and technological change are more fragmented and slower than in other storylines.

- B1: the B1 family describes a convergent world with the same global population that peaks in mid-century and declines thereafter, as in the A1 storyline, but with rapid changes in economic structures toward a service and information economy, with reductions in material intensity, and the introduction of clean and resource-efficient technologies. The emphasis is on global solutions to economic, social, and environmental sustainability, including improved equity, but without additional climate initiatives.

- B2: the B2 family describes a world in which the emphasis is on local solutions to economic, social, and environmental sustainability. It is a world with continuously increasing global population at a rate lower than A2, intermediate levels of economic development, and less rapid and more diverse technological change than in the B1 and A1 storylines. While the scenario is also oriented toward environmental protection and social equity, it focuses on local and regional levels.

For each family, different scenarios have been developed using different modelling approaches. In this work, five Regional Climate Models (RCMs) of the European Union Sixth Framework Programme project ENSEMBLES (Hewitt and Griggs, 2004) from the A1B family have been used. Each RCM is driven by a different General Circulation Model (GCM) as reported in Tab. 4.2, and they have a spatial resolution of 25 km (Stoll et al., 2011). The use of model ensembles is recommended for a realistic assessment of climate change (Fowler et al., 2007).

Table 4.2 Climate models.

Institution	RCM	GCM
Hadley Center for Climate Prediction and Research (HC)	HadRM3Q0	HadCM3Q0
Institute for Atmospheric and Climate Science, ETH Zurich (ETHZ)	CLM	HadCM3Q0
Royal Netherlands Meteorological Institute (KNMI)	RCA	ECHAM5-r3
Max Planck Institute for Meteorology (MPI)	M-REMO	ECHAM5
Swedish Meteorological and Hydrological Institute (SMHI)	RACMO2	ECHAM5-r3

After the publication of the IPCC 2007, a new set of scenarios has been produced with the name of Representative Concentration Pathways (RCPs). Contrary to the SRES scenarios, the RCPs take care of the different climate policies and they allow evaluating the "costs" and "benefits" of long-term climate goals (van Vuuren et al., 2011). For the Fifth Assessment Report of IPCC, the scientific community has defined a set of four RCP scenarios basing on their radiative forcing. These four RCPs include one mitigation scenario leading to a very low forcing level (RCP2.6), two stabilization scenarios (RCP4.5 and RCP6), and one scenario with

very high greenhouse gas emissions (RCP8.5). The RCPs cover a wider range than the scenarios from the SRES (IPCC, 2014). In terms of overall forcing, RCP8.5 is broadly comparable to the SRES A2/A1FI scenario, RCP6.0 to B2 and RCP4.5 to B1. For RCP2.6, there is no equivalent scenario in SRES.

As RCPs data are not available, in this work, all the analysis have been carried out with the SRES scenarios.

4.5.2 FORECASTS

In recent decades, changes in climate are evident and they have caused impacts on natural and human system in all continent and across the oceans (IPCC, 2007). Changes in many extreme events, like droughts, heat waves and heavy precipitations, have been observed since about the 1950. Moreover, in many regions, changing precipitation and temperature are altering the hydrological system, affecting water resources in terms of quantity and quality. The IPCC (2014) states that "Continued emission of greenhouse gases will cause further warming and long-lasting changes in all components of the climate system, increasing the likelihood of severe, pervasive and irreversible impacts for people and ecosystems."

The SRES scenarios show a range of the possible climate forecasts for the 21st century. The most evident characteristic of the future climate system is a general warming. In particular, "Surface temperature is projected to rise over the 21st century under all assessed emission scenarios. It is very likely that heat waves will occur more often and last longer, and that extreme precipitation events will become more intense and frequent in many regions" (IPCC, 2014). Furthermore, for a future warmer climate the SRES models (IPCC, 2007) indicate that precipitation generally increases in the areas of the tropical Pacific and at high latitudes as a consequence of a general intensification of the global hydrological cycle. Instead, in the subtropical and at mid-latitude regions precipitation will decrease; anyway, precipitation intensity is projected to increase but there will be longer periods between rainfall events.

In the EEA (2008) report, focused on the Europe continent, is reported that Europe has warmed about 1° C compared to pre-industrial times. Projections suggest further temperature increases in Europe between 1.0-5.5 °C by the end of the century. Moreover, more frequent and more intense hot extremes and changes in precipitation trend will occur. In particular, dry periods are projected to increase in length and frequency, especially in southern Europe. All this factors will affect the water resources and the ecosystem.

The EEA (2008) focuses also on water quantity, river floods and droughts in Europe. The main key points of this part are:

- Annual river flow is projected to decrease in southern and south-eastern Europe and increase in northern Europe, but absolute changes remain uncertain.
- Regions in southern Europe, which already suffer most from water stress, are projected to be particularly vulnerable to reductions in water resources due to climate change. This will result in increased competition for available resources.
- Climate change is projected to increase the frequency and intensity of droughts in many regions of Europe as a result of higher temperatures, decreased summer precipitation, and more and longer dry periods.
- The regions most prone to an increase in drought hazard are southern and south-eastern Europe, but minimum river flows will also decrease significantly in many other parts of the continent, especially in summer.

In order to analyse the effects of climate change on the study area, the available scenarios have been downscaled and then they have been compared to the actual climate conditions. Moreover, the downscaled scenarios have been used in a numerical model to assess the effects of climate change on the groundwater resources.

4.5.3 DOWNSCALING APPROACHES

To analyse the effects of climate change on the water resource at a regional or local scale, a downscaling of the RCM data is necessary. In fact, using non-processed RCM outputs could bring about unrealistic forecasts

(Homan et al., 2009). This is because of systematic biases and different distributions between the RCM simulation and the observed climate. The two main downscaling approaches are the dynamical downscaling and the statistical downscaling. The first consists in the use of regional climate model, which use boundary conditions from the GCM, to produce high resolution outputs (Mearns et al., 2003). Instead, the statistical downscaling methods use a statistical model, which relates large scale climate variables (predictors) to local variables (predictands; Wilby et al., 2009). Authors have applied a large number of techniques, from the simple delta-change (Prudhomme et al., 2002) to more sophisticated methods as regression models or weather generators (Homan et al., 2009). Murphy (2009) states that the dynamical and the statistical downscaling show similar levels of skill, although the statistical method is better for summertime estimates of temperature while the dynamical methods give slightly better estimates of wintertime precipitation.

In this work, two statistical method have been applied, the delta change method (Hay, 2000; van Roosmalen et al., 2009) and the Cumulative Distribution Function transform method (CDF-t; Michelangeli et al., 2009; Neukum & Azzam, 2012).

In particular, model records have been projected onto the Carpineti weather station position with a weighted average of the model grid-points closest to the station itself, based on a Gaussian weighting function that decreases to 0.5 at the distance of 12.5 km. In the model's datasets, the daily rainfalls and the minimum and maximum temperatures have been processed. Then the transfer method has been applied to the datasets. Finally, results have been shown in terms of monthly average and standard deviation in order to obtain a simple and clear graphical representation and to reduce the uncertainties connected to the RCM selection. This is a common approach in literature (e.g. Goderniaux et al., 2011; Sultana & Coulibaly, 2011; Foster & Allen, 2015). In particular, the daily datasets for each RCM variable have been processed in order to obtain the monthly values. Then, the monthly values of each scenario have been compared obtaining the mean values and the standard deviations.

Finally, the downscaled weather data together with the assessed Potential Evapotranspiration (ET_0) have been used in the numerical modelling of the groundwater resource (section 4.6.2).

DELTA CHANGE METHOD

The Delta change method is a simple and fast statistical method, which has been widely used in hydrological impact studies (Fowler & Kilsby, 2007; Minville et al., 2008; Goderniaux et al, 2009; Blenkinsop et al, 2013).

In detail, the observed time series (Baseline, 1984-2013) have been transformed into the future scenario dataset (Future, 2021-2050) by adding delta change factors. The latter have been calculated from the difference between the future and the present climate as simulated by the RCMs.
The method has been applied for minimum, maximum temperatures (eq. 4.31 and 4.32) and rainfall (eq. 4.33 and 4.34).

$$T_{future,D}(i,j) = T_{obs}(i,j) + \triangle_T(j); \quad i=1,2\ldots,31; \quad j=1,2\ldots,12 \qquad (4.31)$$

$$\triangle_T(j) = \bar{T}_{future,RCM}(j) - \bar{T}_{actual,RCM}(j); \quad j=1,2\ldots,12 \qquad (4.32)$$

$$P_{future,D}(i,j) = P_{obs}(i,j) * \triangle_P(j); \quad i=1,2\ldots,31; \quad j=1,2\ldots,12 \qquad (4.33)$$

$$\triangle_P(j) = \bar{P}_{future,RCM}(j) / \bar{P}_{actual,RCM}(j); \quad j=1,2\ldots,12 \qquad (4.34)$$

Where i and j stand for the ith day of the jth month, $\triangle_T$ and $\triangle_P$ are the monthly delta change factors respectively for temperature and precipitation, $\bar{T}$ and $\bar{P}$ are the average monthly temperature or precipitation for the RCM future and actual period. The resultant series maintain the detail of the station record, scaled and observed data differ only in their means, maxima and minima. The future climate is a slightly perturbed version of the actual with no variability changes. On the other hand, a great series of observed data have been used as baseline for the future simulation, whereas the use of RCM output directly could bring unrealistic simulation (Holman 2009).
To easily analyse the climate variable, the five downscaled scenarios have been processed obtaining a mean values with standard deviations.

CDF-T METHOD

Differently from the delta-change method commonly used in hydrological studies, the CDF-t procedure provides more reliable estimates of future variability and the occurrence of extreme events, making it possible to carry out a proper investigation concerning the intra-annual and inter-annual discharges, as well as low/high flow features. The CDF-t method has been applied by several authors (Déqué, 2007; Michelangeli et al., 2009; Stoll et al., 2011). The approach is based on the assumption that it is possible to find a transformation T allowing translating the cumulative distribution function (CDF) of a RCM variable into the CDF representing the local-scale climate variable at a given weather station. To assess this transformation the observed local data at a weather station and the RCM output for the same period have been compared and analysed. A detailed description of the technical method is reported in Michelangeli et al. (2009). In particular, the CDF-t method compares the baseline observed dataset and the RCM dataset for the same baseline period. Such comparison allows translating the cumulative distribution function (CDF) of the RCM variable into the CDF representing the local scale climate variable at the given weather station. In this work, the baseline period is the thirty-year period 1984-2013, and the observed data are collected at the Carpineti weather station. In this way, the thirty-year period 2021-2050 of the RCM has been downscaled with the transformation (previously obtained for the baseline period) in order to generate the future downscaled scenario (2021-2050).

In this work, to apply the CDF-t method the R package developed from Vrac M. & Michelangeli P.A. and available for free on the CRAN website (http://cran.r-project.org/web/packages/CDFt/index.html) has been used. Therefore, the observed time series (Baseline, 1984-2013) is processed together with the large-scale time series from the SRES scenarios with the R packages obtaining the downscaled time series for each scenario variables. To analyse the changes in the climate variables, the outputs are treated obtaining a mean values of the forecast with a standard deviation.

With reference to rainfall, it must be highlighted that, before applying this procedure, the model series must reflect the same frequency rate as that of the corresponding observed baseline record (1984-2013). This involved pre-filtering the data by estimating, for each month, the observed and the modelled frequency of wet days and then applying the observed frequency to the whole RCMs series by deleting all the simulated wet days with a daily rainfall lower than the one correspondent to the same frequency in the observed data. For example, in February it has been observed a rain event in the 26.7% of the days, therefore to the simulated scenario it has been applied the same frequency putting in descending order the rainfall amounts and deleting the rainfall lower to the one correspondent to the 26.7% of the series.

4.6 NUMERICAL MODELLING

In this work, several numerical models have been developed of both the Mulino delle Vene fractured aquifer (local scale model) and of the Tresinaro stream catchment (large scale model).
The classical way to simulate the groundwater flow processes in aquifers is represented by the solution of the flow equations. In the general case, there is not analytical solution, so we have to employ numerical methods. Different approaches could be applied as the finite elements or finite differences. The finite differences approach solves flow equations in the mesh nodes, whereas the finite elements approach considers the whole element in which the domain was discretised. The software used in this work apply the finite elements method. To build the model several detailed data about the geometry and the properties of the aquifer are necessary. The more data are available, the more the model construction and calibration are facilitated.
Moreover, we have used some rainfall-runoff models to simulate the Mulino delle Vene springs discharge. Rainfall-runoff models allow an easier model construction as the aquifer is considered as a black box and no geological/hydrogeological data are necessary. In particular, the rainfall runoff models need only input (rainfall) and output (spring discharge) data to be calibrated.

4.6.1 FINITE ELEMENTS MODELLING OF A FRACTURED AQUIFER

The simulation of groundwater flow in fractured aquifers is a difficult task (Angelini & Dragoni, 1997). Despite the wide outcrop of rocky aquifers in the mountainous sectors of Italy, mathematical approaches for reproducing their hydrological behaviour have not been exploited extensively to date. This is mainly due both to the heterogeneity of the hydrogeological properties characterizing these systems and to the scarcity of continuous monitoring data. In particular, several Authors have highlighted the lack of wells and boreholes crossing the aquifers, which are generally hosted at greater depths than those that make the water-supplying economic (Angelini & Dragoni, 1997). Unfortunately, boreholes allow hydraulic head values to be gathered and other hydrogeological parameters (permeability and hydraulic gradient), which are required to better calibrate a hydrogeological model, to be estimated. However, there is growing recognition that mountains play a critical role in the hydrologic cycle and the water management requires an understanding of groundwater flow in mountains where most of the recharge occurs (Dragoni & Sukhija, 2008).

The first step in any numerical modelling procedure is the schematic representation of the real system. In particular, the conceptual hydrogeological model of a fractured aquifer has to account for the anisotropy of the medium. The most difficult task is to describe the heterogeneity of the flow parameters due to different groundwater flow processes (i.e. slow flow in the low-permeability rock mass and rapid flow in the channel and fracture network; Kovàcs, 2003).

Three main approaches can be adopted to simulate groundwater in a fractured system: Discrete Fracture Network (DFN), Equivalent Porous Medium (EPM) and hybrid (Francani & Cherubini, 2006). The DFN approach considers the flow within individual fractures or conduits; the matrix is assumed to have negligible permeability. On the contrary, the EPM simplifies the real system with a continuum with a mean permeability. Obviously, using this approach, individual fractures cannot be adequately represented (Shapiro & Andersson, 1983; Teutsch & Sauter, 1998). Finally, the hybrid approach applies either the DFN and EPM methods (Garzonio et al., 2014).

In this work, the EPM approach has been applied both at the local scale and at the large scale. The use of a more complex model has not been possible at this stage for the scarcity of more in detailed geological data especially at the large scale (geometric data of fractures, piezometric surface data in numerous points and tracer tests in the aquifer). Moreover, it has been decided to use the EPM approach for this reasons:

- There are no karstic features;

- The aim of the model is to simulate the discharges of the spring or of the stream and no the flow directions or velocities;

- The main purpose of the large scale model is to assess the effects of climate change in the low flow period, when non-Darcy flow in the fractured system is negligible.

Furthermore, several Authors have demonstrated the efficiency of the EPM approach in case studies having only precipitation and discharge as known data (Cambi & Dragoni, 2000; Dragoni et al., 2013; Scanlon et al., 2003; Hassan et al., 2014).

Hereafter, the main steps of the finite elements modelling procedure and the employed software are described.

PROCEDURE

To build a groundwater model the spatial domain has to be subdivided into a set of finite elements and the time domain into a set of time intervals. This discretization is necessary to represent the problem in a discrete mode resolvable from the groundwater flow software. Every code makes use of different procedure to carry out the spatial discretization but the fundamental steps are always the same, as reported above:

1. Overlook. Build a scale map of the area of interest, defining the physical boundaries.

2. Definition of the area. Indicating the major hydrological properties (boundary conditions like prescribed flow or prescribed head) and the locations of all pumping and observation wells.

3. Mesh. Draw the finite elements grid on the basis of previous point.

4. Check the grid. The generated grid should be conform to the boundaries and interfaces between materials with different properties. Moreover, triangles should not have any obtuse angles and it is better to avoid elongated elements (GHS, 2003).

5. Properties allocation. After creating the mesh, it is possible to start to assign the hydrogeological properties and to define the boundary conditions. This phase depends on the conceptual model that we have obtained from the hydrogeological analysis of the area. Four type of boundary conditions could be applied to a hydrogeological model:

    HEAD: Setting a head boundary condition (first kind, Dirichlet type) means fix the hydraulic head to a known groundwater level at the boundary condition node. The exchange of flux on the point depends on the groundwater situation in the area.

    FLUX: The flux (second kind, Neumann type) boundary condition describes an in- or outflow of water at an element edge or element face. The given value in flow simulations is a Darcy flux perpendicular to the boundary.

    LEAKAGE: The leakage boundary condition (third kind, Cauchy type) uses a leakage function with the river stage as the boundary condition value (L). If the river stage is lower than the groundwater level, the hydraulic gradient points towards the stream, and water flows out from the aquifer. Otherwise, if the river level is higher than the simulated groundwater level, water enters in the model domain. The leakage coefficient (1/T), which controls the exchange of water, is defined as the ratio between the hydraulic conductivity and the thickness of an interface layer that is assumed to separate the river and the aquifer. The leakage boundary was built to simulate aquifer-river exchange but it could be used also to simulate a spring.

    WELL: Well (nodal source/sink type) boundary condition is applied to nodes and it represents a time-constant or time-varying local injection or extraction of water.

6. Calibration. Finally, the model needs to be calibrated, estimating model parameters allowing the best fitting of field measurements. Calibration can be executed manually or automatically with a code that conducts the tests independently but according to the instructions of the user. As stated from Medina et al. (2000), the automatic calibration frees the modeller of the burden of having to deal with parameter modifications (sometimes at the cost of very large computer times). This allows him to concentrate on the really important issue, namely, the identification of the most appropriate conceptual model. Moreover, Medina et al. (2000) asserted that one of the problems in parameter estimation is that many different conceptualizations may lead to a similar model performance. Furthermore, if the model structure is incorrect, its parameters may bear no relationship to their physical counterparts.

Thus, a good match between measured and computed responses does not ensure that the prediction capabilities will be good. This highlight the importance of have an in depth knowledge of the study area and its hydrogeological behaviour to obtain a good conceptual model.

FEFLOW

FEFLOW (Finite Element subsurface FLOW and transport system) is a groundwater modelling software for two or three-dimensional modelling in a regional or local scale (Diersch, 2005).
The program has been under development since 1979 by the Institute for Water Resources Planning and Systems Research Inc. (WASY GmbH) of Berlin (Germany) which has recently become a part of DHI Group (Trefry & Muffels, 2007). The software has been largely applied in recent year to simulate groundwater flow both in porous and in fractured media (Cherubini, 2008; Renz et al., 2009; Brunetti et al., 2013; Garzonio et al, 2014).

TRANSIN

The finite elements code TRANSIN IV (Medina et al., 2000) with the visual interface VISUAL TRANSIN by the Hydrogeology group (GHS – Grupo de Hidrogeologia Subterranea) of the Department of Geotecnical Engineering and Geosciences of the Universitat Politècnica de Catalunya (UPC) has been used (GHS, 2003). The code allows simulating the groundwater flow and the transport for several conditions including simulation in both confined and unconfined aquifer, parameter estimation, error and sensitivity analysis, model selection or experiment design. It can solve a broad range of flow and transport problems have been proved numerous times (Medina & Carrera, 1996; Iribar et al., 1997; Medina & Carrera, 2003; Pujades et al., 2014; Font-Capo et al., 2015). The original code is written in standard FORTRAN-77 and it uses the finite elements method to numerically solve the flow equation.

HYDROGEOSPHERE

HydroGeoSphere has been developed under the leadership of Dr. Edward Sudicky and Dr. Peter Forsyth at the University of Waterloo and Dr. Rene Therrien at the Laval University. The software is a 3-D fully-integrated surface and subsurface flow simulator and transport model. This means that water derived from rainfall inputs is allowed to partition into components such as overland and stream flow, evaporation, infiltration, recharge and subsurface discharge in a natural, physically-based fashion (Brunner & Simmons, 2012). Moreover, the fully-coupled numerical solution approach allows the simultaneous solution of both the surface and variably-saturate subsurface flow equations at each time step (Aquanty, 2013). Solving the surface and subsurface equations simultaneously for both flow and transport allows for a complete coupling of the interactions within and between the domains. These interactions can play a very important role in assessing the impacts of hydrological, chemical or thermal stressors. Without the integrated approach, these interactions cannot be properly quantified because some form of abstraction of the physical process would be necessary.
HydroGeoSphere uses the 2-D Saint Venant equation for surface water flow and the Richards' equation for 3-D unsaturated/saturated subsurface flow. For problems that also involve solute or thermal energy transport, the classical advection-dispersion equation is used in all domains (Aquanty, 2013).
Hydrologic parameters required in the fully coupled simulation are listed in Tab. 4.3. In particular, simulation uses the dual-node approach to calculate water exchanges between the surface and the subsurface domain. The exchange is calculated as the hydraulic head difference between the two domains multiplied by the coupling length (Lc) characterising the soil. Moreover, the Kristensen and Jensen model (Kristensen & Jensen, 1975) is used to calculate the actual evapotranspiration as a function of the potential evapotranspiration (ETP), the soil moisture and the Leaf Area Index (LAI, area covered by leaf over a unit area). The quantity of water extracted is more important near the surface ant it decreases until zero at the root depth (Lr). In addition, a bucket model simulates the interception of rainfall by the canopy; more in detail precipitation excess from the canopy storage coefficient (Cint) reaches the ground surface.
HydroGeoSphere has been used to perform event-based and continuous simulations on widely varying spatial scales ranging from single soil column profiles to large-scale basins, which may include several catchments

(Cey et al., 2006; Goderniaux et al., 2009; Bolger et al., 2011; Levison et al., 2014; Von Gunten et al., 2014; Wildemeersch et al., 2014; Ala-aho et al., 2015; Holding & Allen, 2015; Moeck et al., 2016).

Table 4.3 Parameters used in the HydroGeoSphere model.

Subsurface domain	K	Full saturated hydraulic conductivity	[L/T]
	n	Total porosity	[-]
	Ss	Specific storage	[L^{-1}]
	Alfa	Van Genuchten parameter	[-]
	Beta	Van Genuchten parameter	[L^{-1}]
Surface domain	Lc	Coupling length	[L]
	nx	Manning roughness coefficient	[L$^{-1/3}$T]
	ny	Manning roughness coefficient	[L$^{-1/3}$T]
Evapotranspiration	Le	Evaporation depth	[L]
	LAI	Leaf Area Index	[-]
	Lr	Root depth	[L]
	C1, C2, C3	Transpiration fitting parameters	[-]
	Cint	Canopy storage interception	[L]

4.6.2 RAINFALL-RUNOFF MODEL

In the past, several Authors have used rainfall-runoff model to simulate the outflow from a catchment but they have been developed in order to consider only surface flows. In this work, a modified version of the Hymod model (Cervi et al., 2018) and a multiple reservoirs model developed for this case study have been used. The proposed models allow to simulate the discharge from a spring in a relatively simple way, not demanding for an in-depth knowledge of the geological setting of the aquifer as a traditional hydrogeological model (section 4.6.1). The calibrated and validated models have been used to assess the future springs discharges resulting from the forecasted weather variables of five RCMs downscaled, as described in section 4.5.3, with the CDF-t method.

HYMOD MODEL

The Hydrological model (Hymod) has been firstly proposed by Boyle (2001) starting from the Probability Distributed Moisture (PDM) lumped storage model by Moore & Clark (1981). The Hymod model is constituted of a simple rainfall-excess model connected with two series of linear reservoirs in parallel (Fig. 4.21).

The rainfall-excess model assumes that the soil moisture in the catchment varies in time and in space. In particular, the spatial variability of soil moisture capacity is described by the following distribution function:

$$F_C(c) = 1 - \left(1 - \frac{c}{C_{max}}\right)^{\beta_k}, 0 \leq c \leq C_{max} \tag{4.35}$$

Where $F_C(c)$ [-] is the cumulative probability of a given water storage c [L]; β_k [-] is the degree of spatial variability of the soil moisture capacity within the catchment; C_{max} [L] is the maximum storage capacity in the catchment.

The rainfall-excess model assesses, for each time step, the actual evapotranspiration (AET, function of ETP and of the water capacity of the soil) and the effective rainfall (ER=ER1+ER2) which is used as input to the model part that performs the flow routing to the catchment outlet.

This process is composed of two parallel lines, a quick and a slow one. The water is distributed to each line by a parameter called α [-] varying between 0 and 1.

The quick line is composed by three linear reservoir with residence time K_q [T] in series. The slow line is constituted by a single reservoir with residence time K_s [T]. The total discharge Q(t) from the catchment is equal to the sum at time t of the discharges from each line.

The Hymod model uses 5 parameters which have to be optimize with respect of the observed flow. Parameters description and their initial uncertainty bounds used during calibration are presented in Tab. 4.4.
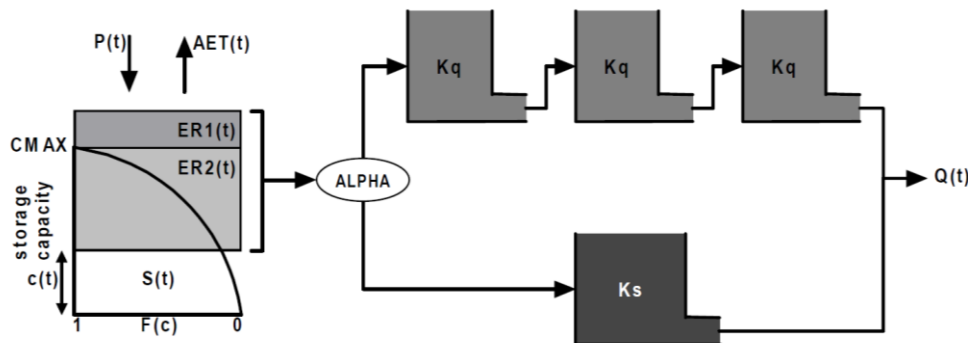
Figure 4.21 Hymod model structure (Wagener et al., 2001).

Table 4.4 Parameters of the Hymod model and their uncertainty range.

Parameter	Description	Prior range
C_{max} [L]	Maximum storage capacity in the catchment	50-700
β_k [-]	Degree of spatial variability of the soil moisture	0.1-2
α [-]	Factor distributing the flow between slow and quick release reservoirs	0-1
K_s [T]	Residence time of the slow line	0.001-0.1
K_q [T]	Residence time of the quick line	0.1-0.99

The model has been widely applied to simulate the outflow from a catchment (Wegener et al., 2001; Vrugt et al., 2003; Montanari, 2005; Bastola et al., 2011; Soundharajan et al., 2013). In the presented case study, the discharge from a spring has been simulated, therefore only the slow component is acting. The water from the water-excess model goes directly to the slow line, meanwhile the quick line is not used. The simplified structure of the used model is reported in Fig. 4.22. The parameters of this modified Hymod model are reduced to 3: the parameters of the rainfall-excess model (C_{max}, β_k) and the residence time of the slow line (K_s).
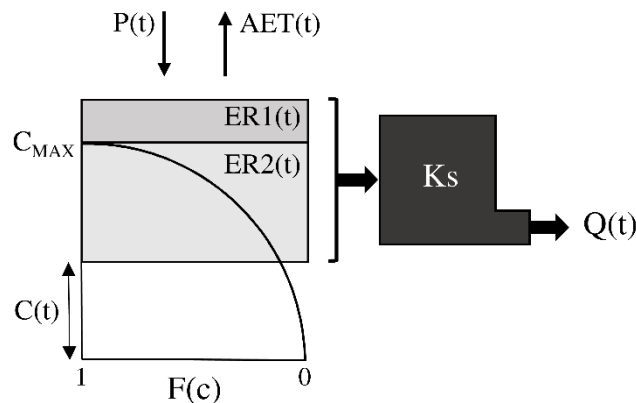
Figure 4.22 Hydrological model (modified Hymod).

MULTIPLE RESERVOIRS MODEL

Multiple reservoirs models have been used for simulating not-porous hydrogeological systems such as karst aquifers (Fiorillo, 2011; Fiorillo, 2013; Katsanou et al., 2015). They are normally ascribed to as grey-box models, i.e. models in which hydrological processes taking place beneath the soil surface are not represented by physical equations but conceptualized as buckets (Davie, 2002). This means that, during a recharge period, each reservoir stores a certain volume of water and releases it with a specific rate. Moreover, once recharge exceeds the amount of water that can flow out from the drainage, the reservoir starts to fill up until the maximum storage of the reservoir is reached. In this case, water surplus feds the beyond reservoir which will start to contribute itself to the total discharge.

In agreement with Tallaksen (1995), the number and the dimensions of the reservoirs were assessed through the recession curve analysis (section 4.3). In particular, the reservoirs volumes are dimensioned on the basis

of the dynamic yields as assessed by equation 4.28. Drainage of each reservoir follows the Maillet exponential discharge law (equation 4.24). In particular, the discharge of a sector can be expressed as follows:

$$Q_{b,i}(t) = \alpha_i W_i(t) \quad (m^3/d) \tag{4.36}$$

where i is the number of the sector, t is the time step (d), $Q_{b,i}$ and α_i are, respectively, the baseflow discharge (m^3/d) and the depletion coefficient (1/d) of the i-th reservoir, $W_i(t)$ is the volume of water in the i-th reservoir (m^3) at the time t. The final discharge of the system is calculated as the sum of the discharges released from each sector.

The sectors have an increasing depletion coefficient, so the last sector identified in the recession curve analysis is the first sector in the model and so on. This trick allows reproducing the process identified in the recession curve analysis, with the last sector of the recession curve working all the year and the early sectors running only when the aquifer is saturated (sectors before full of water).

At each time step, the mass balance equation is solved for each reservoir, computing each discharges and updating the volume stored within the model. Only when the reservoir with the lower depletion coefficient is full, recharge surplus starts to fill the following reservoir and with higher depletion coefficient. The only exception is the reservoir with higher depletion coefficient, so the last one, which is set as unlimited in volume. This reservoir represents the ones with the most rapid flux activated only during the peak of discharge, when all the previous reservoirs are full.

To take into account the variable soil storage in the springs recharge area a rainfall-excess model has been added at the entrance of the model (Fig. 4.23). To resume, the parameters of this model are the two parameters of the rainfall-excess model (C_{max}, β_k) and the two parameters of each sector (α_i, $W_{0,i}$).
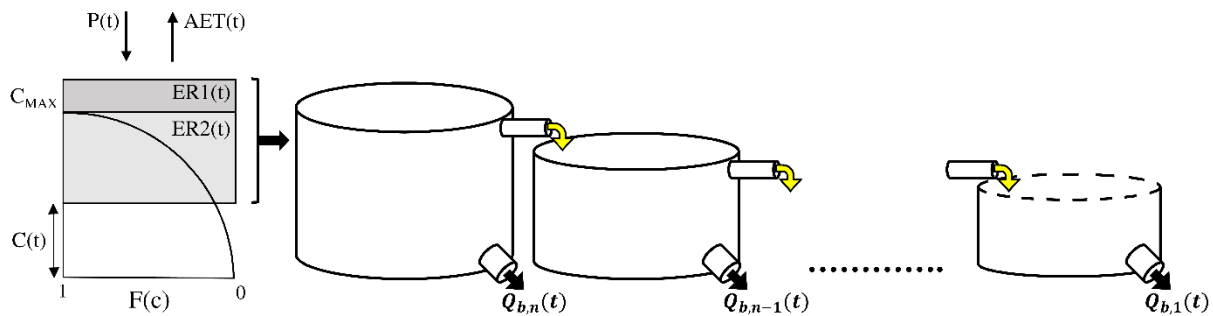
Figure 4.23 General conceptual model to simulate the discharge of a fractured aquifer with recession curve divisible in n-th sectors. The first part is the rainfall-excess model, of which the output is the effective rainfall (ER=ER1+ER2). Then the n-th reservoirs model produce the springs discharge as the sum of each reservoir discharge (pipes with black arrows).

DISCHARGE ANALYSIS

In this work the Mulino delle Vene springs discharge has been simulated in several periods and with different hydrological models. In particular, the thirty years baseline (1984-2013) and future (2021-2050) periods have been studied and compared. To analyse the results several methods and coefficients have been applied as reported above.

• Flow duration curve

Flow duration curves (FDCs) are one of the most informative methods to display the complete range of a discharge from low flows to peaks. They represented the relationship between a discharge value and the percentage of time that this discharge is equalled or exceeded (Vogel & Fennessey, 1994). Wilby et al. (1994) used FDCs to assess the effects of different climate scenarios on stream flow with particular reference to low flows. In this study, the FDCs are calculated on the basis of the whole simulated period (30 years of daily

data). Then the simulated baseline FDC is compared to the forecasted future FDC. Furthermore, some low flow indices are estimated from the resulting FDCs. In particular, the Q95 (daily mean discharge that was exceeded on 95% of days) and the Q80 (daily mean discharge that was exceeded on 80% of days) are used to compare the low flow condition. Moreover, some other percentile of the curves are assessed in order to compare present and future values (Q50, discharge equalled or exceeded 50% of the time; Q05, discharge exceeded on 5% of days).

- Low flow frequency analysis

Unlike the FDC, which shows the proportion of time during which a flow is exceeded, a Low-flow Frequency Curve (LFFC; Smakhtin, 2001) shows the average interval in years ('return period' or 'recurrence interval') that the river falls below a given discharge. Among the several average intervals proposed in literature, 7Q10 (flow that occur for a consecutive 7-days period at the recurrence interval of 10 years) is one of the most commonly used indices and it is usually estimated through a Log-Pearson type III distribution function (Smakhtin, 2001). In this work, the baseline (period 1984-2013) and future (period 2021-2050) low flow series have been used to calculate this statistical distribution.

- Continuous low flow events

As pointed out by Smakhtin (2001), neither FDC nor LFFC provide information about the length of continuous periods below a particular flow value of interest. To overcome this limitation, the duration of longest periods above a flow threshold can be analysed. In this study, the continuous low flow distributions have been analyzed using the spell-duration approach (Institute of Hydrology, 1980), where by spell it is mean the number of days when daily discharges remain below a defined threshold. This threshold can be defined through the FDCs (Beran & Gustard, 1977). When considering rivers or springs with perennial discharges, it is normal to select a threshold flow with an 80% exceedance on the specific FDC (i.e. Q(80)) (Smakhtin, 2001). Results are presented in the form of a histogram showing the number of years where the spell is below the given threshold (Q(80)). The mean number of consecutive days when the discharge is below the threshold is also given for the baseline and future periods.

4.6.3 EFFICIENCY CRITERIA

A comparison between simulated and observed data is necessary to evaluate the goodness of fit of a hydrological model. Several object function can be chosen, for example the efficiency functions as the correlation coefficient, the Nash-Sutcliffe efficiency, the Nash-Sutcliffe efficiency with logarithmic values, and modified forms of these. In this section, a briefly description of these coefficients is reported. In a model performance analysis more than one criteria can be applied. The decision on the more suitable method depends on the goal of the work, for example if it is more important to well simulate low flows than peak flows, then it is better to choose coefficients which give less importance to extreme events. Each criteria has specific characteristics, which have to be taken into account during calibration and evaluation. The most frequently used correlation coefficient and Nash-Sutcliffe efficiency are very sensitive to peak flows. The logarithmic Nash-Sutcliffe efficiency is more sensitive to low flows but it is still susceptible to peak flows. The reaction to peak flow could be suppressed applying the relative efficiency which is sensitive to low flow only (Krause et al., 2005) or the NSE calculated on inverse transformed flow as suggested from Pushpalatha et al. (2012).

CORRELATION COEFFICIENT

The correlation coefficient (r), which ranges from -1 to 1, is an index of the degree of linear relationship between observed and simulated data. If r=0 there is no relationship between the series; if r=1 or -1 there is a positive or negative linear relationship. The squared value of the correlation coefficient is called coefficient of determination (R^2) and it ranges from 0 to 1. Typically values of R^2 greater than 0.5 are considered acceptable (Moriasi et al., 2007). R^2 is calculated as:

$$R^2 = \left(\frac{\sum_{i=1}^{n}(o_i - \bar{o})(s_i - \bar{s})}{\sqrt{\sum_{i=1}^{n}(o_i - \bar{o})^2}\sqrt{\sum_{i=1}^{n}(s_i - \bar{s})^2}} \right)^2 \tag{4.37}$$

Where o_i is the observed variable, $\bar{o}$ is the mean value of the observed variable, s_i is the simulated series, $\bar{s}$ is the mean value of the simulation.

NASH-SUTCLIFFE EFFICIENCY

The Nash-Sutcliffe efficiency (NSE) (Nash & Sutcliffe, 1970) is computed as:

$$NSE = 1 - \frac{\sum_{i=1}^{n}(o_i - s_i)^2}{\sum_{i=1}^{n}(o_i - \bar{o})^2} \tag{4.38}$$

Where o_i is the observed variable, $\bar{o}$ is the mean value of the observed variable, s_i is the simulated series.

The NSE ranges from -∞ to 1 (optimal value). NSE is very commonly used and it is recommended by ASCE (1993). A general performance rating of the coefficient is reported in Tab. 4.5 as in Moriasi et al. (2007).

Table 4.5 Performance rating for NSE (Moriasi et al., 2007).

Performance	NSE
Very good	0.75<NSE≤1.00
Good	0.65<NSE≤0.75
Satisfactory	0.50<NSE≤0.65
Unsatisfactory	NSE≤0.50

LOGARITHMIC NASH-SUTCLIFFE EFFICIENCY

To reduce the sensitivity to the peak values, the NSE is often calculated with the logarithmic values of the variables and it is called logarithmic Nash-Sutcliffe Efficiency (lnNSE). In this coefficient, the influence of the low flow values is greater than in the previous efficiency criteria (Krause et al., 2005). In fact, with the logarithmic transformation, peaks are flattened and low flow values become more pivotal in the statistical analysis. The following formula is used to assess lnNSE:

$$lnNSE = 1 - \frac{\sum_{i=1}^{n}|\ln o_i - \ln s_i|^2}{\sum_{i=1}^{n}|\ln o_i - \overline{\ln o}|^2} \tag{4.39}$$

Where $\ln o_i$ are the observed variable in the logarithmic form, $\overline{\ln o}$ is the mean value of the observed logarithmic variable, $\ln s_i$ are the simulated data always in logarithmic form. The range values of $lnNSE$ is the same of the NSE.

RELATIVE EFFICIENCY CRITERIA

In the coefficient described above the higher values of flow have a greater influence than the lower values. To reduce this, a modification of NSE is possible changing it into a relative form. In particular, the relative efficiency (NSE_rel) can be computed as:

$$NSE_{rel} = 1 - \frac{\sum_{i=1}^{n}\left(\frac{o_i - s_i}{o_i}\right)^2}{\sum_{i=1}^{n}\left(\frac{o_i - \bar{o}}{\bar{o}}\right)^2} \tag{4.40}$$

Where o_i are the observed variable, $\bar{o}$ is the mean value of the observed variable, s_i are the simulated data.

As NSE, the NSE_{rel} ranges from -∞ to 1 (perfect agreement).

INVERSE FLOW EFFICIENCY CRITERIA

This criterion is a modification of the Nash-Sutcliffe efficiency formulated in order to give more relevance to low flow in the coefficient estimation. In particular, the NSE coefficient was calculated on the inverse of the

observed and simulated discharge. This method is not commonly used in literature and it was proposed by Le Moine (2008). The coefficient can be assessed as follow:

$$NSE_i = 1 - \frac{\sum_{i=1}^{n}\left(\frac{1}{o_i} - \frac{1}{s_i}\right)^2}{\sum_{i=1}^{n}\left(\frac{1}{o_i} - \overline{\left(\frac{1}{o}\right)}\right)^2} \qquad (4.41)$$

Where $\frac{1}{o_i}$ is the inverse of the observed variable, $\overline{\left(\frac{1}{o}\right)}$ is the mean value of the inverse of the observed variable, $\frac{1}{s_i}$ is the inverse of the simulated data. The NSE_i has the same range of the normal NSE.

4.7 LAND USE ANALYSIS

Several land use map of the region have allow an historical analysis of the land use in the Mulino delle Vene study area. In particular, ARPAE E-R (Agenzia Regionale per la Prevenzione, l'Ambiente e l'Energia dell'Emilia-Romagna) has produced 4 land use maps for the years 1976, 1994, 2003 and 2008. These maps have been analysed and compared in order to assess the different type of land use to which different albedo are assigned during the evapotranspiration calculation. In particular, the recharge area of the Mulino delle Vene springs has been classified based on the map in agricultural and forested land, and the evapotranspiration with the Penman-Monteith equation has been assessed according to the percentage of surface for each land use type.

Land use map 1976

The land use map of the 1976 is one of the first land use map covering the all region. For the fulfilment, aerial photos from the 1976 to the 1978 have been utilised. In the last years, the map has been digitalised, converting the legend to the Corine Land Cover format in a scale 1:25000 (Corticelli et al., 2011).

Land use map 1994

The land use map of the 1994 comes from the digitalization of the map produced at the beginning of the '90. It is in the scale 1:25000 and the legend has been converted in the Corine Land Cover format in the 2010. (Campiani et al., 2010)

Land use map 2003

The land use map of the 2003 (1:25000) is built with the Quickbird images and the legend respects the Corine Land Cover format (Campiani et al., 2011 a).

Land use map 2008

The land use map of the 2008 (1:25000) is a high precision map and it respects the Corine Land Cover format (Campiani et al., 2011 b). This land use distribution has been used for the Penman-Monteith evapotranspiration assessment as described in section 4.1.1.

5. RESULTS

5.1 HYDROLOGICAL ANALYSIS

5.1.1 RAINFALL ANALYSIS

The daily data from 2004 to 2014 observed at the 9 weather stations have been analysed. In Tab. 5.1 the average monthly rainfall for each monitored weather station are reported and in Fig. 5.1 they are represented. The average yearly rainfall is about 845 mm. Two wet periods are observed in autumn and in spring (100-140 mm/month in November and 60-100 mm in March). The driest month is July with 31 mm of rainfall at the weather station of La Stella. Instead, the wettest month is November with the maximum of 140 mm at the weather station of Villa Minozzo. Moreover, the monthly precipitation in mountainous area is higher than in the plain, this difference is major during the winter reaching 30-40 mm. A similar distribution of the precipitation has been found by Antolini et al. (2016) who analyses daily climate series from 1961 to 2010, finding a large south west/north east gradient, mainly associated with the orography.

Table 5.1 Average monthly precipitation in the weather stations analysed for the period 2004-2014.

	Weather station									
	Baiso	Carpineti	Ponte Cavola	San Valentino	Ca' de Caroli	La Stella	Predolo	Castelnovo Ne' Monti	Villa Minozzo	Average
Month	(mm)	(mm)	(mm)	(mm)	(mm)	(mm)	(mm)	(mm)	(mm)	(mm)
J	59	61	67	53	57	43	44	64	81	59
F	60	64	59	60	63	36	38	60	63	56
M	90	100	92	88	85	58	63	84	96	84
A	84	84	78	90	80	70	65	88	92	81
M	65	69	66	57	61	64	62	75	80	67
J	82	62	57	69	63	78	65	75	68	69
J	36	35	43	34	34	31	38	39	38	36
A	41	37	44	40	35	45	39	48	65	44
S	68	79	72	61	67	68	78	87	89	74
O	97	98	85	90	91	85	84	101	102	93
N	113	125	123	102	104	97	98	125	141	114
D	73	74	76	68	67	49	48	75	88	69
Tot.	870	887	863	809	807	724	723	923	1002	845
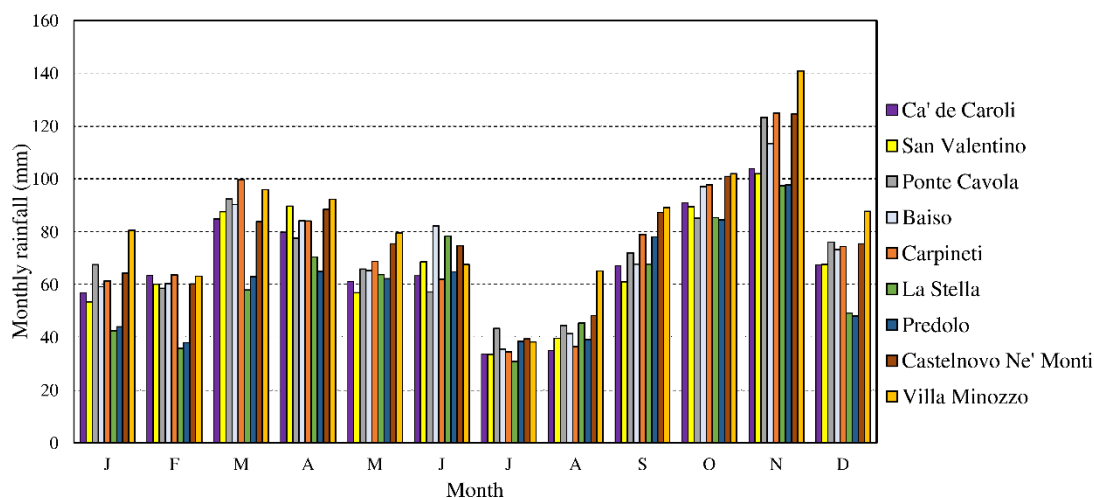
Figure 5.1 Average monthly rainfall in the period 2004-2014.

In Tab. 5.2 the monthly precipitation of the weather stations of Carpineti and Baiso is reported for the two period 1971-1993 (from Vizzi, 2014) and 2004-2014. Comparing the two periods, in both the weather stations a decrease of rainfall in the summer months and an increase in autumn is evident. The mean annual rainfall of the Baiso weather station increases from 809 mm (1971-1993) to 870 mm (2004-2014). Instead, the observed mean annual rainfall at the weather station of Carpineti decreases from 940 mm (1971-1993) to 886 mm (2004-2014).

Table 5.2 Monthly average precipitation from the Baiso and the Carpineti weather stations.

Period	1971-1993		2004-2014	
Weather station	Baiso	Carpineti	Baiso	Carpineti
Month	(mm)	(mm)	(mm)	(mm)
J	51.70	70.70	59.15	61.35
F	54.40	66.70	60.31	63.69
M	70.60	91.30	90.33	99.67
A	85.90	95.70	84.15	84.04
M	73.40	76.30	65.36	68.71
J	55.70	62.30	82.13	61.96
J	37.70	54.80	35.58	34.51
A	66.50	89.60	41.34	36.53
S	83.80	85.00	67.75	78.98
O	89.40	83.10	97.11	97.78
N	83.80	95.10	113.44	124.96
D	56.00	69.70	73.29	74.36

5.1.2 TEMPERATURE ANALYSYS

The observed temperatures in the period 2004-2014, from the weather stations in the area, have been collected and analysed. The assessed average monthly temperature values are reported in Tab. 5.3 for each weather station. Temperatures change from 0÷5 °C in the winter months to 20÷25 °C during the summer. The hottest month is July with an average temperature about 22.2 °C, instead the coldest month is January with an average of 2.9 °C. The yearly average temperature changes from 11.1 °C (Castelnovo Ne' Monti) to 13.8 °C (San Valentino), with an average value over the catchment about 12.1 °C. The temperature trend is reported in Fig. 5.2. A spatial variation of temperature has been identified, in particular temperatures increase towards the north-east. This distribution is in agreement with the correlation between elevation and temperature found for the Emilia-Romagna region by Antolini et al. (2016).

Table 5.3 Average monthly temperature for the period 2004-2014.

	Weather station							
	Carpineti	Ponte Cavola	San Valentino	La Stella	Predolo	Castelnovo Ne' Monti	Villa Minozzo	Average
Month	(°C)	(°C)	(°C)	(°C)	(°C)	(°C)	(°C)	(°C)
J	3.3	1.9	4.2	3.0	2.6	2.2	3.3	2.9
F	4.1	2.7	4.7	3.4	3.0	2.7	3.7	3.5
M	7.8	6.3	8.8	6.9	6.5	6.1	7.0	7.1
A	11.8	10.7	13.3	11.0	10.6	10.2	11.2	11.3
M	16.1	14.6	17.7	15.5	14.9	14.3	15.2	15.5
J	20.1	18.8	21.8	19.4	19.1	18.3	19.3	19.5
J	22.7	21.4	24.5	22.2	21.9	21.0	22.0	22.2
A	22.2	20.8	23.6	21.4	21.1	20.4	21.2	21.5
S	18.1	16.9	19.3	17.4	16.9	16.1	17.1	17.4
O	13.1	12.4	14.3	12.6	12.2	11.6	12.9	12.7
N	8.2	7.3	8.8	7.8	7.4	6.9	7.8	7.7
D	4.5	2.5	4.1	3.8	3.5	3.0	4.0	3.6
Average	12.7	11.4	13.8	12.0	11.6	11.1	12.1	12.1
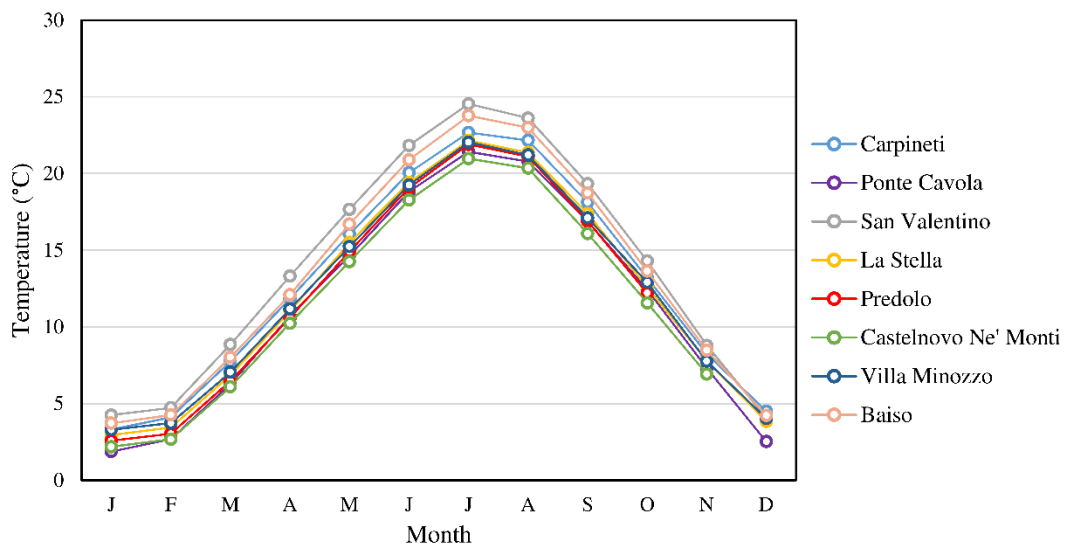
Figure 5.2 Average monthly temperature in the period 2004-2014.

5.1.3 THORNTHWAITE POTENTIAL EVAPOTRANSPIRATION AND EFFECTIVE RAINFALL

The Carpineti weather station is considered as the most important in our study because it is the nearest to the Mulino delle Vene springs, which are the main water source of the study area. Therefore, next analysis has been carried out focusing on data from the weather station of Carpineti.

In particular, the monthly evapotranspiration has been estimated in the period 2004-2014 with the Thornthwaite equation (Tab. 5.4, average values). The effective rainfall of the period, assessed as the difference between the monthly precipitation (P) and evapotranspiration (ET), is reported in Tab. 5.5 along with the percentage of precipitation not evaporated ((P-ET)/P) and the average values. The effective precipitation is about the 52% of the precipitation, in particular, it is about the 0% during the summer but it reached the 90% in some winter months.

Table 5.4 Average monthly potential evapotranspiration (mm) assessed with the Thornthwaite equation over the period 2004-2014.

Month	J	F	M	A	M	J	J	A	S	O	N	D	Tot.
(mm)	9	11	26	46	70	96	113	110	83	54	28	12	659

Table 5.5 Assessed values of monthly effective rainfall (mm) over the period 2004-2014 along with averaged yearly values.

Month	2004	2005	2006	2007	2008	2009	2010	2011	2012	2013	2014	Average
J	53	10	51	7	32	74	75	27	9	89	152	53
F	72	34	38	29	4	40	66	46	65	85	95	52
M	100	22	37	91	31	66	73	89	10	179	109	73
A	80	147	14	0	31	101	0	0	57	65	56	50
M	31	0	0	0	58	0	42	0	1	67	0	18
J	0	0	0	6	56	0	9	0	0	0	0	6
J	0	0	0	0	0	0	0	0	0	0	16	1
A	0	23	0	0	0	0	0	0	0	0	0	2
S	4	2	67	0	0	45	12	0	9	0	22	15
O	42	98	0	107	0	9	94	36	60	57	1	46
N	124	92	13	38	209	60	149	7	147	81	141	97
D	73	97	21	21	130	126	113	14	48	0	46	63
Tot.	581	526	241	299	551	521	634	220	405	623	637	476
(P-ET)/P	55%	54%	37%	41%	59%	60%	59%	40%	52%	66%	53%	52%

5.2 SPRINGS MONITORING

The probe, set at the Mulino delle Vene weir, has collected piezometric level, electric conductivity and water temperature from the 11th March 2013 until the 4th June 2016 at an hourly time step. The discharge from the springs has been assessed as described in section 4.2. Fig. 5.3 and Fig. 5.4 report the observed and assessed variables.

The mean discharge is about 96.8 l/s, maximum average daily value of 462.9 l/s occurrs the 5th April 2013, while minimum is about 28.4 l/s on the 14th November 2013. The observed springs water temperature is constant and it is about 12 °C. The electric conductivity of water is strictly related to the discharge amount, in particular the conductivity values decrease for higher discharge amounts, and higher conductivity values are observed during low flow period.
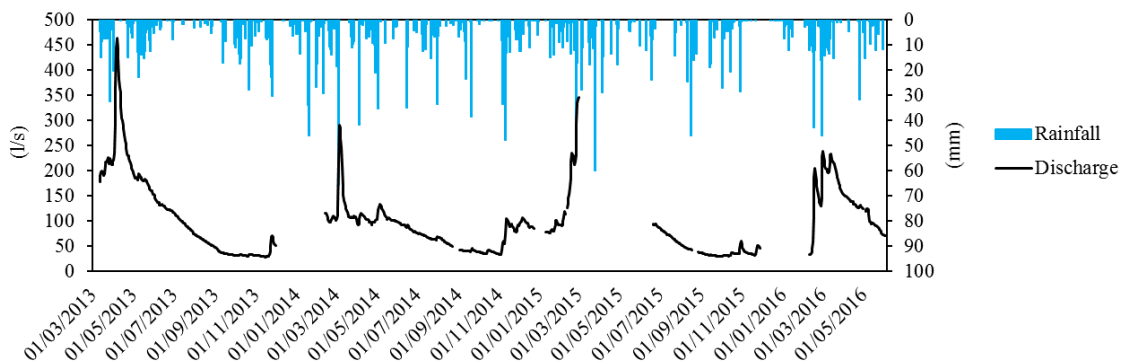
Figure 5.3 Average daily discharge from the Mulino delle Vene springs along with the observed daily rainfall at the Carpineti weather station.
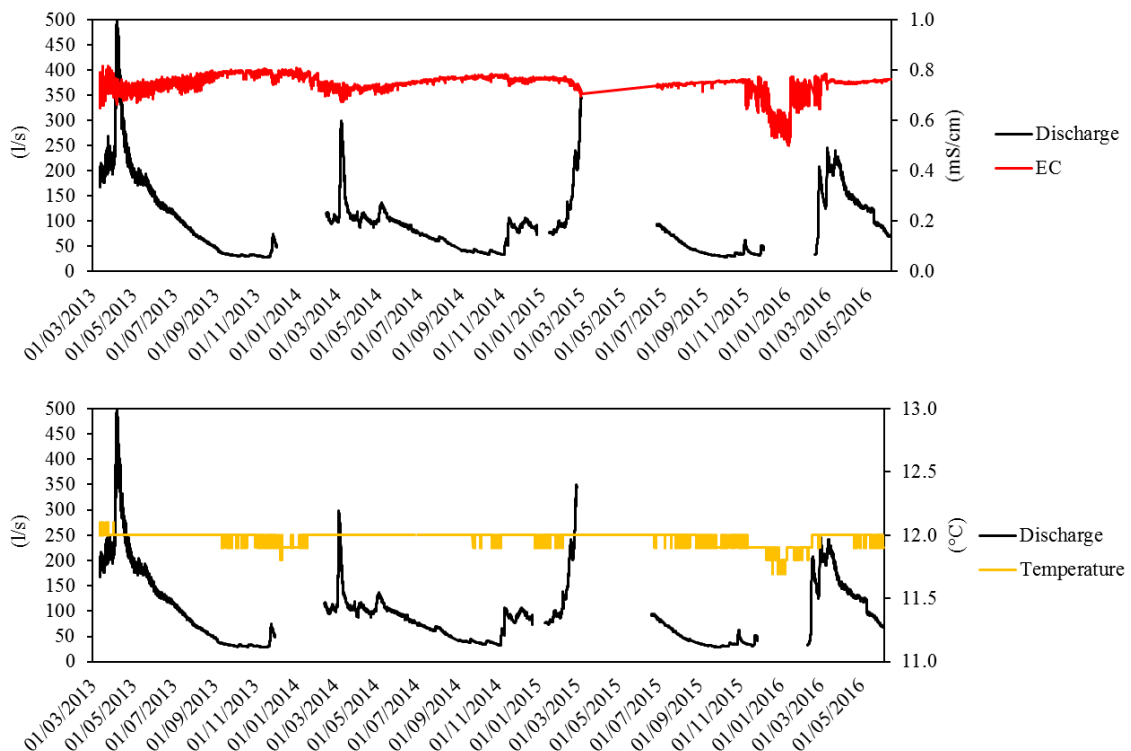
Figure 5.4 Observed electric conductivity (red line) and temperature (yellow line) at an hourly time step and assessed discharge from the Mulino delle Vene springs (black line).

5.3 RECESSION CURVE ANALYSIS

The 2013 springs recession curve is particularly long and the different part of the hydrograph are well detectable. Therefore, the 2013 daily discharge datasets from the Mulino delle Vene springs system has been selected for the recession curve analysis. In particular, the recession curve (Fig. 5.5) starts the 05th April 2013 (Q= 462.4 l/s) and it ends the 16th November 2013 (Q= 28.7 l/s). The period covers a total of 226 days. The recession curve shows three sectors identified by three different slopes. The first part of the curve (1) is the steepest one and lasted 30 days, from the 05th April 2013 to the 05th May 2013. The second part of the curve (2) is gentler and clearly visible up to the beginning of September (4th). The last part of the curve (3) is characterised by lowest slope and ended the 16th November. This means that there are three different sectors (i.e. reservoirs) in the aquifer and they all participate actively in the process, from the beginning of the recession period up to the time when the Mulino delle Vene springs system is fully discharged. The sum of the three discharges at time t=0 (401.2 l/s) is slightly lower than the corresponding peak discharge at the beginning of the observed recession curve (Qmax= 462.4 l/s). This is due to the approximate nature of the exponential curve.

The depletion coefficients (α) and the initial volume (W_0) are assessed for each system composing the recession curve, as described in section 4.3. Data are resumed in Tab. 5.6. The total volume stored by the aquifer at the beginning of the discharge period (dynamic yield) is equal to the sum of the three systems initial volumes and it has been estimated in about 2.45 Mm^3.

Table 5.6 Results of the recession curve analysis. α_i (1/d) and $W_{0,i}$ (m^3) are the depletion coefficient and the dynamic yield of the i-th sector, respectively. $Q_{0,i}$ are the corresponding discharges (here reported in l/s) at the beginning of the recession period (t=0).

	1st sector	2nd sector	3rd sector
$Q_{0,i}$ (l/s)	178.5	171.8	50.9
α_i (1/d)	5.19 x 10^{-2}	3.27 x 10^{-2}	2.58 x 10^{-3}
$W_{0,i}$ (m^3)	2.97 x 10^5	4.55 x 10^5	1.70 x 10^6
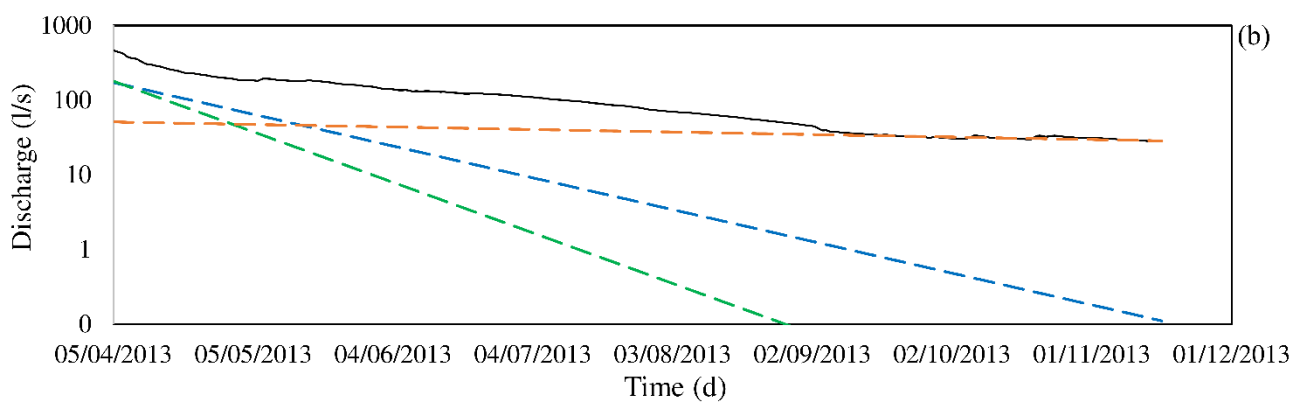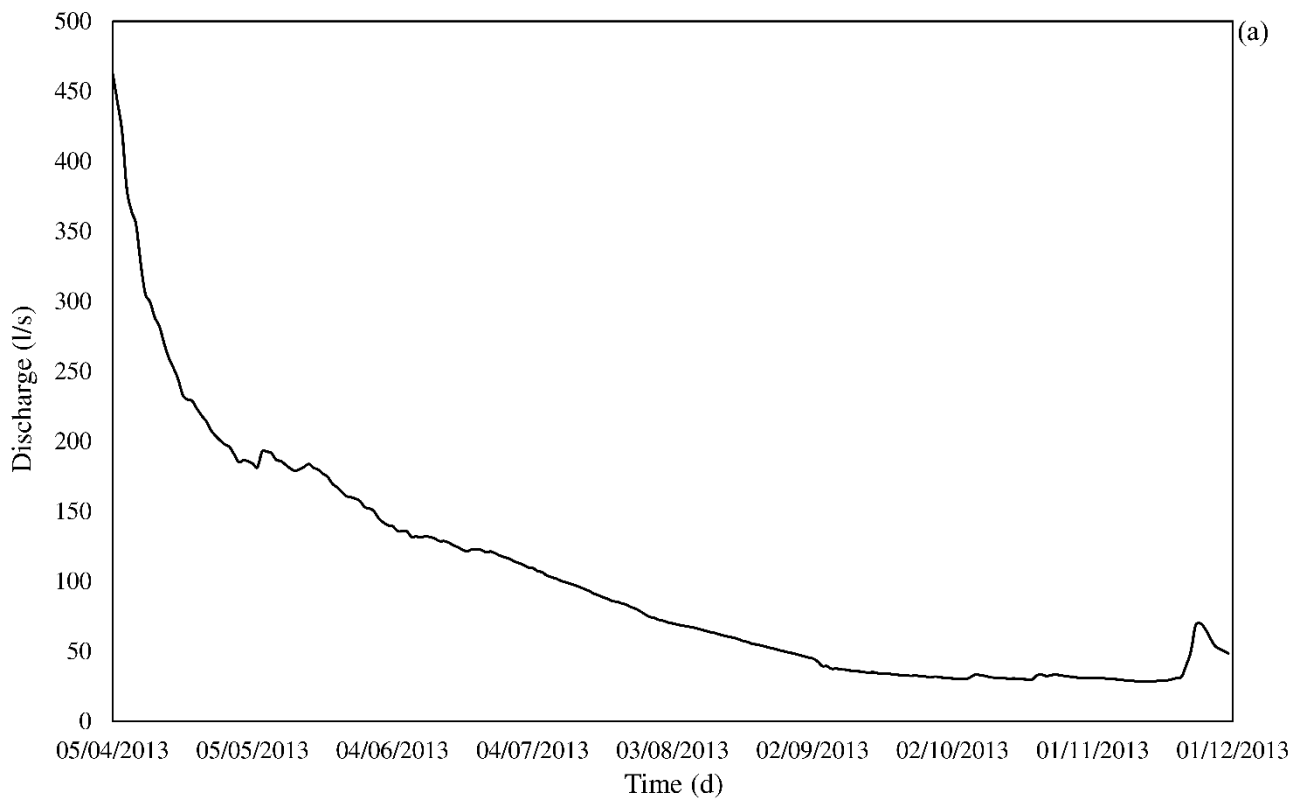
Figure 5.5 a) Recession curve of the Mulino delle Vene springs (l/s), from the 05th April 2013 to the 16th November 2013. b) Semi logarithmic graph of the springs discharge and recession curve analysis. In green the exponential model representing the 1st sector, in blue the 2nd sector and orange the 3rd sector.

5.4 LOW FLOW ASSESSMENT

Hereafter the results of the field surveys executed during the 2015 summer are reported. In particular, the uncertainty in the measures has been assessed analysing the results of the repeated tracer tests. Moreover, low flows have been assessed along the Tresinaro stream length allowing the groundwater contribution to the stream discharge to be determined.

5.4.1 UNCERTAINTY

To assess the uncertainty related to the tracer tests measurements and to the distance between the injection and the measurement points, some repeated measurement have been executed. In particular, the 1st of September 2015 in section n. 2, five repeated measurements have been executed with the same distance of 100 m between the injection and the measurement point. In Fig. 5.6 the observed electric conductivity is reported and in Tab. 5.7 the assessed discharge values. The mean discharge assessed in the five measures is about 0.046 m^3/s with a standard deviation about 0.0029 m^3/s and a coefficient of variation (σ/m) of 6.4%. These results show that the measures are substantially correct and the error is very low and lower to the 10%.
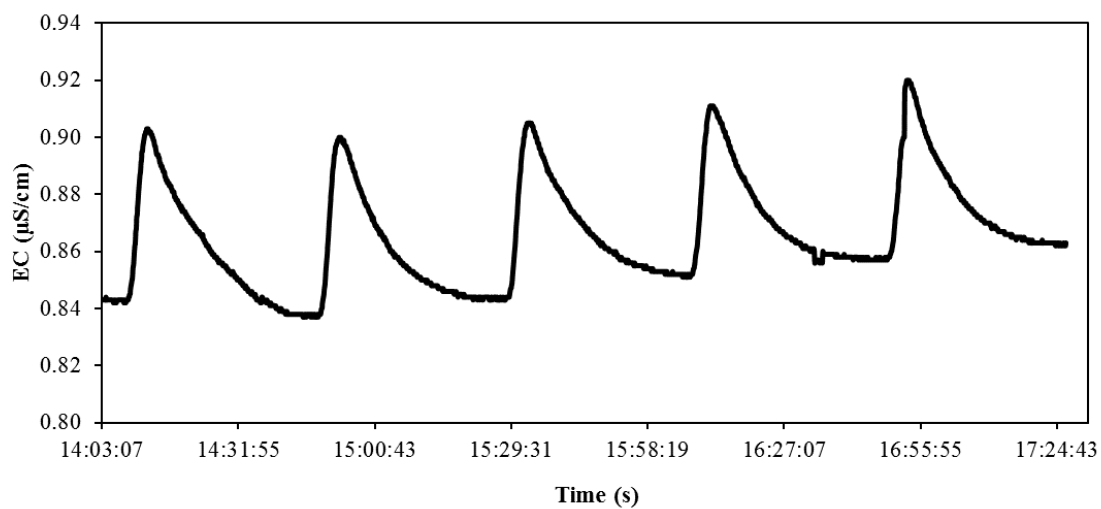
Figure 5.6 Electric conductivity (EC) measured in section n. 2 during the repeated test at the same distance.

Table 5.7 Low flow measures results in section n.2.

Injection number	Q (m^3/s)
1	0.042
2	0.047
3	0.046
4	0.046
5	0.050

The 1st of September 2015, four repeated measures with different lengths have been executed in section n. 6. The measures have the aim to assess the effect of a different distance between the injection and the measurement point in the low flow assessment. In Fig. 5.7 the observed electric conductivity and in Tab. 5.8 the assessed low flow discharges are reported. The mean assessed discharge is about 0.059 m^3/s with a standard deviation about 0.0013 m^3/s and a coefficient of variation of 2.1%. In conclusion, a distance between 120 m and 80 m do not affect the low flow assessment and the error is very low.
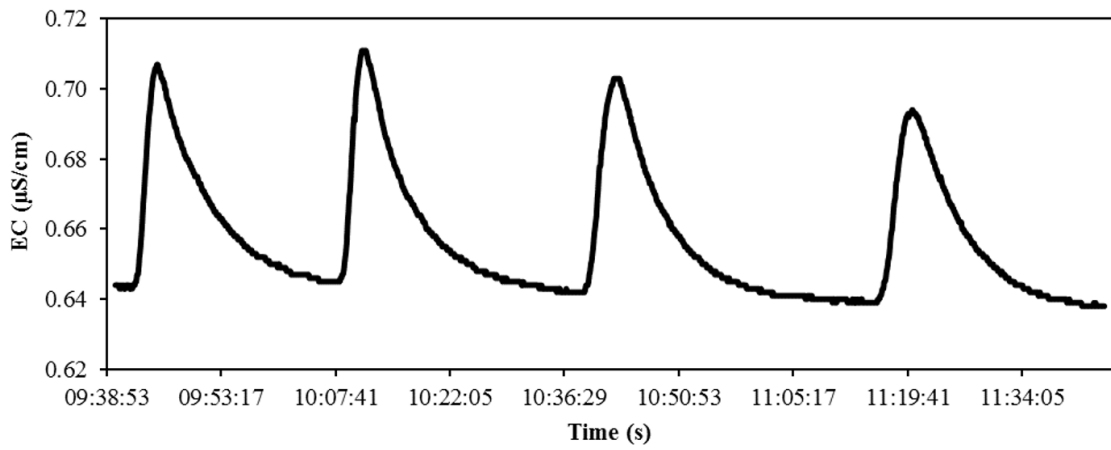
Figure 5.7 Electric conductivity (EC) measured in section n. 6 during the repeated test at variable distance.

Table 5.8 Low flow measures results in section n.6 during the repeated test at different lengths of the segment between the injection and the measurement point.

Injection number	Length (m)	Q (m³/s)
1	120	0.058
2	100	0.613
3	80	0.058
4	60	0.060

59

5.4.2 LOW FLOW

Hereafter the results of the low flow assessment executed during the 2015 summer are reported (Tab. 5.9). After the first analysis, it has been discovered that section n. 13 is located downstream of a channel carrying water from the Secchia River, so its measurement is not relevant. Moreover, the day before the survey of the 23rd of July, a rainstorm affected the higher part of the catchment and therefore the measurements of this day are compromised by the surface runoff. This is particularly evident in the measure of section n. 2 where a discharge higher than average was observed. Furthermore, in section n. 0, the flow assessment is impossible because too much small. In fact, discharge upstream of the village of Carpineti is negligible in the low flow period.

Table 5.9 Assessed discharge in the Tresinaro stream sections (m^3/s).

Section	20/06/2015	02/07/2015	23/07/2015	31/08/2015	22/09/2015	29/09/2015	09/10/2015
14	/	/	0.018	0.012	/	/	/
13	/	/	/	/	/	0.423	/
12	/	/	/	/	/	/	0.043
11	/	/	/	0.054	/	0.042	0.074
10	/	0.069	0.722	0.059	/	0.061	0.092
9	/	/	/	/	/	/	0.088
8	/	/	/	/	/	/	0.090
7	/	0.122	/	0.070	/	0.056	0.080
6	/	0.107	0.126	0.068	0.068	/	/
5	/	0.110	0.103	0.068	/	0.045	/
4	/	/	/	0.051	/	/	/
3	/	/	/	0.050	/	0.041	/
2	0.128	0.063	0.079	0.046	0.039	/	/
1	0.040	0.010	/	/	/	/	/
0	0.000	0.000	0.000	0.000	0.000	0.000	0.000

In Fig. 5.8 the assessed low flows in the monitored sections are reported. In the graph the bar for a standard deviation of 0.0029 m^3/s is marked considering a measurement error equal to the one assessed during the repeated test of the 1st of September. Values for the 23rd of July are not reported because they are affected from the rainstorm and they are not representative of the low flow regime. Fig. 5.9 represents the observed low flow in function of the distance from section 0.
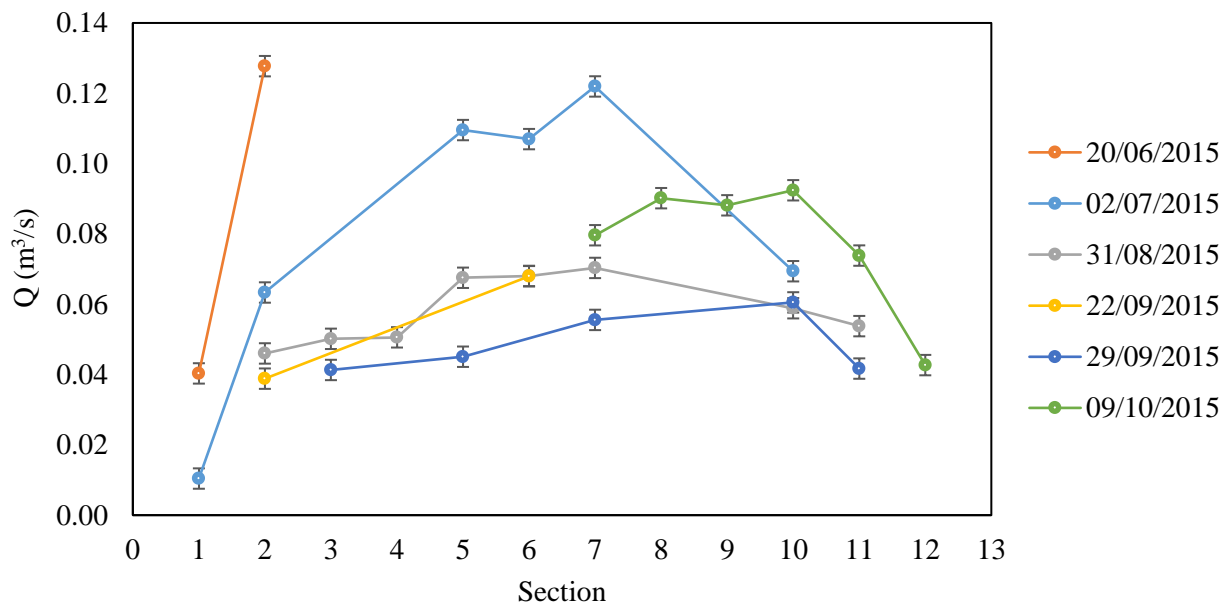
Figure 5.8 Graph of the assessed low flow values in the monitored sections.
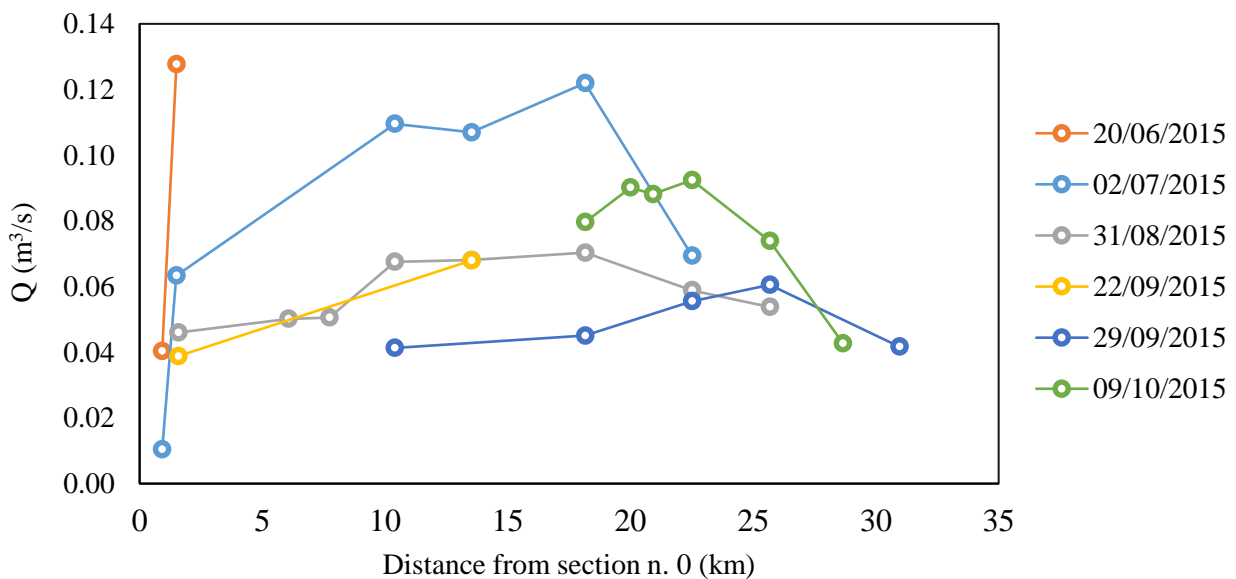
Figure 5.9 Assessed low flow values in the monitored sections as a function of the distance from section 0.

Then the ratio between the variation of flow within two consecutive cross section (DQ) and the distance between the two corresponding sections (D) has been assessed. This coefficient allows an easier explanation of the groundwater inflow into the stream and of the water infiltration from the stream to the aquifer. Results are reported in Fig. 5.10. The assessment shows that the Mulino delle Vene springs are the main source of water of the Tresinaro stream. Downstream the springs, no other groundwater inflow in the stream is made evident. Moreover, after section 10 (22.5 km from section 0), the flow starts to infiltrate in the alluvial fan. From section 6 to section 10 (between 13.5 km to 22.5 km from section 0), during the summer (2nd of July and 31st of August), an important extraction of water has been detected. This occurrence is connected to the agricultural activities settled in this part of the catchment, which use the Tresinaro stream to water the crops.

The extractions of stream water could give problems in model calibration because the amount of extractions is not known exactly.
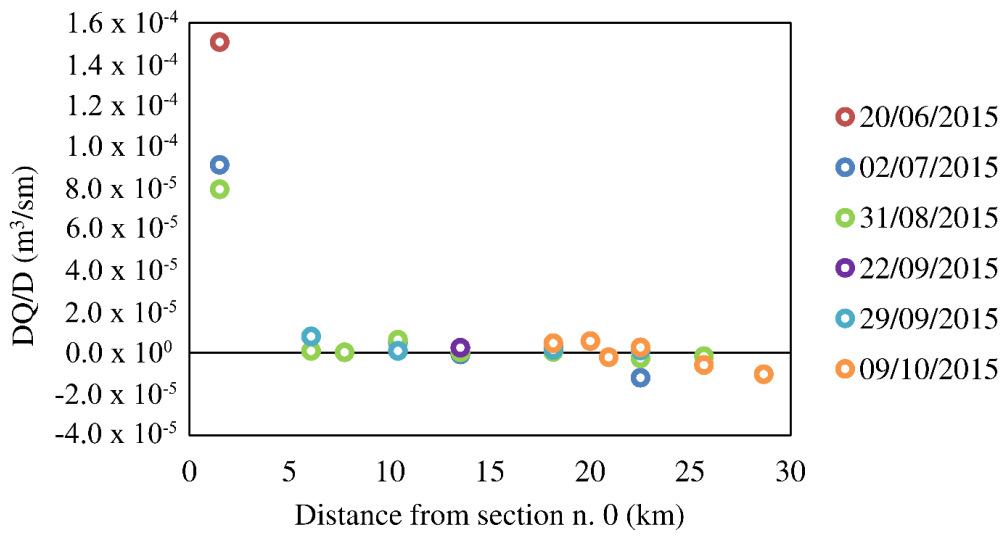
Figure 5.10 Ratio between the variation of flow within two consecutive sections (DQ) and the distance between the sections (D).

5.5 CLIMATE CHANGE SCENARIOS

Hereafter, the results of the downscaling procedure of five RCMs are reported. In particular, we have used the following scenarios:

- HC-HadCM3Q0;
- ETHZ-HadCM3Q0;
- KNMI-ECHAM5-r3;
- MPI-ECHAM5;
- SMHI-ECHAM5-r3.

These projections are based on a A1B SRES IPCC scenario (IPCC, 2007) which describes a consistent economic growth coupled with an increase in population until the mid-21st century, in combination with the rapid introduction of more efficient technologies and balanced energy sources. The dataset covers the period 1961-2050 and it has a spatial resolution of 25 km.

5.5.1 DELTA CHANGE METHOD

As anticipated in section 4.5.3, delta change factors have been calculated on a monthly basis for the 30-years periods of RCM output. The 12 delta change factors for each meteorological variable (rainfall, minimum and maximum temperatures, Tab 5.10) in the periods 1984-2013 (baseline period) and 2021-2050 (future period) have been used to perturb the observed daily database 1984-2013.

Table 5.10 Delta change factors used to perturb the observed database (1984-2013) to generate the future scenario (2021-2050) for each RCMs.

	Month	Jan.	Feb.	Mar.	Apr.	May	Jun.	Jul.	Aug.	Sep.	Oct.	Nov.	Dec.
KNMI	Δ_P	0.90	0.98	0.95	0.85	0.87	1.23	0.81	0.91	0.73	1.17	0.76	0.91
	$\Delta_{T\,max.}$	0.67	1.36	0.06	1.13	1.42	1.03	1.38	1.40	1.47	0.84	0.53	1.18
	$\Delta_{T\,min.}$	0.73	1.46	0.22	0.78	1.17	1.05	1.26	1.36	1.35	1.20	0.20	0.69
MPI	Δ_P	0.88	1.21	1.07	0.94	1.01	1.00	0.99	1.10	0.97	1.12	0.84	0.92
	$\Delta_{T\,max.}$	0.81	1.41	-0.44	0.95	1.25	0.68	1.43	1.31	1.20	0.89	1.34	1.18
	$\Delta_{T\,min.}$	0.73	1.35	0.04	0.54	1.02	0.78	1.21	1.35	1.31	1.10	0.73	0.97
SMHI	Δ_P	0.91	1.03	1.02	0.91	0.88	1.03	0.94	0.82	0.83	1.05	0.73	1.12
	$\Delta_{T\,max.}$	0.74	1.19	-0.07	0.60	1.23	0.84	1.69	1.64	1.45	1.01	0.73	1.19
	$\Delta_{T\,min.}$	0.68	0.92	0.07	0.47	0.78	0.92	1.11	1.63	1.64	1.25	0.05	0.87
ETHZ	Δ_P	0.84	1.09	1.28	0.80	0.93	0.83	0.75	0.95	1.35	1.09	1.02	1.06
	$\Delta_{T\,max.}$	2.59	1.01	0.57	1.43	1.54	2.33	2.76	1.91	2.04	1.62	1.93	2.83
	$\Delta_{T\,min.}$	2.55	0.70	0.99	1.05	1.10	1.96	2.35	2.02	2.35	1.85	2.01	2.90
HC	Δ_P	0.78	0.93	1.10	1.07	1.26	0.91	0.51	0.88	0.85	1.02	1.05	0.99
	$\Delta_{T\,max.}$	3.07	1.48	1.09	1.14	0.71	2.28	2.58	1.92	1.52	1.72	1.21	2.28
	$\Delta_{T\,min.}$	2.53	1.12	1.12	1.30	1.04	1.92	2.03	2.07	1.61	1.66	1.10	2.12

The future daily database for the five scenarios has been processed in order to obtain the future monthly mean and standard deviation of the variables (Tab. 5.11). Moreover, the mean temperature has been calculated. The results are represented in Fig. 5.11 and Fig. 5.12. The average annual rainfall decreases from 810 mm in the baseline period to 784 mm in the future period (-3%). In particular, the decrease is more evident during the

late autumn (in November –10 mm) and the summer (-7 mm in July). The average yearly temperature increases about 1.3 °C (11.5 °C in the baseline, 12.8 °C in the future). The increase is maximum during the summer months, reaching +1.8 °C in August. Minimum and maximum temperatures have the same behaviour of the mean temperature, with a general increase of about 1.3 °C.

Table 5.11 Rainfall and Minimum, Maximum and Mean Temperature for the baseline database (1984-2013) and the forecasted future scenario (2021-2050) downscaled with the delta change method, together with the corresponding mean annual values. Future values are reported as the ensemble means with the standard deviations (±σ).

	Rainfall		Minimum temperature		Maximum temperature		Mean temperature	
	mm		°C		°C		°C	
	Baseline	Future	Baseline	Future	Baseline	Future	Baseline	Future
January	50	43±2	-1.1	0.4±1.0	5.9	7.4±1.1	2.4	3.9±1.1
February	44	46±5	-0.7	0.4±0.3	7.3	8.6±0.2	3.3	4.5±0.2
March	73	75±8	2.3	2.7±0.5	10.5	10.7±0.6	6.4	6.7±0.5
April	89	83±8	5.9	6.6±0.4	14.0	14.9±0.3	9.9	10.8±0.3
May	72	73±11	10.0	10.9±0.2	19.3	20.3±0.3	14.6	15.6±0.2
June	68	69±10	13.7	14.9±0.5	23.5	24.8±0.8	18.6	19.8±0.6
July	34	27±6	16.3	17.8±0.6	26.7	28.6±0.7	21.5	23.2±0.6
August	51	48±5	16.3	18.0±0.4	26.6	28.4±0.3	21.4	23.2±0.3
September	73	69±18	12.4	14.1±0.4	21.8	23.5±0.3	17.1	18.8±0.4
October	92	97±5	8.4	10.0±0.3	15.9	17.3±0.4	12.2	13.6±0.4
November	100	90±13	3.6	4.5±0.8	9.9	11.2±0.5	6.7	7.9±0.6
December	64	65±5	0.2	1.7±0.9	6.6	8.3±0.8	3.3	5.0±0.9
TOT./MEAN	810	784±33	7.3	8.5±0.5	15.7	17.0±0.4	11.5	12.8±0.4
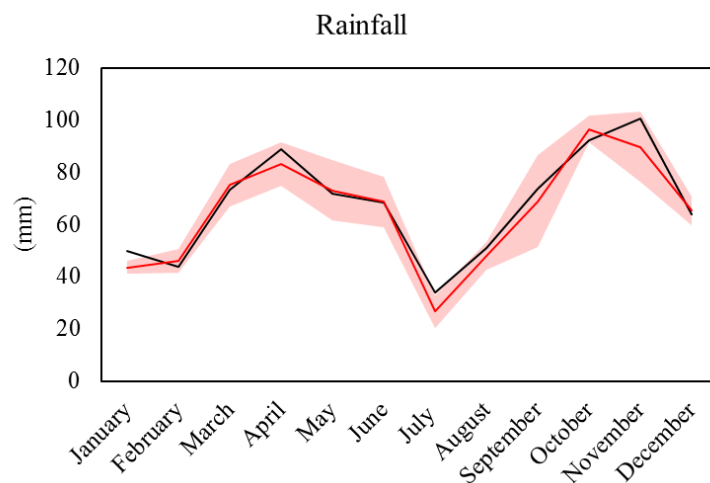
Figure 5.11 Comparison between average monthly rainfall for the baseline period (1984-2013; black line) and the future scenario (2021-2050; red line) downscaled with the delta method. Uncertainty (as ±σ) of the future scenario is also provided (shaded red area).
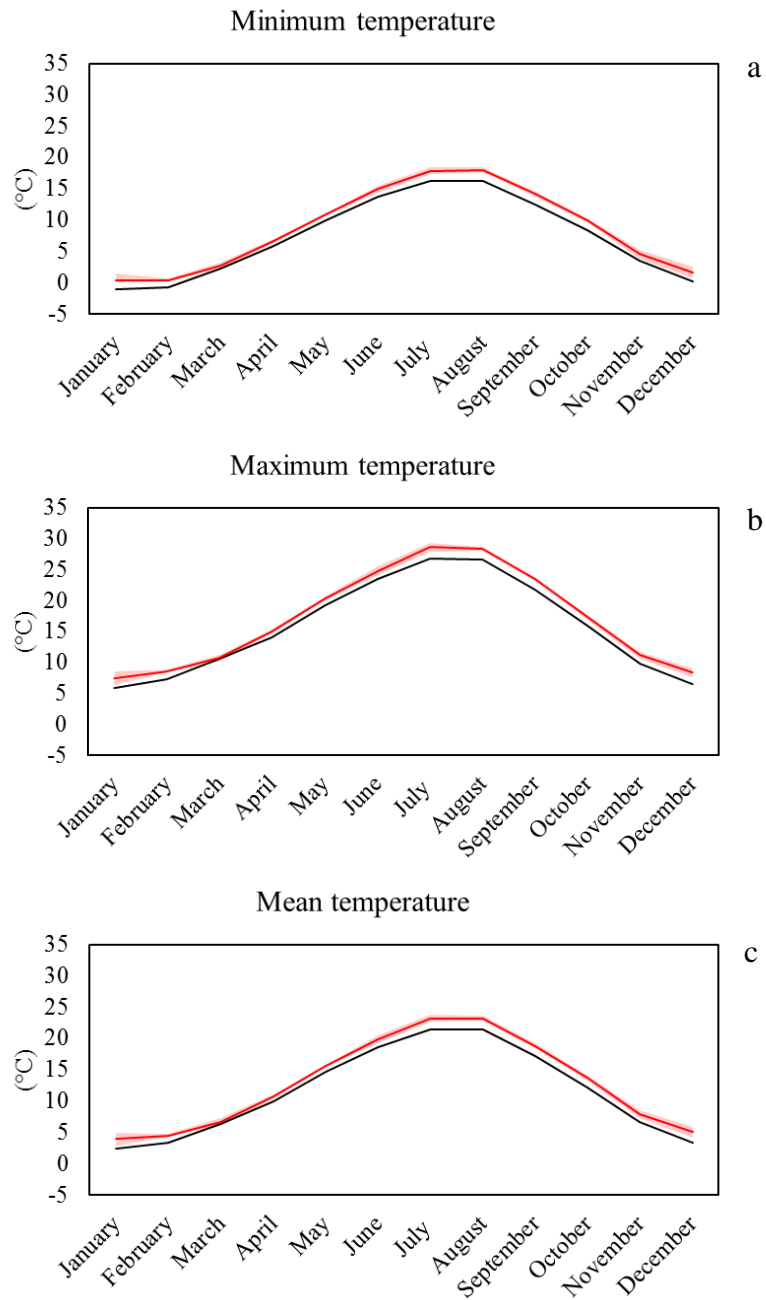
Figure 5.12 Comparison between average monthly temperature data (minimum (a), maximum (b) and mean (c) values) for the baseline period (1984-2013; black line) and the future scenario (2021-2050; red line) downscaled with the delta method. Uncertainty (as ±σ) of the future scenario is also provided (shaded red area).

5.5.2 CDF-T METHOD

The ENSEMBLE database (rainfall, minimum and maximum temperature until 2050) has been downscaled with the CDF-t technique obtaining the forecasts for the period 2021-2050 on the basis of the data observed between 1984-2013. Results of the downscaling (Tab. 5.12) have been processed in order to obtain the monthly mean and the standard deviation of the variables. In particular, the future scenarios have been combined on a single ENSEMBLE mean in order to reduce uncertainties in current climate modelling. The average annual rainfall decreases from 810 mm in the baseline period to 792 mm in the future period (-2.3%). In particular, the rainfall decreases mostly during the summer months (i.e. -30 mm in June) and it increases during the winter months (i.e. +25 mm in February). The average annual temperature increases about +1.3 °C, with maximum change in the summer when it reaches +2.2 °C. The results are represented in Fig. 5.13 and Fig. 5.14.

Table 5.12 Rainfall and Minimum, Maximum and Mean temperatures for the baseline database (1984-2013) and the forecasted future scenario (2021-2050) downscaled with the CDF-t method, together with the corresponding mean annual values. Future values are reported as the ensemble means with the standard deviations (±σ).

	Rainfall		Minimum temperature		Maximum temperature		Mean temperature	
	mm		°C		°C		°C	
	Baseline	Future	Baseline	Future	Baseline	Future	Baseline	Future
January	50	69±10	-1.1	0.8±1.0	5.9	6.8±1.2	2.4	3.8±1.1
February	44	69±6	-0.7	1.1±0.1	7.3	8.4±0.4	3.3	4.7±0.2
March	73	81±5	2.3	2.5±0.3	10.5	10.6±0.4	6.4	6.5±0.3
April	89	86±11	5.9	5.8±0.4	14.0	14.8±0.5	9.9	10.3±0.4
May	72	75±21	10.0	10.2±0.4	19.3	19.7±0.5	14.6	15.0±0.4
June	68	39±10	13.7	14.9±0.5	23.5	24.9±0.6	18.6	19.9±0.5
July	34	28±17	16.3	18.2±0.8	26.7	28.9±0.9	21.5	23.6±0.8
August	51	25±15	16.3	18.2±0.8	26.6	28.6±0.7	21.4	23.4±0.7
September	73	58±23	12.4	14.6±0.6	21.8	23.9±0.5	17.1	19.1±0.4
October	92	103±19	8.4	9.7±0.4	15.9	17.6±0.4	12.2	13.6±0.4
November	100	88±11	3.6	4.9±0.7	9.9	11.5±0.4	6.7	8.2±0.5
December	64	72±12	0.2	1.9±1.0	6.6	8.0±0.8	3.3	4.9±0.9
TOT./MEAN	810	792±45	7.3	8.5±0.4	15.7	17.0±0.4	11.5	12.8±0.4
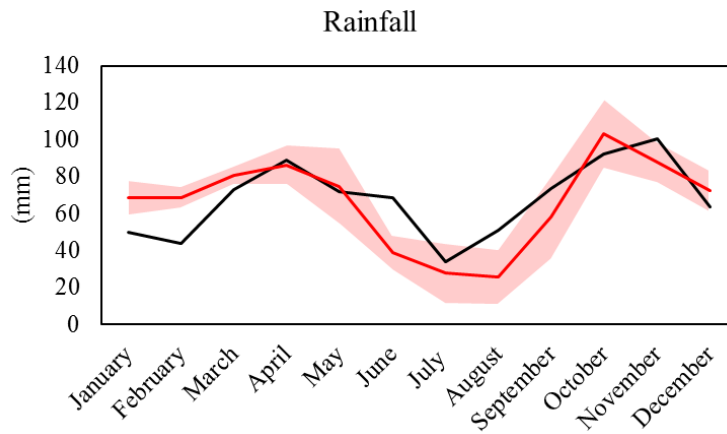
Figure 5.13 Comparison between average monthly rainfall for the baseline period (1984-2013; black line) and the future scenario (2021-2050; red line) downscaled with the CDF-t method. Uncertainty (as ±σ) of the future scenario is also provided (shaded red area).
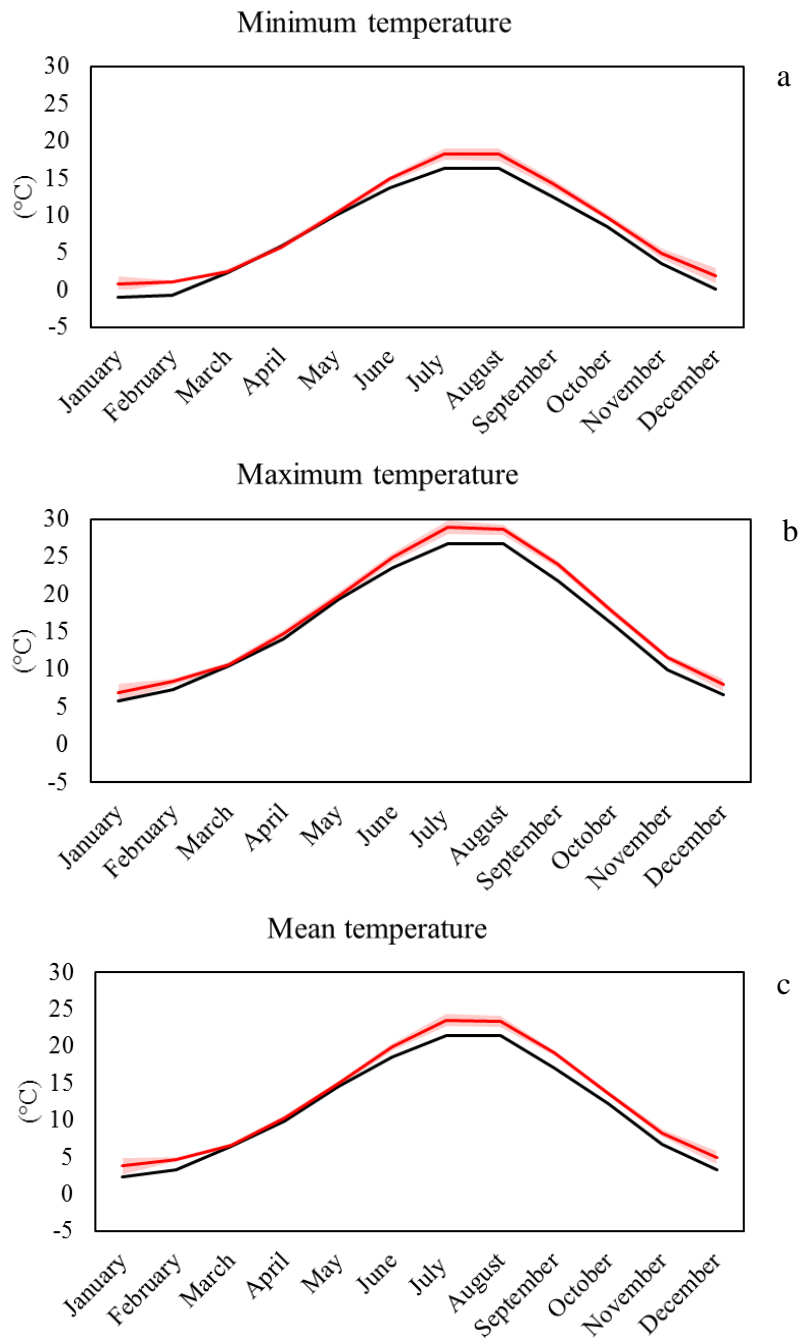
Figure 5.14 Comparison between average monthly temperature data (minimum (a), maximum (b) and mean (c) values) for the baseline period (1984-2013; black line) and the future scenario (2021-2050; red line) downscaled with the CDF-t method. Uncertainty (as ±σ) of the future scenario is also provided (shaded red area).

5.5.3 DISCUSSION

In this work, the 5 SRES scenarios have been downscaled with two statistical downscaling method. Figure 5.15 shows a comparison between the average results of both the applied methods. The downscaled rainfall obtained with the delta method is different from the one downscaled with the CDF-t method. In particular, the delta method gives only a bias to the baseline observed data and the pathway remains the same from the present to the future. Instead, the scenario downscaled with the CDF-t method is subjected also to a change in the pathway from the present. In fact, the CDF-t method allows the changes in the variable trend forecasted from the RCMs to be taken into account. The differences between the two downscaled scenarios are more evident in the winter and in the summer rainfall forecasts. In particular, during the winter months the delta method gives values similar to the baseline values, instead the CDF-t method forecasts an increase of the mean monthly precipitation of about 20 mm. During the summer months, the delta method gives lower values with respect to the actual ones, while the CDF-t method forecasts a marked decrease of rainfall from June to September (maximum decrease of -29 mm in June).

The forecasted temperatures are similar with both the downscaled method. A trend variation of temperature is not forecasted from the SRES scenarios but only an increase of the temperature in all the months. Therefore, the two downscaling methods give similar results.

In conclusion, from the results of this work, it seems evident that the CDF-t method is better than the delta method to downscale variables for which changes in the natural pathway are forecasted, but they are similar for variable maintaining the same trend in the future.
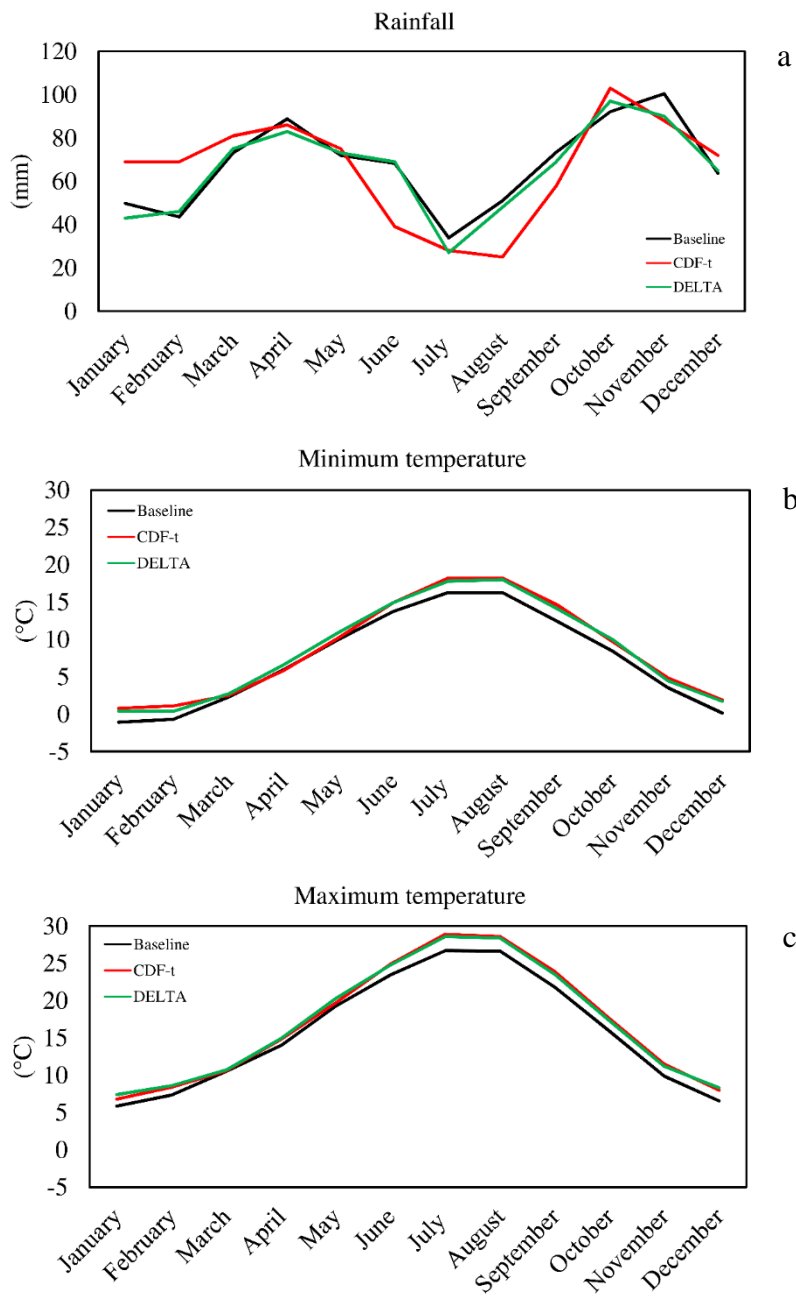
Figure 5.15 Average monthly climate data (rainfall (a), minimum (b) and maximum (c) temperature) for the baseline period (1984-2013; black line) and the future scenario (2021-2050) downscaled with the delta method (green line) and the CDF-t method (red line).

5.5.4 HARGREAVES POTENTIAL EVAPOTRANSPIRATION – BASELINE VS FUTURE

The observed and the downscaled data series have been used to assess the daily potential evapotranspiration with the Hargreaves equation as in section 4.1.1. The assessment has been executed only with the scenario downscaled with the CDF-t method and then the results have been used in the numerical modelling to assess the daily actual evapotranspiration (section 4.1.1). The more simplified delta change scenarios have not been utilised in the modelling part, so the evapotranspiration results have not been calculated nor reported.

The daily ET_0 values are then analysed. Assessed monthly evapotranspiration values are reported in Tab. 5.13. Results are coherent with the typical ranges for ET_0 values found in Allen et al. (1998), which for temperate humid/semi-arid regions indicates daily evapotranspiration between 1-3 mm. The average annual ET_0 is equal to 737 mm in the baseline period and it increases to 774 mm in the future period (+5%). An increasing of monthly evapotranspiration is visible in almost all the months (Fig. 5.16).

Averaged results are higher than the ones assessed with the Thornthwaite equation (section 5.1.3). This is probable due to the different time scale (monthly/daily). In fact, the Hargreaves formula allows the daily variabilities of temperature to be taken into account, whereas the Thornthwaite equation produces only an average monthly result.

Table 5.13 Hargreaves average monthly evapotranspiration for the baseline database (1984-2013) and the forecasted future scenario (2021-2050) downscaled with the CDF-t method, together with the corresponding mean annual values. Future values are reported as the ensemble means with the standard deviations (±σ).

	ET_0	
	mm	
	Baseline	Future
January	22	21±2
February	31	33±2
March	53	52±1
April	67	72±3
May	89	90±3
June	95	100±3
July	106	112±2
August	103	107±2
September	77	84±3
October	49	53±2
November	26	29±1
December	19	20±1
TOT.	737	774±7
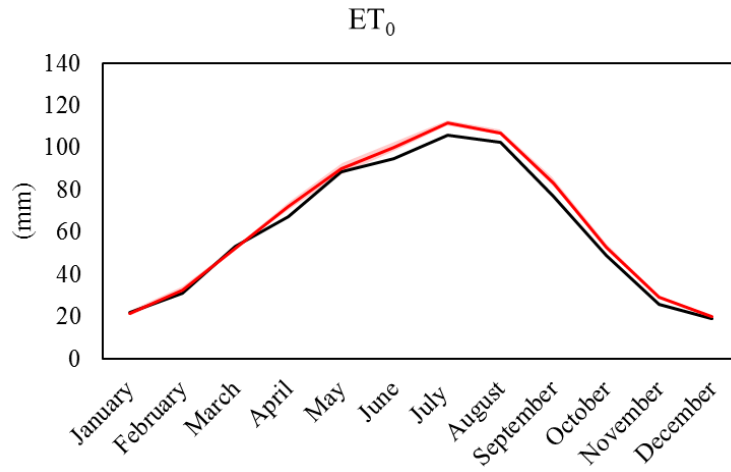
Figure 5.16 Comparison between average monthly Hargreaves evapotranspiration (ET_0) for the baseline period (1984-2013; black line) and the future scenario (2021-2050; red line) downscaled with the CDF-t method.

5.6 LOCAL SCALE MODEL

This work reports the first attempts to model the Mulino delle Vene fractured aquifer starting from data that have been collected in recent years and from the characterization of the aquifer by Cervi et al. (2014). The numerical modelling efforts have been carried out employing both finite elements techniques and some rainfall-runoff models.

Firstly, two finite elements models of the fractured aquifer have been built with the FEFLOW and the TRANSIN codes. The finite elements models of the area have the objective to understand the behaviour of the groundwater flow in the aquifer testing different conceptual models. Moreover, the calibrated models can be used to test different recharge conditions in order to quantify the effects on the springs discharge. Results obtained in this study will help in a better characterization of the area, investigating the hydrogeological interaction between the modelled hydrogeological unit and the surrounding units.

Secondly, the rainfall-runoff models allow forecasting the Mulino delle Vene springs discharge under future climate conditions. The results of these study could be useful to manage the groundwater resource in the Mulino delle Vene area. Moreover, as the Mulino delle Vene springs are the main water source of the Tresinaro stream, climate change impacts on the springs discharge will directly affect the stream discharge causing effects on a larger scale. Therefore, the results of the local scale models show the likely trend of effects of climate change on the catchment.

5.6.1 CONCEPTUAL MODEL

The conceptual model of the aquifer has been built according to the results of Cervi et al. (2014). In particular, Cervi identifies the recharge area as the outcrop of sandstone rock plateau (PAT4) and the Mulino delle Vene springs as the only outlet of the aquifer (Fig. 5.16). Therefore, the first tested local scale model reproduces the PAT4 sandstone formation (one layer) with no boundary conditions set on the borders, at exception of the springs locations. Models allowing a flow input from the west contact borders with sandstone (PAT) have also been tested to investigate the reliability of such a behaviour. Furthermore, the aquifer in the simulation area is known to be one and only, and unconfined (Cervi et al., 2014; Vizzi, 2014), so a phreatic water table has been simulated.

The models have been calibrated, firstly in steady-state condition and with an automatic procedure minimizing the residuals between the observed and the simulated piezometric levels in three observation points in the area (Fig. 5.17), secondly with a manual calibration with the objective to obtain a springs discharge equal to the observed one in addition to reasonable piezometric levels. Moreover, transient state simulation have been executed in order to analyse the transient behaviour of the fractured aquifer and verify the consistency of the model.

The three observation points are two civil wells (point 1-2) and a small lake (point 3). The first well is located in the upper part of a hill (712 m a.s.l.) and it is drill in the PAT4 unit. The second well and the lake are located on the alluvial deposits (Fig. 5.17b), in the bottom of a valley, respectively at the elevation of 608 m a.s.l. and 601 m a.s.l..

The observation points have been monitored three times during the 2013 autumn; observations are reported in Tab. 5.14. The steady-state simulations have been calibrated according to the average observed piezometric levels in each observation point. In particular, a point of the mesh is inserted in correspondence of each point location.
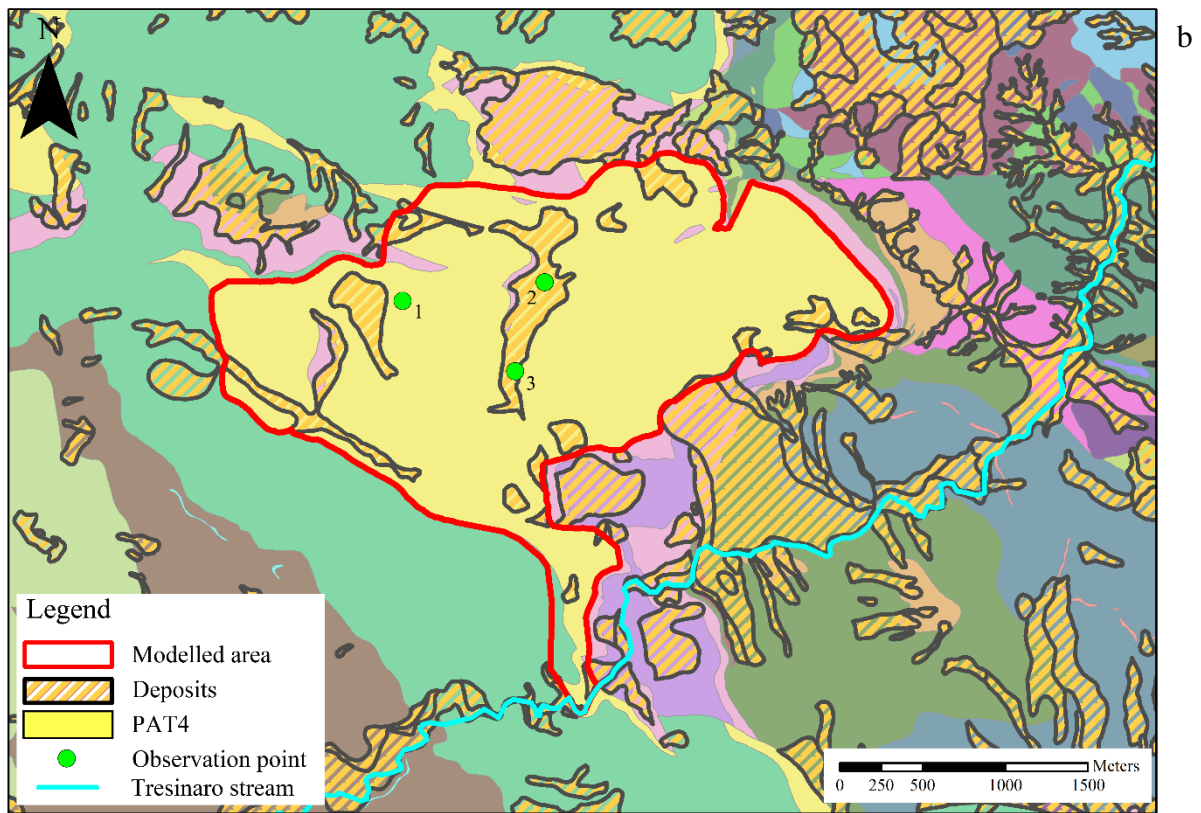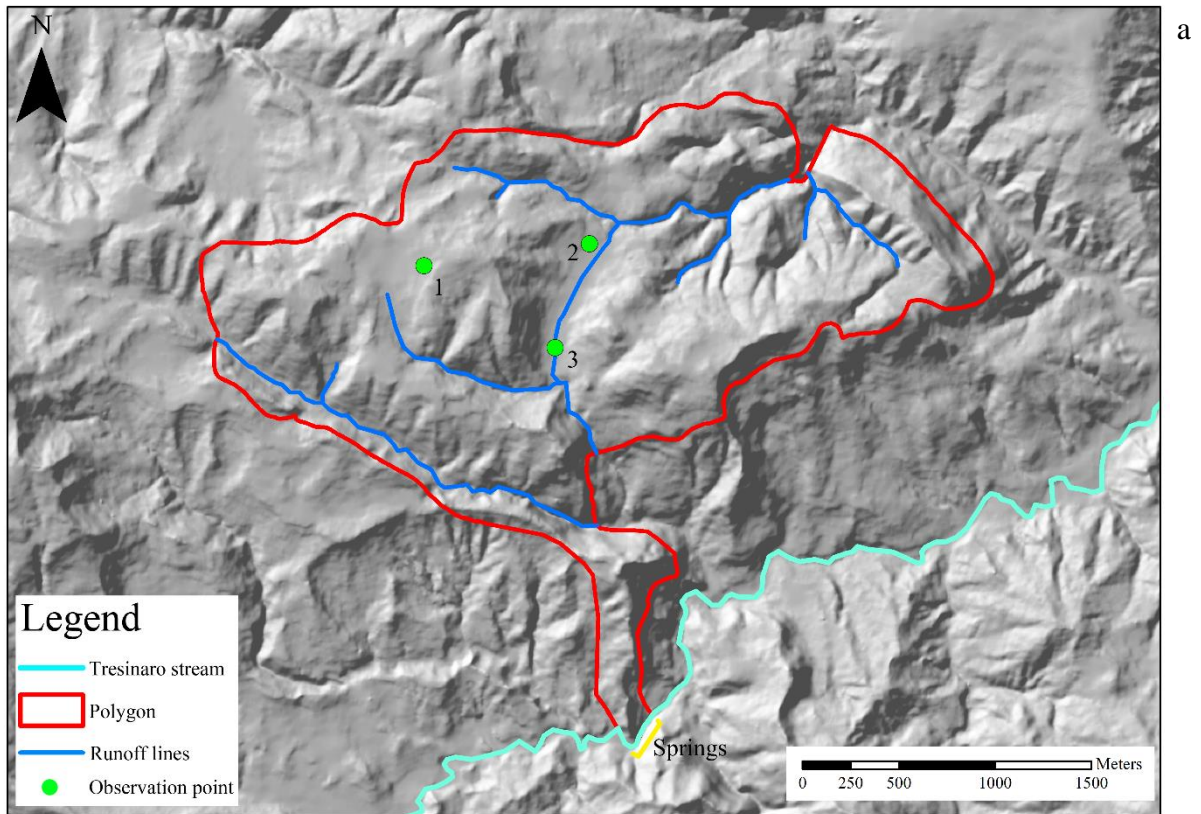
Figure 5.17 a, Digital Terrain Model of the Mulino delle Vene springs area and monitored observation points location. b, Geological map and deposits map along with the observation points location.

Table 5.14 Observed piezometric levels in the observation points.

Observation point	Location	Elevation (m a.s.l.)	Observed piezometric level (m a.s.l.)			Average piezometric level (m a.s.l.)
			25/09/2013	05/11/2013	26/11/2013	
1	Valcava	712.00	704.33	704.74	704.74	**704.60**
2	Pradola	608.00	606.75	606.95	607.01	**606.90**
3	Croveglia	601.00	599.80	599.80	600.30	**599.97**

5.6.2 FEFLOW MODEL

The 3D model has been built according to 8 geological cross sections in the area in addition to the results of the hydrogeological characterization of the Mulino delle Vene springs done by Cervi et al. (2013). Moreover, the data from a DTM with a cell size of 5x5m and the geological map of outcrops and deposits have been utilized. The generated mesh (Fig. 5.18) is composed by 6039 triangular elements with a total area of 5.6 km^2 (one layer composed by 6039 3D elements). This model has been initially used to calibrate model parameters with some steady-state simulations. The recharge has been assessed as the difference between the rainfall, the evapotranspiration (Hargreaves formula, section 4.1.1) and the runoff using data from the meteorological station of Carpineti. In particular, the runoff coefficient is set equal to 0.82, as estimated by Vizzi (2014) for this area. An average daily recharge about 1.6 mm/d has been assessed and it has been assigned uniformly on the model surface in the steady-state simulations.

In order to obtain a simulated piezometric level consistent with the topography, in particular following the valley shapes, boundary conditions of third type (Transfer in FEFLOW) have been applied along the main runoff lines highlighted in the hydrological analysis of the area (blue lines in Fig. 5.17a). In addition, a boundary condition of third type has been applied along the Mulino delle Vene springs line. All the boundaries have been coupled with a variable level equal to the topographic height (Model A).

Later, boundary conditions have been changed to test a different conceptual model. In particular, in a second model (Model B) an inflow from the sandstone units (PAT) has been added. Thereafter the heterogeneous properties of the medium have been taken into account dividing the PAT4 unit from the alluvial deposits. Tests have been made also changing the boundary conditions of the springs into a second type (Flux; Model C). Finally, a model with a higher conductivity area near the springs line and along the main fault of Rio Fontanello has been calibrated manually and also some transient state simulations have been carried out (Model D).

These models, if numerical instability problems do not occur, have been calibrated automatically with the PEST module (Parameter Estimator by Sequential Testing) integrated in FEFLOW. In particular, the automatic calibration minimize the weighted sum of squares of the residuals between measurement and simulation results (the objective function). The search algorithm used in PEST is the Gauss-Levenberg-Marquardt algorithm (GLMA). The GLMA changes the model parameters until a minimum objective function value is found.

The variables used in the automatic calibration are the piezometric levels. Unfortunately, there is not the possibility to calibrate automatically the springs outflow because the PEST tool integrated in FEFLOW 5.3 uses only hydraulic head for calibration. Therefore, a manual calibration has been also executed to maximise the simulated discharge performance.
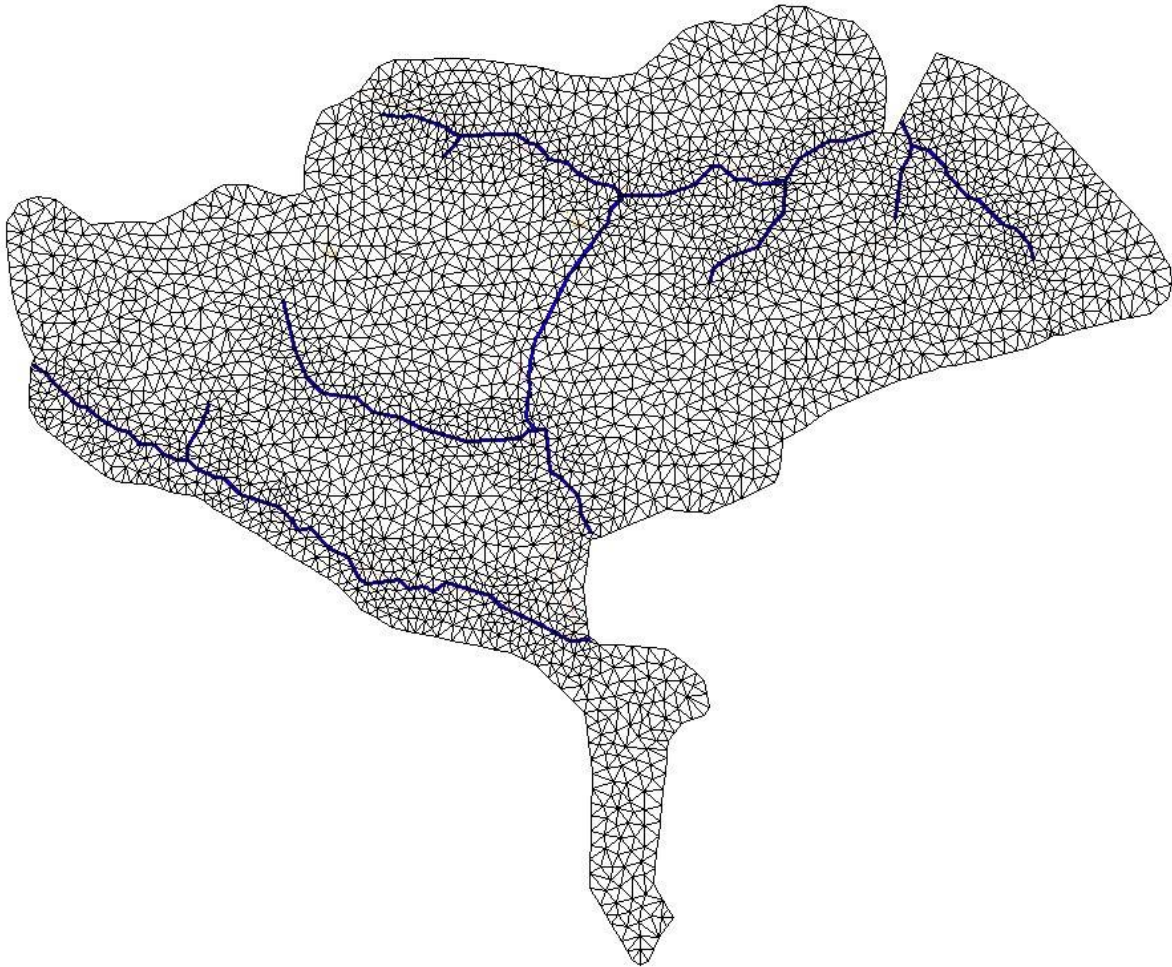
Figure 5.18 FEFLOW mesh and runoff lines (blue lines).

MODEL A

Firstly, Transfer rate in and out parameters and the hydraulic conductivity (K) values have been assigned from literature (Freeze & Cherry, 1979; Allen et al., 1997). After this, they are changed during the automatic calibration procedure of the steady-state simulation in order to better reproduce the mean piezometric level observed (Tab. 5.15). In this first model, the conductivity is considered homogeneous in the modelled volume.

The calibrated parameters are reported in Tab. 5.16, calibrated hydraulic conductivity of the sandstone layer (9.7×10^{-7} m/s) is characteristic of a massive sandstone (Freeze & Cherry, 1979; Civita, 2005). The Fig. 5.19 shows the simulated piezometric surface in the area, instead simulated level in the observation points are reported in Tab. 5.15 (correlation coefficient with the observed ones about 0.996).

Table 5.15 Observed and simulated piezometric level in the observation points.

	Observation point		
	1	2	3
Surface elevation (m a.s.l.)	712.00	608.00	601.00
Observed piezometric level (m a.s.l.)	704.60	606.90	599.97
Simulated piezometric level (m a.s.l.)	694.00	615.00	601.00

Table 5.16 Automatic calibrated parameters and simulated discharge of the springs.

K (m/s)	Transfer rate IN (1/d)	Transfer rate OUT (1/d)	Storativity	Storage (1/m)	Springs discharge (m³/d)
9.7×10^{-7}	1.9	121.5	10^{-2}	10^{-4}	326
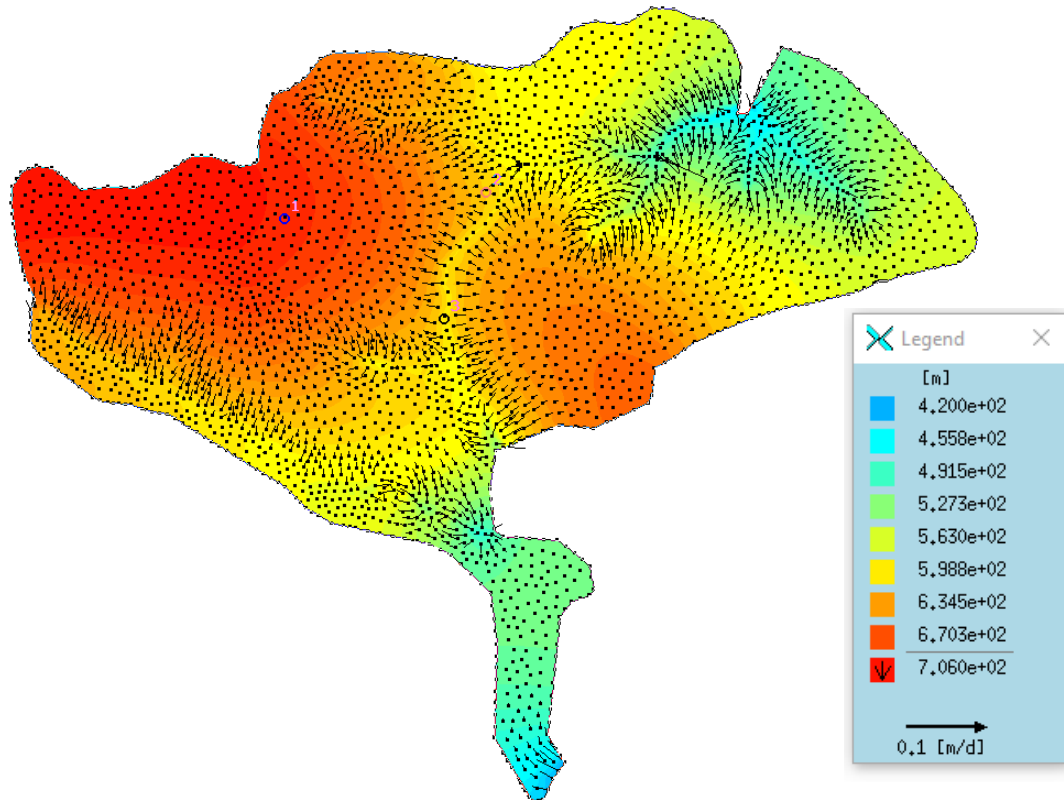
Figure 5.19 FEFLOW results, map of the simulated piezometric level (m a.s.l.).

The simulated output from the springs is about 326 m³/d, therefore it is lower than the mean observed discharge about 8363 m³/d. In this simulation, most of the recharge flows out from the runoff lines before to arrive to the springs. In fact, inserting the Transfer boundary condition along the runoff lines, a big amount of water flows out from them due to the geometric setting of the area (in particular from Rio Fontanello, in correspondence of a fault that cuts the area in proximity of the springs, Fig. 5.20). Nevertheless, a water table in agreement with the topographic surface is not simulated without inserting the transfer boundaries condition along the runoff lines. In particular, a piezometric level higher of the topographic surface is simulated in all the valleys, if the runoff lines are not considered as a boundary (Fig. 5.20). The possible reason for the modelling problems can be the high level of approximation due to the application of an equivalent porous medium instead of a discrete approach.
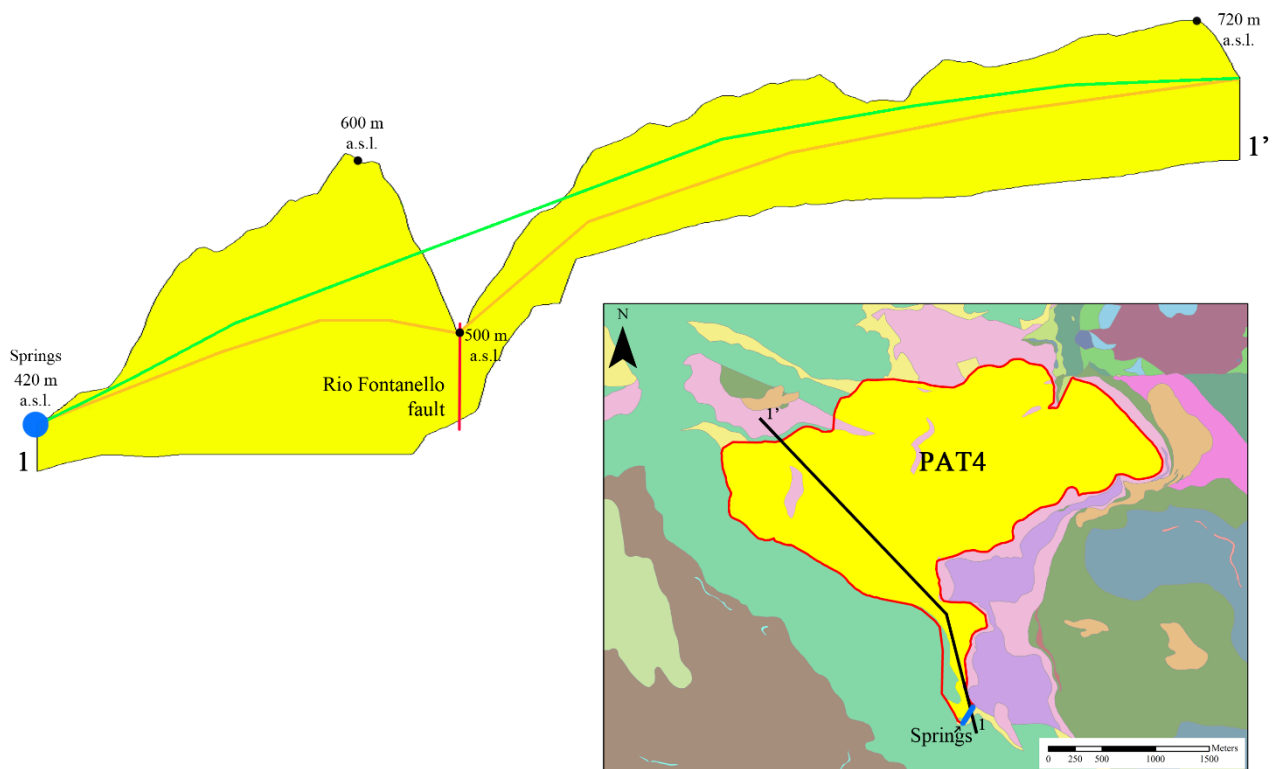
Figure 5.20 Section in the PAT4 plateau. The green line represent the possible simulated piezometric level obtained without inserting the boundary condition along the runoff lines. In orange the possible simulated piezometric level obtained with a boundary condition of third type along the main runoff lines.

MODEL B

Due to the difference between the simulated and the observed springs discharge and the impossibility to simulate such a discharge with the rainfall input of Model A only, a boundary inflow has been added. In particular, the geological and the topographical maps analysis has suggested a possible inflow at the contact with the PAT unit on the west border. In the north, instead, the model border is along the crest and in the south and east borders the marls and clays units surround the PAT4 unit (Fig. 5.21). In addition, some simulations have been done considering a possible exchange of water in all the north and northeast borders. Results always show that the flux exchange is not significant due to the topographic asset. Therefore, a boundary condition of second type has been applied along the west border of the domain in correspondence with the contact with the PAT unit. A similar approach is used by Brunetti et al. (2013) who assigns a specified flux boundary condition to one border of the model to simulate lateral recharge from a nearby unit. Considering only the area at north of the Tresinaro stream, the PAT outcrop area is 2.7 km^2, the 49% of the PAT4 outcrop (5.6 km^2). Considering a uniform recharge about 1.6 mm/d, the PAT unit can supply a recharge amount of 4529 m^3/d. A flux equal 0.018 m/d is used in order to simulate the inflow from the PAT. This value generates an inflow about 5879 m^3/d, that is bigger than the expected; anyway the simulation results are reported to show the behaviour of the simulated groundwater flow.

78
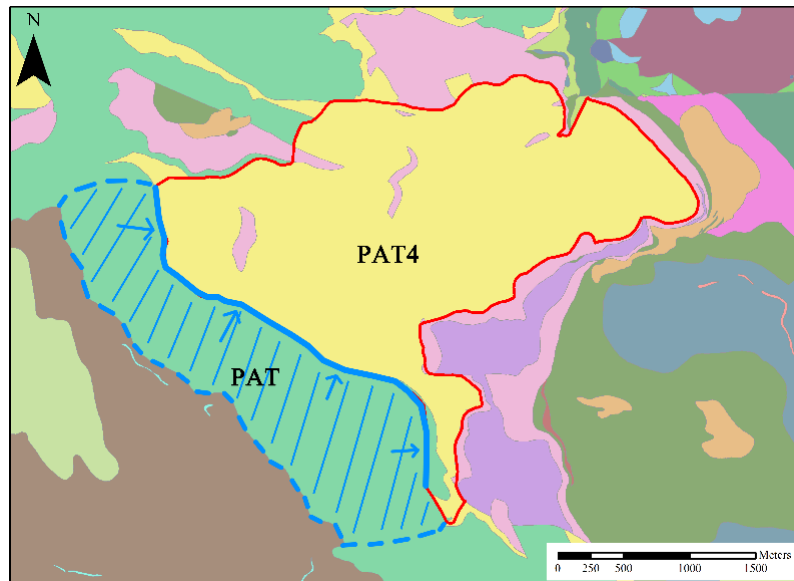
Figure 5.21 Geological map of the Mulino delle Vene springs area (geological map legend as in Fig. 3.3). Red line corresponds to the model border (PAT4 outcrop). Blue line is the contact with the PAT unit where the flux boundary conditions was added. The dashed blue area is the area of the PAT unit at north of the Tresinaro stream which has been considered to assess the possible inflow from the west.

Transfer rate in and out parameters and the conductivity values (K) have been changed during the automatic calibration procedure, in order to better simulate the mean level observed in the observation points (Tab. 5.14) and to be in accordance with the topographic surface. The simulated piezometric levels (Fig. 5.22) are quite consistent with the observed one (correlation coefficient of 0.999, a bit higher than the one of Model A) whereas the springs discharge is underestimated (Tab. 5.17 and Tab. 5.18).

Table 5.17 Calibrated parameters for Model B and simulated discharge of the springs.

K (m/s)	Transfer rate IN (1/d)	Transfer rate OUT (1/d)	Storativity	Storage (1/m)	Springs discharge (m³/d)
1.7×10^{-7}	10^{-3}	15.2	10^{-2}	10^{-4}	1661

Table 5.18 Observed and simulated piezometric level in the observation points.

	Observation point		
	1	2	3
Observed piezometric level (m a.s.l.)	704.60	606.90	599.97
Simulated piezometric level (m a.s.l.)	686.00	611.00	601.00
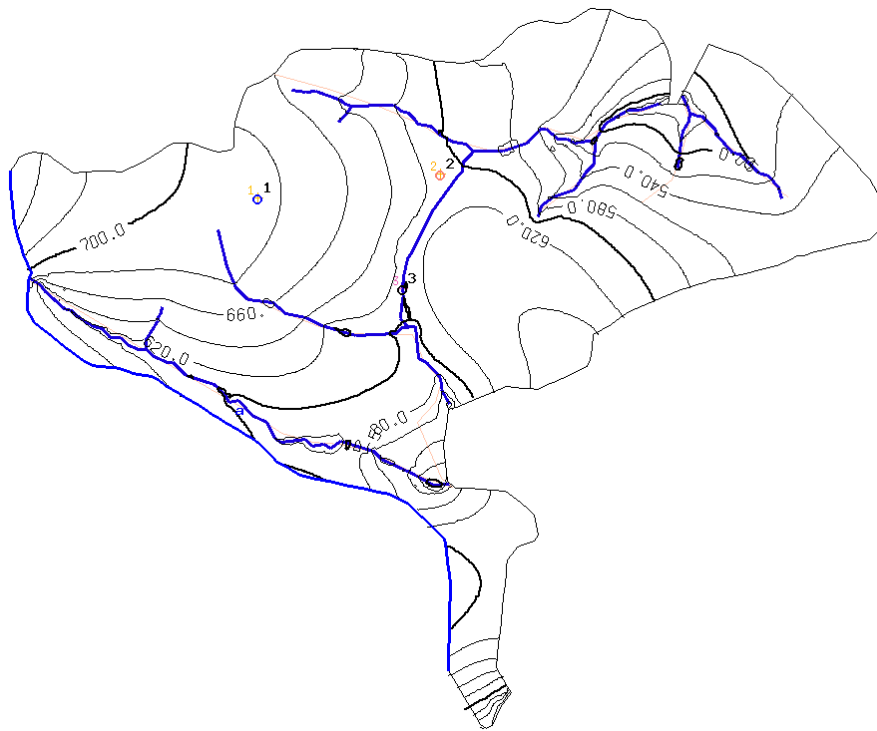
Figure 5.22 Simulated piezometric level. The runoff lines (3rd type boundary condition) and the inflow line from the west (2nd type boundary condition) are in blue.

Previous models consider the PAT4 plateau homogeneous and they do not take into account of the alluvial deposits in the area. Actually, on the main valley some alluvial or slope deposits are identified analysing the deposits map (Fig. 5.17b). Therefore, the deposits have been introduced as zones with higher conductivity values as in Fig. 5.23.
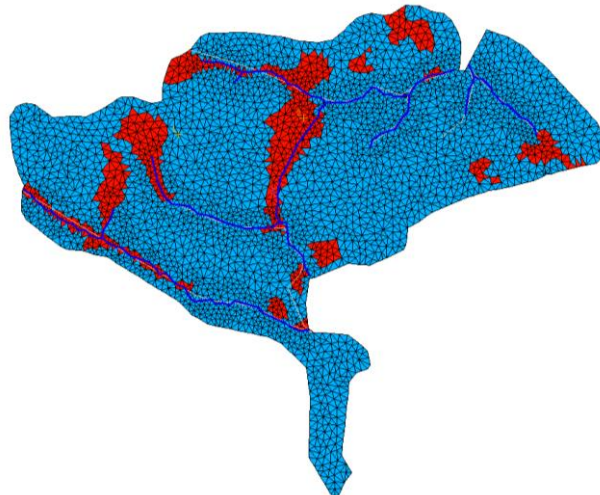
Figure 5.23 Model mesh. In red the deposit elements and in blue the PAT4 elements. The blue lines represent the Transfer boundaries conditions along the main runoff lines.

Thereafter, the model has been calibrated automatically and the final parameter values are reported in Tab. 5.19. As for the previous simulations, the water table in the observation points is simulated correctly (Tab. 5.20; Fig. 5.24) but the discharge of the springs is lower than the observed one. In particular, the correlation coefficient between the simulated and the observed piezometric levels in the observation points is about 0.999.

Finally, to obtain a higher springs discharge, the inflow rate from the west has been increased but then the simulations have became unstable. Therefore, the introduction of influx on the western border is not enough to simulate the observed discharge of the springs.

Table 5.19 Calibrated parameters for Model B with the deposits partition and simulated discharge of the springs.

K PAT4 (m/s)	K Deposits (m/s)	Transfer rate IN (1/d)	Transfer rate OUT (1/d)	Storativity	Storage (1/m)	Springs discharge (m^3/d)
$1.7*10^{-7}$	10^{-5}	53.1	53.1	10^{-2}	10^{-4}	1551

Table 5.20 Observed and simulated piezometric level in the observation points.

	Observation point		
	1	2	3
Observed piezometric level (m a.s.l.)	704.60	606.90	599.97
Simulated piezometric level (m a.s.l.)	686.00	605.00	601.00
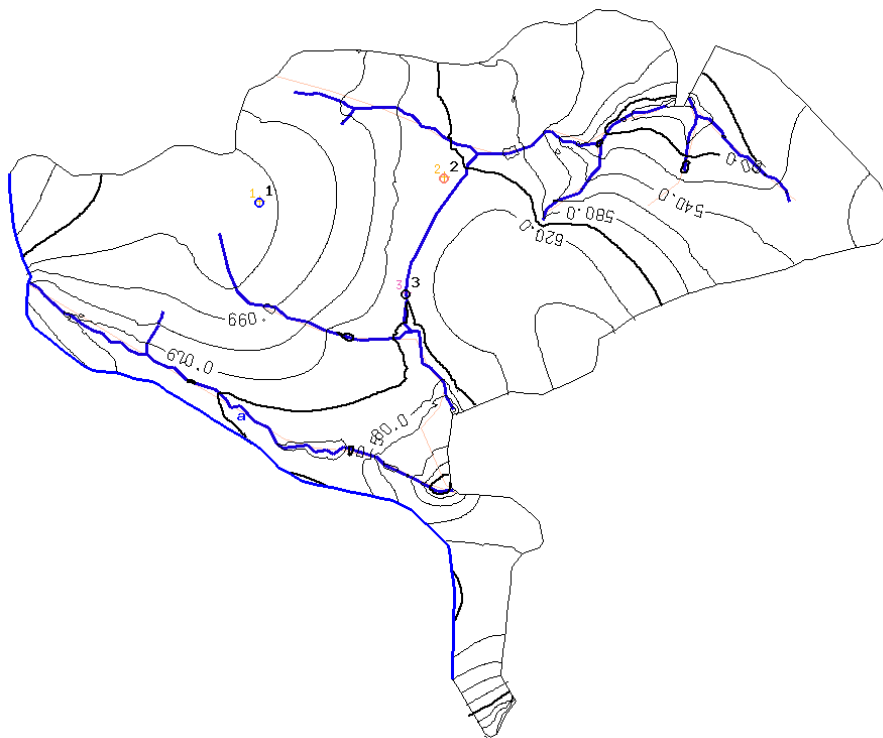
Figure 5.24 Simulated water table. The runoff lines (3rd type boundary condition) and the inflow line from the west (2nd type boundary condition) are in blue.

MODEL C

In this model, a flux boundary condition has been used to simulate the springs discharge along the springs line. The use of the flux condition allows to simulate the exact average observed discharge from the springs. Therefore, this model could be useful to investigate the piezometric surface that allows the flow of the observed springs discharge. Unfortunately, automatic calibration gives problems indicating an instable preconditioning error. Therefore, a manual calibration it has been necessary to face the instability problems. Finally, one of the results of the modelling attempts is reported below (Tab. 5.21, Tab. 5.22, Fig. 5.25). The simulated piezometric surface is not reliable. In fact, the simulated piezometric levels in the observation points are higher than the topographic surface, in particular in correspondence of point 2 and 3 the water table is 60 m above the surface.

Table 5.21 Parameters used in Model C.

K PAT4 (m/s)	K Deposits (m/s)	Transfer rate IN (1/d)	Transfer rate OUT (1/d)	Storativity	Storage (1/m)	Springs discharge (m^3/d)
$6*10^{-5}$	6×10^{-2}	3×10^{-4}	10^{-4}	10^{-2}	10^{-4}	10000

Table 5.22 Observed and simulated piezometric level in the observation points.

	Observation point		
	1	2	3
Observed piezometric level (m a.s.l.)	704.60	606.90	599.97
Simulated piezometric level (m a.s.l.)	671.00	668.00	668.00
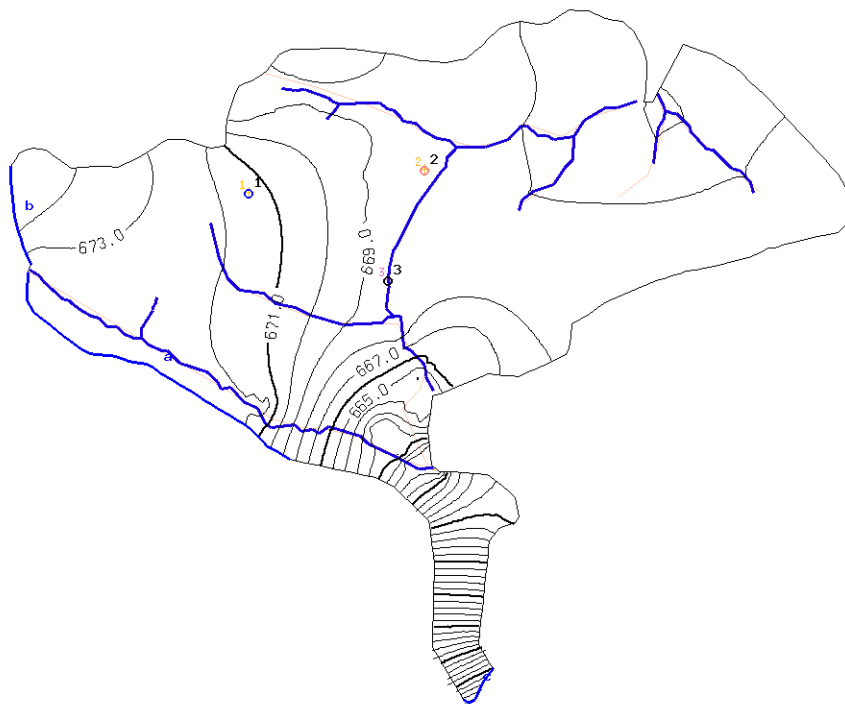
Figure 5.25 Simulated water table of Model C.

MODEL D

Since automatic calibrations are no successful, a manual calibration has been applied. At the beginning, a model similar to Model A has been used but it is impossible to simulate a higher springs discharge as the observed one, also introducing zones with higher conductivity. Thereafter, the boundary conditions of the model with the inflow from the west (Model B) have been tested.

Hereafter the results of the best simulation are reported. In order to increase the flux to the springs the conductivity of the area near the Rio Fontanello fault and the springs (red area in Fig. 5.26) are increased. This modification is necessary to let more water pass from the small volume under the transfer boundary condition along Rio Fontanello (Fig. 5.20). Actually, the fractured system is pivotal in the groundwater flow of the area, therefore zones with higher conductivity are used to reproduce the fractures. The main problem was that the FEFLOW model becomes unstable with such a modification and many simulations stop and do not converge.

Calibrated parameters are reported in Tab. 5.23 and the simulated water table is represented in Fig. 5.27. Moreover, the piezometric levels simulated in the observation points have a correlation coefficient of 0.9901 compared to the mean observed levels (Tab. 5.24).

The total inflow into the model is equal to 14581 m^3/d composed by: 9143 m^3/d (1.6 mm/d) of recharge, 4585 m^3/d from the 2nd type boundary condition and 853 m^3/d from 3rd type boundary conditions. The outflow from the model is 14581 m^3/d, of which 6400 m^3/d from the springs and the rest from the main runoff lines (3rd type boundary condition).
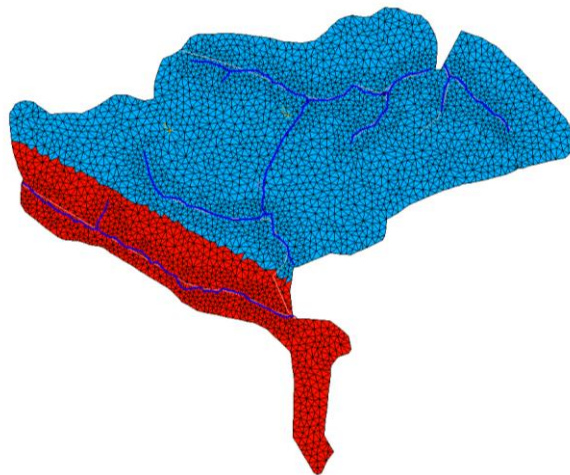
Figure 5.26 Map of the conductivity zone. In red the zone with increased conductivity along the Rio Fontanello fault and near the springs. In blue the remaining part of the PAT4 unit with a low conductivity.

Table 5.23 Manually calibrated parameters.

K PAT4 (m/s)	K fractured zone (m/s)	Transfer rate IN (1/d)	Transfer rate OUT (1/d)	Storativity	Storage (1/m)
5 x 10^{-7}	1 x 10^{-4}	3 x 10^{-4}	30	10^{-2}	10^{-4}

Table 5.24 Observed and simulated piezometric level in the observation points.

	Observation point		
	1	2	3
Observed piezometric level (m a.s.l.)	704.60	606.90	599.97
Simulated piezometric level (m a.s.l.)	698.00	621.00	601.00
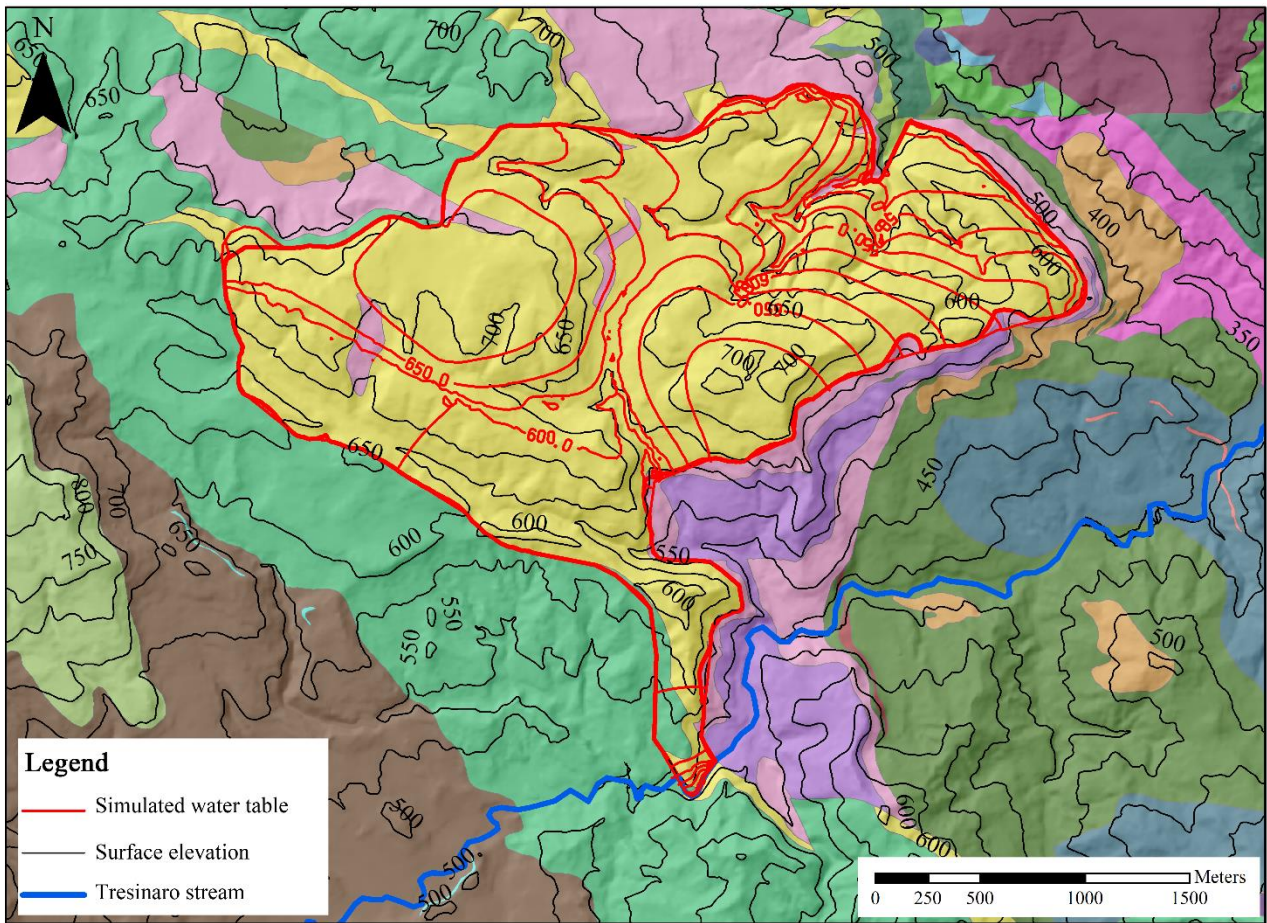
Figure 5.27 Contour map of the simulated piezometric levels (red lines) along with the surface elevation of the area (black lines) and the geological map (Geological map legend as in Fig. 3.3).

The simulated springs discharge (6400 m^3/d) is lower than the observed average springs outflow (8363m^3/d) by the 23%. However, this simulation is the most similar to the observed discharge conditions. For this reason, this model has been used for some transient simulation attempts. In particular, the period between the 11th March 2013 and the 15th November 2013 has been simulated inserting time-variable rainfall as top recharge (weather data from the Carpineti weather station). Storativity and storage values are changed to reproduce the observed discharge. In Tab. 5.25 and in Fig. 5.28 the parameters corresponding to the maximum Nash Sutcliffe Efficiency obtained and the correspondent discharge graph are reported.

Table 5.25 Parameters of the transient simulation.

K PAT 4 (m/s)	K fractured zone (m/s)	Transfer rate IN (1/d)	Transfer rate OUT (1/d)	Storativity	Storage (1/m)
5 x 10^{-7}	1 x 10^{-4}	3 x 10^{-4}	30	2 x 10^{-4}	2 x 10^{-5}
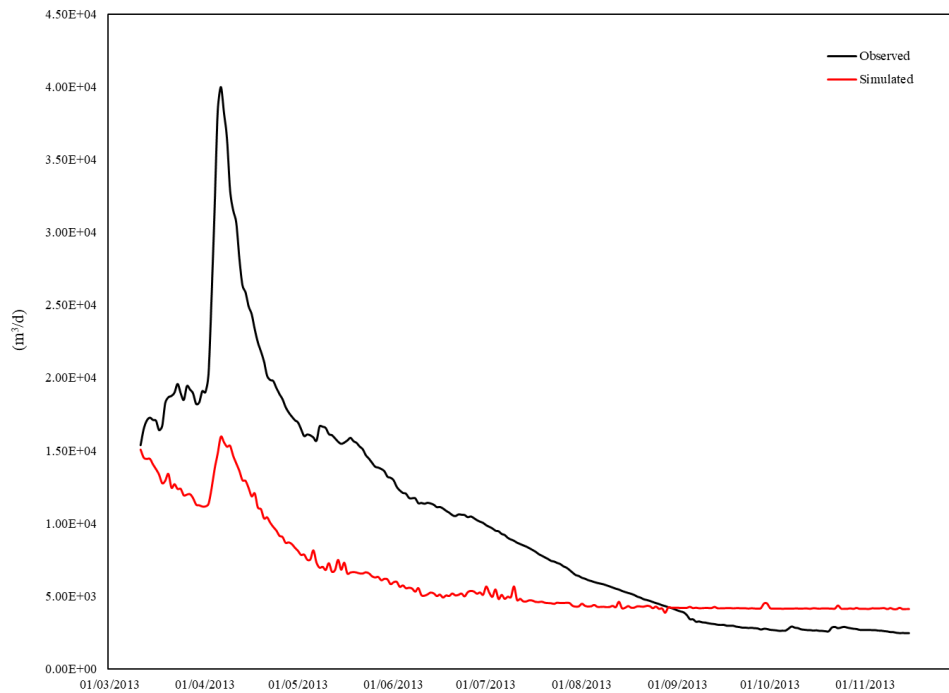
Figure 5.28 Observed and simulated discharge of the Mulino delle Vene springs in the transient state simulation with Model D.

This transient simulation shows two main problems. The first problem is that it cannot simulate the springs discharge inserting the observed rainfall as recharge (maximum NSE obtained in calibration equal to -1.6). It is possible to reproduce the observed discharge only using a rainfall 5 or 10 times higher than the observed one. The second problem is the simulated piezometric level. During rainfall events with a high recharge value, the simulated water table increases a lot (about 100 m) and it exceeds the topographic surface quite everywhere (Fig 5.29).
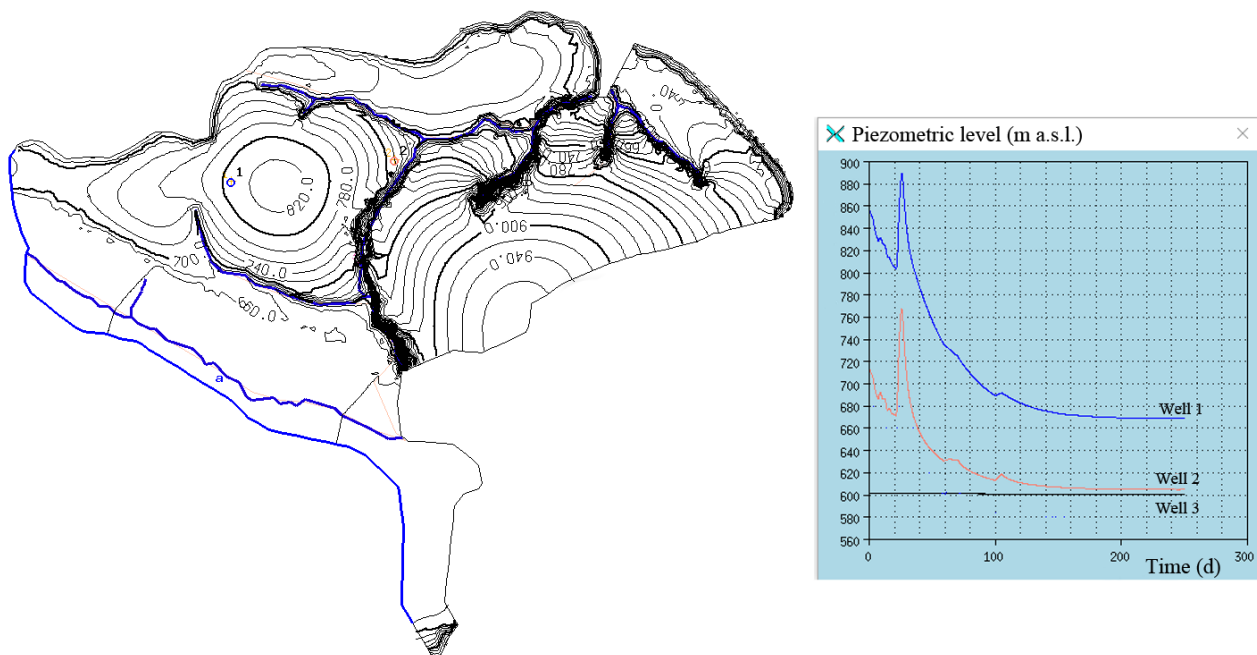
Figure 5.29 Map of the piezometric surface during a recharge event and graph of the simulated piezometric levels in the three observation points during the transient simulation.

From these results, it is clear that this model cannot work in transient state simulation. In particular, from these simulations it appears impossible that the PAT 4 formation only contributes to the springs discharge. This could be an effect of the equivalent porous medium assumption. Actually, the observed springs discharge comes from a complex system of faults and fractures and not from the flow in the entire medium. To simulate this, it is necessary to insert high conductivity areas near the Rio Fontanello and the springs but from the simulations done until now it seems not enough. In fact, a good simulation of both the observed springs discharge and of the piezometric surface has not been achieved neither with a steady-state nor with a transient state simulation. Therefore, a change of the conceptual model will be considered in future studies.

Furthermore, the high instability of the simulations is problematic. In fact, many models did not converge in steady-state and results were not displayed. Moreover, the manual calibration is very difficult especially if the simulation does not converge. For this reason, in the next section a model has been built with a different code.

5.6.3 TRANSIN MODEL

STEADY-STATE SIMULATIONS

The second hydrogeological model of the aquifer has been built with the TRANSIN code considering the DTM of the area and the 8 available geological cross sections (Petronici et al., 2017b). The generated mesh has 3289 nodes and it is restricted along the runoff lines (Fig. 5.30), so the runoff lines correspond to the element borders. The topographic surface as well as the thickness of the modelled layer are very variable. In particular, there is a large difference in elevation between the springs elevation (420 m a.s.l.) and the higher part of the hills (740 m a.s.l., Fig. 5.31). The thickness of the layer is also very variable due to the non-homogeneous characteristics of the area with hills and valleys (Fig. 5.20). In fact, near the observation point 1 the layer thickness is about 150 m and near points 2 and 3 is about 5 or 20 m.
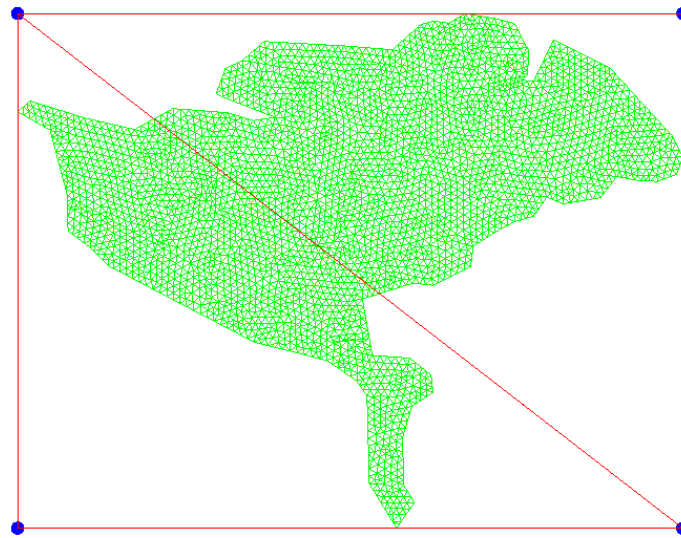
Figure 5.30 Mesh built with TRANSIN.
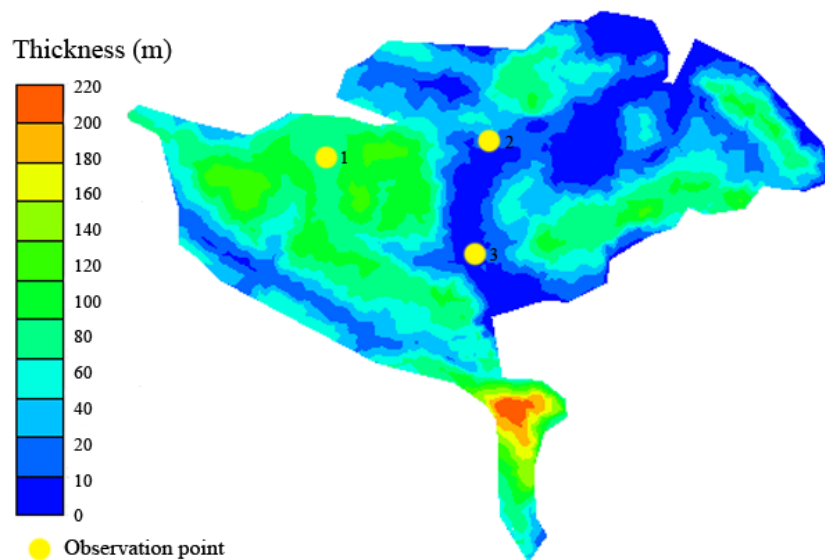
Figure 5.31 Thickness map.

The recharge has been assigned uniformly on the surface area. In particular, it is assessed as the difference between the rainfall and the evapotranspiration from the Hargreaves formula (section 4.1.1), considering an infiltration coefficient equal to 0.82 as assessed by Vizzi (2014) on annual time scale.

The automatic calibration has been carried out in the steady-state condition minimizing the differences between the observed and the simulated piezometric levels in the three observation points in the area (Tab. 5.14). Then, a manual calibration has been used to maximize the reliability of the simulation result. Moreover, a piezometric surface congruent with the topographic height has been investigated.

Finally, two models that reproduce well the observed data have been obtained. In the first model (Model 1), a flux boundary condition has been set along the springs. This model has been used in transient state to simulate the possible transient behaviour of the aquifer. In the second model (Model 2), a leakage condition has been set on the springs and then this model has been used in steady-state condition to simulate the effects of a recharge change on the spring discharge.

MODEL 1 A
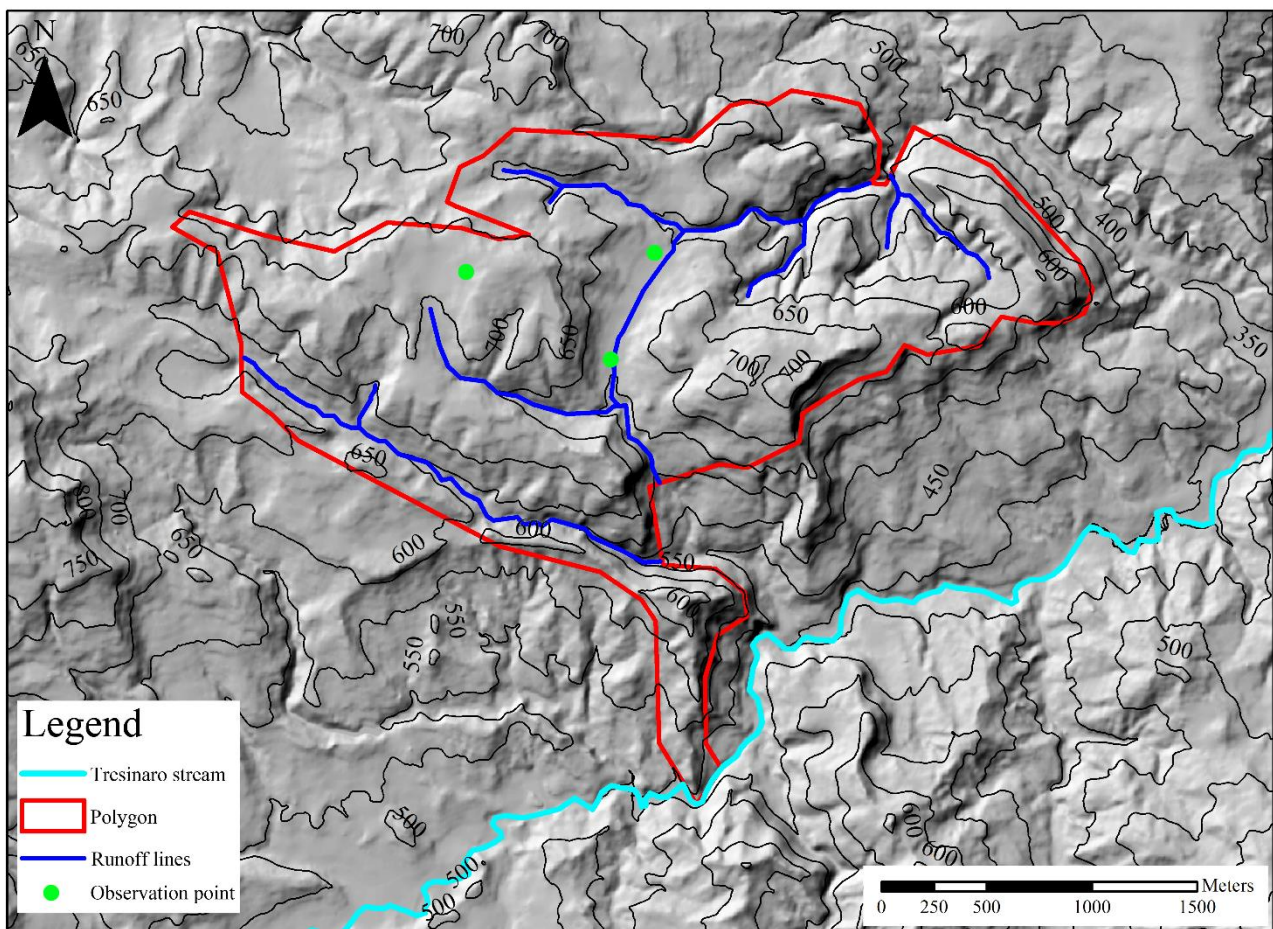
Figure 5.32 Polygon of the Transin model. The blue lines represent the main runoff lines founded in the hydrological analysis of the surface.

In the first model, a flux boundary condition has been applied along the springs line in order to reproduce the observed springs discharge. Moreover, a leakage condition has been applied along the main runoff lines (Fig. 5.32) in combination with a head equal to the topographic surface. Preliminary steady-state simulations have been used to calibrate the hydrogeological properties of the formations. The assigned mean recharge is 1.6 mm/d (9165 m^3/d) and the assigned springs discharge is equal to 9116 m^3/d (105 l/s, average discharge between the 2013 and the 2015). This value is a bit greater (+9.6%) than the average observed value in the period 2013-2016 (8363 m^3/d). Nevertheless, this value it has been used in Model 1 because it is more representative of the

periods that after it has been analysed in the transient state simulations (11th July 2013 - 31st November 2013 and 13th February 2014 - 28th February 2015). Moreover, Model 1A has been split in several areas with different parameters (Fig. 5.33a). In particular, the southern area from the springs to the main fault along Rio Fontanello (A) has been considered as a more permeable area that directs the groundwater flow to the springs. The alluvial and slope deposits have been defined as a different zone (B). Finally, the others part of the PAT4 outcrop have been considered homogeneous and less permeable (C).

The results of the automatic calibration of parameters (hydraulic conductivity, K; leakage coefficient, L), minimizing the differences between the simulated and the observed mean level in the three observation points, are reported in Tab. 5.27. All the values belong to the ranges found by Allen et al. (1997) and Zhang & Hiscock (2010) for sandstone rock masses. Simulated outflow from the runoff lines is about -49 m^3/d. The simulated levels in the observation points are reported in Tab. 5.26 and the simulated piezometric surface in Fig. 5.33b. Simulated levels in point 2 and point 3 have only a difference of few meters from the observed values, instead the simulated level in point 1 is lower than the mean observed value (difference of -18.2 m). The correlation coefficients and the Nash-Sutcliffe efficiency are respectively equal to 0.99 and 0.94, comparing observed and simulated values.

Table 5.26 Automatic calibrated parameters of model 1.

K A (m/s)	K B (m/s)	K C (m/s)	Storage	L stream (1/d)
6.25×10^{-5}	8.68×10^{-5}	9.26×10^{-7}	0.1	7.4×10^3

Table 5.27 Observed and simulated piezometric level (m a.s.l.) and water depth (m) in the three observation points.

Observation point	1		2		3	
Observed	704.6	-7.4	606.9	-1.1	599	-2
Simulated	686.4	-25.8	601.6	-6.4	602	+1
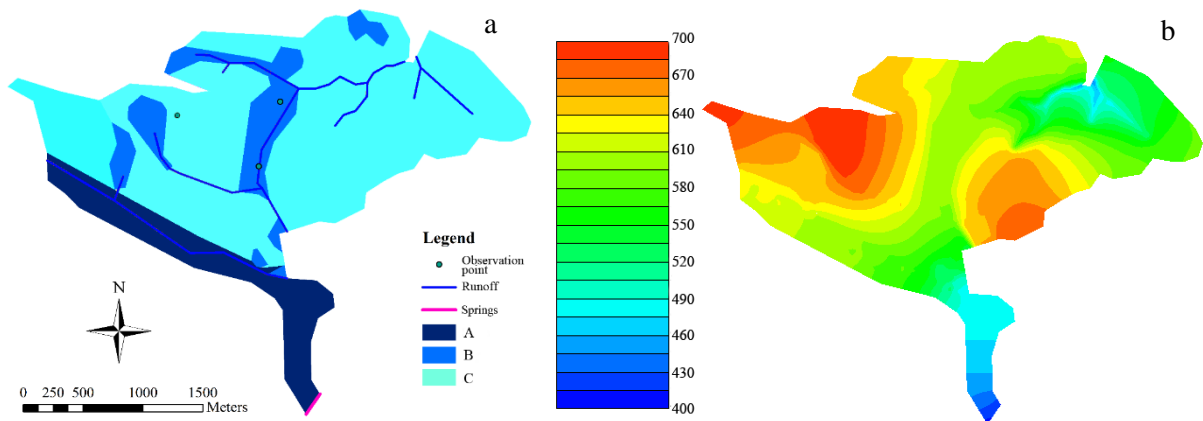
Figure 5.33 a, Modelled area with zones. b, Simulated piezometric surface (m a.s.l.).

MODEL 1 B

To increase the accuracy of the simulation in well 1 a manual calibration has been applied. If the conductivity of the all C area decreases, then the simulated level in well 1 becomes more similar to the observed one but in the other parts of the domain the simulated level exceeds the topographic elevations. Therefore, the domain of Model 1B has been divided into four parts (Fig. 5.34a):

A: Fractured rock mass from the springs to the main fault of Rio Fontanello;

B: Alluvial and slope deposits;

C: Massive sandstone rock mass PAT4;

D: Less fractured sandstone rock mass (hill near the observation point 1).

The results of the automatic calibration of parameters (hydraulic conductivity, K; leakage coefficients, L), minimizing the differences between the simulated and the observed mean level in the three observation points, are reported in the Tab. 5.28. The calibrated permeability for the less fractured sandstone (K D) is very low (2.31×10^{-7} m/s). This is probably due to the higher thickness of the modelled layer in the D zone than in the rest of the domain (Fig. 5.31). In particular, the in-depth sandstones are less fractured/fissured than the surficial ones (as evident comparing the conductivity values from the well test and the outcrops analysis, Tab. 3.1 in section 3.2), therefore the equivalent porous medium conductivity of the layer elements is lower in the D zone (high elements) than in the remaining parts of the domain. Anyway, all the used values belong to the sandstones range found by Allen et al. (1997). The outflows from the runoff lines and from the springs were respectively 49 and 9116 m³/d. The simulated levels in the observation points and the simulated piezometric surface are reported in Tab. 5.29 and Fig. 5.34b. The correlation coefficients and the Nash-Sutcliffe efficiency are respectively equal to 0.99 and 0.99.

Table 5.28 Automatic calibrated parameters of model 1B.

K A (m/s)	K B (m/s)	K C (m/s)	K D (m/s)	Storage	L stream (1/d)
6.25×10^{-5}	8.68×10^{-5}	9.26×10^{-7}	2.31×10^{-7}	0.1	7.4×10^{3}

Table 5.29 Observed and simulated piezometric level (m a.s.l.) and water depth (m) in the three observation points.

Observation point	1		2		3	
Observed	704.6	-7.4	606.9	-1.1	599	-2
Simulated	704.2	-7.8	601.5	-6.5	601.5	+0.5
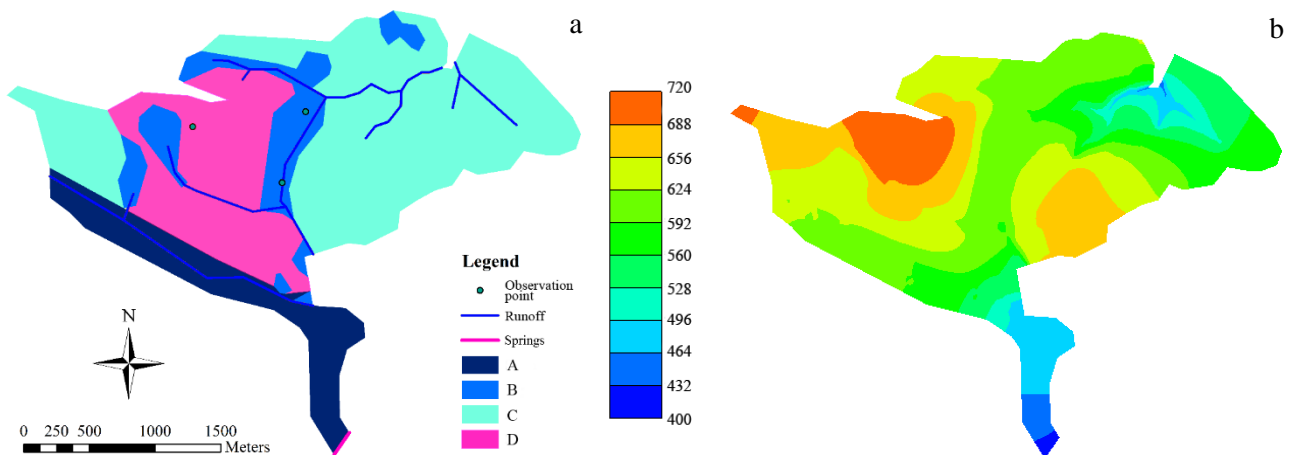
Figure 5.34 a, Modelled area and zones division. b, Simulated piezometric surface (m a.s.l.).

MODEL 1C

The third tested model is similar to Model 1A (Fig. 5.33a), with additional boundary conditions on the West part. In particular, the possibility of a water influx from the PAT sandstone on the West (as in the FEFLOW model) has been tested. The flux has been set equal to the mean infiltrated volume in the PAT area (4578 m^3/d). Then, the model has been automatically calibrated in order to reproduce the mean hydraulic head observed in the three observation points (Tab. 5.30). The parameters resulting from calibration are summarized in Tab. 5.30. As for Model 1A, the simulated level in point 1 is lower than the observed one of about 20 m, instead the other points are better simulated. The simulated piezometric surface is represented in Fig. 5.35. The correlation coefficients and the Nash-Sutcliffe efficiency are respectively equal to 0.99 and 0.92. The springs discharge is always the same of Model 1A, but the outflow from the runoff lines increases to 4373 m^3/d and the automatically calibrated leakage coefficient increases to 207907 d^{-1}. Actually, such a runoff is not evident in the area, for this reason conceptual Model 1C has been considered to be unreliable.

Table 5.30 Automatic calibrated parameters of Model 1C.

K A (m/s)	K B (m/s)	K C (m/s)	Storage	L stream (1/d)
6.02×10^{-5}	1.57×10^{-3}	2.31×10^{-6}	0.1	2.1×10^5

Table 5.31 Observed and simulated piezometric level and water depth (m) in the three observation points.

Observation point	1		2		3	
Observed	704.6	-7.4	606.9	-1.1	599	-2
Simulated	683.4	-28.6	601.3	-6.7	602	+1
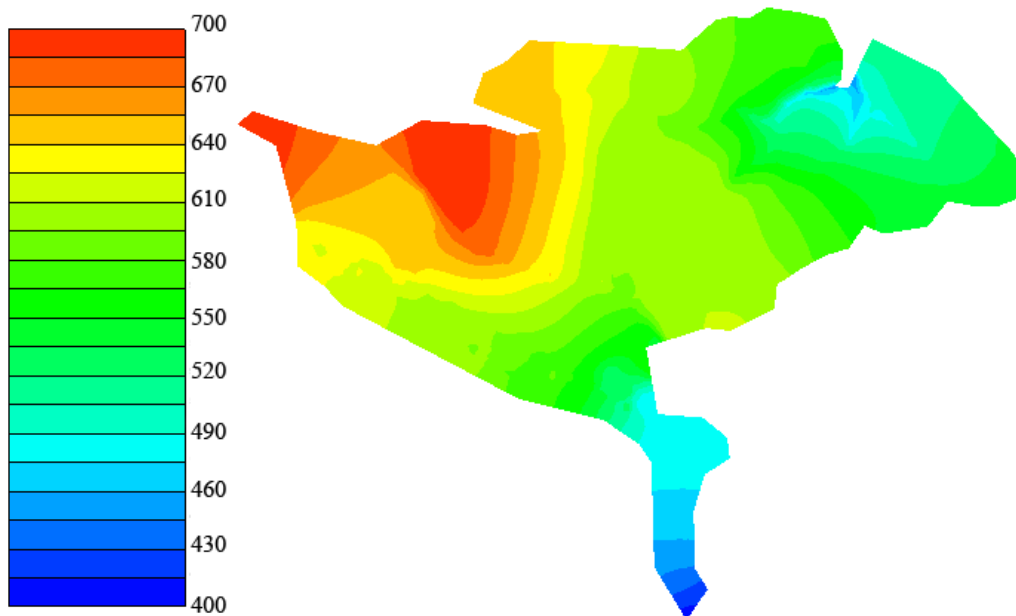
Figure 5.35 Simulated piezometric surface (m a.s.l.).

MODEL 2

In the second model, both the streams and the springs have been represented as leakage lines correlated to a head value equal to the elevation. The assigned mean recharge is 1.6 mm/d (9165 m^3/d). As for Model 1B, to obtain a simulated water table consistent with the topography and the field observations, the PAT4 unit has been divided in four areas (Fig. 5.34a).

Calibration of parameters has been carried out minimizing the differences between the simulated and the observed mean piezometric level in the three observation points. Moreover, it has been searching for a simulated springs discharge equal to the observed one. Resulting parameters (hydraulic conductivity, K; leakage coefficients, L) are reported in Tab. 5.32 and they are in accordance with values reported for sandstones published by Allen et al. (1997). The simulated water table and the level in the observation points are reported respectively in Fig. 5.36 and in Tab. 5.33. The correlation coefficient of the levels in the observation points is about 0.9977 and the Nash-Sutcliffe efficiency is 0.9954. The simulated discharge from the springs is about 8626 m^3/d (94% of the recharge) and the output from the streams is about 539 m^3/d (6% of the recharge). Therefore, the simulated and the average springs discharge (8363 m^3/d, period 2013-2016) differs only about the 3.1%.

Table 5.32 Automatic calibrated parameters of Model 2.

K A (m/s)	K B (m/s)	K C (m/s)	K D (m/s)	Storage	L stream (1/d)	L springs (1/d)
1.16×10^{-4}	1.04×10^{-4}	6.94×10^{-5}	1.16×10^{-7}	0.2	1.1	2.1×10^4

Table 5.33 Observed and simulated piezometric level and water depth (m) in the three observation points.

Observation point	1		2		3	
Observed	704.6	-7.4	606.9	-1.1	599	-2
Simulated	704.2	-7.8	602.4	-5.6	602.4	+1.4
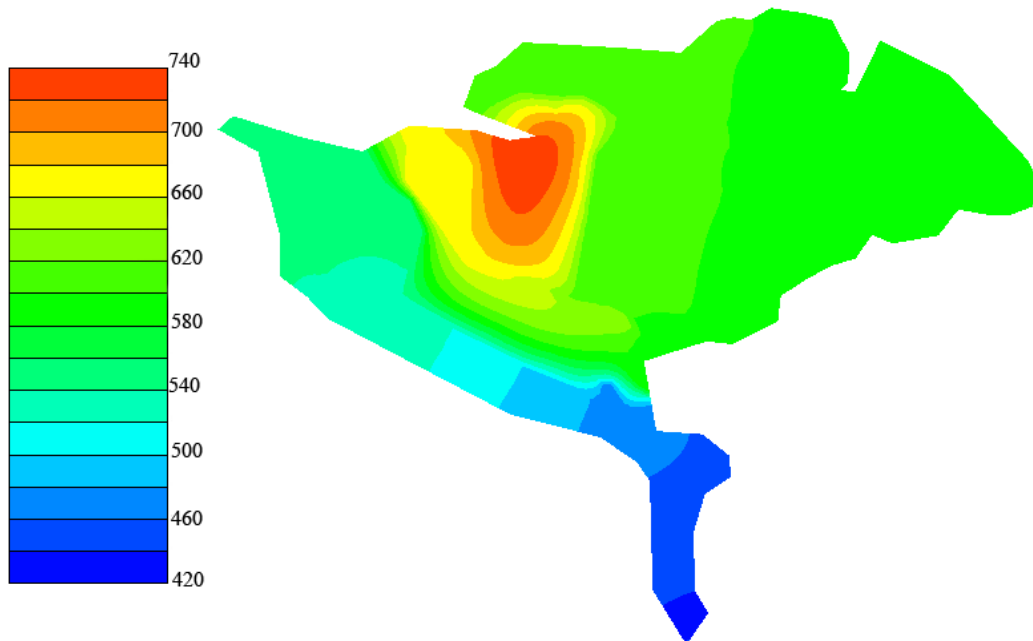
Figure 5.36 Simulated piezometric surface (m a.s.l.).

SIMULATIONS USING EXCEPTIONAL RECHARGE VALUES

Model 2 has been used to investigate the possible behaviour of the aquifer under exceptional recharge conditions. Analysing the historical data from the Carpineti weather station, the driest year is the 2011, with an annual rainfall about 544 mm and an estimated recharge of 351 mm (64% of rainfall). The mean annual recharge is assessed as the difference between the rainfall and the potential evapotranspiration calculated with the Hargreaves formula, and considering an infiltration coefficient equal to 0.82 (Vizzi, 2014). The wettest year occurs in the 1960 with observed precipitation of about 1358 mm. In absence of temperature data, the direct evaluation of the evapotranspiration has not been possible so the recharge has been estimated using the same coefficient assessed for the present-day period. In particular, considering an evapotranspiration percentage equal to the mean assessed during the years 2009-2015, the 1960 recharge amounted to 920 mm (67% of rainfall). Steady-state simulations have been carried out under these exceptional conditions, changing the recharge from the observed mean value (1.6 mm/d) to the two extreme values of 0.96 mm/d (351 mm/year) and 2.5 mm/d (920 mm/year). In addition, the permeability of the D zone has been changed in order to obtain a reliable piezometric surface.

DRIEST CONDITION

The driest condition is registered in 2011. The annual rainfall amount is 544 mm (-40% than the mean value) concentrated at the beginning of spring and in autumn. During almost all the months, a rainfall lower than the monthly mean is observed, varying from the +13% of March to the -94% in August.

To simulate the effects of such a dry condition, a steady-state simulation has been carried out with the Model 2 changing the recharge to the mean annual value assessed for 2011. In this dry condition, the permeability of the D zone (K_D) has been decreased to 6.94×10^{-8} m/s in order to obtain piezometric levels comparable to the observed ones. Without such a change, the simulated water table in point 1 decreases about 100 m. In Tab. 5.34 are reported the parameters used in simulation.

The simulated piezometric surface (Fig. 5.37) decreases in all the area and in particular in the South. In well 1 the piezometric level decreases to 694.5 m (minus 9.7 m from the simulated value of Model 2). In the two observation points in the valley (point 2 and point 3) instead the decrease is about 1.4 m (Tab. 5.35).

The simulated discharge from the springs is equal to the recharge, therefore it amounts to 5499 m^3/d with a decrease about the 36% from the mean simulated discharge of Model 2.

Table 5.34 Parameters used in the driest conditions.

K A (m/s)	K B (m/s)	K C (m/s)	K D (m/s)	Storage	L stream (1/d)	L springs (1/d)
1.16×10^{-4}	1.04×10^{-4}	6.94×10^{-5}	6.94×10^{-8}	0.2	0.65	2.1×10^{4}

Table 5.35 Simulated piezometric level (H, m a.s.l.) and water depth (m) in the three observation points.

Observation point	1	2	3
H	694.5	601	601
Water depth	-17.5	-7	0
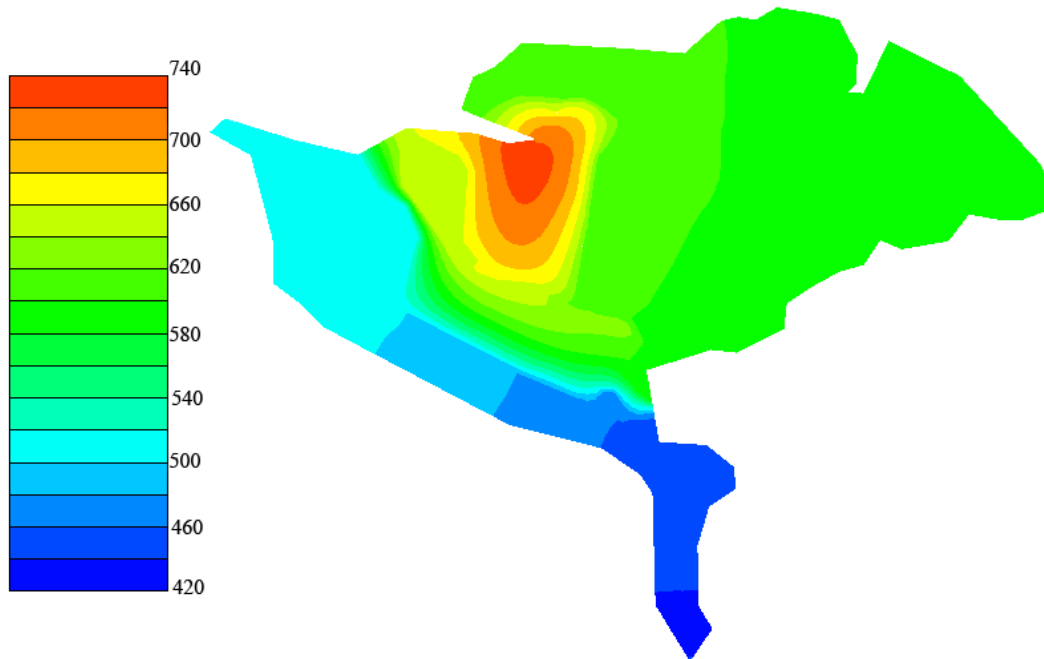
Figure 5.37 Simulated piezometric surface (m a.s.l.).

WETTEST CONDITION

The observed wettest year is 1960 with a total rainfall amount of 1358 mm. A particular wet spring and autumn generate an increase of the rainfall of about the +60% with respect to the average. In particular, the monthly rainfall changes from the +121% of July to the -37% of May if compared to the mean monthly values.

Steady-state simulation in this wet condition has been carried out to evaluate the effects on the springs discharge and on the piezometric surface. The parameters used in this simulation are summarized in Tab. 5.36. The permeability of the D zone (K D) has been changed to 1.96×10^{-7} m/s in order to obtain a water table consistent to the topography surface but major than the ones simulated in the average recharge condition (Model 2).

The simulated levels in the three observation points are reported in Tab. 5.37 and the simulated piezometric surface in Fig. 5.38. Comparing the simulated levels to the ones simulated in the mean condition of Model 2, in all the observation points the level increases. In particular, in well 1 the increase is about 3.8 m, in well 2 about 4.6 m and in point 3 about 1.1 m. The simulated discharge from the springs is about 11170 m^3/d, the 30% more than the mean value of Model 2. The increase of the recharge is not equal to the increase of springs discharge because the outflow from the runoff lines increases to 3450 m^3/d as well. In particular, in the wettest condition, the output from the streams is about the 23% of the recharge and the springs discharge is the 77%.

Table 5.36 Parameters used in the wettest conditions.

K A (m/s)	K B (m/s)	K C (m/s)	K D (m/s)	Storage	L stream (1/d)	L springs (1/d)
1.16×10^{-4}	1.04×10^{-4}	6.94×10^{-5}	1.96×10^{-7}	0.2	1.8	2.1×10^4

Table 5.37 Simulated piezometric level (H, m a.s.l.) and water depth (m) in the three observation points.

Observation point	1	2	3
H	708	607	603.5
Water depth	-4.0	-1.0	+2.5
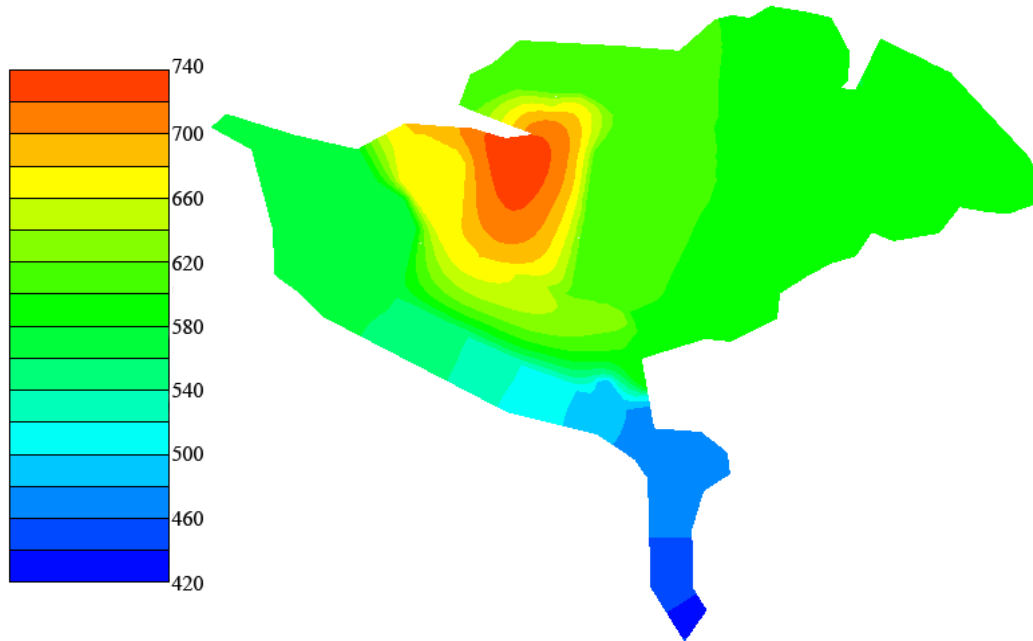
Figure 5.38 Simulated piezometric surface (m a.s.l.).

DISCUSSION

The simulations in the exceptional conditions have allowed a sensitivity analysis of the recharge to be carried out. Moreover, the results show the variations of the levels in the observation points. In particular, in well 1 the level changes from a water depth of -17.5 m in the driest condition to -4.0 m in the wettest condition, with a change of -9.7 m and +3.8 m from the simulated level in the mean recharge condition. The changes are less evident in the observation points 2 and 3, in particular a decrease of 1.4 m is simulated in the dry condition for both the pints and an increase of 4.6 m and 1.1 m in the wet condition respectively for point 2 and point 3. Therefore, the groundwater level in the D zone appears to be the more sensitive to changes in the recharge than the other modelled zones. Results of this study show the vulnerability of the groundwater resources in the area in mean annual conditions simulated with a steady-state. Instead, in transient conditions the water depth could be more variable. In particular, in the dry periods, wells could be completely dried, especially in the highland, whereas in an annual average simulation this issue could not be identified. For this reason, transient state simulations will be considered in future works.

Moreover, the study has identified a possible range of calibrated parameters for the fractured sandstones aquifer. In particular, the conductivity of the aquifer changes from 1.16×10^{-4} m/s in the A zone to 1.16×10^{-7} m/s in the D zone. In particular, the value of the D zone conductivity used in the simulations ranges from 6.94×10^{-8} m/s to 1.96×10^{-7} m/s respectively for the driest and the wettest period. The obtained values belong to the range found by Allen et al. (1997). Moreover, the calibrated conductivities obtained from the modelling are consistent with the ones obtained in the conductivity assessment of the PAT4 outcrops in the area (average value of 6.1×10^{-3} m/s, section 3.2), at exception of the D zone with a lower permeability.

TRANSIENT STATE SIMULATIONS

To investigate the behaviour of the aquifer in transient conditions, transient state simulations have been carried out with both the Model 1 A and Model 1 B. Hereafter the results of these simulations are reported. The storage coefficient of the model has been changed during this phase. In particular, a different storage has been assigned to the South area (A zone). In fact, the South area is supposed to be more fractured, therefore a higher storage is chosen. Initial values are assigned from literature (Allen et al., 1997; Zhang & Hiscock, 2010), and then changed in order to obtain simulated levels in accordance with the observed measurements in the observation points and with the topographic surface. Simulations have been carried out in two different periods, from the 11th July 2013 to the 31st November 2013 and from the 13th February 2014 to the 28th February 2015. During the first period, the piezometric levels in the three observation points in the area have been measured. Both recharge and flux boundary conditions along the springs line are inserted as daily values and changed at each daily time step.

MODEL 1 A

In Tab. 5.38 the parameters used in the simulation are reported. The Fig. 5.39 shows the simulated water table in the three observation points for the 142 days between the 11 July and the 31 November 2013. The difference from the observed values appears to be of the same order of magnitude with respect to the steady-state simulation. In particular, the correlation coefficient between the simulated and the observed piezometric head in each observation point is about 0.81 for point 1, 0.86 for point 2 and 0.95 for point 3. The water table depth in well 1 changes from -30 m to -21 m below the topographic surface (682-691 m a.s.l.), with a variation of 9 m. The level in point 2 and in point 3 are more constant than in well 1, with changes of less than 1 m in this period. In fact, well 1 is located on the top of the hill where the conductivity is supposed to be relatively low (9.26 x 10^{-7} m/s), whereas points 2 and 3 are located on alluvial deposits displaying a higher conductivity (8.68 x 10^{-5} m/s). Fig. 5.39d reports the time-variable function used in the transient simulation, in particular, the daily recharge and the discharge of the springs which has been inserted as variable boundary condition on the springs line.

The simulated water depth in the three observation points from the 13th February 2014 to the 28th February 2015 (380 days) is reported in Fig. 5.40. The maximum variations are simulated for water depths in well 1, varying from -29 m to -17 m (683-695 m a.s.l.).

Table 5.38 Parameters used in the transient simulation.

K A (m/s)	K B (m/s)	K C (m/s)	Storage B-C	Storage A	L stream (1/d)
6.25 x 10^{-5}	8.68 x 10^{-5}	9.26 x 10^{-7}	0.01	0.25	7.4 x 10^{3}
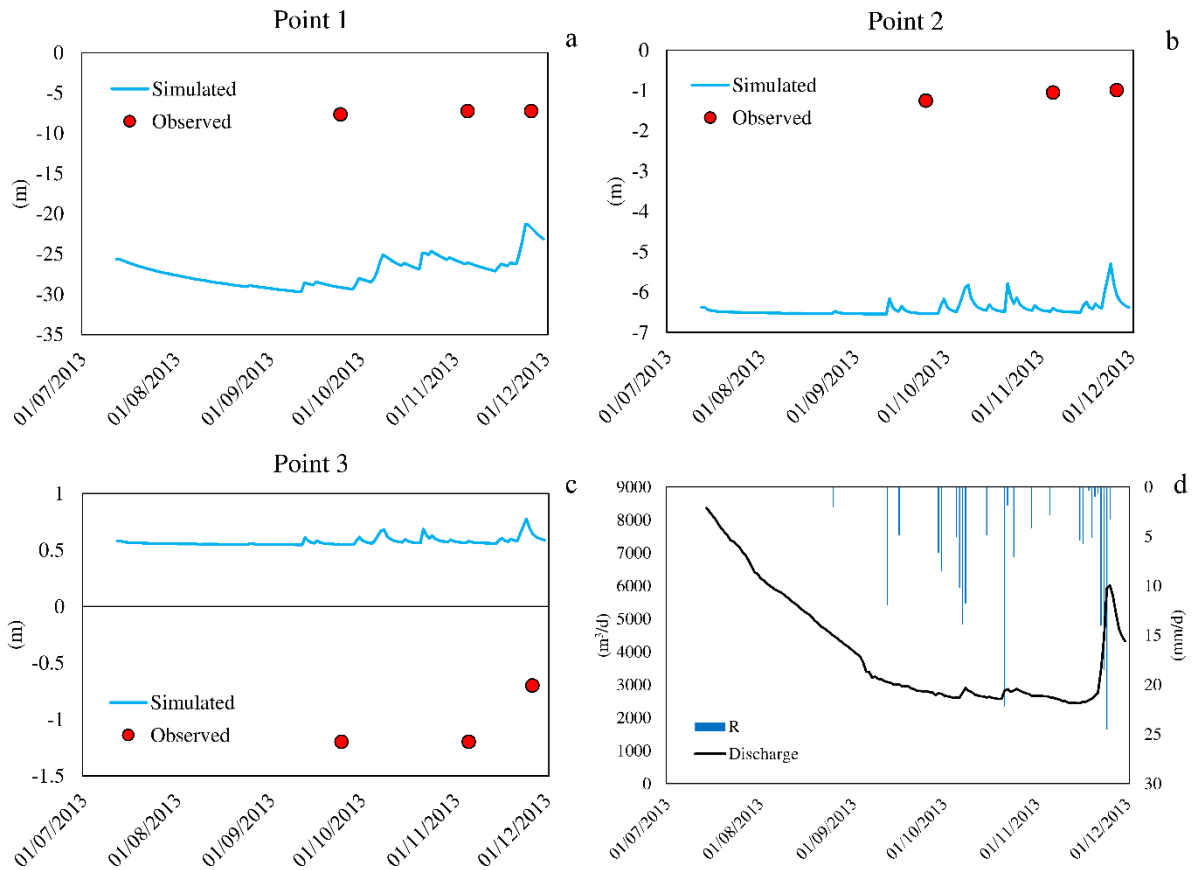
Figure 5.39 a,b,c, Simulated and observed water depth (m) between the 11th July and the 31st November 2013. d, Daily recharge (R, mm/d) and discharge (m^3/d) used in the Transient state simulation between the 11th July and the 31st November 2013.
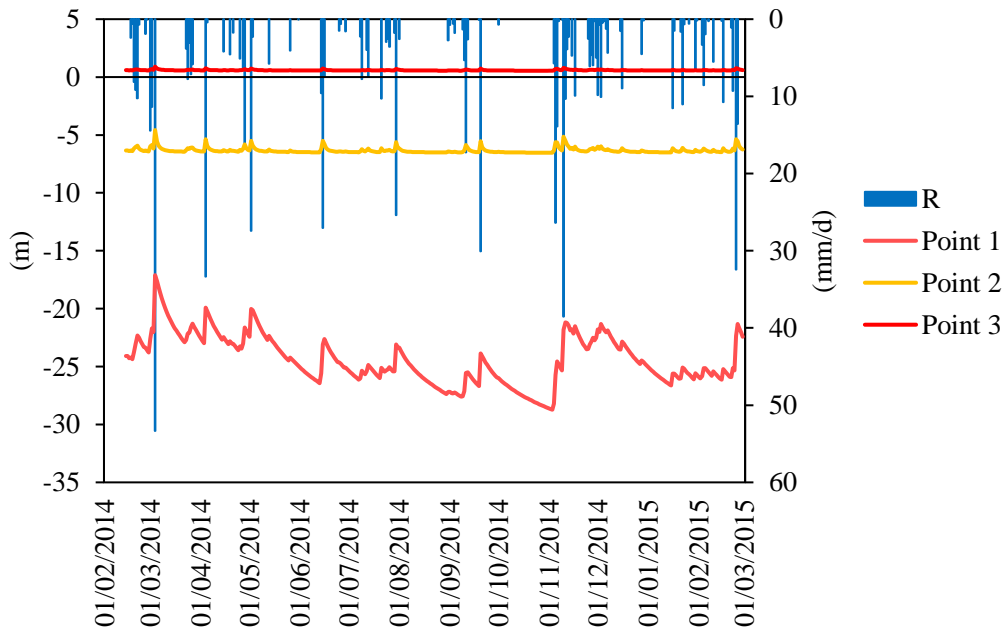
Figure 5.40 Simulated water depth (m) along with daily recharge (R, mm/d) between the 13th February 2014 and the 28th February 2015.

MODEL 1 B

The input to the model is the daily recharge and a variable flux boundary condition is set along the springs with the values reported in Fig. 5.39d. In Tab. 5.39 are reported the parameters used in the simulation. The Fig. 5.41 shows the simulated water depth in the three observation points for the 142 days period between the 11th July and the 31st November 2013. The correlation coefficient between the simulated and the observed water level in each observation point is equal to 0.83 for point 1, 0.84 for point 2 and 0.96 for point 3. The water table depth in point 1 changes from a minimum of -14 m to a maximum of -5 m below the topographic surface (697-706 m a.s.l.), with a variation about 9 m. The levels in point 2 and in point 3 are more stable than in point 1, with changes of less than 1 m in the same period. The mean simulated water depth in the three observation points is about -9 m for point 1, -6.5 m for point 2 and 0.5 m for point 3.

Table 5.39 Parameters used in the transient simulation.

K A (m/s)	K B (m/s)	K C (m/s)	K D (m/s)	Storage (B, C, D)	Storage A	L stream (1/d)
6.25×10^{-5}	8.68×10^{-5}	9.26×10^{-7}	2.31×10^{-7}	0.01	0.25	7.4×10^{3}
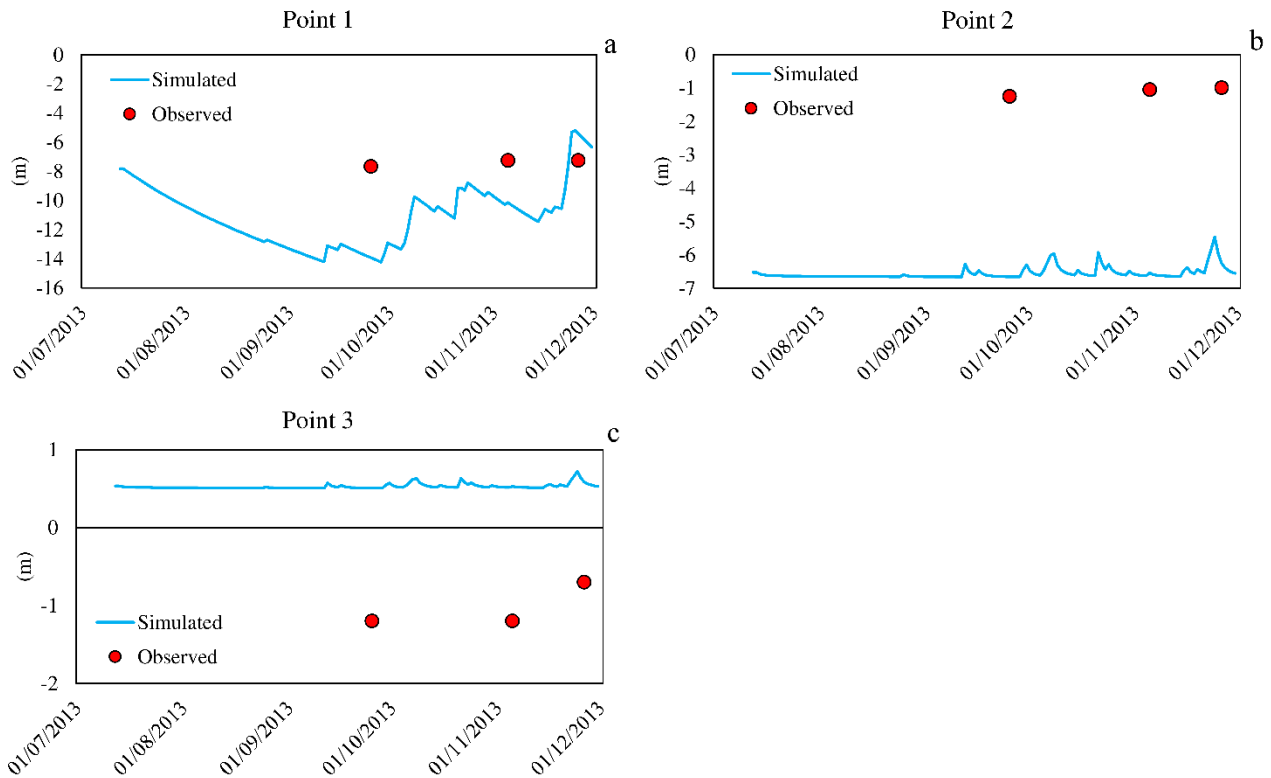
Figure 5.41 a,b,c, Simulated and observed water depth between the 11 July and the 31 November 2013.

The simulated water depth in the three observation points from the 13th February 2014 to the 28th February 2015 (380 days period) is reported in Fig. 5.42. The maximum variations are simulated for water depths in point 1, varying from -11 m to -2 m (700-709 m a.s.l.).
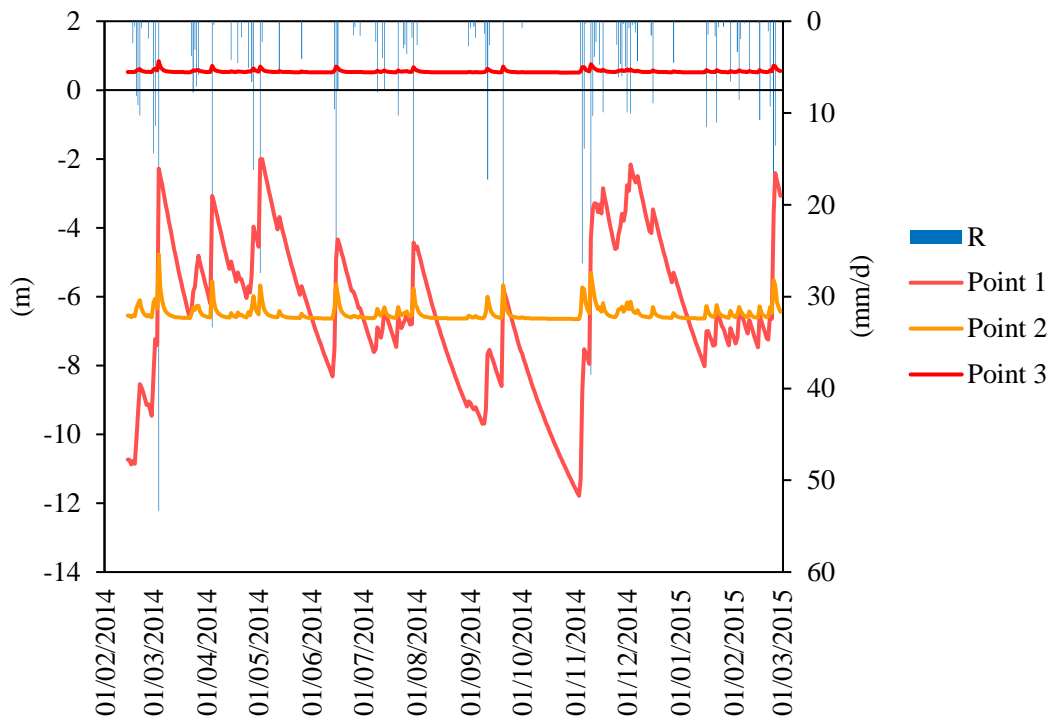
Figure 5.42 Simulated water depth (m) in the three observation points along with the daily recharge (R, mm/d) between the 13 February 2014 and the 28 February 2015.

DISCUSSION

Comparing the results of the transient simulation with Model 1 B and of the sensitivity analysis of Model 2, similar water table depths and calibrated parameters have been assessed. Even if the two models adopt a different boundary condition to represent the Mulino dele Vene springs, they both give reliable and similar results. In particular, the calibrated conductivity of deposits (K B) is 8.68 x 10^{-5} m/s for Model 1B and 1.04 x 10^{-4} m/s for Model 2. In the south area, the calibrated conductivity (K A) are equal to 6.25 x 10^{-5} m/s or 1.16 x 10^{-4} m/s, and in the D zone conductivity values (K D) are 2.31 x 10^{-7} m/s or 1.16 x 10^{-7} m/s respectively for Model 1B and Model 2. Finally, the conductivity of the massive PAT4 (K C), in which observation points are not present and therefore calibration is less reliable, changes from 9.26 x 10^{-7} m/s in Model 1B to 6.94 x 10^{-5} m/s in Model 2. Anyway, all the conductivity values obtained belong to ranges found in literature (Allen et al., 1997; Gómez et al., 2010; Zhang & Hiscock, 2010). Moreover, the well test executed in the area gives a value of conductivity equal to 5 x 10^{-7} m/s for the aquifer. Instead, fracture-network data measurements from PAT4 outcrops have allowed estimating the hydraulic conductivity of the PAT4 ranging from 2.7 x 10^{-2} m/s to 10^{-4} m/s (Petronici, 2014; Vizzi, 2014). Therefore, the assessed conductivity values represent the minimum (well test) and the maximum (outcrop analysis) of the large range of conductivity of the PAT4 unit. In Fig. 5.43 the conductivity values assessed from the observed data and the ranges obtained during calibration are displayed together. In particular, it is evident that the calibrated conductivity values range between the values obtained from the outcrops analysis and the value assessed from the well test.
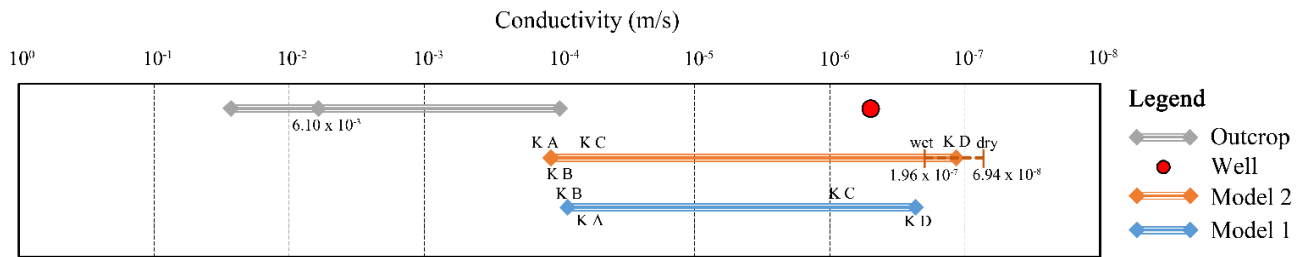
Conductivity (m/s)

Figure 5.43 Graph of the conductivity values obtained from the observations and from the model calibration.

Furthermore, the simulated piezometric levels and its variations in Model 1B and in Model 2 are similar. In the transient simulation of Model 1B the simulated water depth in point 1 changes from -11 m to -2 m (range of 9 m), whereas in point 2 and point 3 the levels are stable with only small changes of about 1 m. Simulations in the two conditions of maximum and minimum annual recharge with Model 2 give a range of water table changes of about 12.5 m for point 1, 6 m for point 2 and 2.5 m for point 3.

Finally, the calibrated parameters obtained from the TRANSIN simulations were inserted in the FEFLOW model. Unfortunately, the FEFLOW simulations are instable for the boundary conditions and the parameters of Model 2, and with errors inserting the parameters of Model 1A, B and C.

5.6.4 RAINFALL-RUNOFF MODEL

As described in section 4.6.2, two rainfall-runoff models of the Mulino delle Vene springs system have been built. At first, the models have been calibrated and validated on the observed springs discharge data (2013-2016). Afterwards, the calibrated models have been used in combination with five RCMs previously downscaled with the CDF-t method (section 4.5.3), to simulate and compare the baseline (1984-2013) and the future (2021-2050) springs discharge.

CALIBRATION AND VALIDATION - MODIFIED HYMOD

The modified Hymod model has been firstly used to simulate the Mulino delle Vene daily discharge. In particular, the calibration period has been set from the 11th of March 2013 to the 4th of November 2014 and the validation period from the 5th of November 2014 to the 31st of May 2016. The model has been calibrated through the relative efficiency and inverse flow efficiency criteria (section 4.6.3), as suggested for low flows simulation by Krause et al. (2005) and Pushpalatha et al. (2012), using the observed daily discharge values. The input of the model is the daily precipitation measured at the Carpineti weather station and the daily potential evapotranspiration assessed with the Hargreaves formula (section 4.1.1). Moreover, the extension of the recharge area, necessary to the model for assess the input volumes, has been set equal to 5.5 km^2 as reported in Cervi et al. (2014). The parameters obtained during calibration are reported in Tab. 5.40. In Tab. 5.41, the obtained values of the efficiency criteria (Erel and NSEi), together with the NSE and the NSEl are resumed. Both calibration and validation gave satisfactory results. Fig. 5.44 and Fig. 5.45 are respectively the graph and the scatter plot of the simulated and observed discharges.

Low flows simulation performance is very good (Moriasi et al., 2007) with an Erel equal to 0.83 in the calibration period and to 0.73 in the validation period and NSEi equal to 0.80 and 0.69 respectively during calibration and validation. In particular, the model correctly reproduces the ending of the recession periods. Instead, the peak values are not well simulated. In particular, the NSE, which takes into account the higher values of the hydrograph, has values equal to 0.58 during the calibration and 0.27 in the validation period. Since the objective is to reproduce the low flow period, the simulation has been considered satisfactory. Moreover, the observed discharge during high flows is more subject to measure errors and less representative of the springs behaviour.

Furthermore, the rainfall-excess model allows assessing the daily actual evapotranspiration (AET, section 4.1.1). During the simulation period, the average yearly actual evapotranspiration is equal to 500 mm with a precipitation about 923 mm, the average effective rainfall is about the 46% of the total rainfall. This value is similar to the one assessed with the Thornthwaite formula (section 5.1.3). In Fig. 5.46 the average monthly precipitation (P) and the average monthly actual evapotranspiration (AET) are reported. The recharge is maximum at the beginning of the springs whereas during the summer the evapotranspiration exceeds precipitation leaking the water stored in the ground.

Table 5.40 Calibrated parameters of the modified Hymod model.

C_{max} (mm)	β_k (-)	K$_s$ (d^{-1})
336.073	0.547	0.015

Table 5.41 Values of the efficiency coefficients in the calibration and validation periods.

Period	NSEi	Erel	NSEl	NSE
Calibration	0.80	0.83	0.79	0.58
Validation	0.69	0.73	0.53	0.27
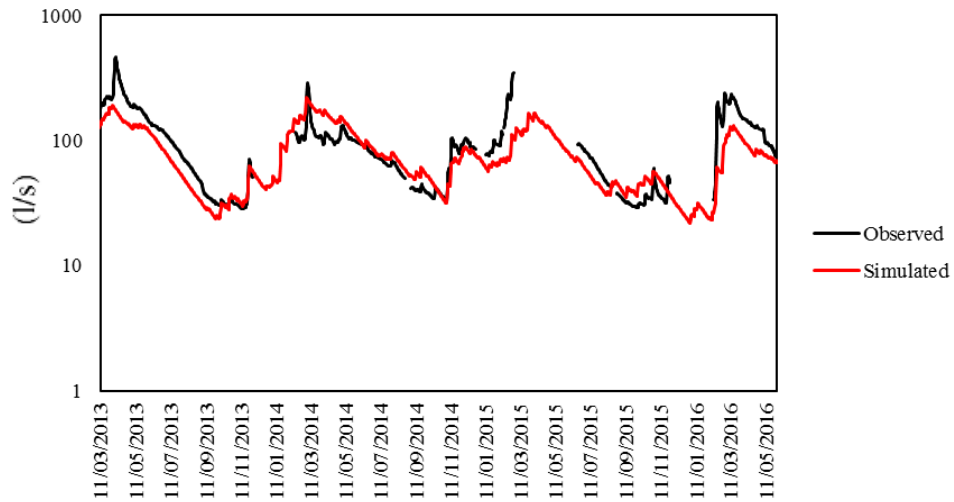
Figure 5.44 Semi-logarithmic graph of the observed (black line) and simulated (red line) discharge in the simulation period (11th of March 2013 - 31st of May 2016).

Figure 5.45 Scatter plot of the springs discharge in the calibration (red) and validation (blue) periods.

Figure 5.46 Average monthly observed precipitation and average monthly simulated actual evapotranspiration in the simulation period (11th of March 2013 - 31st of May 2016) with the calibrated modified Hymod model.

102

CALIBRATION AND VALIDATION - MULTIPLE RESERVOIRS MODEL

On the basis of the results of the recession curve analysis (section 5.3), three sectors have been detected. Thus, the multiple reservoirs model is formed by three reservoirs connected in series and represented in Fig. 5.47. Each reservoir has a deep drainage representing its contribution to the spring's discharge (pipes with black arrows in Fig. 5.47). In addition, a sub-surface drainage (pipes with yellow arrows in Fig. 5.47) connects each reservoir to the following one. The volumes of the reservoirs are equal to those calculated in the recession curve analysis (section 5.3, Tab. 5.6) with the exception of the last one, which has unlimited volume allowing higher discharge to be simulated. Firstly, the output of the rainfall-excess model goes into the sector with the lowest depletion coefficient (corresponding to the 3rd sector identified during the recession curve analysis). Only the water volume over the maximum storage volume of this sector continues into the process and it goes into the second sector, corresponding to the 2nd sector identified in the recession curve analysis. Finally, the water surplus of this reservoir goes in the last sector, which is the one with the higher depletion coefficient (1st sector of section 5.3). This model reproduces the three components identified in the recession curve. In fact, the 3rd sector works for all the hydrological year whereas the 1st and 2nd sector only work when the aquifer is saturated.

This model allows two different approaches to be investigated, the first is the application of the model with all the parameters (7) to be calibrated (Multiple reservoirs model 1), the second is a model with reservoir parameters from the recession curve analysis and only two parameters (C_{max}, β_k) to be calibrated (Multiple reservoirs model 2).
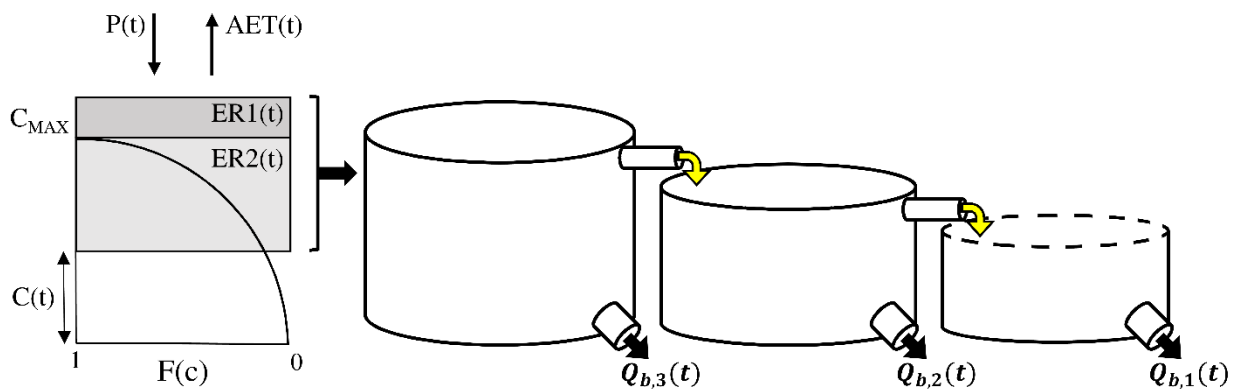
Figure 5.47 Structure of the multiple reservoirs model of the fractured aquifer feeding the Mulino delle Vene springs.

Multiple reservoirs model 1

The model has been firstly calibrated in the period between the 11th of March 2013 to the 4th of November 2014 and then validated in the period from the 5th of November 2014 to the 31st of May 2016.

As for the modified Hymod model, the multiple reservoirs model has been calibrated through the relative efficiency and inverse flow efficiency criteria, as suggested for low flows simulation by Krause et al. (2005) and Pushpalatha et al. (2012), using the observed daily discharge values. The input of the model is the daily precipitation measured at the Carpineti weather station and the daily potential evapotranspiration assessed with the Hargreaves formula. Moreover, the extension of the recharge area is set equal to 5.5 km^2 as reported in Cervi et al. (2014).

Calibration is satisfactory (Fig. 5.48 and Fig. 5.49; Tab. 5.42) with an Erel equal to 0.89 and to 0.72 for the calibration and validation period respectively. NSEi is satisfactory too, with values equal to 0.92 and 0.58. Instead, the NSEl and the NSE coefficients, which give more weight to the high flow values, show a bad simulation performance. The parameters resulting from calibration are reported in Tab. 5.43. Comparing the results of calibration and the parameters identified in the recession curve analysis (see section 5.3) a similarity in the values is evident.

Furthermore, the rainfall-excess model allows assessing the daily actual evapotranspiration (AET). The average annual actual evapotranspiration is about 541 mm, and the effective precipitation is about the 41% of the average annual precipitation of the three years. Analysing the monthly pattern of precipitation and actual evapotranspiration (Fig. 5.50), the water scarcity condition of the summer's months is evident. From May to August, the monthly precipitation is lower than the actual evapotranspiration. The recharge to the aquifer is concentrated between October and November and from January to March.

Table 5.42 Values of the efficiency coefficients in the calibration and validation periods.

Period	NSEi	Erel	NSEl	NSE
Calibration	0.92	0.89	0.81	0.52
Validation	0.58	0.72	0.42	0.13

Table 5.43 Calibrated parameters of the multiple reservoirs model along with the results of the recession curve analysis.

|	C_{max} (mm)	β_k (-)	α_3 (1/d)	W_3 (m^3)	α_2 (1/d)	W_2 (m^3)	α_1 (1/d)
Calibration	206.23	0.139	9.89 x 10^{-3}	1.61 x 10^6	3.27 x 10^{-2}	4.08 x 10^5	6.90 x 10^{-2}
Recession curve analysis (section 5.3)			2.58 x 10^{-3}	1.70 x 10^6	3.27 x 10^{-2}	4.55 x 10^5	5.19 x 10^{-2}
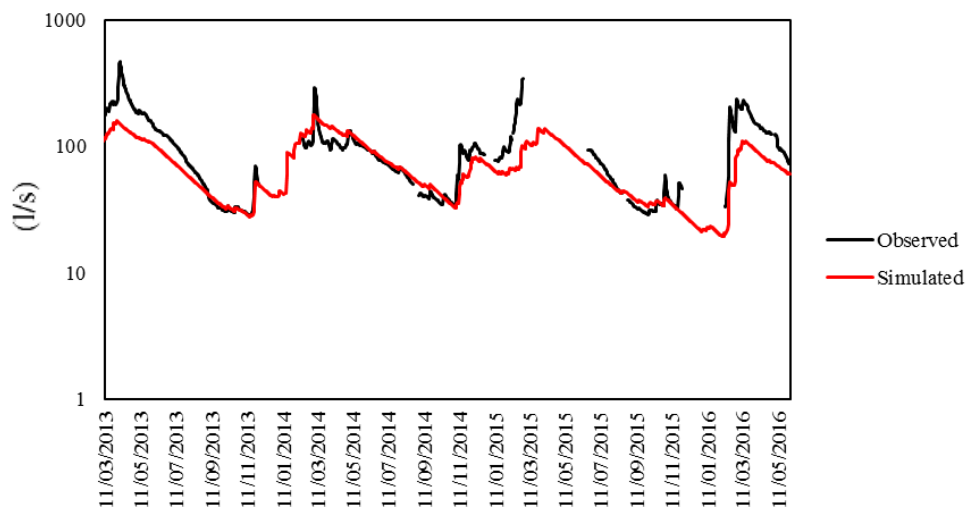
Figure 5.48 Semi-logarithmic graph of the observed (black) and simulated (red) discharges in the simulation period (11th of March 2013 - 31st of May 2016).
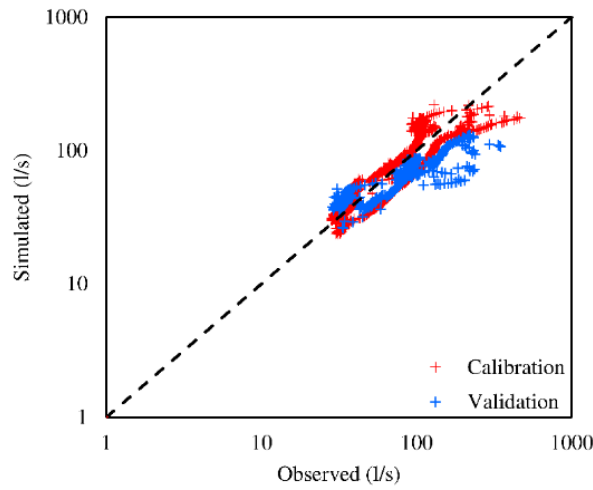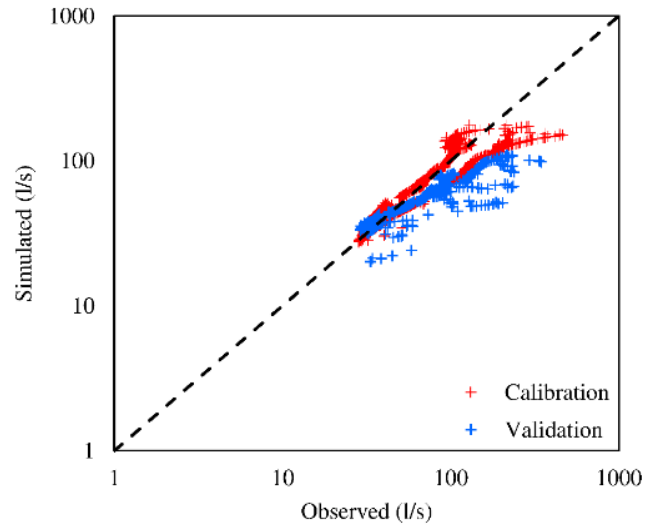
Figure 5.49 Scatter plot in the calibration (red) and validation (blue) period.
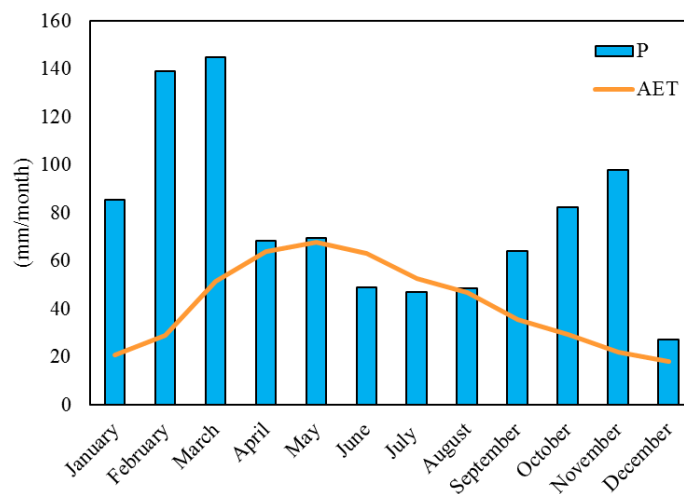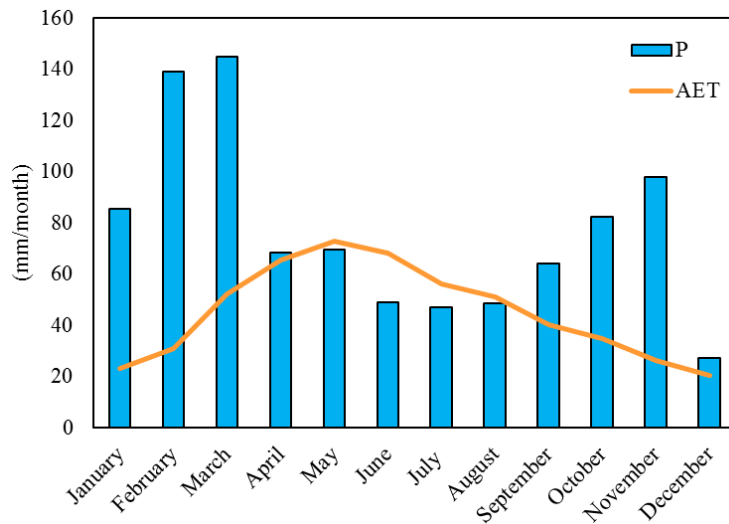

Figure 5.50 Average monthly observed precipitation and average monthly simulated actual evapotranspiration in the simulation period (11th of March 2013 - 31st of May 2016) with the calibrated multiple reservoirs model.

Multiple reservoirs model 2

A second multiple reservoirs model has been built using the parameters from the recession curve analysis and calibrating only the two parameters of the rainfall-excess model (C_{max}, β_k). Parameters resulting from the calibration are reported in Tab. 5.45 along with the used reservoir parameters obtained from the recession curve analysis. The efficiency coefficients drops to lower values (Tab. 5.44) than the previous model both in the calibration and in the validation procedure. In particular, the lowest parts of the hydrograph are always overestimated (Fig. 5.51 and Fig. 5.52).

The rainfall-excess model allows estimating the average annual effective rainfall to the aquifer of about 444 mm (48% of the precipitation) and the average actual evapotranspiration about 480 mm (52% of the precipitation). The mean monthly trend of the actual evapotranspiration (Fig. 5.53) displays a pattern similar to the previous models, with driest condition in the months of June and July.

This model has not been considered satisfactory for the simulation of low flows and, for this reason, it has not been used for the future simulations.

Table 5.44 Values of the efficiency coefficients in the calibration and validation periods.

Period	NSEi	Erel	NSEl	NSE
Calibration	0.67	0.71	0.51	0.17
Validation	0.52	0.68	0.42	0.24

Table 5.45 Calibrated parameters of the multiple reservoirs model along with the results of the recession curve analysis.

Calibration		Recession curve analysis				
C_{max} (mm)	β_k (-)	α_3 (1/d)	W_3 (m^3)	α_2 (1/d)	W_2 (m^3)	α_1 (1/d)
432.21	0.88	2.58×10^{-3}	1.70×10^6	3.27×10^{-2}	4.55×10^5	5.19×10^{-2}
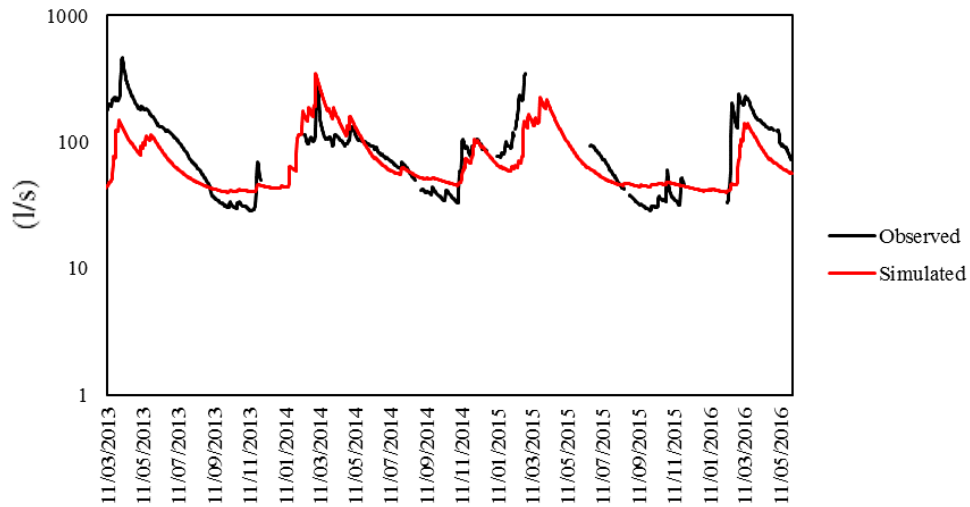
Figure 5.51 Semi-logarithmic graph of the observed (black) and simulated (red) discharges in the simulation period (11th of March 2013 - 31st of May 2016).
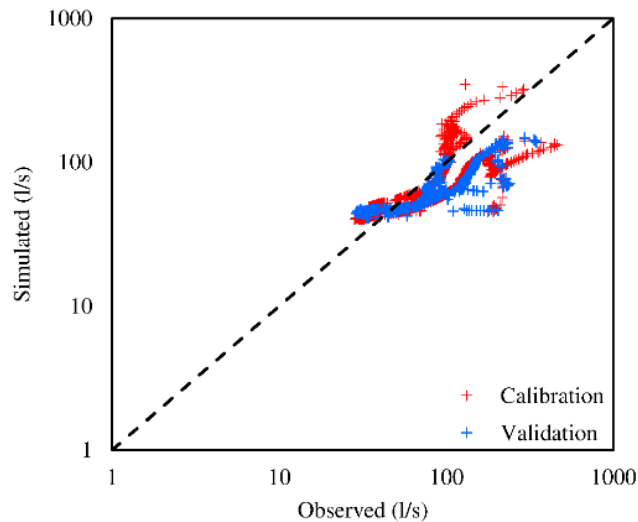
Figure 5.52 Scatter plot in the calibration (red) and validation (blue) period.
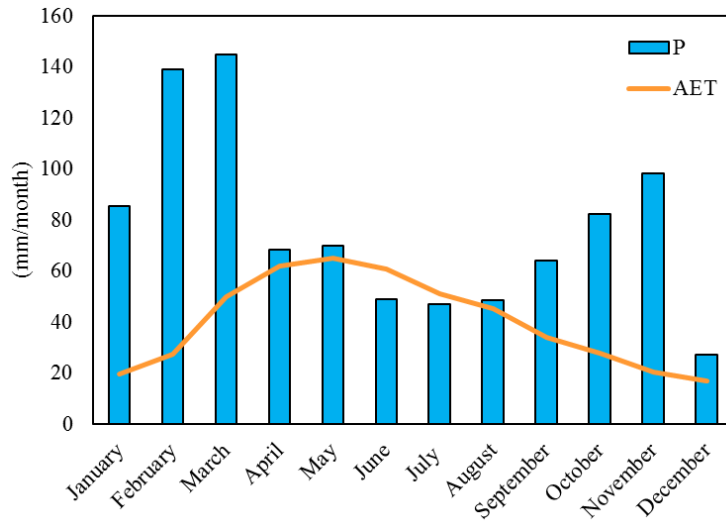
Figure 5.53 Average monthly observed precipitation and average monthly simulated actual evapotranspiration in the simulation period (11th of March 2013 - 31st of May 2016) with the multiple reservoirs model with only two calibrated parameters.

FUTURE SIMULATIONS

The calibrated and validated models have been used to simulate the springs discharge in a baseline (1984-2013) and in a future period (2021-2050). Future scenarios have been previously elaborated and downscaled with the CDF-t approach (section 5.5.2).

MODIFIED HYMOD

Firstly, the hydrological model assesses the daily actual evapotranspiration and effective rainfall with the rainfall-excess model and secondly the daily springs discharge with the bucket model. The modelling results for the future RCMs have been averaged and are here reported as a single series with corresponding uncertainty ($\pm\sigma$). Firstly, the average annual actual evapotranspiration decreases from 454 mm in the baseline period to 435 mm in the future period (Tab. 5.46). The effective precipitation is almost the same, the 44% in the baseline period and the 45% in the future period. The most interesting issue is the change in the monthly pattern of precipitation and evapotranspiration. In particular, in the future the actual evapotranspiration is forecasted to exceed precipitation from June to August whereas this happened only in July in the past (Fig. 5.54). The dryer summers are indicative of a more sensitive water condition that can easily lead to water scarcity or drought.
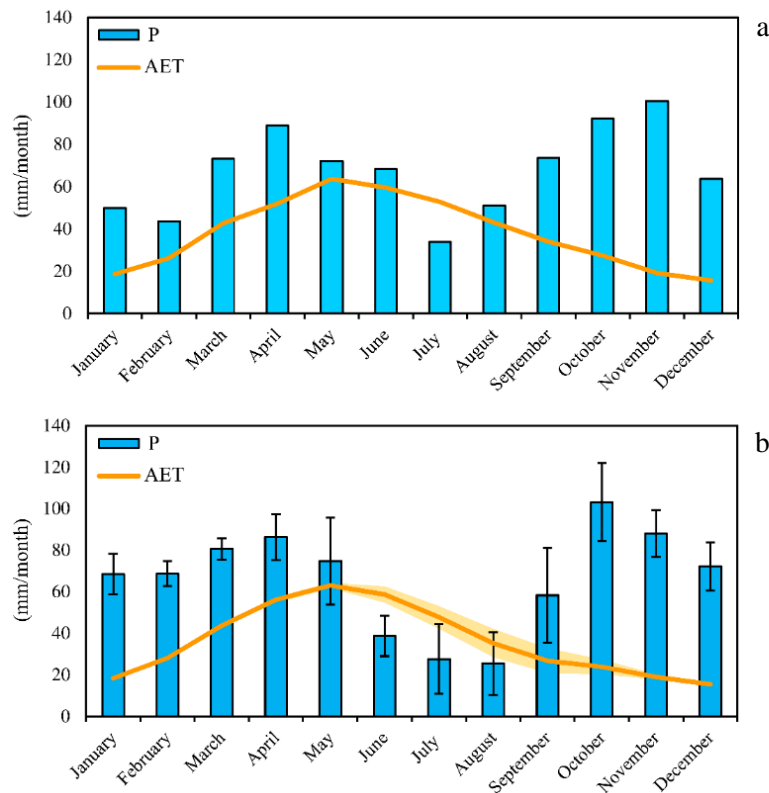
Figure 5.54 Average monthly precipitation (P) and actual evapotranspiration (AET) in the Baseline (a) and in the Future (b) period.

Secondly, the daily discharge has been assessed. The estimated future daily flows from the five RCMs are statistically different from the baseline period, as each P-value obtained through Student's t-test is less than 0.05. Despite the mean annual springs discharges remain almost constant with respect to the baseline (61.8 l/s) and future periods (62.6 l/s), the distribution of the discharge flows within the year changes (Tab. 5.46). The monthly spring discharges are expected to decrease slightly (Fig. 5.55a), starting in July (-7.8%), and reduce continuously until December (-12.9%). The maximum absolute decrease of 10.2 l/s is expected to occur in September and this corresponds to the maximum relative change (-26.3%). Instead, from January to June the future monthly discharge is higher than the baseline one, ranging from the +25.3% of March to the +3.2% of June.

Fig. 5.55b shows the FDCs obtained by processing the simulated daily discharges for the baseline (black curve) and future periods (red curve). By looking closely at the FDCs, the largest negative changes involve discharges close to the lower part of the curve. The median flow Q(50) decreases from 53.3 l/s to 50.6 l/s (-5.1%). On the contrary, high discharges are expected to increase, with Q(05) (i.e. the daily discharge exceeded 5% of the time during the year) going from 133.1 l/s to 154.3 l/s (+15.9%). The Q(95) index decreases from 15.3 l/s (baseline period) to 11.9 (future period; a reduction of -21.8%). At the same time, the 7-day 10-year low flow index (7Q10) shows a drop from 10.6 l/s (baseline period) to 8.0 l/s (future period; a reduction of -25.0%).

Table 5.46 Mean monthly actual evapotranspiration (AET, in mm), effective rainfall (ER, in mm) and discharges (Q, in l/s) for the observed database (Baseline: 1984-2013) and the forecasted Future (2021-2050) scenario together with mean annual values. Future values are reported as mean of the 5 RCMs results with the corresponding standard deviations (±1σ). Relative flow changes (in %) are also reported.

Month	AET		ER		Q		
	Baseline	Future	Baseline	Future	Baseline	Future	Relative changes
Jan.	19	18±1	31	43±7	71.6	74.6±12.4	4.3
Feb.	26	28±1	26	43±5	66.8	82.5±6.5	23.6
Marc.	43	44±1	41	48±4	69.6	87.3±6.2	25.3
Apr.	52	56±1	42	40±6	75.3	87.6±3.8	16.3
May	64	63±1	30	32±13	76.4	83.9±9.6	9.8
Jun.	59	59±4	25	13±5	68.0	70.2±12.4	3.2
Jul.	53	48±5	9	6±5	53.4	49.2±8.9	-7.8
Aug.	43	35±7	12	5±4	40.8	34.5±6.7	-15.5
Sep.	34	27±6	20	14±10	38.7	28.5±9.1	-26.3
Oct.	27	24±3	32	33±11	44.9	35.0±12.8	-22.0
Nov.	19	19±1	50	39±11	60.4	51.6±14.6	-14.7
Dec.	16	15±1	40	44±9	76.1	66.3±15.4	-12.9
Mean	454	435±21	357	359±27	61.8	62.6±5.1	1.2
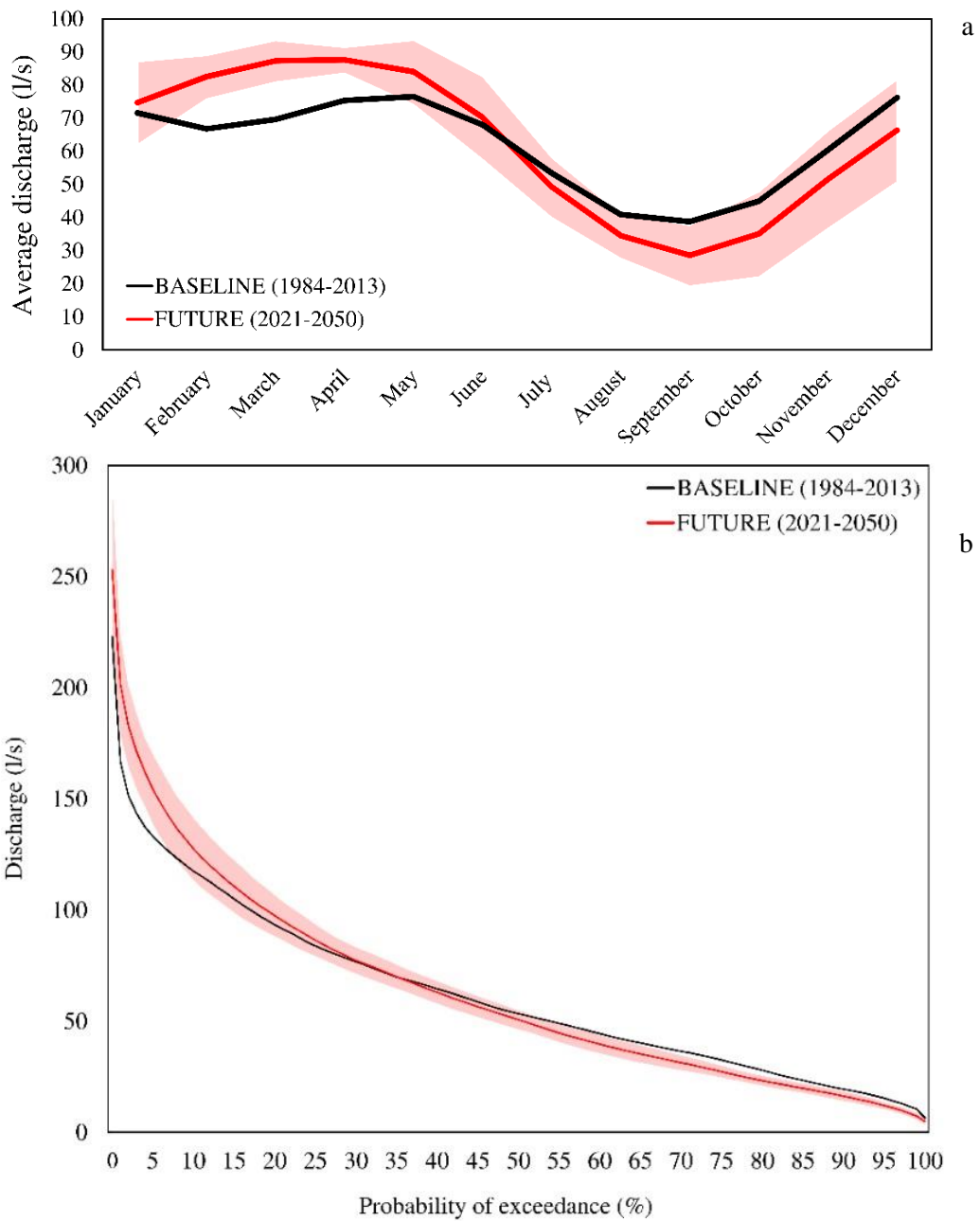
Figure 5.55 a, Average monthly discharge (l/s) for the actual (1984-2013, black line) and future (2021-2050, red line) periods along with uncertainty (±σ, shaded red area). b, Flow duration curves for the Mulino delle Vene springs in the baseline (1984-2013, black line) and future (2021-2050, red line) periods along with uncertainty (±σ, shaded red area).

As touched upon in section 4.6.2, the duration of continuous low flows below the threshold Q(80) has been assessed for each year for the baseline and the future periods. The results are shown in Fig. 5.56, where it can be observed that, by considering both the baseline and the future periods, the majority of the years are characterized by less than 50 days below the corresponding threshold (17 and 14 years, respectively). It is worth noting the slight increase in the number of years with continuous low flow lasting between 51 and 100 days (6 and 9 years, respectively) and between 101 and 150 days (from 2 to 4 years).
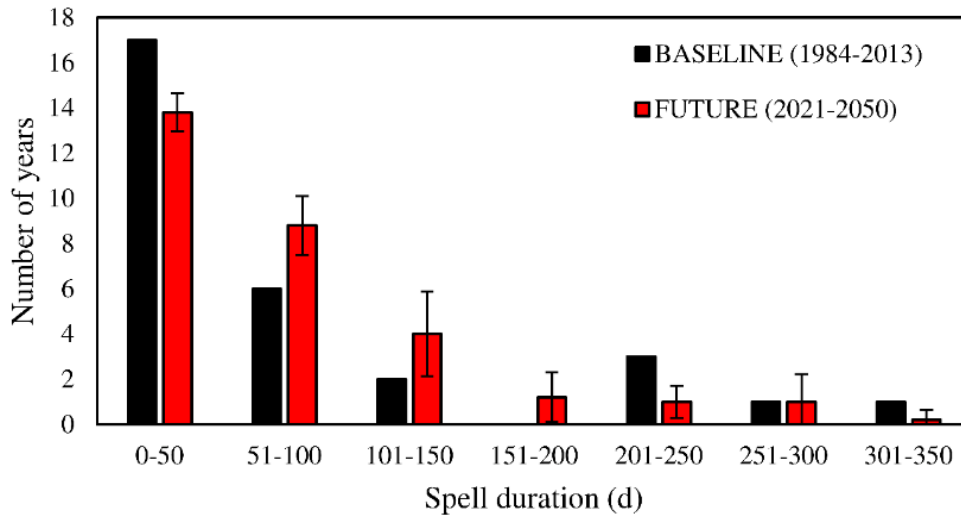
Figure 5.56 Histogram of the low flow duration below the Q(80) threshold (in d) simulated for the baseline (1984-2013, black bar) and future (2021-2050, red bar) periods along with uncertainties (±σ, black line).

MULTIPLE RESERVOIRS MODEL

The multiple reservoirs model with seven calibrated parameters (Multiple reservoirs model 1) has been used to analyse the effects of climate change on the Mulino delle Vene springs discharge. Simulation have been run both in the baseline period (1984-2013) and in the future period (2021-2050).

Firstly, the average annual actual evapotranspiration (Tab. 5.47) decreases from 492 mm (baseline period) to 465 mm (future period). The average effective rainfall increases slightly from 319 mm to 329 mm (respectively the 39% and 41% of precipitation). Comparing Fig. 5.57a and Fig. 5.57b, it is evident the different recharge pattern between the baseline and the future periods. In the baseline scenario, the monthly actual evapotranspiration exceeds precipitation only in July; in the future scenario the monthly actual evapotranspiration is forecasted to exceed precipitation from June to August.

Secondly, the daily discharge from the fractured aquifer of Mulino delle Vene has been assessed. The average annual discharge is almost the same (55.3 l/s in the baseline, 57.4 l/s in the future) but the monthly pattern changed substantially (Fig. 5.57c, Tab. 5.47). From January to June the forecasted future discharge is higher than the baseline one, up to +19.5% in February. Instead, from July to December the average monthly discharge decreases about the 10%. The maximum relative decrease occurs in October with -15.4%.
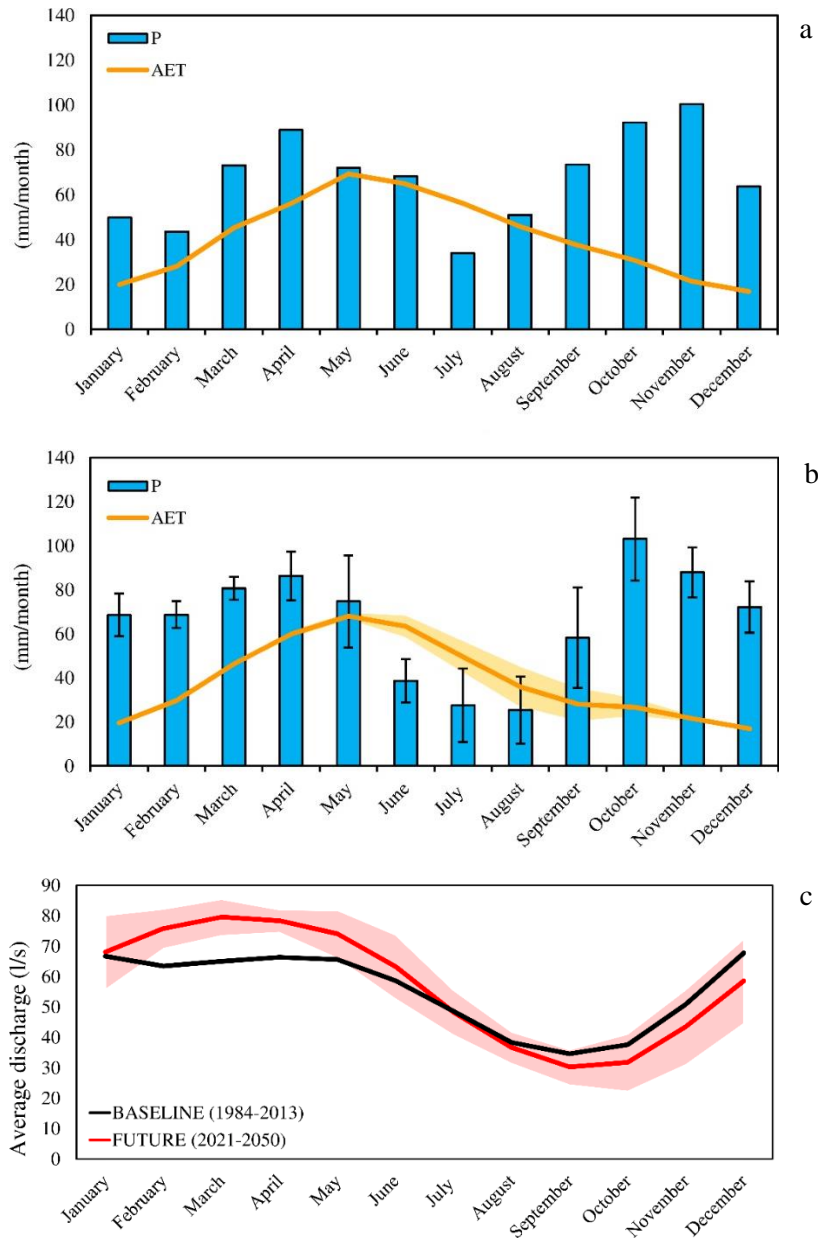
Figure 5.57 a, Average monthly precipitation (P) and actual evapotranspiration (AET) in the Baseline period. b, Average monthly precipitation (P) and actual evapotranspiration (AET) in the Future period. c, Average monthly discharge (l/s) for the actual (1984-2013, black line) and future (2021-2050, red line) periods along with uncertainty (±σ, shaded red area).

Table 5.47 Mean monthly actual evapotranspiration (AET, in mm), effective rainfall (ER, in mm) and discharges (Q, in l/s) for the observed database (Baseline: 1984-2013) and the forecasted Future (2021-2050) scenario together with mean annual values. Future values are reported as mean of the 5 RCMs with the corresponding standard deviations (±1σ). Relative flow changes (in %) are also reported.

Month	AET		ER		Q		
	Baseline	Future	Baseline	Future	Baseline	Future	Relative changes
Jan.	20	20±1	30	44±8	66.7	68.1±12.1	+2
Feb.	28	30±1	23	43±7	63.4	75.8±6.4	+19.5
Marc.	45	46±1	37	43±5	65.0	79.6±5.9	+22.5
Apr.	56	60±2	35	33±6	66.3	78.4±3.7	+18.1
May	69	68±1	23	24±13	65.6	74.1±7.8	+12.8
Jun.	65	63±5	18	8±4	58.6	63.3±10.4	+8.1
Jul.	56	50±7	4	3±3	48.6	48.3±7.3	-0.8
Aug.	46	36±9	7	2±2	38.4	36.7±5.1	-4.3
Sep.	37	28±7	14	10±9	34.6	30.3±5.7	-12.5
Oct.	31	27±4	29	28±14	37.6	31.8±9.3	-15.4
Nov.	21	22±1	58	42±13	50.8	43.5±12.2	-14.5
Dec.	17	17±1	41	48±10	67.8	58.6±13.7	-13.6
Mean	492	465±29	319	329±26	55.3	57.4±5.0	+3.7

The Flow Duration Curves (Fig. 5.58a) shows an increase of the higher discharge values and a decrease of the section of the curve between the 50% and the 90% of the probability of exceedance. In particular, the Q(80) decreases from 24.1 l/s to 21.1 l/s (-12.7%). Q(50) is almost the same with a value respectively about 47.7 l/s and 47.2 l/s in the baseline and future periods (-1.1%). Instead, Q(05) increases from 118.1 l/s to 135.6 l/s (+14.9%) and Q(95) from 9.3 l/s to 10.3 l/s (+11.1%). At the same time, the 7-day 10-year low flow index (7Q10) shows a drop from 8.7 l/s (baseline period) to 7.7 l/s (future period; a reduction of -11.6%).

Fig. 5.58b shows the duration of continuous low flows below the threshold Q(80) for the baseline and the future periods. Most of the years considered are either those where there are less than 50 days below the corresponding threshold (19 and 18 years, respectively). There will be a slight increase in years with continuous low flow lasting between 51 and 100 days (3 and 4 years, respectively) and between 151 and 200 days (from 0 to 2 years).
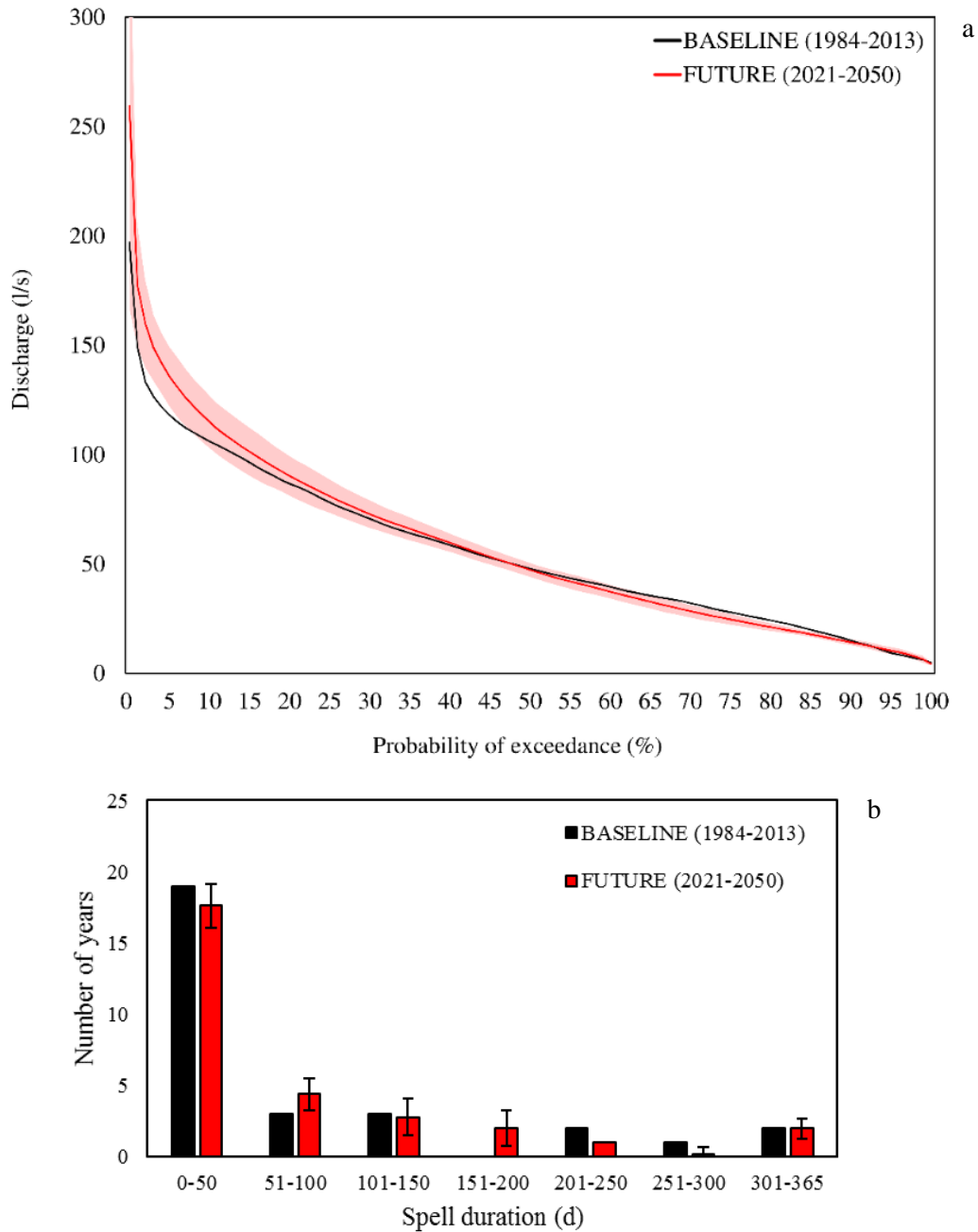
Figure 5.58 a, Flow duration curves for the Mulino delle Vene springs in the baseline (1984-2013, black line) and future (2021-2050, red line) periods along with uncertainty (±σ, shaded red area). b, Histogram of the low flow duration below the Q(80) threshold (in d) simulated for the baseline (1984-2013, black bar) and future (2021-2050, red bar) periods along with uncertainties (±σ, black line).

DISCUSSION

Two hydrological models have been calibrated and validated on the observed discharge data of the Mulino delle Vene springs, and have been then used to forecast the future springs discharges. Even if both the models are calibrated on the same dataset and the rainfall-excess model gives similar results, the different schematic conceptualization produces different discharge results. In particular, the forecasted discharge by the multiple reservoirs model (3 reservoirs) is less influenced by climate change than the one simulated by the single bucket

(modified Hymod model). With only one reservoir, the modified Hymod model is more sensitive to changes in the weather data both for the higher part of the hydrograph and for the lower part. In particular, Q(95) decreases of about 21.8% with the modified Hymod model, whereas it increases of about 11.1% with the multiple reservoirs model. The Q(05) increases by 15.9% with the modified Hymod model and by 14.9% with the multiple reservoirs model. Moreover, the forecasted 7Q10 decreases about the 25.0% with the modified Hymod model, and only about the 11.6% with the multiple reservoirs model. Finally, the duration of continuous low flows below the threshold Q(80) for the baseline and the future periods remained almost the same for the multiple reservoirs model and it changed considerably with the modified Hymod model (years with continuous low flow lasting between 51 and 100 days will increase by a third and between 101 and 150 days will duplicate).

The study demonstrates that the Mulino delle Vene springs will be affected by climate changes. This finding leads to some consideration that can be applied to most springs in the northern Apennines, which are fed by fractured aquifers as the Mulino delle Vene springs. Firstly, results show that the water resources will be reduced during summer and autumn. This issue entails an increasing demand of water supply during the future low flow periods, and the water managers will have to confront with it. On the contrary, the increase in the mean monthly discharges expected from January to June will occur in a period when the flows are already high enough to satisfy the community's water needs.

Moreover, the forecasted changes in springs discharge can affect the stream flow. In fact, the Mulino delle Vene springs is the main source of the Tresinaro stream (section 5.4.2). Furthermore, the Tresinaro stream supplies the porous aquifer in the alluvial plan of the river Po. Here, dozens of wells drawn groundwater for civil and industrial purposes to satisfy the needs of hundreds of thousands of people (Martinelli et al., 2014). The reduction of groundwater quotas released by the mountainous aquifer, related to the forecasted change in the monthly effective rainfall over the catchment area, could result in a change in the recharge process of the aquifer. This is significant because these aquifers are already displaying serious signs of water shortage as a consequence of a severe over-exploitation (Farina et al., 2014).

5.7 LARGE SCALE MODEL

In this work, we have built a simplified distributed model of the Tresinaro stream catchment. In the past, only few studies about the area have been carried on (Petronici et al., 2016; Petronici et al., 2017a) and the database is still under construction. The results of the hydrogeological investigations have allowed the definition of a first conceptual model of the area and then few modelling exercises have been carried out. The large scale model allows an in-depth analysis of the basin hydrological cycle. Moreover, future studies will consider climate change scenarios in combination with the calibrated large scale model in order to evaluate the climate change effects on both the mountainous water resource and the alluvial plain aquifer.

5.7.1 CONCEPTUAL MODEL

Firstly, the Tresinaro hydrological catchment (section 3) defines the boundaries of the modelled area. The closing point of the catchment is set to the Ca' de Caroli stream gauge (98 m a.s.l.; Scandiano, RE), which is in-continuously monitored since 2003. The model boundaries correspond to the surface water divides and it is assumed that there is no water exchange across them for either surface or sub-surface flow, at the exception of the alluvial fan border. Moreover, tracer tests carried out during the 2015 summer show that the major contribution to the stream discharge comes from the Mulino delle Vene springs (section 5.4.2). No other major sources of groundwater have been identified. Therefore, all the geological units have been considered almost impervious at exception of the PAT4 unit, where the main fractured aquifer of the area is hosted.

Furthermore, from a hydrological analysis of the weather variables, a non-homogenous spatial behaviour has been identified (section 5.1.1). Nevertheless, to limit computational time and to simplify simulation, only data from the Carpineti weather station, located close to the Mulino delle Vene springs, have been utilized in the modelling.

5.7.2 HYDROGEOSPHERE MODEL

The 3D model has been built with the HydroGeoSphere finite elements code simulating fully coupled overland flow and variably-saturated groundwater flow (Fig. 5.59). The top layer has a constant depth of 1 m and the surface slice elevation is assigned according to the data from a DTM (5 m x 5 m) of the catchment. The subsurface domain is discretised using 5 layers uniformly distributed between the first layer and the bottom slice which has a constant elevation of 0 m a.s.l.. The mesh is composed of 1084 nodes and 1996 2D triangular elements (Model 1) with a mesh size about 200-600 m. Small elements would have allowed a more reliable representation of the surface domain and a better simulation of the surface-subsurface water interactions, but the computational time would had become too long considering the hardware available at the moment.

A second model has been built increasing the vertical discretization (Model 2). The subsurface domain is separated into two sectors, the first with a depth of 50 m is discretised using 3 uniformly distributed layers, the lower one is discretised using 5 layers.
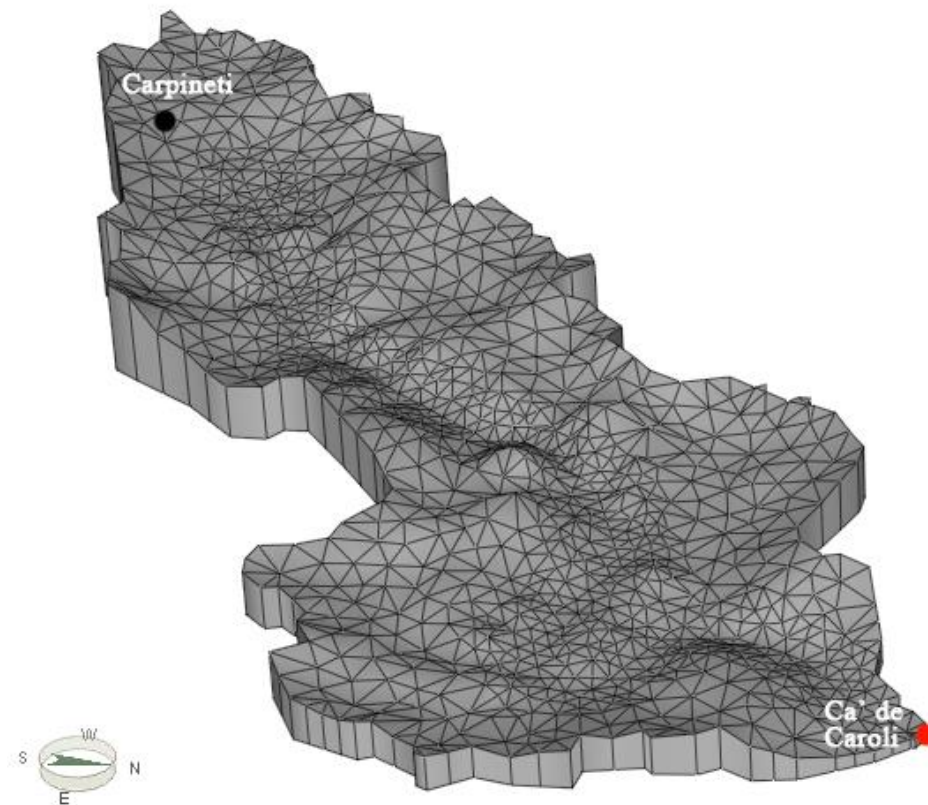
Figure 5.59 3D Hydrogeological model of the Tresinaro stream catchment built with HGS.

SIMULATION PROCEDURE

The first set of simulations have been carried out with reference to the years between the 2003 and the 2014 in order to pre-calibrate model parameters and to reproduce the observed daily discharge at the Ca' de Caroli gauge station, located at the catchment outlet. In order to limit computational time, the evapotranspiration has been introduced on a yearly basis. Instead, rainfall has been entered on a daily basis. In order not to incur in simulation problems, adaptive time stepping has been used based on the transient behaviour of the system. In particular, time steps have been forced so that groundwater piezometric level and surface water level do not vary more than 0.5 m and 0.05 m during each time-step. The calibration objective is to simulate, at least, a flow outlet of the same magnitude of the observed ones. The coarse space discretization has not allowed a better calibration of the model. In particular, at this stage, the observed piezometric levels in the area (the measures from three wells and a lake in the Mulino delle Vene springs area (Fig. 3.5) and one well in the alluvial fan) have not been considered for the calibration. The simulations with different parameters or model scheme have allowed a first sensitivity analysis of the model. In particular, a sensitivity analysis of the recharge has been done decreasing by the 10% the daily recharge.

BOUNDARY CONDITIONS

Two different model geometries have been tested (Model 1 and Model 2) with an increasing geometrical complexity. Moreover, each model havee different boundary conditions. In particular, three types of boundary conditions have been applied to Model 1, two specified fluxes and one surface flow boundary (Critical Depth, CD). In Model 2 a Head (H) boundary condition has been added to the previous ones.

Specified hydrogeological fluxes consist in rainfall (R) and potential evapotranspiration (ETP). Firstly, the rainfall rate [L/T; m/s] has been applied homogeneously over the surface area. The rainfall volumetric inflow [L^3/T] is assessed as a net flux multiplied by the contributing area when projected onto the xy plane. Secondly, the potential evapotranspiration [L/T] has been applied also to the top surface and it has been transformed in

flux by multiplying by the contributing area of the element face. The ETP boundary condition is used in conjunction with evapotranspiration properties.

To assign the specified fluxes boundary conditions, data from the Carpineti weather station (580 m a.s.l., Carpineti, RE) and the Hargreaves formula are used. R is assigned on daily basis; instead mean annual ETP is entered on an annual basis to limit computational time.

Head boundary condition (H), also known as first type or Dirichlet condition, is applied on the nodes corresponding to the alluvial fan border at the outlet of the model (Fig. 5.60). The head is set equal to the stream elevation in the outlet. The head boundary allow a groundwater flow outlet from the aquifer in the alluvial fan.

Furthermore, in the nodes corresponding to the closing point of the catchment at the Ca' de Caroli gauge station a Critical Depth (CD) surface flow boundary condition is applied (Fig. 5.60). CD boundary condition is implemented to simulate conditions at the lower boundaries of a hillslope. In particular, the CD condition forces the depth at the boundary to be equal to the critical depth, which is the water elevation corresponding to the minimum energy. This condition has been used to simulate the catchment outlet from Goderniaux et al. (2009).

No flow boundaries are applied in the other model borders and this corresponds to an impervious condition.
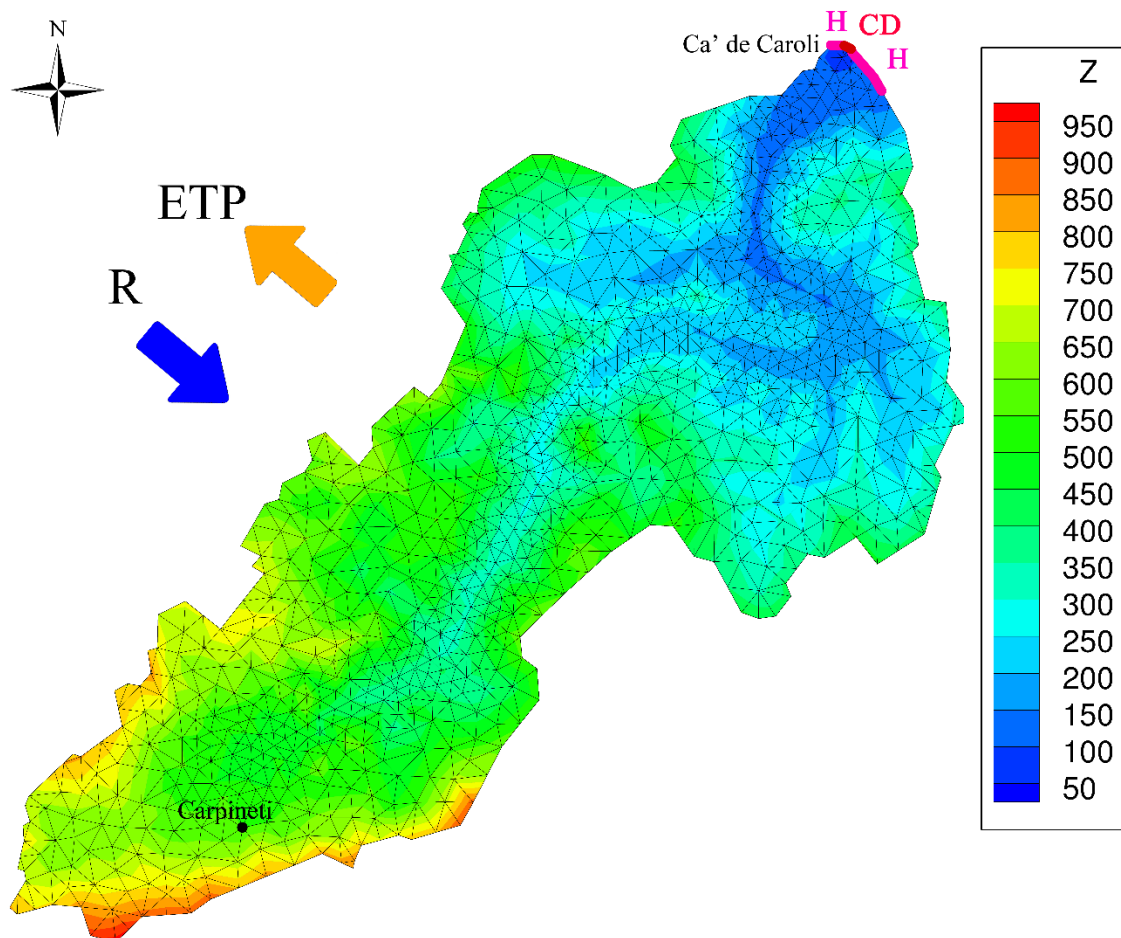
Figure 5.60 Elevation map of the Tresinaro stream catchment. The locations of boundary conditions were specified. The fuchsia line indicates the Head boundary condition (H), the red line the critical depth boundary condition (CD). Moreover, the blue (R) and the orange (ETP) arrows represent the two specified fluxes assigned on the surface area.

POROUS MEDIA PROPERTIES

The geological map of the area is used to define the model zones. In particular, the porous medium is divided in three areas, the alluvial fan zone, the fractured sandstone units (PAT4) and the clay rich units (Fig. 5.61). To simplify the model structure, we have started considering the porous media properties vertically constant (Model 1). Tab. 5.48 lists the parameters of the subsurface domain used in the simulation. The hydraulic conductivity has been changed during the first simulation attempts in order to maximize the reliability of the simulated stream discharge, only final values are reported in Tab. 5.48.

Table 5.48 Porous media properties values.

	K	Van Genuchten parameters		Total porosity	Specific storage
	(m/s)	Alfa (-)	Beta (m^{-1})	(-)	(m^{-1})
Fractured sandstones	10^{-5}			0.01	10^{-4}
Alluvial deposits	10^{-5}	1.9	6	0.25	10^{-4}
Clay-rich units	10^{-9}			0.001	10^{-4}

Figure 5.61 Map of the porous media area.

A second model is built considering for both the PAT4 and the alluvial fan units a constant depth of 50 m. For these simulations, Model 2 is used. Tab. 5.49 summarizes the parameters of the subsurface domain used in the simulation. The hydraulic conductivity has been changed during the first simulation attempts in order to maximize the efficiency of the stream discharge simulation, and only final values are reported in Tab. 5.49.

Table 5.49 Porous media properties values.

	K	Van Genuchten parameters		Total porosity	Specific storage
	(m/s)	Alfa (-)	Beta (m^{-1})	(-)	(m^{-1})
Fractured sandstones	10^{-5}			0.01	10^{-4}
Alluvial deposits	10^{-5}	1.9	6	0.25	10^{-4}
Clay-rich units	10^{-9}			0.001	10^{-4}

SURFACE MEDIA PROPERTIES

The land use map of the catchment (Fig. 5.62) is utilized to define two main zones for the surface flow, the first related to forest and the second to crop. At the moment, the urban areas have not been utilized due to the coarse mesh that does not allow the selection of smaller area than the element size. A third zone is defined along the Tresinaro stream. Tab. 5.50 summarizes the parameter values used in the simulation. As for the hydraulic conductivity, the Manning roughness coefficients (nx and ny) has been changed during the calibration attempts. Values are consistent with literature (Goderniaux et al, 2009; Aquanty, 2013).

Table 5.50 Surface media properties values.

Surface zone	nx - ny	Lc (Coupling length)
	(m$^{-1/3}$s)	(m)
Forest	4.5	10^{-2}
Crop	3	10^{-2}
Stream	0.03	10^{-2}
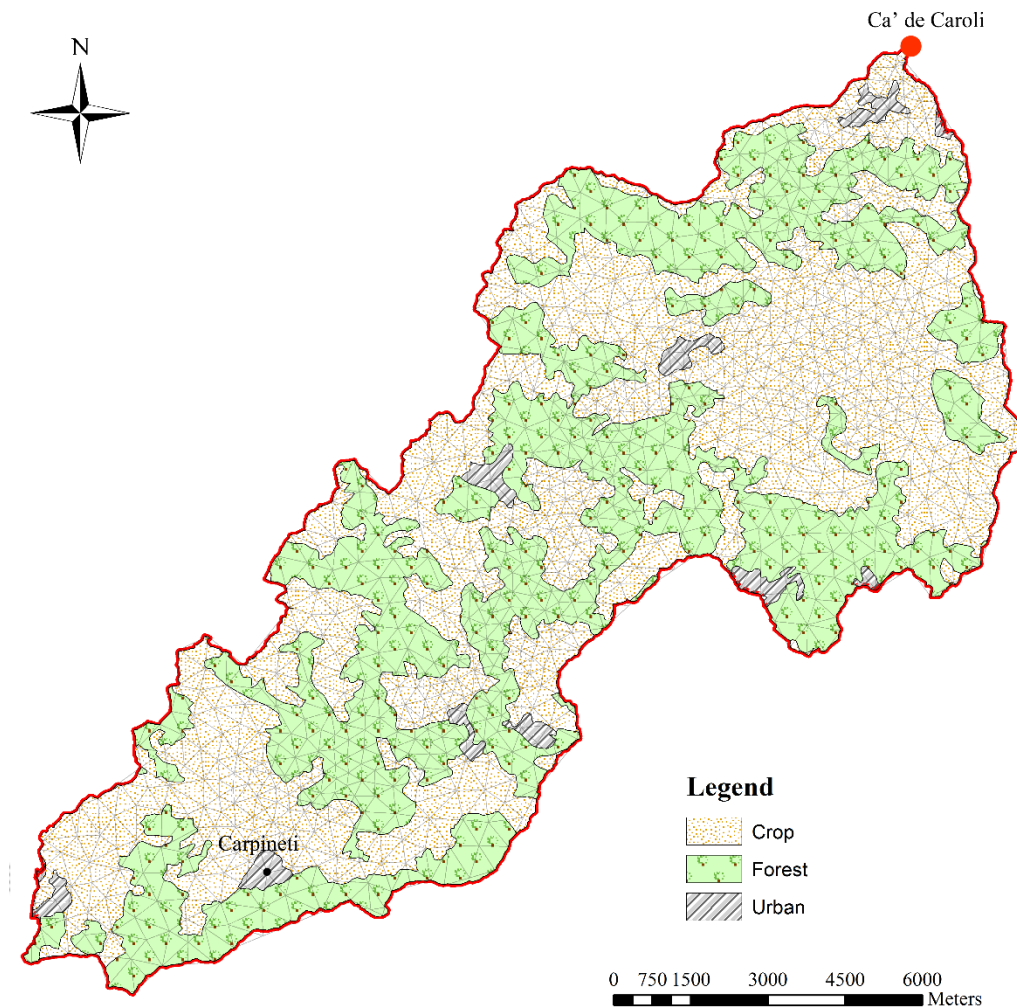
Figure 5.62 Land use map.

EVAPOTRANSPIRATION PROPERTIES

Two evapotranspiration zones are defined in accordance with the land use map (Fig. 5.62). In particular, a zone is related to forest and the other to crop cultivation. As for the surface properties, the urban land is not taken into account due the coarse mesh.

The parameters used to calculate the actual evapotranspiration are defined using values from literature (Krinstensen & Jensen, 1975; Scurloock et al., 2001; Asner et al., 2003; Li et al., 2008; Goderniaux et al., 2009; Aquanty, 2013) and are summarized in the Tab. 5.51. In absence of specific information about the Leaf Area Index (LAI) changes during the years, LAI is reduced during the winter of the 50% as done by Goderniaux et al. (2009).

Table 5.51 Evapotranspiration media properties values.

	Evaporation depth	Root depth	Max LAI	Transpiration fitting parameters			Canopy storage interception
	Le (m)	Lr (m)	(-)	C1 (-)	C2 (-)	C3 (-)	Cint (m)
Forest	2	5.2	6	0.3	0.2	10	10^{-5}
Crop	2	2.1	4	0.3	0.2	10	10^{-5}

121

5.7.3 SIMULATION RESULTS

A sensitivity analysis of the large scale model has been carried out. In particular, two model with increasing discretization complexity have been tested (Model 1 and Model 2). The HGS simulation results which better reproduce the Ca' de Caroli observed discharge are reported below. Moreover, a simulation with decreased daily recharge by the 10% has been executed in order to quantify the effects on the stream discharge and to perform a sensitivity analysis of the recharge variable.

MODEL 1

Model 1 is the more simplified model tested (section 5.7.2). The simulated discharge in the period 2003-2013 is represented in Fig. 5.63. The correlation coefficient between the simulated and the observed discharges is only 0.2. The total simulated discharge amount is larger than the observed one (simulated discharge equal to the 158% of the observed one). Indeed, in this model, the groundwater flow in the alluvial fan is not taken into account and all the output is forced to pass from the critical depth boundary condition. In the simulation period the stream budget is equal to the 66% of the total rainfall, consequently evapotranspiration is about the 44% of the rainfall input, no other output from the model is allowed.
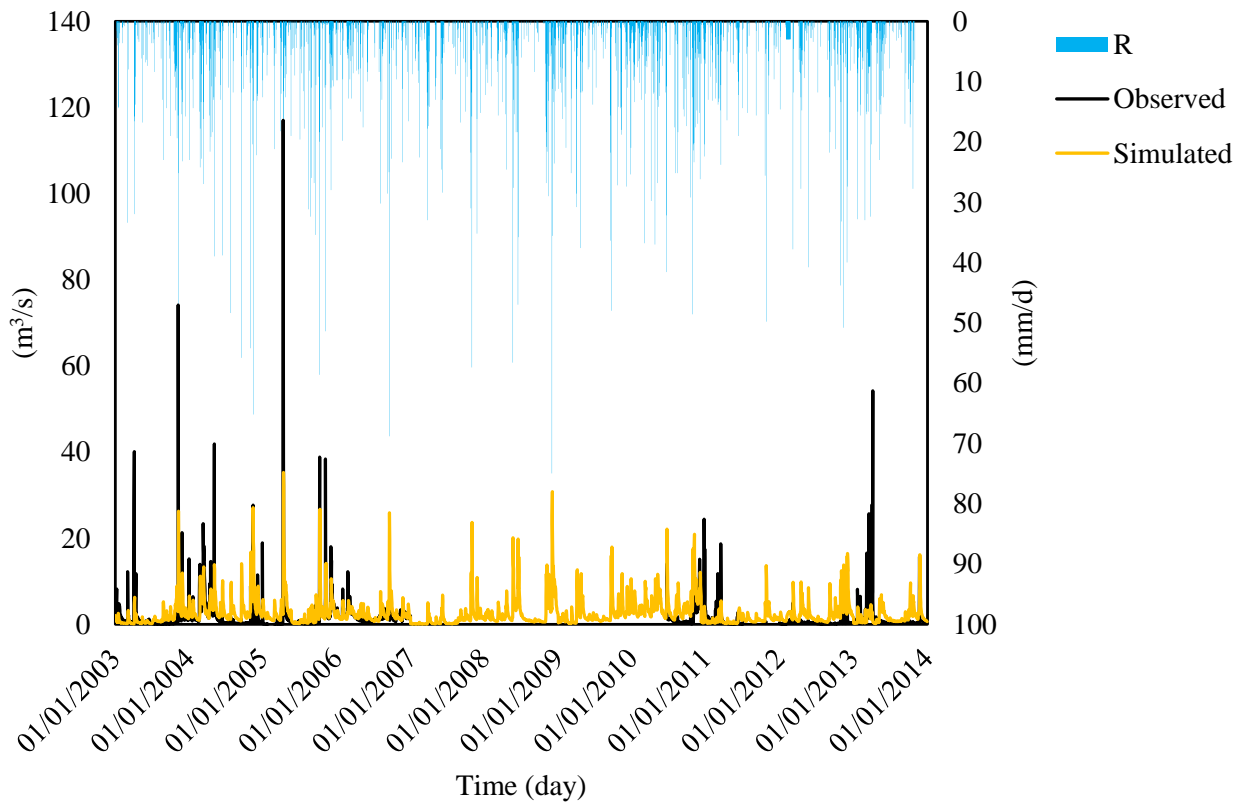
Figure 5.63 Observed and simulated discharges at the Ca' de Caroli gauge station with Model 1, along with the daily rainfall (R) observed at the Carpineti weather station.

MODEL 2

The second tested model allows a groundwater output throughout the alluvial fan (Head boundary condition) and it takes into account some geological pieces of information using vertically limited PAT4 and alluvial fan units. Model parameters are assigned according to literature and then they are changed during simulation achieving the values in section 5.7.2. The simulated discharge in the period 2003-2013 is represented in Fig. 5.64. The correlation coefficient between the observed and the simulated discharge is equal to 0.49. The major errors are found in the peak simulations. In fact, peak events are largely underestimated (up to the 70% of error) whereas low-flow values are well simulated. The average simulated discharge is about 1.77 m^3/s whereas the observed average is 1.62 m^3/s. The simulated discharge range between a minimum about 0 m^3/s (e.g. August 2012) and a maximum of 39.21 m^3/s (11th April 2013). The assessed discharge characteristic values (section 4.6.2) are reported in Tab. 5.52. In particular, the simulated Q(50) is equal to 0.90 m^3/s and the Q(80) is 0.19 m^3/s (Tab. 5.52), respectively overestimating and underestimating the observed data.

Moreover, the total simulated and observed discharges amounts are about the same; in particular the simulated discharge is equal to the 104% of the observed one. In terms of total water budget, in the simulation period the total outflow from the stream is about the 47% of the precipitation (equivalent to 7.06 x 10^3 m^3/s). Moreover, the 5% of the water leaves the model as subsurface flow from the alluvial plain deposits (7.32 x 10^2 m^3/s). Therefore, about the 48% of rainfall is transformed in actual evapotranspiration (7.31 x 10^3 m^3/s). These percentage results are consistent with observations. Indeed, from the observed data, the stream flow water budget amounts to the 48% of the total precipitation (period 2003-2006).

Table 5.52 Observed and simulated characteristic discharge values (m^3/s) and differences in percentage.

	Observed	Model 2	diff.
Q(95)	0.05	0.02	-55%
Q(80)	0.23	0.19	-19%
Q(50)	0.65	0.90	+39%
Q(05)	5.24	6.40	+22%
MEAN	1.62	1.77	+9%
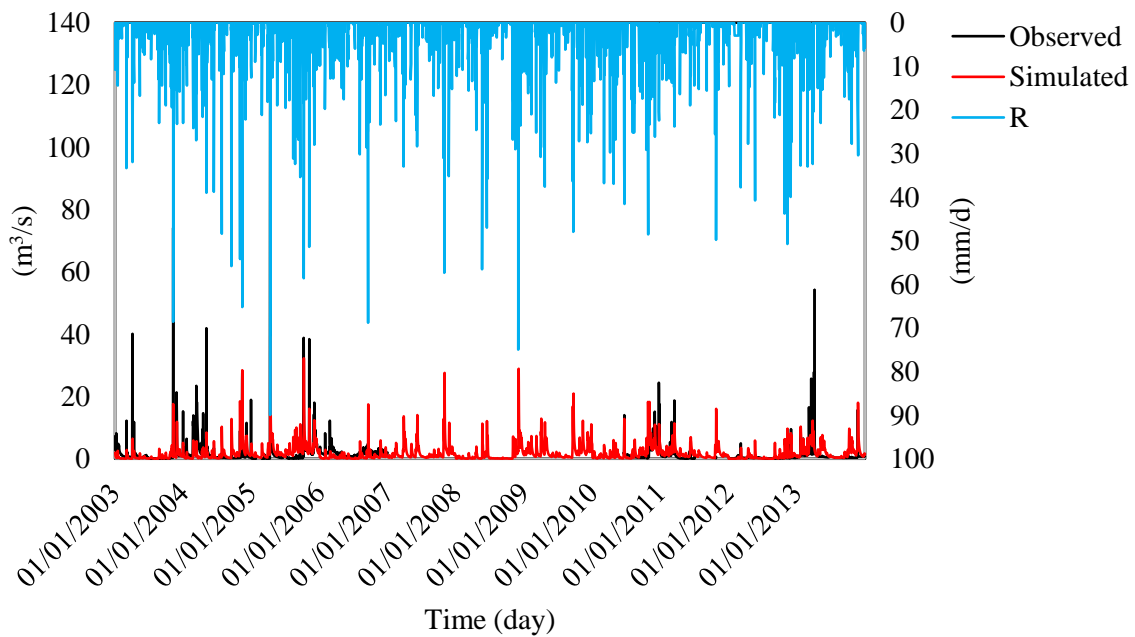
Figure 5.64 Observed and simulated daily discharge at the Ca' de Caroli gauge station with Model 2 along with the daily rainfall (R).

123

MODEL 2-2 PRECIPITATION DECREASE

Model 2 has been used for the sensitivity analysis of the precipitation. A simulation equal to the previous one has been executed decreasing by the 10% the daily precipitation amount. The simulated discharge is reported in Fig. 5.65, the average discharge is equal to 1.42 m^3/s ranging between a maximum about 33.04 m^3/s (11th April 2013) and a minimum about 0 m^3/s (e.g. August 2012). Characteristic discharge values are reported in Tab. 5.53, in particular the simulated Q(50) is equal to 0.64 m^3/s and the Q(80) is 0.13 m^3/s.

The terms of the water budget change from Model 2. In particular, in the simulation period the total outflow from the stream is about the 42% of the precipitation input (5.72 x 10^3 m^3/s with a rainfall of 1.36 x 10^4 m^3/s), subsurface flow to the alluvial plain deposits is the 5% (equivalent to 6.74 x 10^2 m^3/s), and actual evapotranspiration is the 53% (7.19 x 10^3 m^3/s).

Table 5.53 Characteristic discharge values (m^3/s) and differences in percentage simulated respectively with Model 2 and Model 2-2 with a rainfall decreased by the 10%.

	Model 2	Model 2-2 (R-10%)	diff.
Q(95)	0.02	0.01	-43%
Q(80)	0.19	0.13	-33%
Q(50)	0.90	0.64	-29%
Q(05)	6.40	5.20	-19%
MEAN	1.77	1.42	-20%
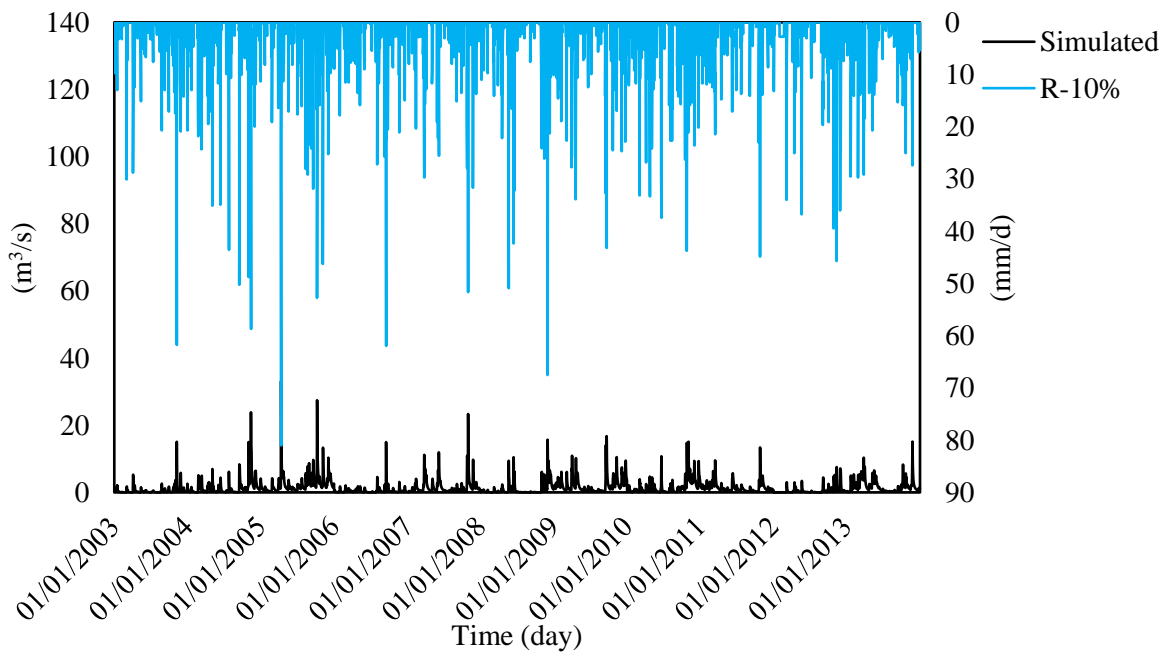
Figure 5.65 Simulated daily discharge at the Ca' de Caroli gauge station obtained with Model 2 after a decrease by the 10% of rainfall along with the daily decreased rainfall (R-10%).

5.7.4 DISCUSSION

The first simulation attempt (Model 1) doesn't account for the outflows in the alluvial fan deposits, the depth of the alluvial fan and of the fractured sandstones. For these reasons, it has been substituted by Model 2, that it has been used for further sensitivity simulations.

Model 2 results are consistent with observations, in particular, the average simulated discharge is about 1.77 m^3/s whereas the observed average is 1.62 m^3/s (+9%). Moreover, the water budget of the stream discharge in the simulation period is equal to the 109% of the observed ones (respectively 3.87 x 10^8 m^3 and 3.54 x 10^8 m^3). Therefore, the water balance components are well simulated (Fig. 5.67a,b).

Furthermore, the simulation with a decreased precipitation (Model 2-2) allows the assessment of the effects of a change in precipitation on the catchment water cycle. First at all, the reduction by the 10% of the precipitation affects the Tresinaro discharge with a reduction by the 20% of the average discharge (from 1.77 m^3/s to 1.42 m^3/s; Tab. 5.53). Furthermore, a decrease of all the characteristic discharge values is assessed (Tab. 5.53) with a maximum decrease for the low-flow values (Q(95) decreased by the 43%, Tab. 5.53).

Fig. 5.66 represents the cumulative distribution functions of the Tresinaro stream discharge observed or simulated at the Ca'de Caroli gauge station, at the output of the modelled area. The graph points out the underestimation of high discharge values and the good estimation of the low part of the curve (discharge minor of Q(50)).
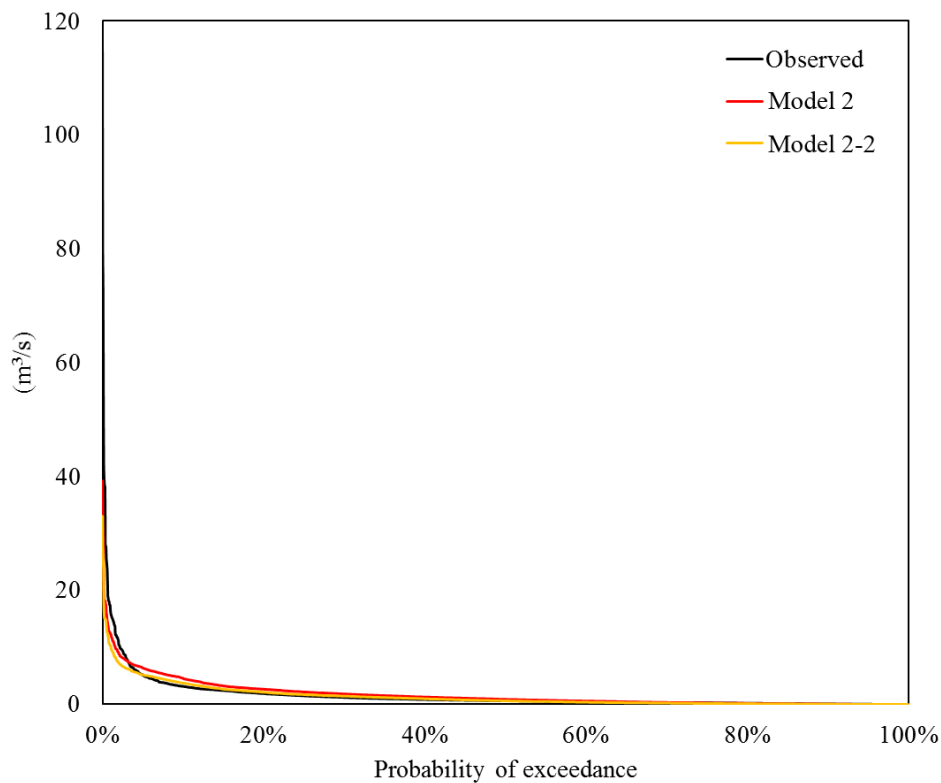
Figure 5.66 Cumulative distribution functions of the observed and simulated Tresinaro stream discharges at the Ca' de Caroli gauge station.

Finally, the components of the water cycle change (Fig. 5.67). In particular, the total evapotranspirated volume (actual evapotranspiration) is about the 48% of the rainfall with Model 2 (equivalent to 7.31 x 10^3 m^3/s) and about the 53% of precipitation with Model 2-2 (equivalent to 7.19 x 10^3 m^3/s). Instead, the water budget of the stream decreases from the 47% (7.06 x 10^3 m^3/s, Model 2) to the 42% (5.72 x 10^3 m^3/s, Model 2-2) of the total

rainfall. The simulated subsurface flow is the 5% of the rainfall for both the simulations (equivalent to 7.32 x 10^2 m³/s for Model 2 and 6.74 x 10^2 m³/s for Model 2-2).

		Observed (a)	Model 2 (b)	Model 2-2 (c)
INPUT	R	100%	100%	100%
OUTPUT	Actual Evapotranspiration	-	-48%	-53%
	Runoff	-48%	-47%	-42%
	Subsurface flow	-	-5%	-5%
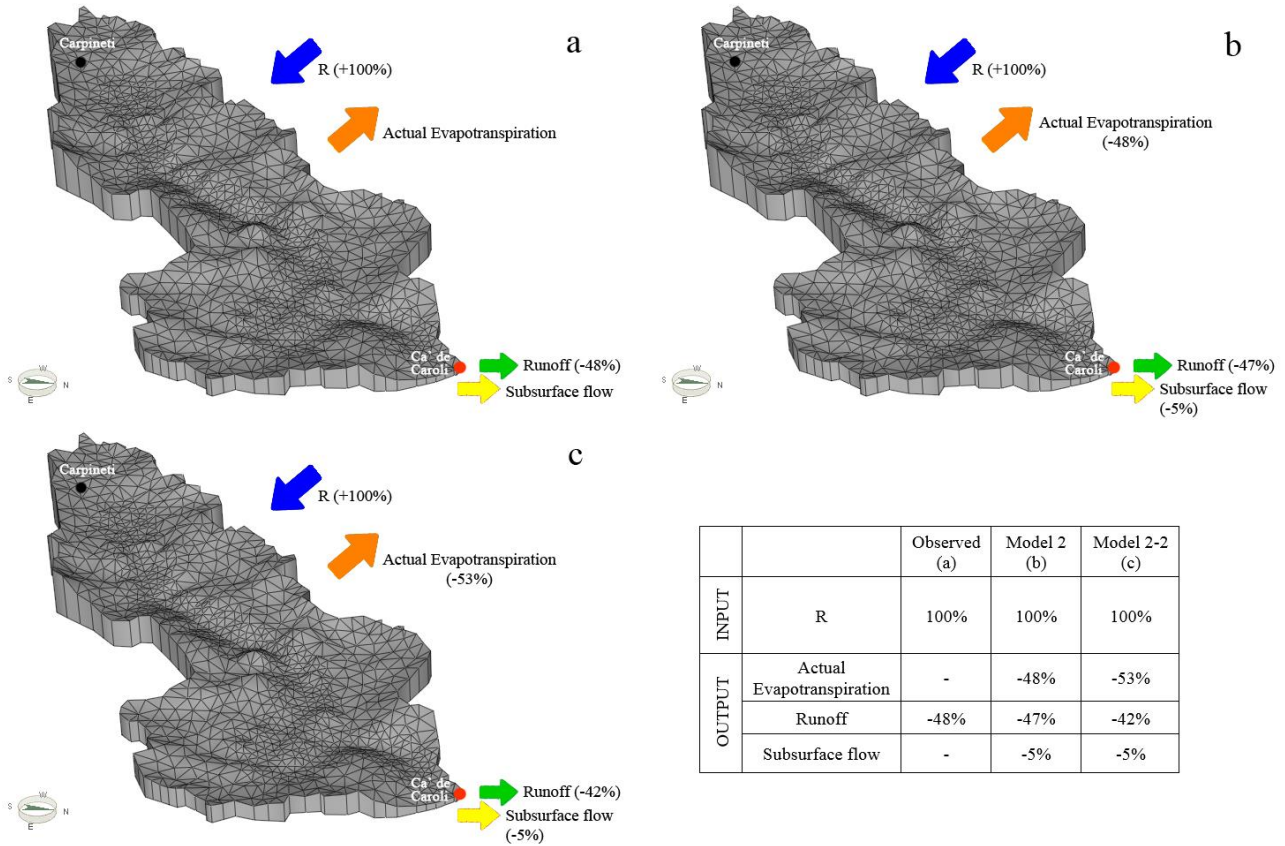
Figure 5.67 Schematic representation of the total water budget in the simulation period (2003-2013) respectively for the observed data (a), for the simulation of Model 2 (b) and for the simulation of Model 2-2 (c), along with the resuming table of the water budget components.

During simulations, computational time has limited the calibration efforts. Indeed, one simulation takes up to one months of time and instability problems sometimes cause the block of the run. To overcome the problems the mesh has been simplified with larger elements and average data have been utilized. To optimize the simulation procedure and to allow a more detailed mesh to be used, the use of a computational centre is recommended.

Further studies should improve the model starting from this:

- Decreasing the mesh size;
- Using piezometric levels measured in some observation points during the calibration procedure and increasing the number of monitored points;
- Using a distribution of precipitation assessed from the data of the different weather stations in the area;
- Carrying out some surveys in the area to validate the geological model.

5.8 LAND USE ANALYSIS

An in-depth analysis of the 4 available land use maps has been carried out on the recharge area of the Mulino delle Vene springs in order to investigate the land use trend in the last decades and to assess the different land use types to be used in the Penman-Monteith evapotranspiration assessment. Hereafter a description of the land use analysis for each map is given.

Land use map 1976

In Fig. 5.68 the land use map with the different types of land use in the recharge area of the Mulino delle Vene springs is shown. To simplify the classification the different type have been associated in Agricultural land (Arable land) and Forest (Forest, Shrub, Sparse shrub). Then the percentage of land for each type has been assessed. In particular, the Forest occupies 52% of the total recharge area and the Agricultural land the 48%.
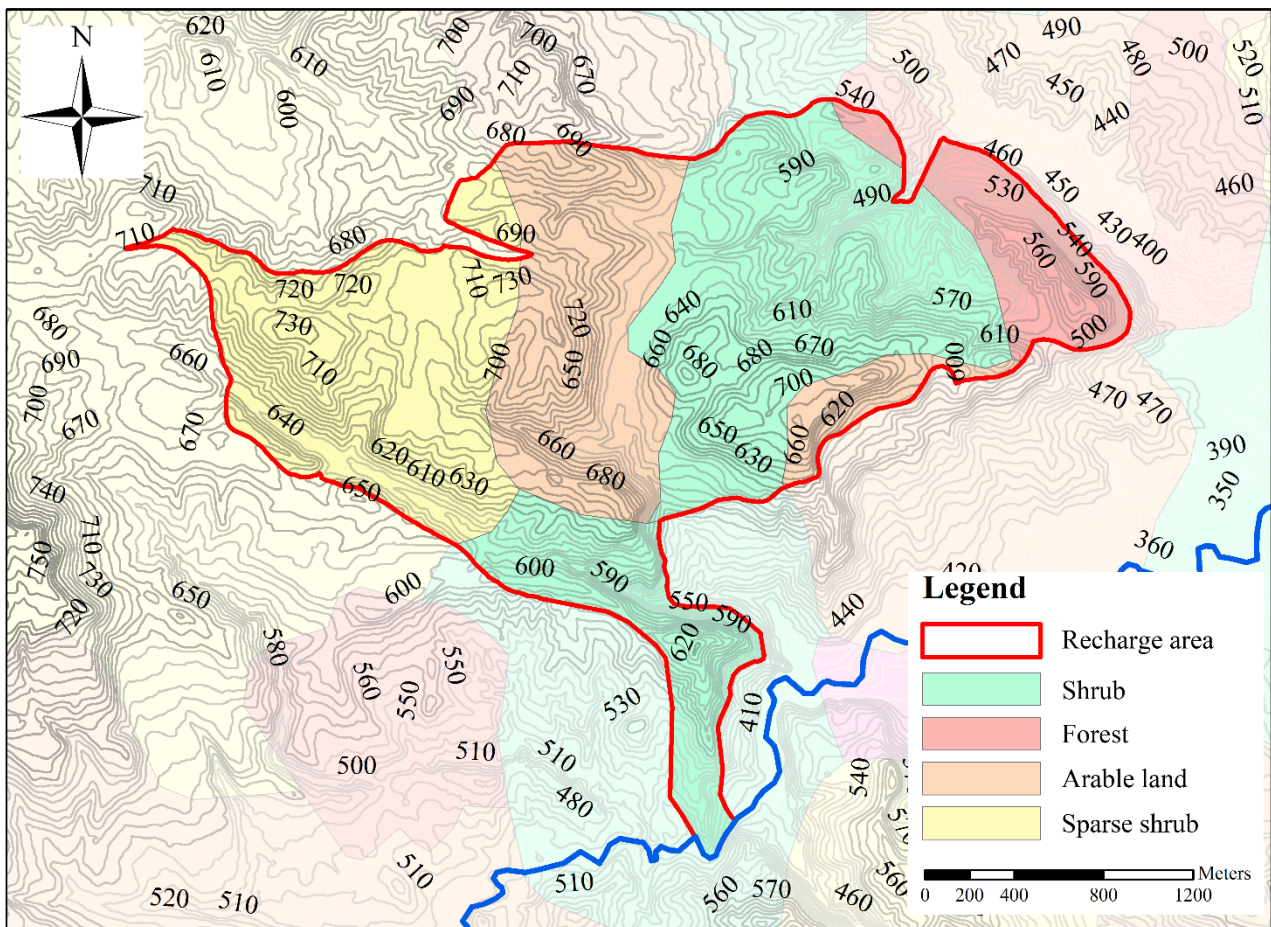
Figure 5.68 Land use map of the 1976.

Land use map 1994

The land use map of the Mulino delle Vene area is reported in Fig. 5.69. The different land use types have been associated in Agricultural land (Arable land, Rural land), Forest (Forest, Chestnut trees, Shrub) and Urban land. Then the percentage of land for each type has been assessed. In particular, the Forest covers the 52% of the total recharge area, the Agricultural land the 46% and the Urban land the 2%.
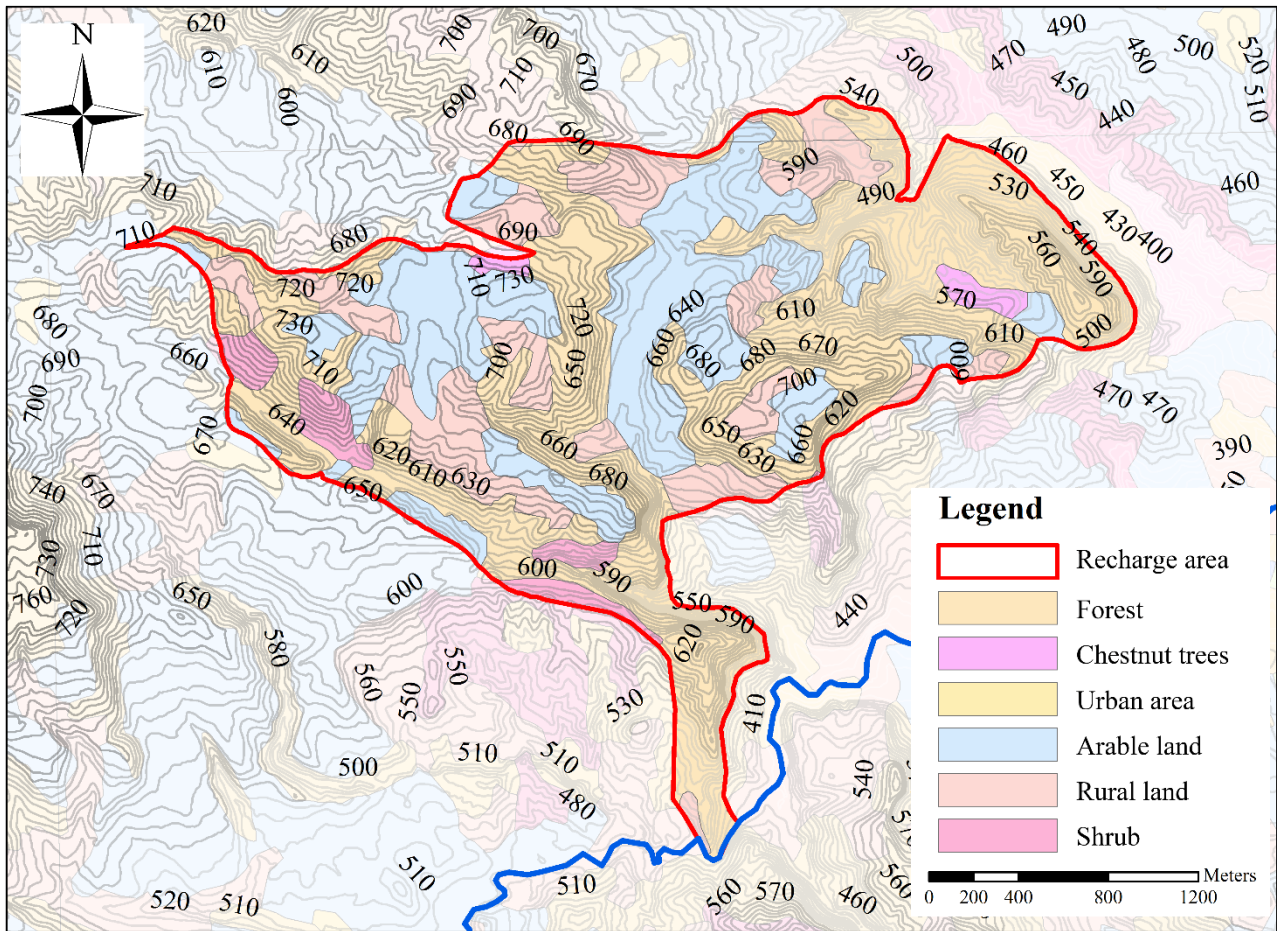
Figure 5.69 Land use map of the 1994.

Land use map 2003

From the 2003 land use map, the agricultural land is equal to the 43% of the recharge area and the forest is equal to the 57%. An image of the land use map in the springs area is reported in Fig. 5.70.
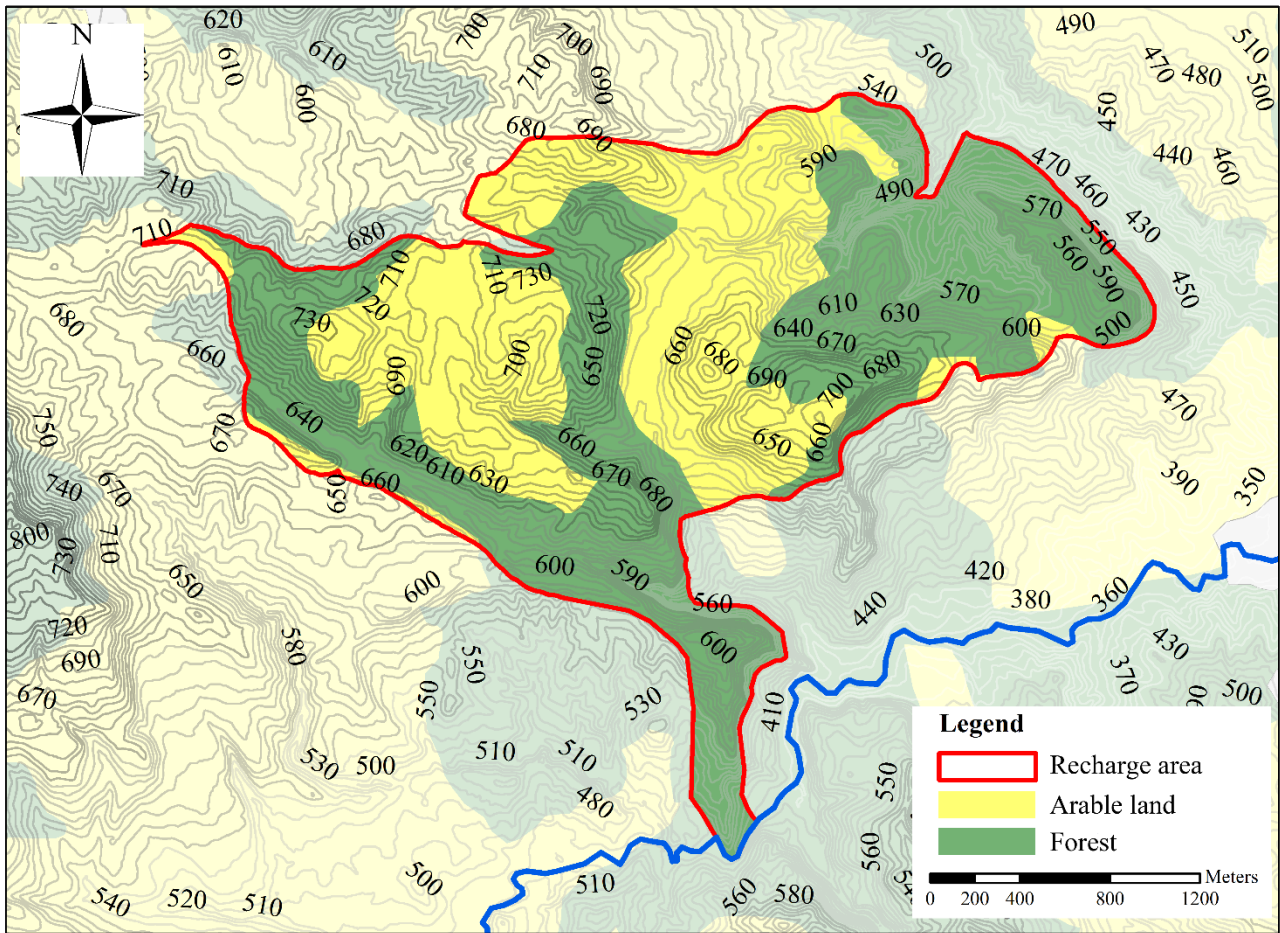
Figure 5.70 Land use map of the 2003.

Land use map 2008

The 2008 land use map in the springs area is represented in Fig. 5.71. The land use types have been classified in Forest (forest, forest mixed and shrub), Agricultural land (arable land, rural land) and Urban area. In particular, the Agricultural lands are the 41% of the springs recharge area, the forest is the 58% and the Urban lands are the 1%. To simplify the evapotranspiration assessing, the Urban areas have not been considered and they have been assimilated to agricultural land. Therefore, in the potential evapotranspiration estimation (Penman Monteith equation, section 4.1.1) the following weights of the land have been utilised: Agricultural land 42%, Forest 58%. These weights have been considered constant during the period 2009-2015 in which the potential evapotranspiration with the Penman-Monteith formula has been assessed in order to calibrate the Hargreaves results.
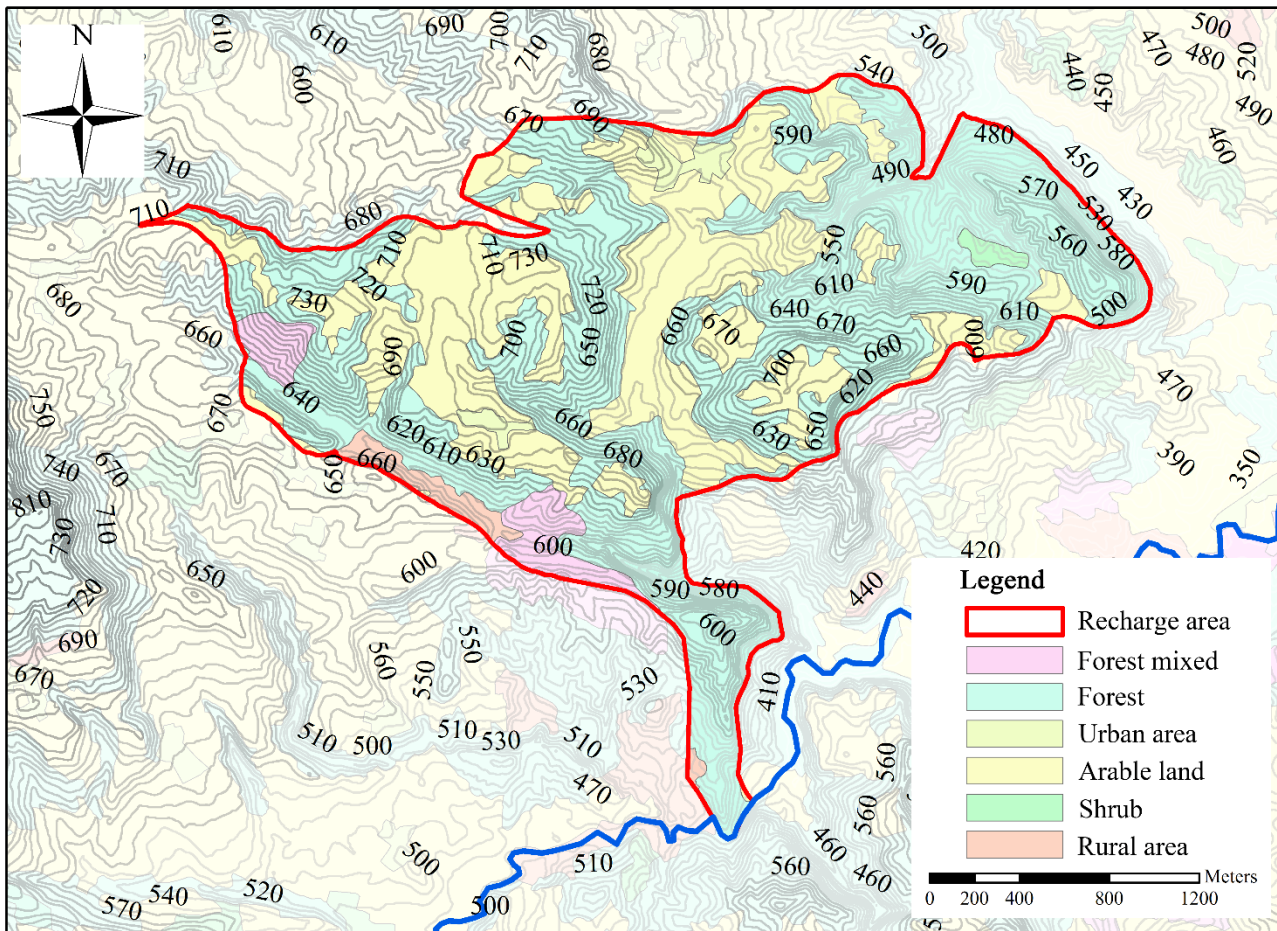
Figure 5.71 Land use map of the 2008.

COMPARISON

In the analysed period (1976-2008) the land use of the recharge area of the Mulino delle Vene springs change considerably (Fig. 5.72). In particular, the forest increases from the 52% to the 58% (+6%) while the agricultural land decreases from the 48% to the 41% (-7%). Urban lands are almost negligible in the area.
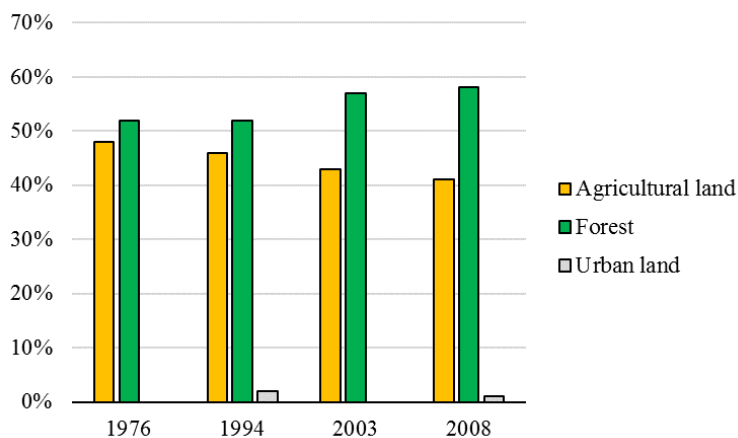
Figure 5.72 Assessed percentage of the three land use type in the four land use map.

130

6. CONCLUSION

The objectives of this research are the following:

- Hydrological analysis of the Tresinaro stream catchment and of the main groundwater resources in the area, the Mulino delle Vene springs;
- Numerical modelling of the hydrogeological systems analysed;
- Evaluation of the effects of climate change on the groundwater – surface water resources of the Tresinaro stream catchment using the numerical models developed during the research.

This objectives have been set in response to the growing water stress problems affecting Italy and in particular the Apennines area. They respond to a lack of researches carried out in the field of climate change and groundwater relationship, especially in the northern Apennines. The case study analysed in this work is representative of the several mountainous aquifers of the Apennines. Therefore, it is expected that they all will react to climate change in a similar way.

Moreover, this research has allowed further efforts in the numerical modelling of fractured aquifers, which is still a challenge in hydrogeological studies.

6.1 CLIMATE CHANGE SCENARIOS

To assess the climate change impacts on the groundwater resources of the Tresinaro stream basin, five RCMs have been analysed. The climate change scenarios have been statistically downscaled from RCMs using two downscaling techniques: the delta change method and the Cumulative Distribution Function transform (CDF-t) method. The delta change method projects changes only to the mean values of the climate variables whereas the CDF-t method takes into account also of the variable statistical distributions in the time. The two techniques are used to generate the future daily climatic series for the 30-year time period between the 2021 and the 2050 (future), starting from the 30-year time period of observed daily data between the 1984 and the 2013 (baseline), and using five different RCM scenarios from the A1B family. Comparing future downscaled data with baseline data, an increase of temperature into the future is forecasted at each month (+1.3 °C) with both the techniques. Instead, the average annual rainfall decreases by the 3% or the 2.3% respectively with the delta change or the CDF-t method. Moreover, the CDF-t method forecasts a change in the monthly rainfall distribution. In particular, rainfall decreases mostly during the summer months (e.g. -30 mm in June) and it increases during the winter months (e.g. +25 mm in February). Results are consistent with the forecasts presented in the IPCC reports (IPCC, 2007).

Afterwards, downscaled scenarios have been used in combination with the calibrated rainfall-runoff models to evaluate the effects of climate change on the Mulino delle Vene springs discharge.

6.2 NUMERICAL MODELLING

In this work, several numerical models have been developed of both the Mulino delle Vene fractured aquifer (local scale model) and of the Tresinaro stream catchment (large scale model).

Firstly, this study represents the first modelling attempts of the Mulino delle Vene fractured aquifer. The area has been object of studies and analysis since 2013; in particular, the springs discharge is in continuous monitored and the conductivities of several outcrops in the recharge area have been assessed (Petronici, 2014). Moreover, the aquifer feeding the springs has been identified by Cervi et al. (2014) and Vizzi (2014) with a sandstone plateau (Pantano sandstones, unit of Santa Maria, PAT4) affected by a network of faults and joint. The springs represent the one and only outflow of the hydrogeological structure. Unfortunately, there are only few information about the piezometric levels and the flow behaviour in the fractured rock mass. This study has allowed a first investigation of the groundwater flow behaviour of the aquifer and a sensitivity analysis of the hydrogeological parameters. Further investigation efforts will include in-continuous monitoring of the piezometric levels in the observation points and tracer tests.

More in detail, two finite elements models of the fractured aquifer feeding the Mulino delle Vene springs have been built respectively with the FEFLOW and the TRANSIN code. The FEFLOW model has allowed the analysis of different conceptual models. Even if calibration is not successful, the models are very important to better understand the complexities of the groundwater flow system. In particular, results suggest the possibilities of some inflow in the PAT4 fractured aquifer from close geological units. The main result of this work is that it pointed out that the hydrogeological catchment feeding the Mulino delle Vene springs is likely to be more extended than the PAT4 unit. It is reliable that the hydrogeological catchment includes also the surrounding sandstone unit (Pantano sandstones, PAT) and that all these units are connected throughout the system of fractures and faults at a regional scale.

The TRANSIN code has allowed the calibration of the system in steady-state conditions (Nash-Sutcliffe efficiency larger than 0.9) and the comparison of different conceptual models. The calibration procedure has allowed the assessment of a range of possible calibrated conductivity values for the sandstones unit ranging from 1.16×10^{-4} m/s to 1.16×10^{-7} m/s, respectively for the more fractured rock mass (area near the main fault) and the less fractured rock mass (hill near observation point 1). In particular, the sensitivity analysis of the recharge has allowed the assessment of a small range of hydraulic conductivity for the less fractured rock mass depending on the climate condition, ranging from 6.94×10^{-8} m/s to 1.96×10^{-7} m/s respectively for the driest and the wettest period. These conductivity values belong to ranges found in literature (Allen et al., 1997; Gómez et al., 2010; Zhang & Hiscock, 2010) and to the range found with the field tests in the area (Petronici, 2014; Vizzi, 2014). Moreover, some transient state simulations with the objective to investigate the water table fluctuations have been executed.

The results of the two codes highlight the complexity inherent in the numerical modelling of fractured aquifers. Even if the TRANSIN model gives satisfactory results (Nash-Sutcliffe efficiency higher than 0.9), the FEFLOW results and the heterogeneity of the system suggest that more observation points of the piezometric level spread on the modelled area are necessary for a good calibration.

At this moment, 3D numerical EPM models of the groundwater flow in the fractured aquifer have been built. The DFN modelling approach should have allowed a more realistic groundwater flow simulation due to the deterministic and stochastic description of the discontinuities. Future studies will focus on the application of the DFN approach in the modelling of this aquifer. In particular, both outcrop-scale fractures and lineaments can be considered for DFN model generation and subsequent conductivity and specific storage determination (Voeckler & Allen, 2012). Moreover, the outcrops scale measurements have to be integrated with tracer tests and groundwater levels monitoring in a larger number of wells. Information from wells are fundamental to have data about the rock mass at depth and tests will allow the hydrogeological parameters of the aquifer to be estimated.

Secondly, some rainfall-runoff models have been used to simulate the Mulino delle Vene springs discharge. In particular, two rainfall-runoff models have been developed and calibrated successfully on the observed daily springs discharge data. The first model is inspired to the Hymod model structure (modified Hymod model) and the calibration performance is very good (Erel equal to 0.83 in the calibration period and to 0.73 in the validation period). The second model belongs to the multiple reservoir models group and the calibration is satisfactory (Erel equal to 0.89 and to 0.72 for the calibration and validation period respectively), as well. Afterwards, these models have been used in combination with climate change scenarios to assess the climate change effects on the springs discharge.

Finally, a large scale model of the Tresinaro stream catchment has been built with the finite elements code HydroGeoSphere. This model is a physically based, spatially distributed, integrated surface-subsurface hydrological model and it enables a more realistic representation of the system. Some sensitivity analysis have been executed and the effects of a decrease in the rainfall has been assessed. In particular, the reduction by the 10% of the precipitation affects the Tresinaro discharge with a reduction by the 20% of the average stream discharge. This study outlines the usefulness of a computer centre to reduce the computational time of

simulations. The calibration of the Tresinaro stream catchment model will be possible only if simulation will take less computational time.

6.3 CLIMATE CHANGE IMPACT ON THE SPRINGS

The RCMs data are used in combination with the rainfall-runoff models to assess the climate change impacts to the Mulino delle Vene springs discharge. Moreover, the results of this work lead to considerations that can be applied to several springs in the northern Apennines, which have similar hydrogeological characteristics with respect to the Mulino delle Vene springs. Springs fed by fractured aquifer represent the main sources of water in the Apennines, and the decreasing of their yield would lead to water resources management problems.

Considering results achieved in this study, it is very likely that water stress into the future will be exacerbated. Even if the average annual effective recharge does not change in the future, the springs discharge during low flow periods will decrease due to the different rainfall pattern throughout the year. In particular, if compared to the baseline data, the future 7Q10 decreases about the 25% and the duration of continuous low flows below the threshold Q(80) changes severely as the years with continuous low flow lasting between 51 and 100 days will increase by a third and between 101 and 150 days will duplicate (results of the modified Hymod model).

This is of concern because it also means that the groundwater quantities supplying the Tresinaro stream and then the alluvial plain aquifer will decrease, while they are already intensively exploited. Furthermore, the water demand in the future might increase, due for example to an intensification of irrigation practices during the dry periods. The findings of this work are supported by the results of several Authors, which analysed the effect of climate change in other Italian regions (Cambi & Dragoni, 2000; Gattinoni & Francani, 2010).

The present work, together with the results of these Authors, highlight the sensitivity of the Italian water resources to changes in the climate. The changes in groundwater intra-annual discharges, together with the changes to rainfall pattern, can also influence the river network in terms of its hydrological and ecological behaviour and potentially alter the process of recharging the porous aquifers in the alluvial plain. To face the increasing water stress problems, the delineation of integrated practices for the management of water resources is a key point in the future that needs to be solved as soon as possible. In fact, efficient resource management is of great importance, for both mitigation and adaptation purposes (Howells et al., 2013).

6.4 GENERAL CONCLUSIONS AND PERSPECTIVES

This research has allowed the development and comparison of several numerical models of the fractured aquifer feeding the Mulino delle Vene springs (local scale models) and of an integrated surface-subsurface model of the Tresinaro stream catchment (large scale model) in the northern Apennines. The results offer numerous additional general remarks to be pointed out.

First of all, the most innovative part of the work is represented by the application of the rainfall-runoff models to assess the climate change effects on the Mulino delle Vene springs discharge. No other works about the application of rainfall-runoff models for the simulation of groundwater resources in the northern Apennines have been carried out so far. Their use and combination with sophisticated climate change scenarios constitutes an innovation and advances the study of climate change impacts on groundwater resources. Furthermore, results achieved in this work are specific to the case study of the Tresinaro stream catchment but the developed methodology and the main conclusions drawn can be applied easily to other case studies worldwide.

Secondly, the problems related to the finite elements models of the fractured aquifer of Mulino delle Vene are evident. In fact, the few information available about the groundwater system in the area have complicated the local modelling efforts. Further investigations will help in the improvement of the finite elements models. One more difficulty, using the large scale model, is the computing time. Future studies will focus on the calibration of a more detailed model of the area. The calibrated large scale model will allow the assessment of the climate

change effects on the catchment water resources and on the mountainous water supply to the alluvial plain aquifer.

In addition, the present study focuses on the direct impacts of climate change on groundwater resources but other factors may also affect indirectly the groundwater resources. Examples of such factors are the evolution of land use or changes in agricultural practices that can be considered in the modelling. This might also help in making decisions for appropriate land-use development planning to safeguard the water resources in the catchment.

Finally, as groundwater and surface water are inseparable components of the hydrologic cycle, several Authors (Goderniaux et al., 2009; Holman et al., 2012) recommended the use of an integrated code, asserting that concrete conclusions can only be made if groundwater - surface water interaction is included in climate change impact studies. Instead, a simple numerical model could be easily applied with even good results. In particular, this work has pointed out the good capacity of simple rainfall-runoff models to reproduce and simulate the springs discharge behaviour in the future. Therefore, before starting with numerical modelling, the real objectives of the work must be accurately pointed out. If the objectives are strictly related to quantity problems, a rainfall-runoff model, as the ones developed in this study, could be applied with satisfactory results. If the objectives are related to the water quality, integrated models have to be taken into account being conscious of the big amount of data and of the large computational time needed to carry out the simulations.

REFERENCES

Ahrens C.D. (2006) Meteorology Today: Introduction to Weather Climate and Environment, 2008. Brooks/Cole, Belmont, California, US.

Ala-aho P., Rossi P. M., Isokangas E., & Kløve B. (2015) Fully integrated surface–subsurface flow modelling of groundwater–lake interaction in an esker aquifer: Model verification with stable isotopes and airborne thermal imaging. Journal of Hydrology, 522, 391-406.

Allen D.J., Brewerton L.J., Coleby L.M., Gibbs B.R., Lewis M.A., MacDonald A.M., Wagstaff S.J. & Williams A.T. (1997) The physical properties of major aquifers in England and Wales. British Geological Survey Technical Report WD/97/34. Environment Agency R&D Publication 8, 312 pp.

Allen R.G., Pereira L.S., Raes D. & Smith M. (1998) Crop evapotranspiration: Guidelines for computing crop water requirements, Irrig. and Drain. Paper No. 56, United Nations Food and Agriculure Organization.

Allen D.M., Mackie D.C. & Wei M. (2004) Groundwater and climate change: a sensitivity analysis for the Grand Forks aquifer, southern British Columbia, Canada. Hydrogeology Journal, 12, 270-290.

Alley M.W. (2001) Ground Water and Climate. GROUND WATER, 39(2).

Amit H., Lyakhovsky V., Katz A., Starinsky A. & Burg A. (2002) Interpretation of spring recession curves, Ground Water, 40(5), 543-551.

Angelini P. & Dragoni W. (1997) The problem of modeling limestone springs: the case of Bagnara (North Apennines, Italy), Ground Water, 35(4), 612-618.

Antolini G., Auteri L., Pavan V., Tomei F., Tomozeiu R. & Marletto V. (2016) A daily high-resolution gridded data set for Emilia-Romagna, Italy, during 1961-2010. International Journal of Climatology, 36, 1970-1986.

Aquanty Inc. (2013) HGS, HydroGeoSphere User Manual 2013. Pp. 459.

ASCE (1993) Criteria for evaluation of watershed models. J. Irrigation Drainage Eng. 119(3), 429-442.

Asner G.P., Scurlock J.M.O. & Hicke J.A. (2003) Global synthesis of leaf area index observations: implications for ecological and remote sensing studies. Global Ecology & Biogeography, 12(3), 191–205.

Bastola S., Murphy C. & Sweeney J. (2011) The role of hydrological modelling uncertainties in climate change impact assessment of Irish river catchments. Advances in Water Resources, 34, 562-576.

Batelaan O. & De Smedt F. (2001) WetSpass: a flexible, GIS based, distributed recharge methodology for regional groundwater modeling. In: Gehrels H., Peters J., Hoehn E., Jensen K., Leibundgut C., Griffioen J., Webb B., Zaadnoordijk W.J. (eds) Impact of human activity on groundwater dynamics, IAHS Publ 269, IAHS, Wallingford, UK, 11–17.

Bates B.C., Kundzewicz Z.W., Wu S. & Palutikof J.P. (2008) Climate Change and Water. Technical Paper of the Intergovernmental Panel on Climate Change, IPCC Secretariat, Geneva, 210 pp.

Barthel R. & Banzhaf S. (2016) Groundwater and surface water interaction at the regional-scale–A review with focus on regional integrated models. Water Resources Management, 30(1), 1-32.

Bekele E.G. & Knapp H.V. (2010) Watershed modeling to assessing impacts of potential climate change on water supply availability. Water Resources Management, 24(13), 3299-3320.

Beran M.A. & Gustard A. (1977) A study into the low-flow characteristics of British rivers. Journal of Hydrology, 35, 147–157.

Berg M.A. & Allen D.M. (2007) Low flow variability in groundwater fed streams. Canadian Water Resources Journal, 32(3), 227-246.

Berger K. (2004) The Hydrologic Evaluation of Landfill Performance (HELP) Model: Engineering Documentation for HELP 3.80 D—Enhancements Compared to HELP 3.07. Tech. Rep. Institute of Soil Science, University of Hamburg.

Blessent D., Therrien R. & Mac Quarrie K. (2009) Coupling geological and numerical models to simulate groundwater flow and contaminant transport in fractured media. Computers & Geosciences, 35(9), 1897-1906.

Blenkinsop S., Harpham C., Burton A., Goderniaux P., Brouyere S. & Fowler H.J. (2013) Downscaling transient climate change with a stochastic weather generator for the Geer catchment, Belgium. Climate Research, 57, 95-109.

Bolger B.L., Park Y.J., Unger A.J. & Sudicky E.A. (2011) Simulating the pre-development hydrologic conditions in the San Joaquin Valley, California. Journal of hydrology, 411(3), 322-330.

Borah D.K. & Bera M. (2003) SWAT model background and application reviews. In 2003 ASAE Annual Meeting (p. 1). American Society of Agricultural and Biological Engineers.

Boyle D.P. (2001) Multicriteria calibration of hydrological models. PhD Thesis, Department of Hydrology and Water Resources, University of Arizona, Tucson.

Brunner P. & Simmons C.T. (2012) HydroGeoSphere: A fully integrated, physically based hydrological model. Ground Water, 5(2), 170-176.

Brunetti E., Jones J.P., Petitta M. & Rudolph D.L. (2013) Assessing the impact of large-scale dewatering on fault-controlled aquifer systems: a case study in the Acque Albule basin (Tivoli, central Italy). Hydrogeology Journal, 21, 401-423.

Cambi C. & Dragoni W. (2000) Groundwater, recharge variability and climatic changes: considerations arising from the modelling of a spring in the Umbria-Marche Apennines. Hydrogeology, 4, 11-25. ed. BRGM, Orlean, ISSN: 0246-1641.

Campiani E., Corticelli S., Garberi M.L. & Mariani M.C. (2010) Uso del suolo 1994 – Documentazione. Community network, Regione Emilia-Romagna.

Campiani E., Corticelli S., Garberi M.L. & Mariani M.C. (2011) a. Uso del suolo 2003 – Documentazione. Community network, Regione Emilia-Romagna.

Campiani E., Corticelli S., Garberi M.L. & Mariani M.C. (2011) b. Uso del suolo 2008 – Documentazione. Community network, Regione Emilia-Romagna.

Cey E., Rudolph D. & Therrien R. (2006) Simulation of groundwater recharge dynamics in partially saturated fractured soils incorporating spatially variable fracture apertures. Water Resources Research, 42(9).

Cervi F., Marcaccio M., Petronici F. & Borgatti L. (2014) Hydrogeological characterization of peculiar Apenninic springs. Proceedings of the International Association of Hydrological Sciences, 364, 333-338.

Cervi F., Corsini A., Doveri M., Mussi M., Ronchetti F. & Tazioli A. (2015) Characterizing the recharge of fractured aquifers: a case study in a flysch rock mass of the northern Apennines (Italy). In Engineering Geology for Society and Territory-Volume 3 (pp. 563-567).

Cervi F., Petronici F., Castellarin A., Marcaccio M., Bertolini A. & Borgatti L. (2018) Climate change potential effects on the hydrological regime of freshwater springs in the Italian northern Apennines. Science of the Total Environment, 622, 337-348

Cherubini C. (2008) A modelling approach for the study of contamination in a fractured aquifer. Geotech. Geol. Eng., 26, 519-533.

Citrini D. & Noseda G. (1987) Idraulica, Casa Editrice Ambrosiana, Italy.

Civita M. (2005) Idrogeologia applicata ambientale, Casa Editrice Ambrosiana, Milan, Italy.

Corticelli S., Campiani E. & Garberi M.L. (2011) Uso del suolo 1976 – Documentazione. Community network, Regione Emilia-Romagna.Citrini D. & Noseda G. (1987), Idraulica, 2° Edizione, Editore CEA.

D'Agostino D.R., Scardigno A., Lamaddalena N. & El Chami D. (2014) Sensitivity analysis of coupled hydro-economic models: quantifying climate change uncertainty for decision-making. Water Resources Management, 28, 4303-4318.

Davie T (2002) Fundamentals of Hydrology. 200 pp.

Déqué, M. (2007) Frequency of precipitation and temperature extremes over France in an anthropogenic scenario: Model results and statistical correction according to observed values. Global and Planetary Change, 57(1), 16-26.

DHI (2007) MIKE SHE User Manual: Reference Guide, vol. 2. Danish Hydraulic Institute, Denmark.

Diersch H.J.G. (2005) FEFLOW finite element subsurface flow and transport simulation system, reference manual. WASY Institute for Water Resources Planning and Systems Research, Berlin.

Diodato, N., Guerriero, L., Fiorillo, F., Esposito, L., Revellino, P., Grelle, G., & Guadagno, F. M. (2014). Predicting monthly spring discharges using a simple statistical model. Water resources management, 28(4), 969-978.

Dragoni W. & Sukhija B.S. (2008) Climate change and groundwater: a short review. Geological Society, London, Special Publications, 288(1), 1-12.

Dragoni W., Mottola A. & Cambi C. (2013) Modeling the effects of pumping wells in spring management: the case of Scirca spring (central Apennines, Italy). Journal of hydrology, 493, 115-123.

Dragoni W., Giontella C., Melillo M., Cambi C., Di Matteo L. & Valigi D. (2015) Possible response of two water systems in Central Italy to climatic changes. Advances in Watershed Hydrology, Water Resources Publications, USA, 397-424.

EEA (2008) Impacts of Europe's changing climate – 2008 indicator based assessment. Joint EEA-JRC-WHO Report. 246 pp.

Eisenlohr L., Király L., Bouzelboudjen M. & Rossier Y. (1997) Numerical simulation as a tool for checking the interpretation of karst spring hydrographs. Journal of Hydrology, 193(1), 306-315.

Farina M., Marcaccio M., Zavatti A. (2014) Esperienze e prospettive nel monitoraggio delle acque sotterranee. Il contributo dell'Emilia-Romagna. Pitagora Editrice, Bologna, 560 pp.

Feyen L., V`azquez R., Christiaens K., Sels O. & Feyen J. (2000) Application of a distributed physically-based hydrological model to a medium size catchment. Hydrology and Earth System Sciences 4(1): 47–63.

Ficklin D.L., Luo Y., Luedeling E. & Zhang M. (2009) Climate change sensitivity assessment of a highly agricultural watershed using SWAT. Journal of Hydrology, 374(1), 16-29.

Fiorillo F., Esposito L. & Guadagno F. M. (2007) Analyses and forecast of water resources in an ultra-centenarian spring discharge series from Serino (Southern Italy). Journal of Hydrology, 336(1), 125-138.

Fiorillo F. (2011) Tank-reservoir drainage as a simulation of the recession limb of karst spring hydrographs. Hydrogeology journal, 19(5), 1009-1019.

Fiorillo F. (2013) Spring hydrographs recession and analysis of the Caposele spring (Southern Italy) during dry periods, Italian Journal of Engineering Geology and Environment, 1, 51-64.

Font-Capo J., Pujades E., Vazquez-Sune E., Carrera J., Valasco V. & Monfort D. (2015) Assessment of the barrier effect caused by underground constructions on porous aquifers with low hydraulic gradient: A case study of the metro construction in Barcellona, Spain. Engineering Geology. 196. pp 238-250.

Forkasiewicz J. & Paloc H. (1967) Le regime de tarissement de la Foux de la Vis. Etude preliminaire. Chronique d'Hydrogéologie, BRGM 3(10), 61-73.

Foster S.B. & Allen D.M. (2015) Groundwater-surface water interactions in a mountain to coast watershed: effects of climate change and human stressors. Advances in Meteorology 2015, 22 pp.

Fowler H.J., Blenkinsop S. & Tebaldi C. (2007) Linking climate change modelling to impacts studies: recent advances in downscaling techniques for hydrological modelling. International journal of climatology, 27(12), 1547-1578.

Fowler H.J. & Kilsby C.G. (2007) Using regional climate model data to simulate historical and future river flows in northwest England. Climatic Change, 80, 337-367.

Francani V. & Cherubini C. (2006) Approcci modellistici e confronto per lo studio del flusso e del trasporto nei mezzi fratturati. Atti del convegno GEOFLUID (Gestione delle acque sotterranee e geologia applicata all'ambiente), Piacenza, 4 Ottobre 2006, DIIAR, Politecnico di Milano, 39-55.

Freeze R.A. & Cherry J.A. (1979) Groundwater, Prentice-Hall Inc., Englewood Cliffs, New Jersey, United States, 604 pp.

Garnier M., Harper D.M., Blaskovicova L., Hancz G., Janauer G.A., Jolankai Z., Lanz E., Lo Porto A., Mandoki M., Pataki B., Rahuel J.L., Robinson V.J., Stoate C., Toth E. & Jolankai G. (2015) Climate change and European water bodies, a review of existing gaps and future research needs: Findings of the Climate Water Project. Environmental Management, 56, 271-285.

Garzonio C.A., Piccinini L. & Gargini A. (2014) Groundwater modeling of fractured aquifers in mines: the case study of Gavorrano (Tuscany, Italy). Rock Mech Rock Eng, 47(3), 905-921.

Gattinoni P., Scesi L. & Francani V. (2005) Tensore di permeabilità e direzione di flusso preferenziale in un ammasso roccioso fratturato [Hydraulic conductivity tensor and preferential flow directions in the fractured rock mass], Quaderni di Geologia Applicata, Pitagora Editrice, Bologna, 12(1), 79-98.

Gattinoni, P. & Francani, V. (2010) Depletion risk assessment of the Nossana Spring (Bergamo, Italy) based on the stochastic modeling of recharge. Hydrogeology journal, 18(2), 325-337.

Gburek W.J., Folmar G.J. & Urban J.B. (1999) Field data and ground water modeling in a layered fractured aquifer. Ground Water 37(2):175–184.

Ghirotti R. (2016) Valutazione dei deflussi di base e modellazione idrologica di un bacino dell'Appennino Settentrionale. Master thesis, Università di Bologna, 177 pp.

GHS (2003) Visual Transin. Developed in the Department of Geotechnical Engineering and Geosciences y Grupo de Hidrologia Subterránea (ETCG), UPC-CSIC, Barcelona (Spain). Available at: http://h2ogeo.upc.edu/en/investigation-hydrogeology/software. Accessed the 9/3/2017.

Gleeson T. & Manning A.H. (2008) Regional groundwater flow in mountainous terrain: Three-dimensional simulations of topographic and hydrogeologic controls. Water Resources Research, 44(10).

Goderniaux P., Brouyère S., Fowler H.J., Blenkinsop S., Therrien R., Orban P. & Dassargues A. (2009) Large scale surface–subsurface hydrological model to assess climate change impacts on groundwater reserves. Journal of Hydrology, 373(1), 122-138.

Goderniuax P., Brouyere S., Blenkinsop S., Burton A., Fowler H.J., Orban P. & Dassargues A. (2011) Modeling climate change impacts on groundwater resources using transient stochastic climatic scenarios, Water Resources Research, 47, W12516.

Goderniaux P., Brouyere S., Wildemeersch S., Therrien R. & Dassargues A. (2015) Uncertainty of climate change impact on groundwater reserves – Application to a chalk aquifer. Journal of Hydrology, 528, 108-121.

Golder Associates Ltd. (2006) FRED (FracManReservoirEdition) Version 6.54: Redmond, Washington, Golder Associates.

Gómez A.A., Rodríguez L.B. & Vives L.S. (2010) The Guarani Aquifer System: estimation of recharge along the Uruguay–Brazil border. Hydrogeology Journal, 18 (7), 1667–1684.

Green T.R., Taniguchi M., Kooi H., Gurdak J.J., Allen D.M., Hiscock K.M., Treidel H. & Aureli A. (2011) Beneath the surface of global change: Impacts of climate change on groundwater. Journal of Hydrology, 405(3), 532-560.

Hassan S.T., Lubczynski M.W., Niswonger R.G. & Su Z. (2014) Surface–groundwater interactions in hard rocks in Sardon Catchment of western Spain: an integrated modeling approach. Journal of hydrology, 517, 390-410.

Hay L.E., Wilby R.L. & Leavesley G.H. (2000) A comparison of delta change and downscaled GCM scenarios for three mountainous basins in the United States. Journal of the American water resources association, 36, 387-398.

Hewitt C.D. & Griggs D.J. (2004) Ensembles-based predictions of climate changes and their impacts, Eos Trans. AGU, 85(52), 566-566.

Hiscock K., Sparkes R. & Hodgson A. (2011) Evaluation of future climate change impacts on European groundwater resources. Climate change effects of groundwater resources: a global synthesis of findings and recommendations. CRC, London, 351-365.

Holding S. & Allen D.M. (2015) From days to decades: numerical modelling of freshwater lens response to climate change stressors on small low-lying islands. Hydrology and Earth System Sciences, 19, 933-949.

Holman I.P., Tascone D. & Hess T.M. (2009) A comparison of stochastic and deterministic downscaling methods for modelling potential groundwater recharge under climate change in East Anglia, UK: implications for groundwater resource management. Hydrogeology Journal, 17, 1629-1641.

Holman I.P., Allen D.M., Cuthbert M.O. & Goderniaux P. (2012) Towards best practice for assessing the impacts of climate change on groundwater. Hydrogeology Journal, 20, 1-4.

Howells M., Hermann S., Welsch M., Bazilian M., Segerström R., Alfstad T., ... & Wiberg D. (2013). Integrated analysis of climate change, land-use, energy and water strategies. Nature Climate Change, 3(7), 621-626.

House A.R., Thompson J.R. & Acreman M.C. (2016) Projecting impacts of climate change on hydrological conditions and biotic responses in a chalk valley riparian wetland. Journal of Hydrology, 534, 178-192.

Huntington J.L. & Niswonger R.G. (2012) Role of surface-water and groundwater interactions on projected summertime streamflow in snow dominated regions: An integrated modeling approach. Water Resour. Res., 48, W11524.

IAH-Italy (2017) La risposta naturale all'emergenza idrica viene dalle falde sotterranee. Comunicato stampa IAH Italia del 27 Luglio 2017.

Institute of Hydrology (1980) Low Flow Studies (1–4), Wallingford, UK.

IPCC (2007) Climate Change 2007: The Physical Science Basis. Contribution of Working Group I to the Fourth Assessment Report of the Intergovernmental Panel on Climate Change [Solomon S., Qin D., Manning M., Chen Z., Marquis M., Averyt K.B., Tignor M. & Miller H.L. (eds.)]. Cambridge University Press, Cambridge, United Kingdom and New York, NY, USA, 996 pp.

IPCC (2014) Climate Change 2014: Synthesis Report. Contribution of Working Groups I, II and III to the Fifth Assessment Report of the Intergovernmental Panel on Climate Change [Core Writing Team, Pachauri R.K. & Meyer L.A. (eds.)]. IPCC, Geneva, Switzerland, 151 pp.

Iribar V., Carrera J., Custodio E. & Medina A. (1997) Inverse modelling of seawater intrusion in the Llobregat delta deep aquifer. J. Hydrol., 198, 226–247.

ISTAT (2012) Statistiche focus. Giornata mondiale dell'acqua 21 Marzo 2012. (https://www.istat.it/it/archivio/57514)

Istat (2014) Statistiche dati Istat. url: http://dati.istat.it/Index.aspx.

Jayakrishnan R.S.R.S., Srinivasan R., Santhi C. & Arnold J.G. (2005) Advances in the application of the SWAT model for water resources management. Hydrological processes, 19(3), 749-762.

Jones J.P., Sudicky E.A. & McLaren R.G. (2008) Application of a fully-integrated surface-subsurface flow model at the watershed-scale: A case study. Water Resources Research, 44(3).

Katsanou K., Maramathas A. & Lambrakis N. (2015) Simulation of karst springs discharge in case of incomplete time series. Water resources management, 29(5), 1623.

Kovàcs A. (2003) Geometry and hydraulic parameters of karst aquifer: a hydrodynamic modeling approach. Unpublished PhD thesis, University of Neuchathel, Switzerland, 131 pp.

Kovács A. & Perrochet P. (2008) A quantitative approach to spring hydrograph decomposition. Journal of Hydrology, 352, 16-29.

Krause P., Boyle D.P. & Base F. (2005) Comparison of different efficiency criteria for hydrological model assessment, Advances in Geosciences, 5, 89-97.

Kreins P., Henseler M., Anter J., Herrmann F. & Wendland F. (2015) Quantification of climate change impact on regional agricultural irrigation and groundwater demand. Water Resources Management, 29, 3585-3600.

Kristensen K.J. & Jensen S.E. (1975) A model for estimating actual evapotranspiration from potential evapotranspiration. Nordic Hydrology, 6, 170–188.

Kundzewicz Z.W. & Doll P. (2009) Will groundwater ease freshwater stress under climate change?. Hydrological Sciences-Journal-des Sciences Hydrologiques, 54(4), 665-675.

Le Moine N. (2008) Le bassin versant de surface vu par le souterrain: une voie d'amélioration des performance et du réalisme des modéles pluie–débit? PhD Thesis, Université Pierre et Marie Curie, Antony, 324 pp.

Levison J., Larocque M. & Ouellet M.A. (2014) Modeling low-flow bedrock springs providing ecological habitats with climate change scenarios. Journal of hydrology, 515, 16-28.

Li Q., Unger A.J.A., Sudicky E.A., Kassenaar D., Wexler E.J. & Shikaze S. (2008) Simulating the multi-seasonal response of a large-scale watershed with a 3D physically-based hydrologic model. Journal of Hydrology, 357 (3–4), 317–336.

Liu H., Chen X., Bao A. & Wang L. (2007) Investigation of groundwater response to overland flow and topography using a coupled MIKE SHE/MIKE 11 modeling system for an arid watershed. Journal of Hydrology 347: 4–459.

Liuzzo L., Noto L.V., Arnone E., Caracciolo D. & La Loggia G. (2015) Modifications in water resources availability under climate changes: a case study in a Sicilian Basin. Water resources management, 29(4), 1117-1135.

Long J.C.S., Remer J.S., Wilson C.R. & Witherspoon P.A. (1982) Porous media equivalents for networks of discontinuous fractures. Water Resources Research, 18(3), 645-658.

Maillet E. (1905) Essais d'hydraulique souterraine et fluviale. Outline of underground and river Hydraulics, Lib Sci A Herman, Paris, 218 pp.

Mango L.M., Melesse A.M., McClain M.E., Gann D. & Setegn S.G. (2011) Land use and climate change impacts on the hydrology of the upper Mara River Basin, Kenya: results of a modeling study to support better resource management. Hydrology and Earth System Sciences, 15(7), 2245.

Markstrom S.L., Niswonger R.G., Regan R.S., Prudic D.E. & Barlow P.M. (2008) GSFLOW-Coupled Ground-water and Surface-water FLOW model based on the integration of the Precipitation-Runoff Modeling System (PRMS) and the Modular Ground-Water Flow Model (MODFLOW-2005), U.S. Geol. Surv. Tech. Methods, 6-D1, 240 p.

Martinelli G., Chahoud A., Dadomo A. & Fava A. (2014) Isotopic features of Emilia-Romagna region (North Italy) groundwaters: Environmental and climatological implications. Journal of Hydrology, 519, 1928-1938.

Mearns L.O., Giorgi F., Whetton P., Pabon D., Hulme M. & Lal M. (2003) Guidelines for use of climate scenarios developed from regional climate model experiments. Data Distribution Centre of the Intergovernmental Panel on Climate Change.

Medina A. & Carrera J. (1996) Coupled estimation of flow and solute transports parameters. Water Resour. Res., 32 (10), 3063–3076.

Medina A., Alcolea A., Carrera J. & Castro L.F. (2000) Modelos de flujo y transporte en la geosfera: Código TRANSIN IV. (Flow and transport modelling in the geosphere: The code TRANSIN IV). IV Jornadas de Investigación y Desarrollo Tecnológico de Gestión de Residuos Redioactivos de ENRESA. Technical publication 9/2000: 195-200.

Medina A. & Carrera J. (2003) Computational different type of data. Geostatistical inversion of coupled problems: dealing with computational burden and different types of data. Water Resour. Res., 32 (10), 3063–3076.

Michelangeli P.A., Vrac M. & Loukos H. (2009) Probabilistic downscaling approaches: Application to wind cumulative distribution functions. Geophysical Research Letters, 36, L11708, doi:10.1029/2009GL038401

Minville M., Brissette F. & Leconte R. (2008) Uncertainty of the impact of climate change on the hydrology of a nordic watershed. Journal of Hydrology, 358, 70-83.

Moeck C., Brunner P. & Hunkeler D. (2016) The influence of model structure on groundwater recharge rates in climate-change impact studies. Hydrogeology Journal, 24, 1171-1184.

Moisello U. (2003) Idrologia Tecnica, Edizione La Goliardica Pavese s.r.l, 824pp.

Montanari A. (2005) Large sample behaviors of the generalized likelihood uncertainty estimation (GLUE) in assessing the uncertainty of rainfall-runoff simulations. Water Resources Research, 41, W08406.

Moore R.J. & Clarke R.T. (1981) A distribution function approach to rainfall runoff modelling. Water Resources Research, 17 (5), 1367-1382.

Moore R.J. (2007) The PDM rainfall-runoff model. Hydrology and Earth System Sciences Discussions, European Geosciences Union, 11 (1), 483-499.

Morari F., Lugato E. & Borin M. (2004) An integrated non-point source model-GIS system for selecting criteria of best management practices in the Po Valley, North Italy. Agriculture, ecosystems & environment, 102(3), 247-262.

Moriasi D.N., Arnold J.G., Van Liew M.W., Bingner R.L., Harmel R.D. & Veith T.L. (2007) Model evaluation guidelines for systematic quantification of accuracy in watershed simulations. Trans ASABE 50(3), 885–900.

Murphy J.M. (1999) An evaluation of statistical and dynamical techniques for downscaling local climate. J. Climate, 12, 2256-2284.

Nakićenović N. & Swart R. (eds.) (2000) Special Report on Emissions Scenarios. A Special Report of Working Group III of the Intergovernmental Panel on Climate Change. Cambridge University Press, Cambridge, United Kingdom and New York, NY, USA, 599 pp.

Nash J.E. & Sutcliffe J.V. (1970) River flow forecasting through conceptual models, Part I - A discussion of principles, Journal of Hydrology, 10(3), 282–290.

Neukum C. & Azzam R. (2012) Impact of climate change on groundwater recharge in a small catchment in the Black Forest, Germany. Hydrogeology Journal, 20, 547-560.

Papani G., De Nardo M.T., Bettelli G., Rio D., Tellini C. & Vernia L. (2002). Note Illustrative della Carta Geologica d'Italia alla scala 1:50,000, Foglio 218 "Castelnuovo ne' Monti". EL. CA. Firenze, Servizio Geologico d'Italia—Regione Emilia-Romagna.

Paradi D., Martel R., Karanta G., Lefebvre R., Michaud Y., Therrien R. & Nastev M. (2007) Comparative study of methods for WHPA delineation. Groundwater, 45(2), 158-167.

Petronici F. (2014) Modellazione idrogeologica di un acquifero fratturato. Master Thesis, Department of Civil, Chemical, Environmental and Material Engineering, University of Bologna, Bologna, Italy. 143 pp.

Petronici F., Ghirotti R., Borgatti L., Marcaccio M. & Cervi F. (2016) Hydrological modelling of the Tresinaro stream catchment (northern Apennines) with HEC-HMS code: preliminary results. Abstract Book, XXXV Convegno Nazionale di Idraulica e Costruzioni Idrauliche Bologna, 14-16 Settembre 2016.

Petronici F., Hermans T., Goderniaux P., Cervi F., Dassargues A. & Borgatti L. (2017a) Integrated modelling of the Tresinaro stream catchment (northern Apennines, Italy) to assess the sensitivity of water resources to a changing climate. Abstract Book, International Conference on Ecohydrology, Soil and Climate Change, 21-23 September 2017, Figueira da Foz, Portugal.

Petronici F., Pujades E., Jurado A., Cervi F., Dassargues A. & Borgatti L. (2017b) Hydrogeological modelling of a fractured aquifer: the Mulino delle Vene case study (northern Apennines, Italy). Abstract Book, International Conference on Ecohydrology, Soil and Climate Change, 21-23 September 2017, Figueira da Foz, Portugal.

Piccinini L. & Vincenzi V. (2010) Impacts of a railway tunnel on the streams baseflow verified by means of numerical modelling. Aqua Mundi, 1(2), 123-134.

Prudhomme C., Reynard N. & Crooks S. (2002) Downscaling of global climate models for flood frequency analysis: Where are we now? Hydrol Process 16(6):1137–1150.

Pujades E., Vazquez-Sune E., Carrera J., Vilarrasa V., De Simone S., Jurado A., Ledesma A., Ramos G. & Llorest A. (2014) Deep enclosures versus pumping to reduce settlements during shaft excavations. Enginnering Geology, 169,100-111.

Pulido-Velazquez D., Garcia-Arostegui J.L., Molina J.L. & Pulido-Velazquez M. (2015) Assessment of future groundwater recharge in semi-arid regions under climate change scenarios (Serral-Salinas aquifer, SE Spain). Could increased rainfall variability increase the recharge rate? Hydrological Porcesses, 29, 828-844.

Pushpalatha R., Perrin C., Le Moine N. & Andreassian V. (2012) A review of efficiency criteria suitable for evaluating low-flow simulations. Journal of Hydrology, 420, 171-182.

Raposo J.R., Dafonte J. & Molinero J. (2013) Assessing the impact of future climate change on groundwater recharge in Galicia-Costa, Spain. Hydrogeology Journal, 21(2), 459-479.

Rayne T.W., Bradbury K.R. & Muldoon M.A. (2001) Delineation of capture zones for municipal wells in fractured dolomite, Sturgeon Bay, Wisconsin, USA. Hydrogeology Journal, 9(5), 432-450.

Renz A., Rühaak W., Schätzl, P. & Diersch H.J. (2009) Numerical modeling of geothermal use of mine water: challenges and examples. Mine Water and the Environment, 28(1), 2-14.

Romanowicz A.A., Vanclooster M., Rounsevell M. & La Junesse I. (2005). Sensitivity of the SWAT model to the soil and land use data parametrisation: a case study in the Thyle catchment, Belgium. Ecological Modelling, 187(1), 27-39.

Scanlon B.R., Mace R.E., Barrett M.E. & Smith B. (2003) Can we simulate regional groundwater flow in a karst system using equivalent porous media models? Case study, Barton Springs Edwards aquifer, USA. Journal of hydrology, 276(1), 137-158.

Scesi L. & Gattinoni P. (2007) La circolazione idrica negli ammassi rocciosi, casa editrice Ambrosiana.

Schaffranek R.W. (1987) Flow model for open-channel reach or network. US Geol Surv Prof Pap 1384

Scibek J. & Allen D.M. (2006) Modelled impacts of predicted climate change on recharge and groundwater levels. Water Resources Research, 42, W11405.

Scibek J., Allen D.M., Cannon A.J. & Whifield P.H. (2007) Groundwater-surface water interaction under scenarios of climate change using a high-resolution transient groundwater model. Journal of Hydrology, 333, 165-181.

Scurlock J.M.O., Asner G.P. & Gower S.T. (2001) Worldwide Historical Estimates of Leaf Area Index, 1932-2000, prepared for the Oak Ridge National Laboratory. ORNL/TM-2001/268, Oak Ridge, Tennessee.

Shapiro A. & Andersson J. (1983) Steady state fluid response in fractured rock: a boundary element solution for a coupled, discrete fracture continuum model. Water Resources Res., 19(4), 959-969.

Smakhtin V.U. (2001) Low flow Hydrology: A Review. Journal of Hydrology, 240, 147-186.

Snow D.T. (1968) Rock fracture spacings, openings, and porosities, Journal of Soils Mechanics of the Foundations Division, ASCE, 94, 73-91.

Soundharajan B., Adeloye A.J. & Remesan R. (2013) Assessing climate change impacts on operation and planning characteristics of Pong Reservoirs, Beas (India). In Considering hydrological change in reservoir planning and management: Proceedings of H09, IAHS-IASPEI Assembly, Gothenburgh, Sweden (Vol. IAHS Publication 362, pp. 207-212). Wallingford: IAHS Press.

Stoll S., Franssen H.H., Butts M. & Kinzelbach W. (2011) Analysis of the impact of climate change on groundwater related hydrological fluxes: a multi-model approach including different downscaling methods. Hydrology and Earth System Sciences, 15(1), 21.

Sulis M., Paniconi C., Rivard C., Harvey R. & Chaumont D. (2011) Assessment of climate change impacts at the catchment scale with a detailed hydrological model of surface-subsurface interactions and comparison with a land surface model. Water Resources Research, 47(1).

Sultana Z. & Coulibaly P. (2011) Distributed modelling of future changes in hydrological processes of Spencer Creek watershed. Hydrological process, 25, 1254-1270.

Surrette M., Allen D. M. & Journeay M. (2008) Regional evaluation of hydraulic properties in variably fractured rock using a hydrostructural domain approach. Hydrogeology Journal, 16(1), 11.

Tallaksen L.M. (1995) A review of baseflow recession analysis. Journal of Hydrology, 165, 349-370.

Taylor R.G., Scanlon B., Döll P., Rodell M., Van Beek R., Wada Y., ... & Konikow, L. (2013) Ground water and climate change. Review article. Nature Climate Change, 3(4), 322-329.

Tazioli A. (2011) Experimental methods for river discharge measurements: comparison among tracers and current meter. Hydrological Sciences Journal, 56(7), 1314–1324.

Terenziani M. (2014) Caratterizzazione idrogeologica di acquiferi fratturatu nella valle del Torrente Tresinaro (sorgente del Monte Lusina e sorgenti del Mulino delle Vene), Dipartimento delle Scienze Chimiche e Biologiche, Università degli studi di Modena e Reggio Emilia, 54 pp. (unpublished)

Teutsch G. & Sauter M. (1991) Groundwater modeling in karst terranes: scale effects, data acquisition and field validation. Conference on hydrology, ecology, monitoring and management of ground water in karst terranes, Nashville, USA, 17-34.

Thornthwaite C.W. (1946) An approach toward a ratioanl classification of climate. Trans. Am. Geophys. Union, vol. 27, n.1.

Toews M.W. & Allen D.M. (2009) Evaluating different GCMs for predicting spatial recharge in an irrigated arid region. Journal oh Hydrology, 374, 265-281.

Touhami I., Chirino E., Andreu J.M., Sanchez J.R., Moutahir H. & Bellot J. (2015) Assessment of climate change impacts on soil water balance and aquifer recharge in a semiarid region in south east Spain. Journal of Hydrology, 527, 619-629.

Trefry M.G. & Muffels C. (2007) FEFLOW: A Finite-Element ground water FLOW and transport modelling tool. Ground Water, 45(5), 525-529.

Van Roosmalen L., Sonnenborg T.O. & Jensen K.H. (2009) Impact of climate and land use change on the hydrology of a large-scale agricultural catchment. Water Resources Research, 45(7).

Van Vuuren D.P., Edmonds J., Kainuma M., Riahi K., Thomson A., Hibbard K., Hurtt G.C., Kram T., Krey V., Lamarque J.F., Masui T., Meinshausen M., Nakicenovic N., Smith S.J. & Rose S.K. (2011) The representative concentration pathways: an overview. Climatic Change, 109, 5-31.

Vezzoli R., Mercogliano P., Pecora S., Zollo A. L. & Cacciamani C. (2015) Hydrological simulation of Po River (North Italy) discharge under climate change scenarios using the RCM COSMO-CLM. Science of The Total Environment, 521, 346-358.

Vizzi L. (2014) Studio idrogeologico delle sorgenti di Mulino delle Vene. Master Degree Thesis, Dipartimento delle Scienze Chimiche e Biologiche, Università degli studi di Modena e Reggio Emilia, 101 pp. (unpublished)

Voeckler H. & Allen D.M. (2012) Estimating regional-scale fractured bedrock hydraulic conductivity using discrete fracture network (DFN) modeling. Hydrogeology Journal, 20(6), 1081–1100.

Voeckler H.M., Allen D.M. & Alila Y. (2014) Modeling coupled surface water − groundwater processes in a small mountainous catchment. Journal of Hydrology, 517, 1089-1106.

Vogel R.M. & Fennessey N.M. (1994) Flow duration curves. I. A new interpretation and confidence intervals. Journal of Water Resources Planning and Management, 120(4), 485–504.

von Gunten D., Wöhling T., Haslauer C., Merchán D., Causapé J. & Cirpka O.A. (2014) Efficient calibration of a distributed pre-based hydrological model using grid coarsening. Journal of Hydrology, 519, 3290-3304.

von Gunten D., Wöhling T., Haslauer C.P., Merchán D., Causapé J. & Cirpka O.A. (2015) Estimating climate-change effects on a Mediterranean catchment under various irrigation conditions. Journal of Hydrology: Regional Studies, 4, 550-570.

von Gunten D., Wöhling T., Haslauer C.P., Merchán D., Causapé J., & Cirpka O.A. (2016) Using an integrated hydrological model to estimate the usefulness of meteorological drought indices in a changing climate. Hydrology and Earth System Sciences, 20(10), 4159.

Vrugt, J. A., Gupta H. V., Bouten W. & Sorooshian S. (2003) A Shuffled Complex Evolution Metropolis algorithm for optimization and uncertainty assessment of hydrologic model parameters, Water Resources Research, 39(8), 1201.

Wagener T., Boyle D.P., Lees M.J., Wheater H.S., Gupta H.V. & Sorooshian S. (2001) A framework for development and application of hydrological models. Hydrology and Earth System Sciences Discussions, European Geosciences Union, 5(1), 13-26.

Wang M., Kulatilake P.H.S.W., Panda B.B. & Rucker M.L. (2001) Groundwater resources evaluation case study via discrete fracture flow modeling. Engineering Geology, 62(4), 267-291.

WHI, Waterloo Hydrogeologic Inc. (1997) Visual MODFLOW, version 2.6.

WHI, Waterloo Hydrogeologic Inc. (1999) UnSat Suite with Visual HELP, version 2.1.03.

Wilby R., Greenfield B. & Glenny C. (1994) A coupled synoptic hydrological model for climate change impact assessment. Journal of Hydrology,153, 265–290.

Wilby R.L., Charles S.P., Zorita E., Timbal B., Whetton P. & Mearns L.O. (2004) Guidelines for the use of climate scenarios developed from statistical downscaling methods. Supporting material for the Intergovernmental Panel on Climate Change. Available at http://www.ipcc-data.org/guidelines/dgm_no2_v1_09_2004.pdf.

Wildemeersch S., Goderniaux P., Orban P., Brouyère S. & Dassargues A. (2014) Assessing the effects of spatial discretization on large-scale flow model performance and prediction uncertainty. Journal of hydrology, 510, 10-25.
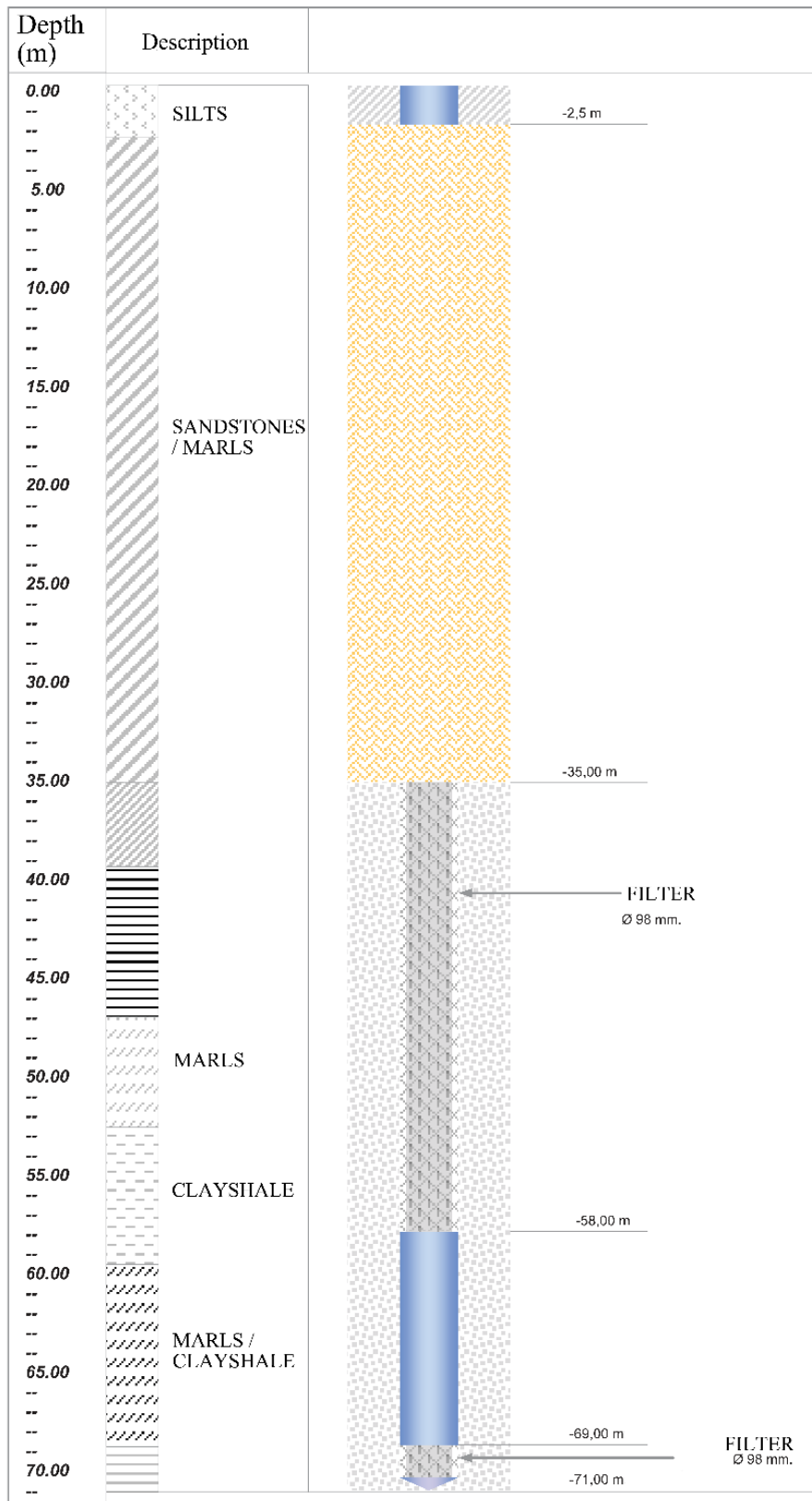
WMO, World Meteorological Organization (1974) International Glossary of Hydrology. WMO, Geneva.

Woldeamlak S.T., Batelaan O. & De Smedt F. (2007) Effect of climate change on the groundwater system in the Grote-Nete catchment, Belgium. Hydrogeology Journal, 15, 891-901.

Xevi E., Christiaens K., Espino A., Sewnandan W., Mallants D., Sørensen H. & Feyen J. (1997) Calibration, validation and sensitivity analysis of the MIKE SHE model using the Neuenkirchen catchment as case study. Water Resources Management 11: 219–242.

Zhang H. & Hiscock K.M. (2010) Modelling the impact of forest cover on groundwater resources: A case study of the Sherwood Sandstone aquifer in the East Midlands, UK. Journal of Hydrology, 392, 136-149.

APPENDIX

A. Schematic section of the stratigraphy detected during the drilling of well 4.

Depth (m)	Description	

SILTS

SANDSTONES / MARLS

MARLS

CLAYSHALE

MARLS / CLAYSHALE

-2,5 m

-35,00 m

FILTER
Ø 98 mm.

-58,00 m

-69,00 m

FILTER
Ø 98 mm.

-71,00 m

Studio geologico Dott.ssa Maria Cristina Cavazzoni, Carpineti (RE).

Figure Appendix-1 Stratigraphy of well 4.

150